Aerodynamic Modelling and Control of Vertical Axis Wind Turbines

A thesis presented in fulfilment of the requirements for the degree of Doctor of Philosophy

Conaill Eoin Soraghan

2014

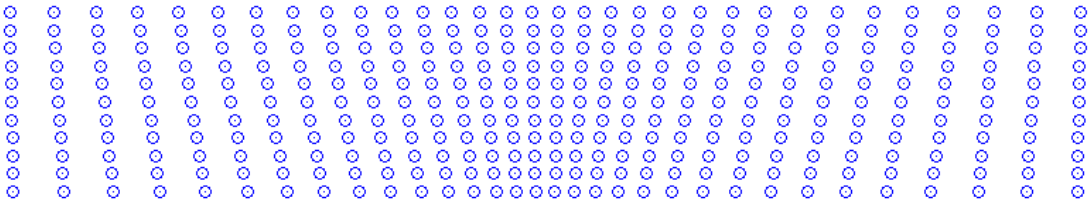

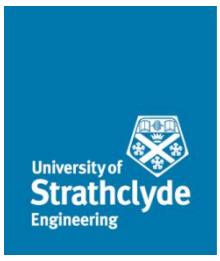

Centre for Doctoral Training in Wind Energy Systems

Department of Electronic and Electrical Engineering

The University of Strathclyde

Glasgow, UK

Declaration

This thesis is the result of the author's original research. It has been composed by the author and has not been previously submitted for examination which has led to the award of a degree.

Signed: _____

Date: _____

Abstract

Designing a structure which harnesses energy from the wind offshore is a radically different design challenge compared to that which the industry standard three-blade Danish model horizontal axis wind turbine (HAWT) has evolved to serve. Vertical axis wind turbines (VAWTs) may prove to be suitable candidates for the offshore sector due to the potential to locate heavy and complex mechanical components near the water surface providing ease of access and a low centre of gravity. Unlike their horizontal-axis counterparts, VAWT designs have not benefited from forty years of intense research and development. Therefore many challenges lie ahead for VAWT technology but lessons can be drawn from the development of HAWT technology. The main aims of this thesis are to create a design tool capable of investigating the performance of large scale, variable pitch VAWTs and to provide analyses of rotor design and control systems that would align utility scale VAWTs with aerodynamic performance and operational flexibility of state of the art HAWTs.

The design tool developed is based on the double multiple streamtube (DMS) adaptation of blade element momentum theory and it incorporates tip loss effects, flow curvature, dynamic stall, flow expansion and variable pitch. Validation demonstrates good estimation of local wind flow conditions and aerodynamic performance for both fixed pitch and variable pitch rotors. The model has been developed to investigate in particular V-rotor performance and the potential of variable pitch for VAWTs. A contribution is made to DMS modelling, which involves capturing the effects of varying degrees of streamtube expansion occurring along the blade. This contribution is referred

to as fanning and is particularly significant when implementing or designing pitch regimes.

Three novel investigations are provided that contribute to fixed pitch VAWT rotor design and control. Firstly, a method for applying lift to drag ratio to VAWTs is introduced, which accounts for azimuthal variation in aerodynamic performance. Secondly, the impact of wind shear on V-rotor rotor design is analysed. Thirdly, a solution for smoothing power fluctuations from aggregated VAWTs is proposed, which is based on controlling the phase of each rotor so peaks in individual generated power do not occur simultaneously.

A holistic approach to the way in which cyclic variable pitch can benefit VAWT operation is provided. Five control objectives are identified that span the entire operating envelope for any wind turbine, namely providing high torque during start-up, maximising power coefficient in below rated conditions, alleviating cyclic loading, power limiting in above rated conditions and aerodynamic braking in extremely high winds. Two test case turbines are designed, a similarly rated H-rotor and V-rotor, and for each turbine and each objective, a cyclic pitch regime is developed and analysed.

(Cover image: Fanning phenomenon for a three blade H-rotor with tapered blades. $\sigma = 0.16$, $\lambda = 4.5$.)

Acknowledgements

First and foremost, I would like to acknowledge Prof. Bill Leithead and Dr. Julian Feuchtwang for their unyielding endeavour for quality. I would also like to thank Dr. Hong Yue for her support and supervision throughout this research.

During the course of this project, I have collaborated with a selection of experts with remarkable knowledge and experience in the field of vertical axis wind turbine technology and I would like to thank them individually. Dr. Brian Kirke for engaging in valuable discussions about variable pitch for VAWTs and inviting me to observe water tunnel testing. Dr. Uwe Paulsen for inviting me to join and learn from the Deepwind research group in DTU Risø for a month and extending such a warm reception. Lastly, Peter Jamieson for being a constant source of ideas and inspiring me with a continuous ambition to innovate.

I want to thank my friends near and far, including the Lions, Silverbacks and Dolphins, for the endless entertainment and the Marckmanns who treated me like family while I lodged with them in Denmark. Finally, a special thanks to my family for all the encouragement, support and pragmatic advice over the years.

Nomenclature

a	Induction factor	
A	Area of an actuator surface	[m^2]
B	Number of blades	
C_L, C_D	Coefficient of lift and drag forces	
C_N, C_T	Coefficient of normal and tangential forces (in blade frame of reference)	
C_R, C_S	Coefficient of radial and sideways force (in the rotor path of rotation frame of reference)	
C_P	Coefficient of power	
C_Q	Coefficient of torque	
C_x	Coefficient of thrust in the streamwise direction	
C_{x_BE}	Coefficient of thrust in the streamwise direction due to blade element principles	
C_{x_Mom}	Coefficient of thrust in the streamwise direction due to momentum principles	
c	Chord length	[m]
$D_{Qi,j}$	An expression capturing the instantaneous forces and moment arms that contribute to torque for a particular blade segment at location (i, j) on the swept area	
d	Moment arm for a bending moment	[m]
h	Height of a blade segment (aligned with the z-axis)	[m]
l	Blade length	[m]
F_N	Instantaneous force (Normal)	[N]
$M_{B\text{-}f}$	Flapwise blade bending moment (contribution from a blade segment)	[Nm]
$M_{B\text{-}rf}$	Flapwise root blade bending moment	[Nm]
$M_{B\text{-}re}$	Edgewise root blade bending moment	[Nm]
$M_{OT\text{-}x}$	Overturning moment in the windward direction	[Nm]
$M_{OT\text{-}y}$	Overturning moment in the cross-wind direction	[Nm]
N_s	Number of blade segments	
N_t	Number of azimuthal stations	
P	Power	[W]
Q	Torque	[N.m]
Q_A	Aerodynamic torque provided by a rotor	[N.m]
Q_{DT}	Drive train torque provided by generation	[N.m]
Q_d	Torque demand output form a controller	[N.m]
R	Radius for an H-rotor	[m]
r	Local radius for a V-rotor blade station	[m]
U_{blade}	Wind speed due to wind field local to a blade	[$m.s^{-1}$]

U_e	Equilibrium wind speed between tandem actuator surfaces	[m.s^{-1}]
U_{inf}	Free stream wind speed	[m.s^{-1}]
U_{rec}	Wind speed when ambient pressure has recovered	[m.s^{-1}]
U_u, U_d	Streamwise wind velocity; upstream and downstream	[m.s^{-1}]
U_W	Wind speed in wake	[m.s^{-1}]
W	Net wind incident on a blade	[m.s^{-1}]
α	Angle of attack; measured clockwise from chord line to *W*	
α_{ss}	Aerofoil static stall angle	
β	Pitch angle; measured from tangent of rotation to chord line	
β_d	Pitch angle demand output from a controller	
γ	Coning angle; measured from the vertical to a V-rotor blade	
θ	Azimuthal position; measured anticlockwise from downwind x-axis	
λ	Tip speed ratio	
μ	Dynamic viscosity of air	[kg.(ms)$^{-1}$]
ρ	Density of air	[kg.m^{-3}]
σ	Rotor solidity	[Nc/R]
φ	Flow angle; measured from the tangent of rotation to *W*	
Φ	Phase difference for phase-shifting aggregated VAWT control	
ψ	Angle measured between radial vector pointing out of path of rotation and streamtube in streamwise direction	
ω	Rotor speed	[rad.s^{-1}]

Subscripts

D	drag
d	Downstream
e	Equilibrium (streamtube expansion context)
i	Blade segment number
j	Azimuthal position
L	Lift
N	Normal (to blade)
opt	Optimal
R	Radial (normal to rotor path of rotation)
rec	Recovery (pressure recovery between actuator surfaces)
S	Sidewards (tagential to rotor path of rotation)
T	Tangential (to blade)
u	Upstream
x	Windward direction

y	Cross wind direction
z	Vertical direction

Contents

Chapter 1

Introduction to Thesis

1.1 Research Motivations

Driven by the harmful risks posed by climate change, dwindling natural resources and the economic objective of energy security, there has been a major shift towards renewable energy technologies in the past twenty years. Of these technologies, wind energy systems are one of the most reliable and economical, to the extent that wind power has become mainstream generation in many countries [1]. Throughout the 20th century, wind turbines developed significantly and the state of the art today for the onshore sector is the three blade, variable speed, pitch regulated horizontal axis wind turbine (HAWT) [2]. A major challenge over the next decade will be how to effectively harness the potential of offshore wind where the resource is more abundant, but is situated in a challenging environment.

The approach adopted by the offshore wind industry in this early stage has been to implement proven onshore HAWT technology and engineer substantial foundations suitable for the offshore environment. Consequently construction has been expensive and excessive operation and

maintenance costs have been incurred [3]. There has been some recent interest in the need for a redesign of wind turbines that exploit the offshore environment rather than tolerate it [4, 5]. Despite inherently poor aerodynamic performance, vertical axis wind turbine (VAWT) technology is emerging as an attractive option for the offshore sector because it can provide the significant structural benefit of locating the heavy and mechanically complex generating components near the base of the structure, thus providing ease of access and improved structural stability. As a result, there has been a recent surge in VAWT research [6-10] and commercial designs of large-scale offshore VAWTs [11-15].

As the industry standard onshore wind turbine converged towards the three bladed, variable speed, pitch regulated HAWT over the past two decades, research and development of the VAWT diminished. The consequence of this combined with the current renewed interest in VAWTs for offshore has led to primitive VAWT designs emerging. In order to improve VAWT performance, there is a wealth of areas of HAWT design where lessons can be drawn.

For any wind turbine design study, a model which estimates the aerodynamic performance of the turbine is necessary. There is not currently an off-the-shelf VAWT aerodynamic code available so there is a need to develop a bespoke VAWT model. The main requirements of this model are to sufficiently capture the complex aerodynamics associated with VAWTs, permit any piecewise linear blade rotor configuration including the relatively novel V-rotor, and accurately capture the effects of variable pitch regimes.

The V-rotor is a concept that was originally proposed by Ljungstroem [16] whereby the vertical blades of the more conventional H-rotor VAWT are inclined at a coning angle. The main benefits are that deadweight supporting

structure is minimised by removing the tower and any cross arms, the coning angle improves start-up capability and the straight blades protrude from a drive-train housed at the base of the structure, so the configuration lends itself to the offshore environment. Sharpe patented an augmentation of the original V-rotor configuration which include sails on the blades to mitigate excessive overturning moments [17]. While research of this concept is ongoing at Cranfield University [11, 18], the aerodynamics of this rotor are not well understood, particularly how to capture the aerodynamics accurately in an actuator surface framework.

A major limitation of current offshore VAWT designs is that they are stall regulated. Some of the significant improvements in wind turbine performance over the past two decades have been due to the move towards variable speed operation and pitch control of HAWTs. These developments have not only improved energy capture below rated wind speed, but have achieved other objectives above rated, including the ability to limit power, alleviate transient and cyclic structural loads, and supply overspeed protection by providing aerodynamic braking in extreme wind speeds [19-21]. Active variable pitching has been demonstrated in the past for VAWTs [22-25], but only for fixed speed machines employing a single pitch regime which could not vary to suit the operating condition. These primitive turbines demonstrated very poor aerodynamic performance and ultimately, the pitch mechanisms required were regularly dismissed as too complicated in the context of relatively small turbines. Passive pitch techniques for VAWTs were investigated [26, 27] but the pitch regimes involved are inherently limited to achieving a solitary control objective and a passive system will always incur a lag. It is therefore relevant and timely that the potential benefits of active blade pitch for variable speed VAWTs be

reconsidered following a typical variable speed strategy with several different operational modes.

1.2 Aims of Research

The overarching research goal is to provide a design tool capable of VAWT aerodynamic performance evaluation and then to use it for rotor design and control system analysis, and exploration of variable pitch for piecewise linear bladed VAWTs. The thesis has the four following aims:

Aim 1: Develop a double multiple streamtube (DMS) aerodynamic evaluation tool which can model any piecewise linear blade VAWT rotor configuration and variable pitch regime.

Aim 2: Utilise the bespoke model to investigate the aerodynamic performance and design of the V-rotor and H-rotor concept.

Aim 3: Address the issue of fluctuating power output associated with aggregated VAWTs due to torque ripple by providing a wind farm control based solution.

Aim 4: Examine how variable pitch should be employed by VAWTs to achieve the whole range of control objectives that are currently achieved by state of the art pitch regulated HAWTs.

1.3 Original Contributions

The original contributions of this thesis underpinning each aim are provided.

Novel Aerodynamic Model

- A double multiple streamtube (DMS) design tool is built for aerodynamic estimation of variable pitch VAWTs with piecewise linear blades.

- In this model the flow state method [28] for calculating induction factors has been applied to the DMS method for the first time. It provides a more accurate way of capturing dynamic stall hysteresis compared to standard iterative blade element momentum techniques.
- A contribution to DMS modelling referred to as fanning is introduced in this thesis. This stems from the variation in degree of streamtube expansion along a VAWT blade and is particularly important for V-rotors. Fanning is crucial for accurately implementing or designing variable pitch regimes for VAWTs.

H-Rotor and V-Rotor Design

- A new measure of performance for VAWTs, effective lift to drag ratio, is introduced and utilised to compare the performance of H-rotors and V-rotors with each other and with state of the art HAWTs.
- Novel analysis is provided evaluating the impact of wind shear on V-rotor design.

Phase-shifting VAWT Farm Control

- A dynamic model of a VAWT farm is developed.
- A novel wind farm control based approach to smoothing aggregated power is proposed and the VAWT farm is then used for controller design.

Pitch Control for VAWTs

- Pitch regimes are designed for the full operating strategy for an active pitch H- and V-rotor with a holistic approach which considers the whole operating envelope.

- For the first time it is demonstrated that pitch control of VAWTs has the potential to provide alleviation of cyclic loads and the above rated control objectives of power limitation and overspeed protection.

1.4 List of Publications

Soraghan, C. E., Leithead, W. E., Yue, H. and Feuchtwang, J. "*Double Multiple Streamtube Model for Variable Pitch Vertical Axis Wind Turbines*", AIAA 31st Conference on Applied Aerodynamics, San Diego, 2013.

Soraghan, C. E., Leithead, W. E. and Jamieson, P. "*Influence of Lift to Drag Ratio on Optimal Aerodynamic Performance of Straight Blade Vertical Axis Wind Turbines*", EWEA Conference, Vienna, 2013.

Soraghan, C. E., Leithead, W. E. and Yue, H. "*Control Based Power Smoothing for Aggregated Vertical Axis Wind Turbines*", EWEA Conference, Copenhagen, 2012.

A journal paper is under review for the Wiley Wind Energy Journal: Soraghan, C. E., Leithead, W. E., Feuchtwang, J., Yue H., "*An Exploration of Pitch Options for Vertical Axis Wind Turbines*", 2014

1.5 Thesis Structure

The thesis is structured as follows. Chapter 2 provides the necessary background VAWT information with particular focus on straight blade rotor design, variable pitch and turbine control. Chapter 3 is a review of VAWT aerodynamics and aerodynamic modelling. In Chapter 4 the novel double multiple streamtube model is developed. Chapter 5 describes three original investigations for fixed pitch VAWTs, namely effective lift to drag analysis, impact of wind shear on V-rotor design and phase-shifting control for smoothing aggregated VAWT power output. Chapter 6 is an exploration of how variable pitch should be employed for an H-rotor and a V-rotor for the various modes spanning the operating envelope. Finally conclusions and further work are provided in Chapter 7.

Chapter 2

Background: VAWT Rotor Design and Wind Turbine Control

2.1 Introduction

Figure 2-1: Musgrove VAWT 850 H-rotor at the Carmarthen Bay test site [31]

A vertical axis wind turbine (VAWT) has a rotor with blades that revolve about a vertical axis of rotation. One of the largest straight bladed VAWTs to be tested was the 0.5MW rated Musgrove VAWT 850 shown in Figure 2-1. VAWT technology is well understood and a thorough exploration of turbine design and modelling is provided in [29, 30]. In this chapter, the topics of VAWT rotor design, variable pitch and wind turbine control, that are central

to this thesis, are reviewed. The focus is on lift-driven straight blade VAWTs because this thesis ultimately aims to contribute to the area of VAWT pitch control which is only realistic with straight blade rotors.

At the heart of VAWT engineering is the following dilemma. Although they have inherently poorer aerodynamic performance than their horizontal counterparts, VAWTs boast structural features which allow tailoring to specific environments. This chapter begins with the challenges and opportunities that have driven VAWT rotor design, before covering a brief history of VAWT technology in Section 2.2. The V-rotor concept is reviewed in Section 2.3. In Section 2.4 the state of the art of variable pitch for VAWTs is reviewed. Finally, in Section 2.5 a general background in wind turbine control theory is provided, which is required for analysis of improvements to VAWT control and the way in which new control strategies can impact turbine design.

2.2 VAWT Rotor Design

2.2.1 Rotor Definitions

In order to discuss VAWT rotors, the following definitions are required.

The two straight blade VAWT concepts that are cental to this thesis are the H-rotor and V-rotor illustrated in Figure 2-2. An H-rotor has straight vertical blades and a V-rotor has straight blades, which protrude at an angle to the vertical that will be referred to as the coning angle, γ. The chord length is c, the blade length is l and the rotor radius is R. A ϕ-rotor [32] has curved blades connected at the top and base of a tower.

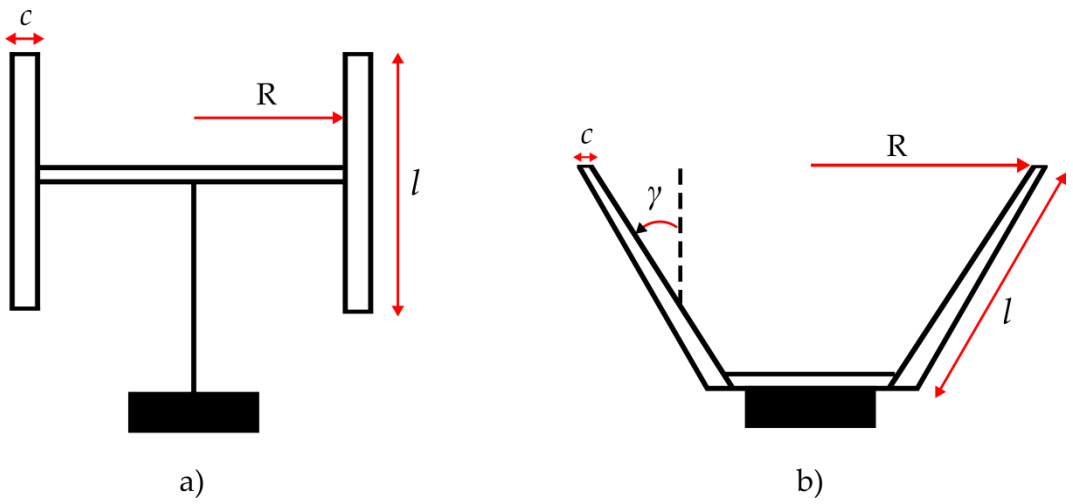

Figure 2-2: a) H-rotor b) V-rotor

Power coefficient, C_P, is the proportion of power in the wind that is converted into electrical power, P, by the wind energy system.

$$C_P = \frac{P}{\frac{1}{2}\rho A {U_{inf}}^3} \tag{2-1}$$

ρ is the density of air, A is the cross sectional area of the rotor and U_{inf} is the free stream wind speed upstream of the turbine.

Tip speed ratio, λ, expresses the speed of the blade tips due to rotation of the rotor with radius R at angular velocity ω as a ratio of U_{inf} as in (2-2). The optimal tip speed ratio, λ_{opt}, is the value of λ that maximises a $C_P - \lambda$ curve.

$$\lambda = \frac{\omega R}{U_{inf}} \tag{2-2}$$

Rotor solidity, σ, is a measure of the proportion of the swept area that is occupied by blades. Many different expressions exist that capture the essence of σ for VAWTs. The expression that is used exclusively throughout this thesis is given by (2-3) where B is the number of blades and c is the chord length [33]. Note that c will vary on a tapered blade and the radius will vary

on a V-rotor. However, for any rotor geometry, σ will refer to the solidity at the tip. The optimal solidity, σ_{opt}, is the solidity which maximises C_P.

$$\sigma = \frac{Bc}{R} \tag{2-3}$$

The blade aspect ratio is the ratio of blade length to chord length for un-tapered straight blades. The rotor aspect ratio is the ratio of blade length to rotor radius, which is only applicable to H-rotors.

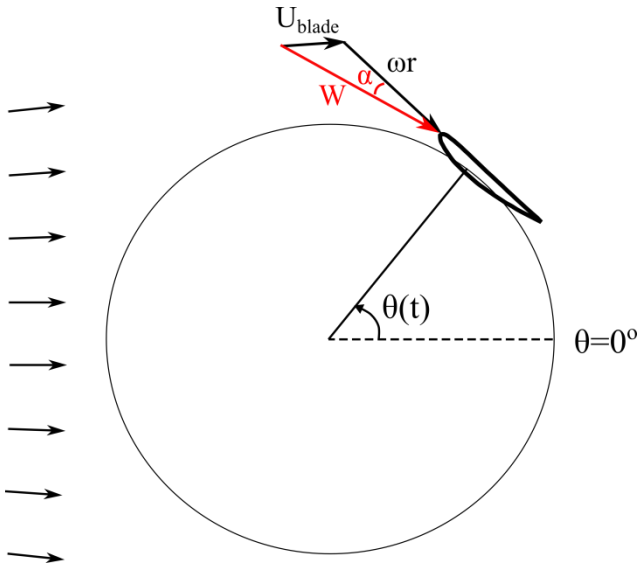

Figure 2-3: Plan view of a straight blade VAWT.

Figure 2-3 provides the convention for rotor azimuthal position, θ that is used throughout this thesis. The furthest downstream position is associated with $\theta = 0^o$ and the blades rotate anticlockwise. U_{inf} is the free stream wind speed and r is the local blade radius. The net wind incident on a VAWT blade, W, is obtained from the addition of two wind vectors: the incident wind in the streamwise direction local to the blade, U_{blade}, which accounts for streamtube expansion and any slowing of the wind due to energy extraction; and wind due to rotation of the blade, ωr, which is tangential to the path of rotation. Angle of attack, α, is measured clockwise between the chord line and W, and is restricted to the interval [-180°, 180°].

Stall is the phenomenon that causes a reduction in lift as α increases. It occurs when α exceeds the critical stall angle and the laminar fluid flow over the low pressure surface of an aerofoil transitions into turbulent flow.

2.2.2 VAWT Design Challenges

In order to introduce some of the key issues with VAWT performance, field test data for the Musgrove VAWT 850 from [34] is reproduced in Figure 2-4. This straight blade VAWT, which is shown in Figure 2-1, was operational throughout the early 1990s and remains one of the largest straight blade VAWTs to have been tested. More on VAWT history and performance follows in Section 2.2.4.

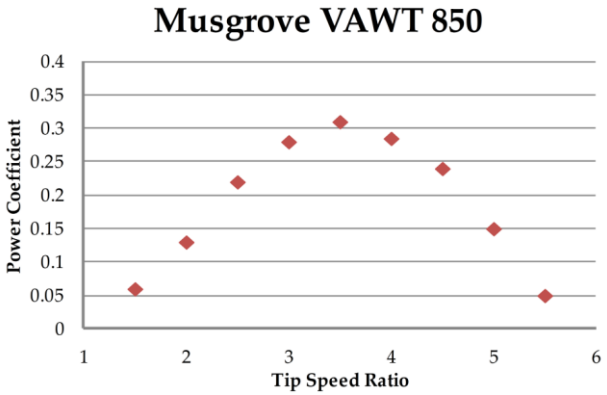

Figure 2-4: Musgrove VAWT 850 H-rotor C_P-λ curve reproduced from [34]

Two of the fundamental issues with VAWT aerodynamics are captured in Figure 2-4; poor aerodynamic performance and low rotational speed. One of the most significant issues associated with VAWTs is that they are inherently inferior to their horizontal counterparts in terms of aerodynamic efficiency. The Betz limit states that the maximum possible power coefficient, C_{Pmax}, from a horizontal axis wind turbine (HAWT) is 16/27, or approximately 0.59 [35]. State of the art HAWTs can attain a C_{Pmax} of around 0.5 [6] while the VAWT 850 has C_{Pmax} of only 0.3. Furthermore, VAWTs must operate at a low

ω. λ_{opt} is 3.5 for the VAWT 850 in Figure 2-4, which is significantly lower than that of state of the art HAWTs, at around $\lambda_{opt} = 8$ [6].

The following are the reasons for poor performance of this type of wind energy system:

Cyclical Nature of Aerodynamics – Both W and α, vary with θ, and hence time, t. Therefore an optimal lift to drag ratio cannot be sustained by the rotor and instead, the aerodynamic characteristics are constantly varying. Figure 2-5 is a plot of α against θ generated by the aerodynamic code developed in Chapter 4 for a fixed pitch H-rotor VAWT with B=3, R=18.75m and c=1.25m. It illustrates how α varies with both θ and λ. α passes through 0^o twice per revolution for each blade at approximately $\theta = 90^o$ and $\theta = 270^o$. Also, it is clear that the range of α experienced by the blade decreases with λ. For $\lambda < 2$ the blade is in deep stall for a significant portion of the path of rotation and for $\lambda > 6$ a very small range of α is experienced by the blade.

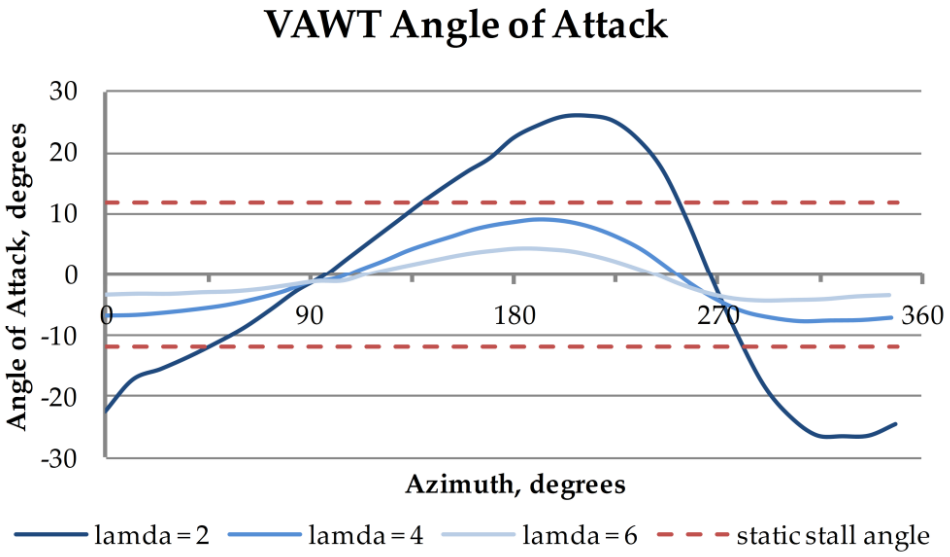

Figure 2-5: Variation of angle of attack with azimuth and tip speed ratio

Torque Ripple – The cyclic nature of α and W manifests as cyclic variation in driving torque known as torque ripple. There will be localised regions of the

path of rotation providing good aerodynamic performance and a surge in aerodynamic torque is generated every time a blade passes through one of these regions [36]. Without the ability to sufficiently vary ω, torque ripple can manifest as power fluctuations. One constant speed VAWT demonstration from the Carmarthen Bay test facility exhibited cyclic variation in power output of 22% of the mean value [37].

Inability to Self-Start – It was recognized by Watson [38] that the inability of VAWTs to self-start arises from the existence of a band of λ below the operating condition for which the net amount of energy extracted by each blade each revolution is negative. Self-starting problems can be overcome electrically if the load is a synchronous alternator or a DC generator which can function as a motor and can be used to drive the turbine up to operating speed [26].

Low Rotational Speed – Efficient generation of electricity from a lift driven wind turbine requires high design λ[2]. However, the range of α experienced decreases with λ [30] and suitably high α are required in order to generate a significant amount of lift and hence driving torque. HAWTs can achieve high λ while maintaining suitable α by introducing twist along a blade. VAWTs, on the other hand, are limited by the fact that any twist will improve performance in one half cycle of the rotor, while incurring penalties in the other half cycle. Consequently VAWTs typically operate at much lower λ, and hence lower ω. This is a disadvantage because power, P, is related to torque, Q, by the relationship given in (2-4) so for a particular power rating, low ω implies a high torque rating.

$$P = Q\omega \tag{2-4}$$

Low ω significantly impacts drive train architecture because either a gearbox with a large gear ratio or a direct drive generator with many pole pairs is required for electricity generation and both of these entail high costs [6].

Excessive Weight and Cost – The combination of poor aerodynamics requiring a large structure for a specified power rating, and heavy drive trains due to the low ω and high Q translates into high material costs and excessive weight which must be supported by a large foundation.

Any new VAWT design must address these fundamental issues. In this thesis, a tool capable of exploring the design options which impact these fundamental issues for fixed pitch VAWTs is presented. Furthermore, it is used to demonstrate how variable pitch can successfully address the above issues.

2.2.3 VAWT Design Opportunities

In spite of the significant disadvantages, the following opportunities provided by the vertical axis concept are driving resurgence in interest, in particular for the offshore environment [7-15].

Ease of Accessibility – VAWTs have the potential to locate the heavy and mechanically complex drive-train components near the base of the structure providing simplification of construction and operations and maintenance (O&M).

Low Centre of Gravity – A structure with the heavy components near the base has a much lower centre of gravity. Structural stability is, thereby, considerably enhanced.

Scalability of Designs –Wind turbine rotors are subject to the square-cube scaling law which dictates that if the surface area of a rotor increases by the square of a multiplier, the mass increases by the cube of that multiplier [6].

Therefore, as wind turbines are scaled up to achieve higher power outputs, excessive weight has to be supported by the slender tower of a HAWT configuration. The VAWT configuration is suitable for very large designs because the heavy drive train can be positioned near the base of the structure and tower size can be reduced with concepts such as the V-rotor.

Simple Blade Design – Current state of the art HAWTs blades have a complex twist profile to accommodate variation in local flow conditions along the blade and this requires a challenging and expensive manufacturing process. VAWTs benefit from more consistent flow conditions along the blade so simpler, piecewise manufacturing solutions are possible.

No Yaw Drive – A VAWT does not require a yaw drive. A fixed pitch VAWT requires no knowledge of the wind direction so control is simplified. For variable pitch VAWTs, however, a direction of the wind is required so the pitch regime can be adjusted, but the whole rotor does not need to be yawed as is the case with HAWTs.

Offshore Candidate – VAWT technology is emerging as a potential candidate for harnessing offshore wind. This is driven mainly by the ease of accessibility to mechanical components for bottom fixed turbines and the low centre of gravity for floating wind energy systems. An investigation recently commissioned by Sandia National Labs [39] concluded that VAWTs have significant advantages over HAWTs in offshore applications, and that H- or V-rotor designs are likely to be more cost effective.

It should be noted that currently there is a lot of interest in VAWTs at the micro-generation scale due mainly to their simple designs and successful companies have emerged such as Quiet Revolution and X-wind. Also, the vertical axis concept has been adopted to suit the marine energy sector [40] and a lot of work is on-going regarding blade pitching for these turbines [41-

44]. A motivation for this thesis is that VAWTs are a potential candidate for offshore wind energy systems at the utility scale so the focus is on multi-megawatt turbines, in particular straight blade VAWTs.

2.2.4 Evolution of VAWTs

VAWTs are by no means a new endeavour. The technology dates back to the ancient Persian and Chinese civilisations in the 12th Century [30]. Blades made from cloth or reeds were attached to a rotating vertical axis, and these so called panemones were used to grind grain or pump water. Mills of this type continued to operate in areas of the middle-east into the 20th century. The world's first wind powered electricity generator was constructed by James Blyth in July 1897 in Marykirk, Scotland [45] and it is known that Blyth experimented with both horizontal and vertical axis wind turbines. An early step in the development of VAWTs was the work of Finnish engineer Sigurd J. Savonius who invented and patented a drag-driven VAWT with an S-shaped rotor in 1930 [46]. Subsequently, Georges Darrieus developed lift-driven VAWTs because, unlike drag driven devices, they have the capability of operating at $\lambda > 1$ which is advantageous for efficient generation of electricity. He patented the lift-driven straight and curved blade VAWT concept in 1953 [47]. This patent also included active pitch control which will be a central technology throughout this thesis.

Throughout the 1960s and up until the early 1990s lift-driven VAWTs were extensively researched and tested at the medium to large scale. There are two classifications of lift-driven VAWT rotors; curved blade and straight blade.

The curved bladed ϕ -rotor concept, or 'egg-beater', was pioneered by Sandia National Laboratories in the USA [39] and the National Research

Council (NRC) of Canada [48]. This design aims to eliminate bending moments so the blades exist essentially in tension, and the rotor geometry which minimises bending moments is known as the troposkein rotor [49]. At Sandia labs, prototype ϕ -rotors with diameters of 5m [50], 17m [51] and 34m [52] were developed and tests demonstrated C_{Pmax} ranging between 0.3 and 0.4. The largest installed ϕ -rotor turbine was the NRC 3.8MW rated Eole turbine shown in Figure 2-6 a). Poor performance led to downrating the rating to 2.7MW and the turbine was shut down in 1993 due to a bearing problem [53]. However, it successfully operated for six years and confirmed that megawatt scale VAWTs were technically feasible.

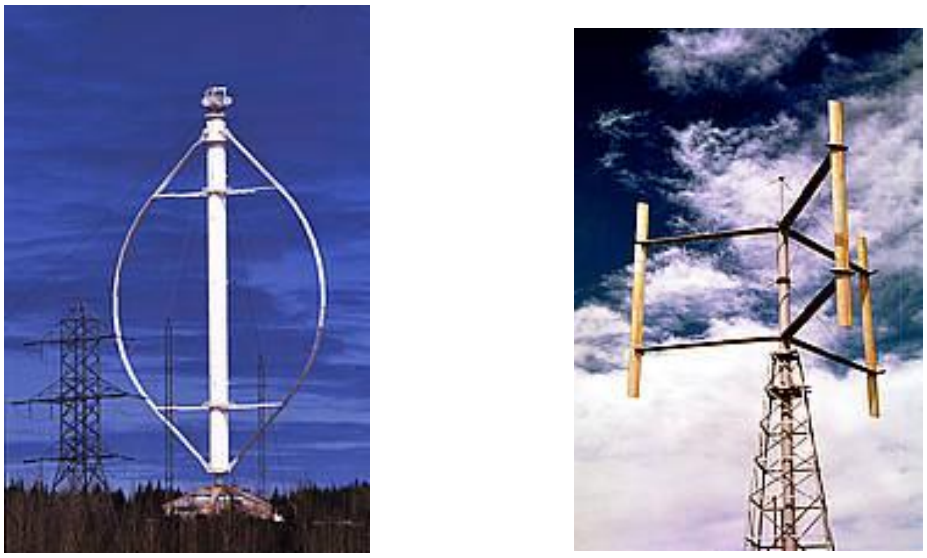

a) Eole 3.8MW ϕ-rotor **b) McDonnell 40 kW Giromill**

Figure 2-6: Lift-driven VAWT prototypes. Both pictures provided by Gipe [32].

The straight bladed H-rotor concept was taken forward in the UK and championed by Peter Musgrove [54]. This concept simplifies the curved troposkein design into a configuration which is more aerodynamically efficient and easier to manufacture. Two prototypes at the hundred kW scale were built in the 1980s. The 135 kW rated VAWT 450 had a reefing

mechanism to shed power in above rated conditions [55]. It achieved a C_{Pmax} of 0.31 at λ = 3. The larger VAWT 850 [34] was rated at 500 kW and is shown in Figure 2-1. Experimental results are provided in Figure 2-4 demonstrating low C_P. The reefing mechanism was not included in the larger VAWT 850 and the turbine only operated for one year before a blade failure in 1990. A review of the Musgrove turbine tests concludes that the concrete tower was prohibitively expensive in order to withstand the cyclical fatigue due to pulsating torque and thrust [56].

Blade pitching is appealing for VAWT design because it provides the potential to sustain effective angles of attack for generating lift. In the late 1970s it was shown theoretically that variable pitch could enhance start-up performance and increase peak aerodynamic efficiency [57]. The H-rotor configuration lends itself to variable pitch VAWTs and with this enhancement the concept was dubbed the cycloturbine [58] and giromill [59]. Demonstrations of these concepts are reviewed in Section 2.4.4. The largest variable pitch H-rotor was the 40 kW McDonnell Giromill which is shown in Figure 2-6 b). The prototypes that were developed operated at fixed ω and failed to deliver the theoretical improvements to peak aerodynamic performance [22, 24, 25, 60].

The period of development of lift-driven VAWTs throughout the late 20th century is well documented [29, 30],[39],[48],[54],[56] and the following key challenges for VAWT design, that hindered their commercialisation, emerged; poor start-up performance, low peak aerodynamic performance, pulsating torque and power output, and low operational rotor speed. The wind industry learned that the VAWT concept is fundamentally inferior to the HAWT concept onshore and naturally, research and design of VAWTs diminished in favour of HAWTs towards the end of the 20th century. As

previously noted, there has been resurgence in VAWT literature and designs over the past decade [7-15]. Evidence of this resurgence is clear from Figure 2-7 which presents the incidence of publications with the keyword "Vertical axis wind turbine" in the title. Data from the Compendex Engineering Village [61] dates back to 1973 and the active period of VAWT research throughout the late 1980s is evident. The Science Direct data [62] does not include this period, but both datasets display a spike in activity in the past five years.

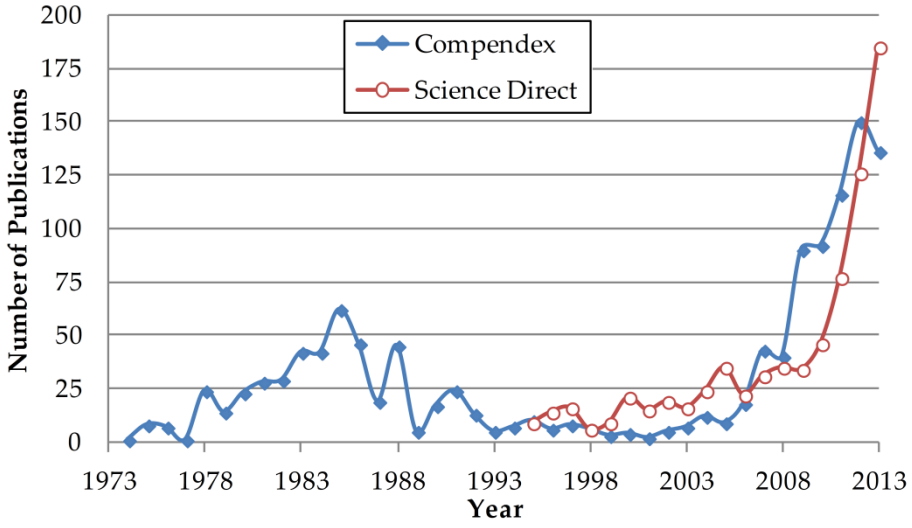

Figure 2-7: Incidence of VAWT publications

Despite the inherent problems with VAWTs, the recent interest stems from two visions for VAWTs. Firstly, the simplicity due to insensitivity to wind direction and uniform blade design make them ideal as small scale stand-alone systems. Alternatively, at the very large scale, as discussed earlier, the VAWT configuration is suitable for the offshore environment. Offshore presents a radically new design challenge where structural factors and reliability may be as important as aerodynamic performance and where foundation and O&M costs make up a significant portion of project lifetime costs. One concept that emerged which is tailored to operational challenges

offshore is the V-rotor with sails [17]. A full review of the V-rotor design is provided in Section 2.3.

Of all the offshore utility scale VAWT projects emerging, the furthest advanced are Deepwind [12], MODEC Skwid [14] and Vertiwind [13] shown in Figure 2-8. A common trait among these offshore VAWT designs is that they are stall-regulated machines, while pitch regulation has become the industry standard for HAWTs [63]. There are a lot of lessons to be learned from the development of HAWTs over the past two decades. This thesis will provide a range of analyses exploring some design possibilities that could bring large scale VAWT performance in line with that of the current state of the art HAWTs.

a) Deepwind 1kW

b) MODEC Skwid 500 kW

c) Vertiwind 35 kW

Figure 2-8: Offshore VAWT prototypes

2.3 V-Rotor VAWT

The V-rotor VAWT has straight blades which protrude at an angle to the vertical that will be referred to as the coning angle, γ. With straight blades, this configuration lends itself to blade pitching. The main benefits of this concept are that the heavy and complex mechanical drive train is situated at the base of the structure, and the deadweight supporting structure is

minimised by removing the tower and any cross arms. Furthermore it has good start-up capability. However, achievable aerodynamic performance diminishes with γ and overturning moments are extremely large leading to excessive loading on the bearing connecting blades to the drive train.

2.3.1 Development of the V-Rotor

The idea of inclining the blades of an H-rotor to create a V-rotor was originally proposed by Olle Ljunstrom in his 1973 paper [16], which assessed a variety of innovative VAWT configurations. An early reference to a coning angle appeared in Baker's 1983 paper [64] in which he refers to γ as the angle of tilt. This paper investigates the inability for low solidity, straight bladed VAWTs to self-start. The aim of the paper was to identify rotor alterations which can reduce the negative C_T that is experienced in low λ during startup. It was shown analytically that increasing γ reduces the range of α experienced throughout the rotor cycle and reduces the amount of time dwelt in the negative C_T region, so increasing γ improves start-up capability.

The invention of the V-rotor is credited to Derek Taylor of the Open University. His original idea was first developed into a prototype in 1986 and wind tunnel test results were published by Robotham and Sharpe [65]. This initial model scale prototype had two 615mm blades inclined at 45° to the vertical axis. The wind tunnel tests demonstrated C_{Pmax} consistently lower than 0.2 but the authors argued that this is due to the low Reynolds number of approximately 300,000. This early investigation had a focus on above rated control. Each blade had the ability to set a fixed pitch at three positions along the span near the tip. It was demonstrated that a blade tip area of 5% was sufficient for both power regulation and overspeed protection when the fixed pitch could be set anywhere between 0 and 25° (positive pitch was associated

with nose in pitch). Enhancement of torque at all operating speeds was demonstrated using small negative pitch settings.

Following this Sharpe et. al. published the design and free-air tests of a 5kW V-rotor prototype [66]. It had an 8.8m diameter and blades which tapered from 460mm at the root to 230mm at the tip. A cable was connected to the 70% span position to support the blade. Performance measurements experienced difficulties due to the lag between the time of wind measurement and the time at which the wind arrived at the turbine leading to fluctuations of the C_P-λ curve and an excessively high C_{Pmax} value of 0.5. Filtering results and binning tip speed ratios provided more realistic performance curves with a C_{Pmax} of 0.275 occurring at λ_{opt} = 5.5 which is a much higher λ_{opt} than most similarly rated VAWTs. The ability to pitch a portion of the blade for above rated control was ignored for the 5kW design and there was no discussion on above rated control in [66].

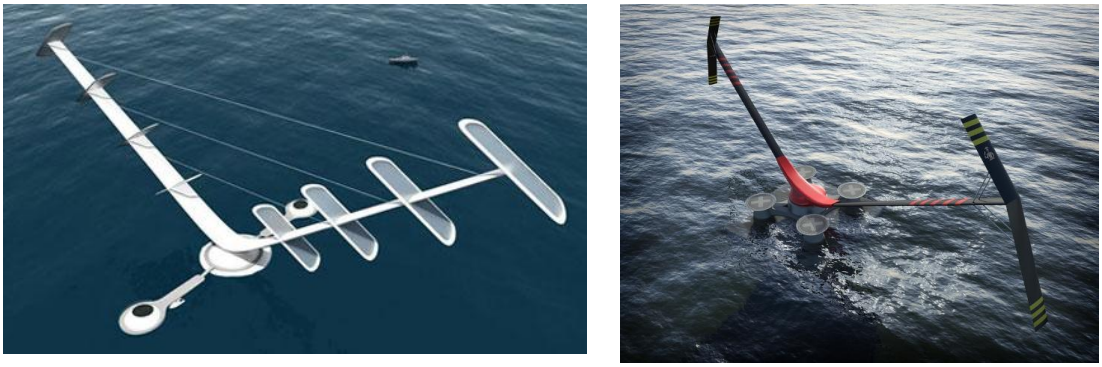

a) V-rotor with sails **b) Aerogenerator X**

Figure 2-9: V-rotor augmentations

Sharpe designed and patented an augmentation to the V-rotor [17] which included sails along the blades to counter the additional component of overturning moments and blade bending moments induced by γ (see Section

2.3.2). This configuration is shown in Figure 2-9 a). The V-rotor with sails concept was further developed as part of the of the Novel Offshore Vertical Axis demonstrator (NOVA) project [67]. This project had the aim of demonstrating that the radical yet simple V-rotor design could provide reductions in cost of electricity generated from offshore wind. The work was completed in 2010 and the NOVA V-rotor, illustrated in Figure 2-9 b), was renamed the Aerogenerator. A 5MW and 10MW version were designed and details of the design optimisation which led to the 10MW version are available [11]. Minimising overturning moment is the objective of the design optimisation and consequently the blades are at 40^{o} from vertical, notwithstanding the 30% reduction in driving torque. This design optimisation was based on static loading which is not sufficient for such a design because the mass of the sails at the tips of the blades will inevitably induce dynamic motion of the rotor and consequently fatigue induced by dynamic loading is significantly increased. The aerodynamic modelling approach was published [18] describing the BEM based model that was developed to assess the Aerogenerator design. The results show that the model captures curved bladed VAWT performance well, but there is a stated lack of confidence in the predictions for the V-rotor.

2.3.2 Excessive Loading Associated with V-Rotors

A major disadvantage of the V-rotor concept is the excessive blade bending moments and overturning moments. This is mainly a consequence of the geometry of the rotor and to a lesser degree, due to compensating for induced vertical aerodynamic forces.

The geometry of the V-rotor does not permit many options for support of the blades and incurs excessive blade bending moments where the blades are attached to the hub. Figure 2-10 shows an H-rotor and a V-

rotor with similar swept areas. The diagram indicates the variables required to determine blade root bending moments at the connection point, which is between a blade and a cross beam for the H-rotor, and between a blade and the hub for the V-rotor. F_N is the instantaneous normal force per unit blade span shown here at a blade tip, d_H is the moment arm from the cross beam to a tip for an H-rotor, d_V is the moment arm from the hub to a tip for the V-rotor and $M_{B\text{-}rf}$ is the flapwise blade root bending moment. For a fixed pitch blade with no pitch offset at $\theta = 0^o$, the flapwise force is in the direction of F_N. $M_{B\text{-}rf}$ is significantly larger on the V-rotor for two reasons. Firstly the V-rotor moment arm is considerably larger, and secondly the two halves of H-rotor blades generate $M_{B\text{-}rf}$ that act in opposite directions so they partially cancel out, whereas the connection point for the V-rotor must withstand $M_{B\text{-}rf}$ generated by the whole blade without any cancelation.

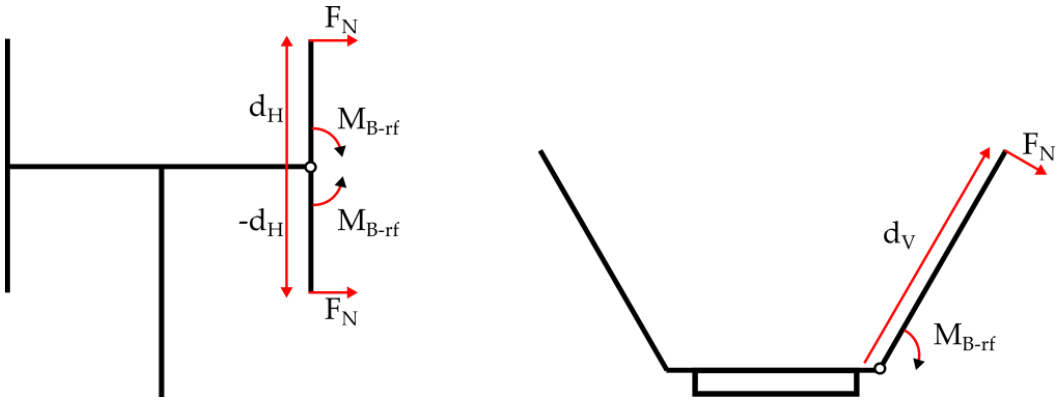

Figure 2-10: Blade root bending moment for an H-rotor and a V-Rotor

A difference between the aerodynamics of H-rotors and V-rotors is that the latter induces vertical aerodynamic forces. For a V-rotor to apply a thrust force on the free stream wind, a component of force must be generated in the vertical direction which increases the overturning moment.

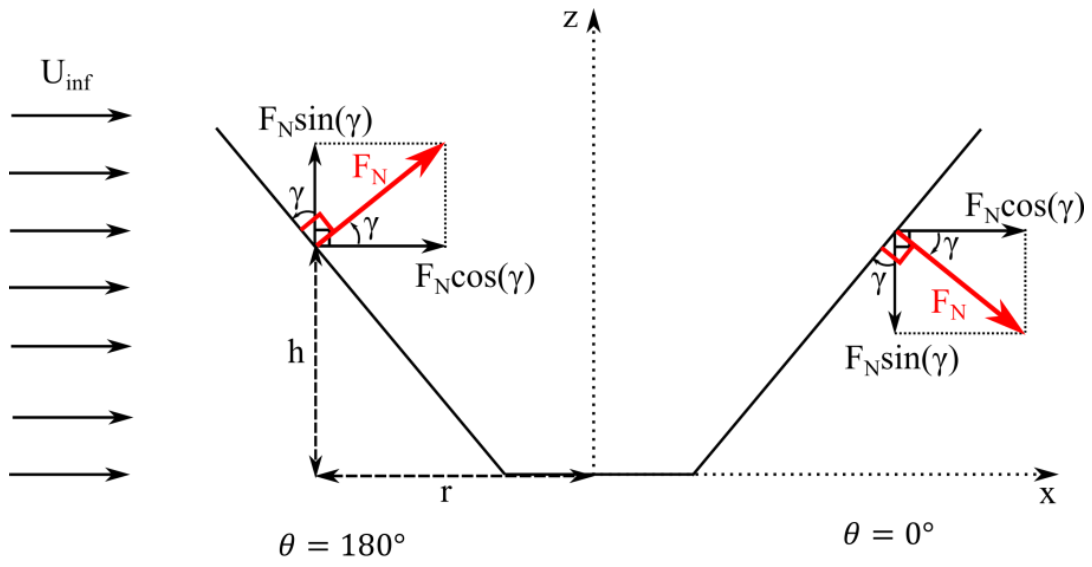

Figure 2-11: Normal aerodynamic force on a V-rotor blade resolved into windward and vertical components.

A wind turbine blade can only generate aerodynamic forces in a plane which contains the chord and is perpendicular to the span. In Figure 2-11 the normal blade forces, F_N, in this plane of interest are for the furthest upwind and furthest downwind positions. The component $F_N\cos(\gamma)$ is the force on the blade in the streamwise direction. This force applied with moment arm h provides a contribution to overturning moment which is similar to an H-rotor with the same thrust and radius. The component $F_N\sin(\gamma)$ acts to deflect the wind and deform the blade clockwise in both the upwind and downwind positions in this schematic. This force applied with moment arm r provides an additional contribution to overturning moment which is not present on an H-rotor. While a ϕ-rotor does have γ which departs from 0^o for most of the blade, the additional overturning moment generated by the bottom half of the blade is cancelled by the opposite forces acting on the top half of the blade.

According to HAWT BEM principles, a wind turbine rotor provides the optimal performance when the wind is slowed by a factor of 1/3 [2]. Only

the component $F_N\cos(\gamma)$ from the normal blade force contributes to providing thrust force on the free stream wind. Therefore, as γ increases, a larger F_N is required to create the optimal blockage. This can be achieved by increasing local flow speed by permitting a faster ω, which is a benefit for electricity generation based on a spinning generator, but ultimately increasing the blade forcing will incur penalties in terms of fatigue of the blade.

2.4 Variable Pitch for VAWTs

This section introduces the convention used throughout this thesis for pitch angles and the various forms of pitch are defined. Fixed pitch and passive pitch are discussed briefly and a full review of active pitch demonstrations and theoretical studies is provided.

2.4.1 Variable Pitch Definitions

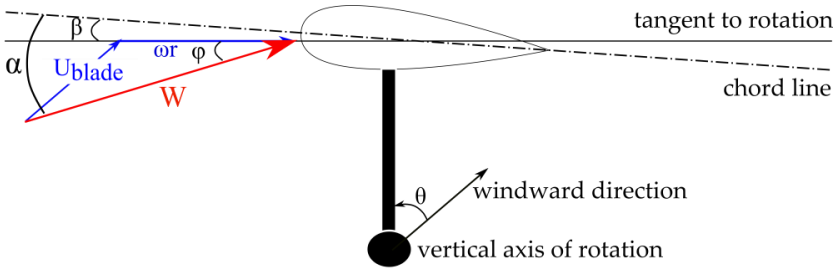

Figure 2-12: Relation between pitch angle, β, flow angle, φ, and angle of attack, α.

All angles (with the exception of θ) are measured with a clockwise direction of positivity. Blade pitch angle, β, is measured from the tangent to rotation to the chord line. Flow angle, φ, is measured from the tangent to rotation to the net wind speed vector, W. Angle of attack, α, is measured clockwise from the chord line to W and is restricted to the interval [-180°, 180°]. These angles are illustrated in Figure 2-12 for a downstream azimuthal position, θ = 45°

therefore φ is negative. β can be manipulated to adjust α according to (2-5). β is positive in Figure 2-12 so α is negative with a larger magnitude than φ.

$$\alpha = \varphi - \beta \tag{2-5}$$

VAWT blade pitch can be either fixed pitch or variable pitch. **Fixed pitch** implies an offset value of β is kept the same at every azimuthal position. Variable pitch exists in two forms; **passive pitch** whereby the blades are free to pitch about a spanwise axis and β is determined directly by the wind forces on the blades themselves; and **active pitch** whereby some mechanism actively controls the degree of blade pitch such as an actuator or a central cam with pushrods connected to the blades.

A further classification exists between two fundamentally different forms of variable pitch; cyclic pitch and responsive pitch. **Cyclic pitch,** which can be achieved passively or actively, refers to pitch regimes that are functions of θ. A pitch regime for cyclic pitch refers to the mapping of θ to β for $\theta \in [0^o, 360^o]$ and will be written as $\beta(\theta)$ for shorthand. Alternatively, **responsive pitch**, which can only be achieved actively, refers to adjusting β in response to changes in conditions such as wind speed.

A pitch regime proposed by Staelens in a theoretical optimisation study [68] is reproduced in Figure 2-13, which has been adapted to suit the convention followed in this thesis, in order to introduce some key aspects of variable pitch design.

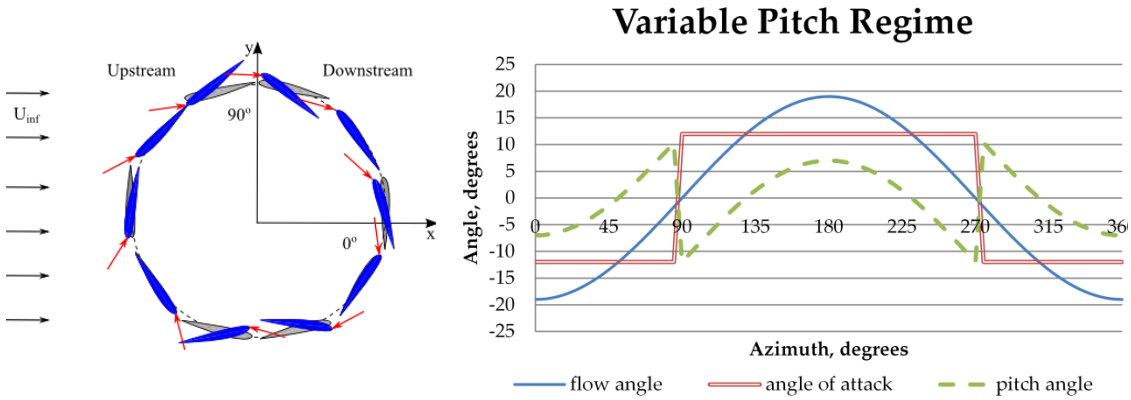

a) Plan view of an idealised pitch regime

b) Variation in angle of attack, flow angle and pitch angle with azimuth

Figure 2-13: A VAWT pitch regime taken from [68]

The impact of this pitch regime on the aerofoils in the x-y plane is provided in Figure 2-13 a) and in b) the three angles α, β and φ are plotted against θ. The pitch regime in Figure 2-13 was designed to maximise aerodynamic performance by sustaining α at 12° upstream and -12° downstream. In the upstream pass, β is negative when $\varphi < 12°$ to increase $|\alpha|$ and β is positive when $\varphi > 12°$ to avoid stall, while downstream the opposite is true. This example demonstrates some of the main challenges of variable pitch for VAWTs. Any pitch regime is designed to achieve some predefined objective. A pitch regime depends on the range of φ, which is very sensitive to λ (see Figure 2-5). There are two flipping regions in the vicinity of 90° and 270° where the sign of β must change. The results of this optimisation are unreliable because the VAWT model used was basic and maintaining a fixed value of α is not a sufficient objective for attaining the optimal aerodynamic performance, instead the torque generated should be maximised. A full review of this investigation is provided in Section 2.4.5.

2.4.2 Fixed Pitch

The simplest form of blade pitch is fixed pitch where a constant offset value of β is maintained for all θ. This has the major benefit of avoiding the need for a complicated pitching mechanism and controller, however, it has very limited flexibility. It has been shown that fixed pitch has the ability to aid self-start [64] and improve peak VAWT aerodynamic performance [69].

It has been shown previously that fixed pitch can successfully achieve redistribution of loads without any penalty to energy conversion. Scheurich and Ferriera [70] demonstrated that power and instantaneous loads are decoupled in a VAWT. For an exemplary small-scale H-rotor VAWT, two independent modelling approaches, a potential flow panel model and a method that is based on the vorticity–velocity formulation of the Navier–Stokes equations, demonstrate that $+3^{o}$, 0^{o} and -3^{o} of fixed pitch will generate the same average power output. They argued that fixed pitch causes a change in bound circulation by a constant value which leads to a redistribution of loading. Although the current thesis adopts the simpler BEM approach, a central argument to this thesis is that pitching for VAWTs should be exploited for purposes other than extracting more energy from the wind, particularly in above rated conditions.

Fixed pitch regimes are used in this thesis to benchmark performance of non-pitching turbines because fixed pitch is as mechanically simple as a zero pitch VAWT.

2.4.3 Passive Pitch

Passive techniques exploit the fact that if the blade pivots about a position near the leading edge, aerodynamic forces will always produce a pitching moment tending to reduce $|\alpha|$ and so reduce the tendency for the blades to

stall. A comprehensive review of this theory and turbines that use this principle can be found in both [26] and [27]. A passive pitch system will always involve a lag between the instantaneous forcing on the blade which influences β and the instantaneous β. VAWT blade pitching is a dynamic situation where β is continuously varying, so this lag is significant. In addition, passive pitch turbines have limited flexibility because the pitch regime cannot be manipulated to achieve multiple objectives. The variable pitch analysis in this thesis explores how pitching can benefit the entire operating envelope, so passive pitching techniques are not explored any further.

2.4.4 Active Pitch VAWT Review

Active pitch for VAWTs involves a mechanism which forces the blades to pitch according to some predefined regime. The simplest form enforces variation in β which is a first order sinusoidal function of θ. More sophisticated pitch regimes include higher order sinusoidal terms or may not be restricted to sinusoidal variations. The ideal mechanism would set $\beta(\theta)$ to suit the operating conditions.

It has been demonstrated that aerodynamic performance of a VAWT can be improved by varying β to alter α, however, active pitch should also be employed to achieve other objectives. The potential for variable pitch to improve aerodynamic performance was shown by Holme [57] in 1977. A VAWT was simulated in a vortex code and when variable pitch was applied, an 8% increase in C_{Pmax} was achieved. In 1979, De Vries noted in [71] that blade pitching could not only provide improvements to power efficiency of a VAWT, but also be employed to control the power output at constant angular velocity and varying wind speed. However, with the rise of the Danish concept in the subsequent decade, interest in variable pitch VAWTs

diminished. Investigations and demonstrations were carried out confirming the ability of variable pitch to increase the aerodynamic efficiency of VAWT technology, but very little can be found in the literature addressing how a variable pitch VAWT operating strategy should be designed.

Primitive small-scale versions of variable pitch VAWTs appeared in the 1970s with the main motivation of exploiting variable pitch to improve aerodynamic performance. The first commercially available VAWT with active pitching was the Pinson **cycloturbine** [58] which had a pitch control mechanism that was activated by a camshaft. The pitch regime used was considered to be first-order sinusoidal because $\beta(\theta)$ consisted of a constant term and one sinusoidal term. Grylls et. al. [22] published the results of both theoretical studies and wind tunnel tests for a constant speed cycloturbine. Their cited reasons for employing variable pitch were to improve self-starting and increase C_P. The amplitude of the sinusoidal pitch could be adjusted to achieve these two objectives. A multiple streamtube model which lacked streamtube expansion, predicted an improvement in peak aerodynamic performance as pitch variation amplitude increased to 3^o, achieving C_P of up to 0.46, and that a further increase in pitch angle range led to a degration in power performance. Experimental results for a 2.4m diameter prototype failed to achieve C_P exceeding 0.2 with any pitch regime, while regimes with large pitch amplitudes of 20^o did improve start-up capability. While the form of $\beta(\theta)$ was limtied, this was an early step towards utilising different pitch regimes with the same turbine to suit the whole operating envelope of a VAWT. One conclusion was that the power output was insensitive to the location of maximum pitch within a band of θ spanning 40^o, which supports the idea that variable pitch can be used to redistribute the loading of a VAWT.

Another early active pitch VAWT was the **giromill**. A feasibility study was completed in 1975 [59] which concluded that it had the potential to reduce the cost of energy production but that was based on simulations with a C_P of 0.5. Prototype testing at the 2m diameter scale was completed [72] and it did achieve excellent power coefficient. However, a relatively small wind tunnel was used which acted as a duct. Nevertheless, a 40kW giromill was commissioned [23] with testing scheduled to take place the following year. A comprehensive account of the fabrication of the turbine was published [73], however, no performance results were ever published.

Madsen and Lundgren [24] designed a constant speed active pitch VAWT that was inspired by the Voith-Schneider propeller in 1980. This paper presents field test data compared to actuator cylinder predictions for a 9m^2 swept area VAWT. The pitch regime was a simple sinusoidal function of θ and was selected as a means to validate the novel actuator cylinder model, as opposed to emerging from an optimisation procedure. This turbine was tested in the field which avoids the ducting effect of a wind tunnel and a C_{Pmax} of only 0.25 was attained.

In 1986, Vanderberghe and Dick published aerodynamic estimations and test results for a small scale constant speed variable pitch VAWT with 1m diameter [25]. Due to observations that the flow characteristics of a VAWT are significantly different between the up and downstream portions of the path of rotation, this turbine had the ability to implement cyclic pitch regimes that, while still sinusoidal in nature, could differ significantly up and downstream. Their work on optimal pitch regimes is reviewed in the following section. As with Madsen's Voith-Schneider turbine the sophisticated pitch regimes were not able to achieve the theoretical high aerodynamic efficiency attributed to variable pitch VAWTs and the tests

demonstrated a C_{Pmax} of only 0.12. One reason for this is the high solidity (Nc/R) of 0.6. In the following year the same authors completed a similar pitch optimisation for a VAWT with a lower solidity of 0.3 and achieved a C_{Pmax} of 0.25 [60].

More recently in 2004, a constant speed variable pitch VAWT was designed by Cooper and Kennedy [74], which operates at an extremely low λ of less than 1. Pitching of up to 180^o permits successful self-starting because it acts partially as a drag device, which explains the low operating λ. Test result show a great degree of spread in performance with some reasonable C_P, but the average is below 0.1. Also Hwang et. al. designed a 3 kW constant speed variable pitch straight blade VAWT in 2005 [75]. The focus of the work was to develop a control system that implements a simple pitching regime. The design involves a point of eccentricity that can be moved, which pitches all of the blades at once. This work was followed by an extension that enabled individual control of each blade [76]. In both of these studies there is a lack of test results and no analysis of the effect of λ on choice of $\beta(\theta)$ or any consideration of other control objectives.

As has been mentioned, variable pitch blades revolving around a vertical axis has been adapted to harness energy in water current flows [41-44]. One particular design stands out because it claims to have achieved outstanding hydrodynamic performance. Finn Kaare of Water Power Industries (WPI) generated experimental results demonstrating C_{Pmax} of 0.49 [41]. This is in line with state of the art HAWT performance and theoretical performance as predicted by vorticity and BEM models of vertical axis turbines with the ability to pitch (see section 2.4.5). Each blade has individual control of the pitch angle and the controller constantly updates β based on measurements of the conditions. With this functionality it is claimed that

they achieved the excellent C_{Pmax} in an open water test, however, closer inspection reveals that the turbine was in the mouth of a river lock which would confine flow expansion and artificially increase C_P to a value that could not be achieved in a tidal stream.

There have been various attempts to commercialise active pitch VAWTs, but to date none have achieved the predicted aerodynamic performance and ultimately all have failed. One common feature of previous work is constant speed operation of the turbine, but a VAWT would benefit from variable speed operation to improve performance below rated by maintianing optimal ω as wind speed varies [77]. Variable pitch VAWTs require struts, hinges and attachments points that all add parasitic drag to the rotor. This is the perhaps the major reason that variable pitch is too cumbersome for small scale VAWTs. However, within the design space of offshore wind energy systems, the turbines involved are much larger than those discussed in this section, which failed to demonstrate a benefit of active pitching. At the large utility scale, pitch actuators could be used eliminating a lot of the sources of parasitic drag. The demonstrations reviewed in this section also reinforce the argument that the value of variable pitch for VAWTs is not only the improvement in aerodynamic performance, but the ability to provide control in above rated conditions.

2.4.5 Optimal Pitch Studies Review

In addition to demonstrator projects, there have been some theoretical studies published which focus on how to optimise $\beta(\theta)$.

The early Giromill and Cycloturbine configurations had simple optimisation procedures because the turbines were only capable of pitch regimes with one sinusoidal term known as first-order sinusoidal pitch

regimes, thus an optimisation consisted of running the turbine for a range of values for the constant offset and maximum amplitude of the sinusoid as in [22]. It was clear that the flow field differed significantly between the up and downwind pass and when VAWT designs emerged that permitted more sophisticated pitch regimes, more refined optimisations could be considered. Madsen and Lundgren's Voith-Schneider turbine [24] had the ability to implement more sophisticated pitch regimes, but no optimisation of the pitch regime was published, instead a pitch regime was selected as a means of validating their actuator cylinder aerodynamic estimation code.

Vandenberghe and Dick [60] carried out a numerical optimisation for their small scale VAWT which had the capability of pitch regimes of the form (2-6)

$$\beta(\theta) = A_0 + \sum_{n=1}^{3} B_n \cos(n\theta) + \sum_{n=1}^{3} C_n \sin(n\theta) \quad \textbf{(2-6)}$$

The objective of the optimisation was to maximise C_P and simulations of a vorticity based model suggested C_{Pmax} of almost 0.5 could be attained. This promising prediction was not achieved in wind tunnel tests and instead the turbine reached a C_{Pmax} of 0.25 [25]. Very few experimental test results are available in the literature for active variable pitch VAWTs so despite the major discrepancy between prediction and wind tunnel tests, this turbine and the optimal pith regimes that emerged from the optimisation procedure are used for validation of the model developed in Chapter 4 .

A theoretical optimisation of pitch regime was conducted by Zervos et. al. in 1984 [78]. A vortex model was used to determine the local force on the blades while a streamtube model was used to determine performance such as C_P. An optimisation procedure was followed which attempted to maximise tangential force at each azimuthal position. It was revealed that

optimal pitch regimes tend to be asymmetric so a basic sinusoidal variation is suboptimal. While this study revealed the importance of investigating non sinusoidal pitch regimes, the numerical results could be disputed because in operation at λ high enough to avoid dynamic stall, performance improvements are demonstrated both up and down stream. This could stem from the fact that the model used did not capture streamtube expansion. This paper was one of the first to explicitly state that to achieve optimal blade pitch variation, a control mechanism would be required that alters $\beta(\theta)$ to suit λ.

Throughout the 1990s the lack of interest in VAWT was mirrored in the lack of investigations of pitch regimes. There was a steady stream of work from Kirke and Lazauskas [79-82], however, these studies were tailored to the passive pitch concept and were focused entirely on simple sinusoidal regimes.

More active pitch optimisations began to appear over the past decade. In 2002 Kosaku carried out an optimisation of the pitch regime for variable pitch VAWTs by combining momentum theory and calculus of variations [83]. It was demonstrated in this paper that variable pitching can improve self-starting capability and it investigates how the optimal pitch regime should vary with λ. A basic aerodynamic estimation code was used for simulations which modelled the turbine as a single actuator surface inside a single streamtube (see Section 3.4). Consequently high aerodynamic performance with C_{Pmax} of 0.5 was forecast.

In 2003 Staelens et. al. published a paper on the improvement of straight blade VAWT performance in terms of increased power output by varying its pitch [68]. Three different pitch regimes with varying degrees of complexity were simulated in a momentum based model. The first pitch

regime was designed to maintain α just below the static stall angle throughout the rotor cycle and is reproduced in Figure 2-13. The other two pitch regimes incorporated modifications to model realistic limitations on pitch systems. The first modification was a limit on $|\beta|$ and the second modification was a limit on $|d\beta/dt|$ to ensure smooth variations in β. All three regimes demonstrated improvement in power production. However, the objective of maintaining a fixed $|\alpha|$ does not necessarily create the maximum driving torque, instead the torque generated by the rotor should be maximised. The induction at any specific location has an effect on the rest of the rotor energy extraction so a procedure should be designed which considers the impact of upstream pitching on downstream locations. In this exploration, only one λ was considered and there was no analysis of how variable pitch could be used for anything other than improving aerodynamic performance. In addition the simulation tool used was an actuator surface based model called CARDAAV, created by Paraschivoiu [84], which did not account for streamtube expansion. This is a key feature of VAWT aerodynamics that significantly reduces aerodynamic performance and leads to complexity when defining which azimuthal positions are associated with which streamtube. This phenomenon is investigated further in Section 4.4.2 and is particularly important when applying pitch regimes which are defined as a function of azimuthal position.

The most comprehensive optimisation of pitch regime to date was proposed by Paraschivoiu et. al. [85]. A 7kW straight blade VAWT was simulated and an optimisation procedure searched for the pitch regime which maximised aerodynamic performance. The cyclic pitch regime was assumed to be of the form (2-7).

$$\beta(\theta) = x_1 \cos\theta + x_2(\sin\theta)^{x_3} \quad \textbf{(2-7)}$$

A genetic algorithm was employed to determine the best optimisation values x_1, x_2 and x_3 with the objective function of maximising C_P. The CARDAAV model was used to determine the power coefficient with any choice of parameters for the cyclic pitch regime. The optimisation presented in this paper was incomplete for two reasons. Firstly, the CARDAAV did not account for streamtube expansion. The second issue concerns the optimisation procedure. Imposing any particular form of $\beta(\theta)$ such as (2-7) limits the optimisation. Furthermore, the assumed form in (2-7) is not well-defined. The paper does not indicate any restrictions on the optimisation parameters but if x_3 is non-integer then $\beta(\theta)$ will be complex for any θ where $\sin(\theta)$ is negative. Despite this, the result of the optimisation was that $x_3 = 3.009$. Hence, the optimisation reported in [85] cannot be based on (2-7). A refined version is suggested in (2-8).

$$\beta(\theta) = x_1 \cos\theta + x_2 \mathrm{sgn}(\sin\theta)|\sin\theta|^{x_3} \quad \textbf{(2-8)}$$

This form implies the symmetry $\beta(\theta) = -\beta(\theta+\pi)$ which limits the set of pitch regimes that were considered. Consequently the optimisation cannot account for the significant differences in a VAWT flow field between the up and downstream regions.

The pitch regimes and associated C_P-λ curves resulting from the optimisation reported in [85] are reproduced in Figure 2-14. The optimal pitch regime and a sinusoidal pitch regime that was also analysed as part of the study in Figure 2-14 a) confirm that the regimes considered here do have an inherent symmetry. The C_P-λ curves shown in Figure 2-14 b) suggest that the aerodynamic model is over-predicting because C_P is exceeding 0.4 which is optimistic based on most VAWT testing to date. While the optimal pitch has

produced a C_{Pmax} of 0.45 which is in line with modern HAWT performance, the zero pitch simulation also has a very high C_{Pmax} of 0.425 which is unrealistic compared to most published data on fixed pitch VAWTs. While this study did demonstrate potential aerodynamic improvements with VAWT pitching, there is a potential for a more complete investigation of optimal VAWT pitch regimes using a comprehensive aerodynamic model, relaxing the restriction of pitch regimes to any predetermined cyclic forms, and undertaking the optimisation on a streamtube by streamtube basis.

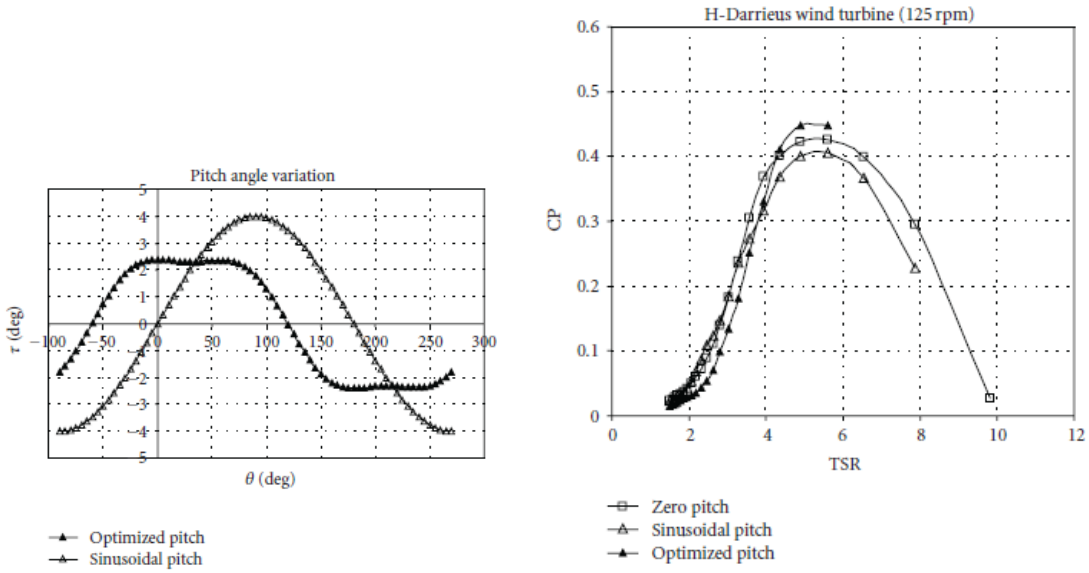

a) Optimised pitch regime and a sinusoidal pitch regime.

b) C_P-λ curves for three different pitch regimes.

Figure 2-14: Output from an optimal pitch investigation for a simulated 7 kW variable pitch straight blade VAWT [85].

Several theoretical investigations into optimal pitch regimes for VAWTs appeared in 2012 [86-89]. All of these papers approach the opportunity of variable pitch from the same position; that it can improve peak power coefficient. The papers lack substantial novel contributions and simply support the argument that variable pitch can improve the aerodynamic performance of VAWTs by avoiding stalled conditions. The

work by Miau to design a variable pitch VAWT [87] contains exceedingly high performance improvements which could be down to simplistic modeling, however, the paper is important because it explicitly states that an important feature would be the ability to vary the pitch regime to suit the range of operating conditions experienced by the rotor. This is an important aspect in the design of a control strategy for a variable pitch VAWT.

The optimal pitch regime investigations reviewed in this section have revealed that there is the potential for a more general investigation. It is clear that a simple sinusoidal pitch variation will be suboptimal and the differences in flow field up and downstream should be accommodated in the optimal pitch regime, therefore assumed forms for $\beta(\theta)$ with inherent symmetries should be avoided. Previous variable pitch investigations made no accommodation for flow expansion which impacts aerodynamic performance and the application *of* $\beta(\theta)$. It has been established that variable pitch can improve start-up capability and improve C_{Pmax}, but it must be demonstrated that VAWTs can be controlled with as much flexibility as their horizontal counterparts. Blade pitching can make this possible but current research remains focussed on the potential of variable pitch to improve aerodynamic performance. While this is important, the current thesis, particularly Chapter 6, adopts a much more holistic approach which addresses how variable pitch should be employed for the entire operating envelope of a VAWT including above rated objectives such as load alleviation, power limitation and overspeed protection.

2.5 Wind Turbine Control

Control is one of the most important drivers in the development of wind turbines. Originally the control system was intended to protect the turbine,

but the introduction of pitch regulation for HAWTs significantly improved the aerodynamic performance and power quality while at the same time protecting the turbine in high winds. It is important to understand how control has been employed for HAWTs in order to anticipate the major challenges in applying pitch control to VAWTs.

This section begins by stating the objectives of a state of the art wind turbine control system. Following this, the way in which a wind turbine control system is designed is explored in Section 2.5.2. Variable speed control below rated is described in Section 2.5.3. Fixed pitch VAWTs achieve above rated control by designing the rotor to operate in stall and Section 2.5.4 reviews this form of control. Section 2.5.5 then addresses how the entire operating strategy can be improved when pitch control is possible. Finally section 2.5.6 reviews previous work on control of VAWTs.

2.5.1 Objectives of a Wind Turbine Control System

The controller in a wind turbine is responsible for modifying the objectives of the wind turbine in response to changes in the environmental conditions in order to meet a range of objectives. The role of the controller is to ensure the wind turbine operating conditions, such as ω in a variable speed machine, remain sufficiently close to their design operating points while the wind fluctuates.

The ideal power curve for a wind turbine is shown in Figure 2-15. In very low wind speeds, the turbine does not operate because there is insufficient power in the wind in comparison to the drive-train losses. At the cut-in wind speed the turbine begins generating power. As the wind speed increases, the power generated grows in proportion to the cube of the wind speed when the turbine operates at C_{Pmax}. Eventually a rated wind speed is

reached which is the wind speed at which the turbine can achieve the full rated power of the drive-train. For higher wind speeds, power has to be shed in order for it to remain within the drive-train limits. For wind speeds exceeding the cut-out wind speed, the turbine must be shut down to avoid extreme loads. A thorough description of this full operating envelope is available in [2].

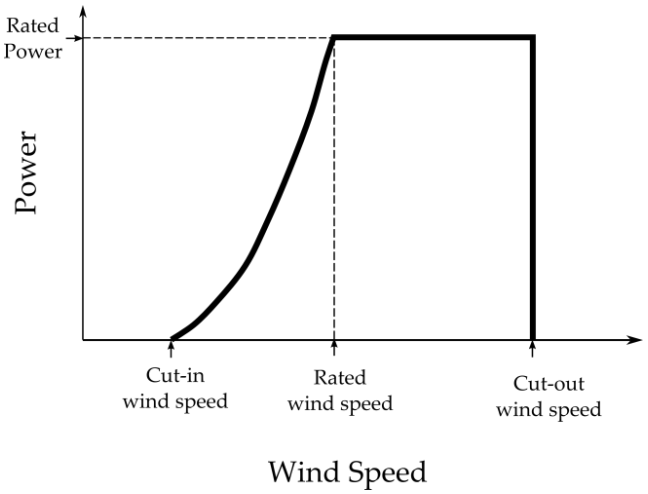

Figure 2-15: An ideal wind turbine power curve.

There is a fundamental difference in the primary objective of the control system between above and below rated conditions. Below rated, the control system must optimise the energy capture whereas in wind speeds above rated the turbine must shed energy. Older wind turbines had stall regulated rotors that enabled power limitation at high wind speeds to be achieved passively, i.e. without a control system. Furthermore, the generator was connected directly to the grid. Consequently, ω was a fixed by the grid frequency. However, as wind turbines have grown more sophisticated, the objectives of their controllers have become steadily more comprehensive [90]. Today most multi-megawatt wind turbines have the ability to continuously vary operating points of the rotor. The controlled actions are generator

reaction torque to vary ω and blade pitch angle; i.e. pitching the blades along the longitudinal axis, to alter the aerodynamic efficiency of the rotor. The objectives of the control system in these variable speed, pitch regulated wind turbines are [91]:

- Optimisation of energy capture
- Alleviation of loads throughout the wind turbine
- Power limitation in high wind speeds

2.5.2 Control System Design

Appropriate design of a wind turbine control system consists of both the synthesis of wind controller laws [92] and the appropriate choice of operating strategy and controller implementation [77]. Wind control laws synthesis methods are concerned with the local behaviour of the system and employ linear models of the plant. The focus in this section in on the choice of operating strategy because it is within the scope of this thesis with regard to VAWT control.

The operating strategy for a wind turbine is defined by a mapping of wind speed to a steady state of the turbine operating point such as aerodynamic torque, rotor speed, pitch angle etc. An ideal power curve is, thereby, also defined. However, the controller itself should not rely on an input of wind speed. The turbine rotor experiences a spatially and temporally distributed wind field and the presence of the turbine itself disturbs the wind field. Hence, any measurement of point wind speed is of limited value. Instead, the point on the operating strategy at which the turbine is operating at any given time must be inferred from measurements on the wind turbine itself such as generated power and ω. The standard

context in which to define an operating strategy is the Q/ω plane [93] as shown in Figure 2-16 for a stall regulated machine.

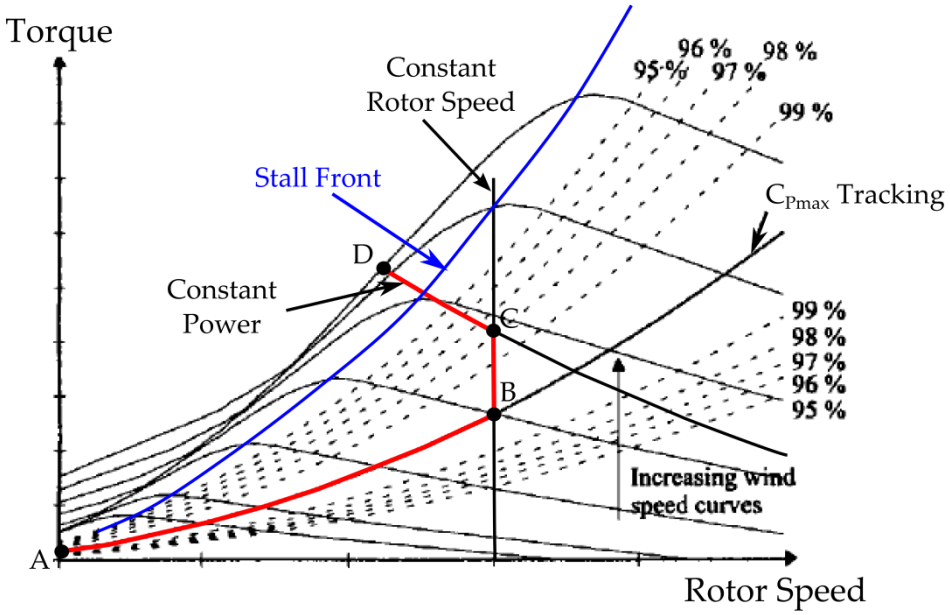

Figure 2-16: The Q/ω plane in which an operating strategy is defined for a stall regulated variable speed wind turbine.

The Q/ω plane is populated by constant wind speed curves; a curved line lying entirely within the section of the plane within which the constant wind speed curves lie, represents a potential operating strategy. The torque referred to here can be either the aerodynamic torque provide by the rotor, Q_A, or the drive train reaction torque, Q_{DT}, since operating strategies can be defined with respect to either or a combination of both. The operating strategy shown in Figure 2-16 consists of the locus of operating points making up the thick line labelled ABCD. The operating state of the turbine does not always perfectly follow the desired operating strategy curve due to variation of wind speed and other factors [93]. The effect of turbulence and changes in mean wind speed and direction is to displace the operational state of the turbine. The controller is required to drive the state of the turbine to track the operating strategy curve as tightly as possible.

The on-design loads for a wind turbine correspond to the loads encountered by the turbine when it operates in steady state on the operational strategy. Since the wind speed continuously changes, the operating point of the wind turbine continuously fluctuates about the operating strategy. The off-design loads correspond to these deviations from the operating strategy. The operating strategy provides an idealized description of how a turbine should behave. It does not, however, provide information regarding the impact of off-design loads on the fatigue life of the turbine or the power train and structural dynamics.

A variable-speed wind turbine operating strategy can be divided into the two fundamentally separate regions with contrasting control objectives:

below rated: refers to all of the operating points for wind speeds lower than rated. This region is indicated as AB and BC in Figure 2-16. AB allows variation of ω when the wind speed change to maintain λ_{opt}. BC holds a constant ω as wind speed increases.

above rated: refers to the operating points for wind speeds above rated. CD is the above rated region in Figure 2-16. The intent here is to reduce ω as wind speed increases to drive the turbine into stall in such a way that the turbine maintains constant power.

It is important to emphasise that Figure 2-16 is one particular choice of operating strategy to suit a variable speed stall regulated turbine. A range of options of operating strategies are available and a full investigation of how to select a strategy based on turbine design and controller objective priority is provided in [77].

2.5.3 Variable Speed Control Below Rated

The primary objective below rated is to maximise energy capture which is achieved by tracking the line on the Q/ω curve which corresponds to maximum aerodynamic efficiency.

A frequently used equation of motion for the wind turbine rotor is (2-9). The net toque on the rotor is the difference in Q_A and the sum of Q_{DT} and viscous damping with coefficient *f*. *J* is the moment of inertia of the rotor.

$$\omega(t) = \frac{1}{J}\int \left(Q_A - (Q_{DT} + f\omega)\right)dt \qquad \textbf{(2-9)}$$

If the turbine is at a steady state operating point on the below rated operating strategy, it is dynamically stable. If ω is displaced from its steady state value its operating point of the turbine system causes ω to return to the original steady state operating point [77]. If the wind speed changes, ω changes according to (2-9) until the turbine reaches a new steady state operating point. Provided the controller adjusts Q_{DT} appropriately, that new operating point will be on the operating strategy curve.

The controller that realises the above adjustment in response to changing wind speed in below rated conditions has the structure in Figure 2-17. It is a single input single output (SISO) feedback system. The control action is generator torque demand, Q_d. The output, y, is the displacement from the operating strategy curve. It is a function of the two measured plant variables ω and Q_{DT}. Its exact form depends on both the precise control objectives and on the current operating point. A range of options for y are provided in [77] for tracking the AB and CD sections in Figure 2-16. When tracking BC, y can be chosen to be simply $\omega - \omega_o$, where ω_o is the rated rotor speed of the turbine. Since the objective of the controller is to reduce the off-

design fluctuations relative to the operating strategy curve, its reference point is set to zero; that is, the control task is disturbance rejection.

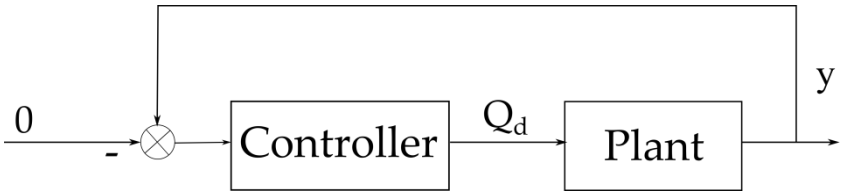

Figure 2-17: SISO feedback control for below rated.

2.5.4 Stall Regulation Above Rated

In above rated operating conditions, stall regulation of variable speed turbines relies on the operating point of the wind turbine being deliberately driven into stall, thus limiting the power generated. There are several options available to drive the turbine towards stall including tracking the constant power curve (as in CD in Figure 2-16), constant ω or constant toque, Q, the merits of which are investigated in [77]. A significant disadvantage is that the dynamics become unstable when in stall because an unstable pole exists. A consequence of the unstable dynamics is that if the rotor speed is displaced from a steady state operating point on the operating strategy curve at a given wind speed, the rotor speed does not return to its original value, and the discrepancy continues to grow. This instability is general to all variable speed turbines in the stall region. Consequently, the wind turbine must be controlled to track the operating curve extremely closely. Furthermore, for many choices of above rated control strategy, its open loop transfer function has a non-minimum phase zero, [92]. This imposes nonlinear dynamic responses of the turbine that must be accounted for by the controller at the expense of controller performance. The crossover frequency of a controller is

the frequency at which the open loop magnitude bode plot crosses 10dB. Crossover frequency indicates the performance of the controller because signals lower than this frequency are amplified while higher frequencies are attained. The aforementioned controller dynamics limit the performance of variable speed stall controlled turbines because the unstable pole imposes a lower bound on the controller frequency while the non-minimum phase zero imposes an upper bound. While the advantage of a stall regulated turbine is its mechanical simplicity, a drawback is that in above rated conditions, the turbine must operate far from the optimal aerodynamic operating point. The structure must withstand regular transient loads incurred when entering and leaving stall.

2.5.5 Pitch Regulation Above Rated

The ability to pitch the blades introduces the option of varying Q_A in (2-9) and, thus, more options in the choice of operating strategy. While pitch regulation has previously been rarely explored for VAWTs, it is important to understand what pitching might provide and how it might impact on turbine design.

With this new degree of freedom, the system is multi-input multi-output (MIMO) as illustrated in Figure 2-18. The plant, P, which models a wind turbine, is fed by two controlled signals: torque Q_d, as before, and pitch angle demand, β_d. These signals are the output of two decoupled controllers. The two plant outputs y_1 and y_2 are again dependent on the choice of operating strategy but, in general, are functions of the three measured plant variables, ω, Q_{DT}, and β. One choice of operating strategy is to maintain constant ω and constant P but other possibilities are discussed in [77].

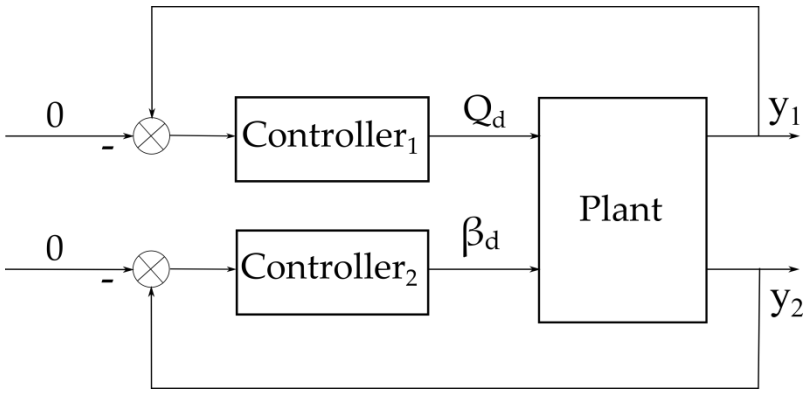

Figure 2-18: MIMO feedback control for above rated.

2.5.6 Control of VAWTS

Early VAWTs were simple constant speed machines such as the Musgrove, cycloturbines and giromills discussed earlier, and the Sandia ϕ-rotors [39]. However, the flexibility of operation and performance improvements provided by variable speed has caused this mode of operation to become industry standard. All of the emerging utility scale designs for offshore VAWTs are variable speed and in this thesis, the VAWTS considered are all variable speed.

With the exception of the Musgrove VAWT450, all previous VAWTs employed stall regulation for power limitation. Full demonstration of stall control for a 225 kW direct driven VAWT is discussed in [94]. It was shown in this paper that the controller can stabilise the nonlinear system using an adaptive current feedback loop. A comparison of five different start-up algorithms was published for the stall regulated Sandia 17m ϕ-rotor assessing the impact on energy production [95]. An investigation of the trade-off between high power generation and effective control for a stall regulated VAWT was provided in [96].

A recurring theme of this thesis is the exploration of whether the performance and flexibility of operation of VAWTs could match that of

HAWTs and whether pitch regulation can assist in meeting that goal. It should be emphasised that VAWT cyclical pitch has been demonstrated in the past as reviewed in Section 2.4. However, pitch regulation for VAWTs is underdeveloped. A goal for VAWT control is that variable pitch should not only increase aerodynamic performance, but also, it should address similar issues to those of pitch regulated HAWT control. Additional complexity for the former is introduced by the need for cyclic pitch as well as non-cyclic pitch in order to address the azimuthal dependence of certain aspects.

2.6 Summary

In this chapter the challenges and opportunities of VAWT design are introduced and a brief history of VAWT development is provided. Despite their inherent poor aerodynamic performance, VAWT technology has structural benefits which make it a potential candidate for robust offshore wind energy systems which has driven a resurgence in interest in the past decade. There is a particular focus throughout this chapter on straight blade VAWTs, variable pitching and wind turbine control.

The V-rotor concept is discussed because it is a configuration suitable for the offshore environment and has straight blades therefore could benefit from variable pitch. There is potential to improve the aerodynamic modelling of this class of turbine.

A review is provided of the previous demonstrations and studies of variable pitch VAWTs. Most previous simulation studies of variable pitch VAWTS have indicated significant improvements in aerodynamic performance but physical demonstrations never achieved the predicted high power coefficients. This may be in part due to the fact that, for the main part, the aerodynamic models employed did not account for streamtube

expansion. Cyclic pitching was only ever experimentally tested with constant speed machines whereas variable speed operation has become industry standard due to the ability to improve performance below rated by operating at the rotor speed that achieves C_{Pmax} as wind speed varies. Previously, variable pitch has only been used for the objectives of improving start-up performance and attaining better aerodynamic performance below rated. There are other VAWT control objectives that could be met by cyclic pitching, including redistribution of loads, power limiting and overspeed protection above rated but they remain to be investigated.

Finally, this chapter introduces some essential elements of wind turbine control. Variable speed operation below rated is described. Stall and pitch control for above rated wind turbine operation are introduced. As discussed, most VAWTs to date are stall controlled.

In the late 20th century, utility scale lift-driven VAWT demonstrations were carried out. However, with the rise of the Danish concept HAWT over the past two decades, interest in large scale VAWTs diminished. Therefore VAWTs have not been developed into a mature technology and in order to explore both V-rotors and the potential improvements of variable pitch, many issues remain to be explored. A major impediment is that no industry standard aeroelastic code is available for general VAWT design studies, so a suitable design tool needs to be developed. In the next chapter the VAWT aerodynamics characteristics that must be captured in a model to accurately represent the aerodynamics are reviewed.

Chapter 3

A Review of VAWT Aerodynamics

3.1 Introduction

The time-varying orientation of a VAWT blade relative to the incoming wind leads to extremely complex aerodynamics. In order to facilitate investigations of how to effectively design and control a VAWT, the aerodynamics must be understood and captured in a suitable model. This chapter presents some key aspects of VAWT aerodynamics and reviews modelling approaches with particular focus on the double multiple streamtube (DMS) method.

This section begins with an investigation of the cyclical nature of the aerodynamics in Section 3.2 to highlight the complexity of what must be captured in an aerodynamic estimation model. Section 3.3 is an examination of the aerodynamic phenomena associated with VAWTs that must be included in any VAWT model. Subsequently, in Section 3.4 the main aerodynamic modelling approaches are introduced. The DMS method is reviewed because this is the core modelling approach underpinning the model developed in this thesis.

3.2 Cyclic Nature of VAWT Aerodynamics

The fundamental shortcoming of VAWT technology is poor aerodynamic performance, which stems from the cyclical nature of $\varphi(t)$ (or $\alpha(t)$ in the case of non-pitched VAWTs).

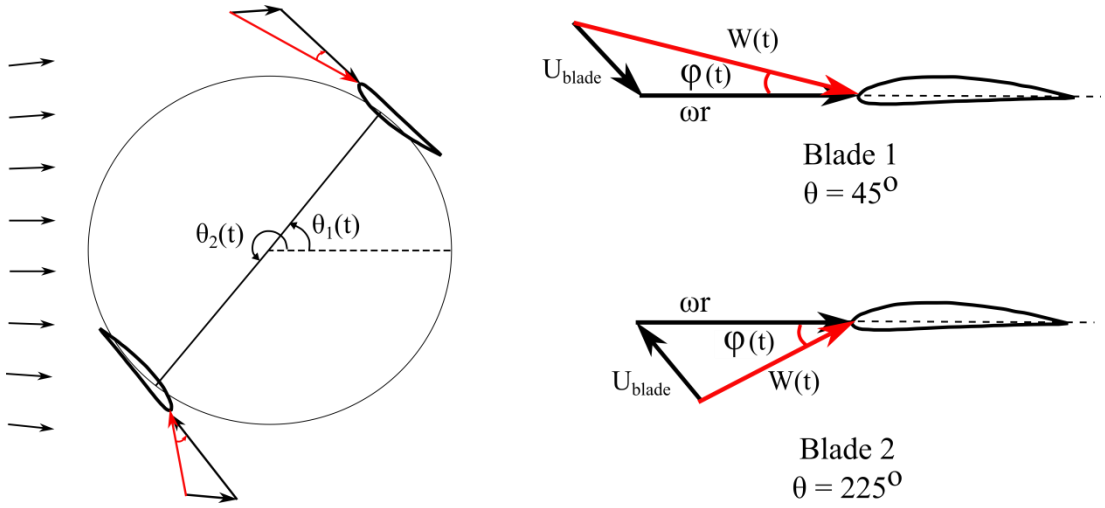

Figure 3-1: Angle of attack at two different locations in the path of rotation of a fixed pitch VAWT.

Net wind speed incident on a VAWT blade, W, consists of two components; wind speed due to rotation of the blade, ωr, which is in the direction of the tangent to rotation; and wind speed from the wind field at the blade, U_{blade}, which varies its orientation relative to the blade as azimuth changes. This is illustrated in Figure 3-1 which shows these components for two different locations around the path of rotation, $\theta = 45^{o}$ and $\theta = 225^{o}$.

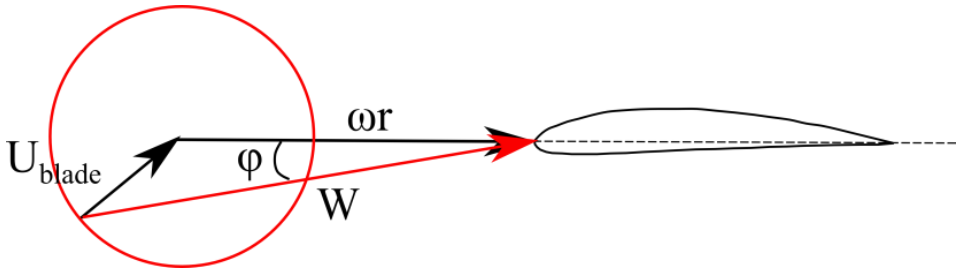

Figure 3-2: Range of flow angles for a VAWT in the aerofoil frame of reference, λ = 3.

Figure 3-2 is an illustration of φ and W at $\theta = 135^o$ when $\beta = 0^o$. This position has a positive φ; however, the circle maps out all the other possible φ and W combinations in the non-physical situation that induction is the same at all azimuthal positions.

In every cycle of the rotor, a VAWT blade will experience both positive and negative φ. This aspect presents challenges for VAWT analysis because anything which improves performance in one half cycle, such as imposing twist or fixed pitch, will be accompanied by negative consequences in the other half cycle.

In every revolution, a VAWT blade will pass through $\varphi = 0^o$ near $\theta = 90^o$ and $\theta = 270^o$. At these two specific locations lift and hence driving torque of a zero-pitch VAWT will go to zero, while at the same time vorticity is shed into the wake.

Figure 3-2 also illustrates why VAWT performance varies with λ. This figure is drawn for $\lambda = 3$. A lower value of λ would lead to a circle with larger radius, implying a larger range of φ. For $\lambda < 1$ the radius of the circle is larger than ωr (when induction is neglected), so $|\varphi|$ would exceed 90^o at certain θ which causes very deep stall for most aerofoils. Alternatively for high λ, the circle becomes very small as W is dominated by ωr. Therefore, the range of φ experienced by the blades and the lift generated are very low. Even when operating at a design λ with a reasonable range of φ, the cyclic nature of $\varphi(t)$ prevents sustaining optimal lift to drag ratio.

The time varying nature of $\varphi(t)$ for zero pitch VAWTs dictates the physics of the energy extraction. A VAWT wake is composed mainly of shed vorticity which is a consequence of the variation of the blade's bound circulation as $\varphi(t)$ varies. This differs fundamentally from the wake of a HAWT which is dominated by trailing vorticity due to the finite span of the

blade. A good examination of the structure of a VAWT wake is reported in [97]. In this thesis, Ferreira demonstrated that it is the time derivative of the bound vorticity that influences the exchange of energy of the VAWT, while the absolute value of the bound vorticity dictates the blade loading. Understanding the vorticity structure is necessary for a true understanding of how the VAWT wake behaves, however, more simple approaches are available for capturing the general performance of a VAWT as will be discussed in Section 3.4.

Blade pitching can benefit VAWT technology because it provides a facility to mitigate the adverse impacts of the cyclic nature of VAWT aerodynamics. In below rated conditions the primary control objective is to maximise the aerodynamic torque provided by the rotor. Aerofoil theory states that there is a specific α which optimises lift to drag ratio in order to maximise the driving torque [6]. Variable pitch makes it possible for a VAWT to approach this optimal by sustaining good lift to drag ratios for large portions of the rotor cycle, but there will always be the flipping regions where very little energy can be converted. In above rated conditions, the primary control objective is to protect the turbine. In Chapter 6 it is shown that the cyclic nature of the aerodynamics can be manipulated to alleviate cyclic loading and shed excess power.

3.3 Aerodynamic Phenomena Associated with VAWTs

In this section, the significant aerodynamic phenomena associated with VAWTs are introduced. The section begins with an introduction to induction factors to provide a context in which to frame the complex aerodynamic phenomena.

3.3.1 Induction Factor

An induction factor expresses the fractional decrease in wind speed between the free stream wind speed and some energy extracting device such as a wind turbine rotor. The induction factor, a, quantifies how much a body slows the wind. Therefore the speed of the wind field local to a rotor blade, U_{blade}, can be expressed as a function of the induction factor.

$$U_{blade} = U_{inf}(1 - a) \quad \textbf{(3-1)}$$

Induction factor is commonly referred to as the axial induction factor because in the context of simple steady state HAWT analysis, the free stream wind speed is assumed to be aligned with the axis of rotation of the rotor. With VAWTs the free stream is orthogonal to the axis of rotation of the rotor.

3.3.2 Tip Loss

Similar to HAWT blades, vortices are shed off the end of VAWT blades. This leads to much lower aerodynamic efficiency at the tip of the blades and the effect is known as tip loss. The original work on tip loss was reported by Goldstein but he did not give a closed form solution for the tip loss effects [98]. In 1957 Prandtl simplified this work [99] in a theory which only applies to lightly loaded turbines as it assumes that the wake does not expand.

Prandtl represented the helical vortex structure in the far wake as solid disks with specific spacing, d, which move at the speed of the wake. To account for the effect of tip loss within an actuator surface based model for a HAWT, Prandtl proposed that the induction factor becomes af, where $f \in [0,1]$ is the tip loss factor given in (3-2), a decreasing function of blade span that reaches 0 at the tip of the blade.

$$f = \frac{2}{\pi} arcos(\exp(-\pi \frac{s}{d})) \quad \textbf{(3-2)}$$

s is the length from the hub to the blade segment and the distance d for HAWTs is given by

$$d = \frac{2\pi R}{B} sin\eta = 2\pi(1-a)\frac{RU_{inf}}{BW} \quad \textbf{(3-3)}$$

η is the angle at which the wake protrudes from the rotor plane. The major difference for VAWTs is that the streamwise pitch of the vorticity sheets shed is not uniform thus an average must be taken. Sharpe provides an expression in [29] that incorporates d for H-rotor VAWTs

$$\pi\frac{s}{d} = \frac{U_{inf}}{U_w} B \frac{s}{R} \quad \textbf{(3-4)}$$

In this case s is the distance from the blade tip. Substituting (3-4) into (3-2) provides an expression for f for VAWTs.

$$f = \frac{2}{\pi} arcos(\exp(-\frac{U_{inf}}{U_w} B \frac{s}{R})) \quad \textbf{(3-5)}$$

3.3.3 Flow Curvature

The aerodynamic characteristics of an aerofoil differ for curvilinear and rectilinear flow [100]. The effect is to introduce a virtual camber and a virtual angle of attack and it can be accurately modelled by augmenting the normal force, F_N. Figure 3-3 a) shows a symmetrical aerofoil moving in a curved path. It has the same aerodynamic characteristics as the cambered aerofoil in Figure 3-3 b) which is moving in a rectilinear flow field with a virtual angle of incidence.

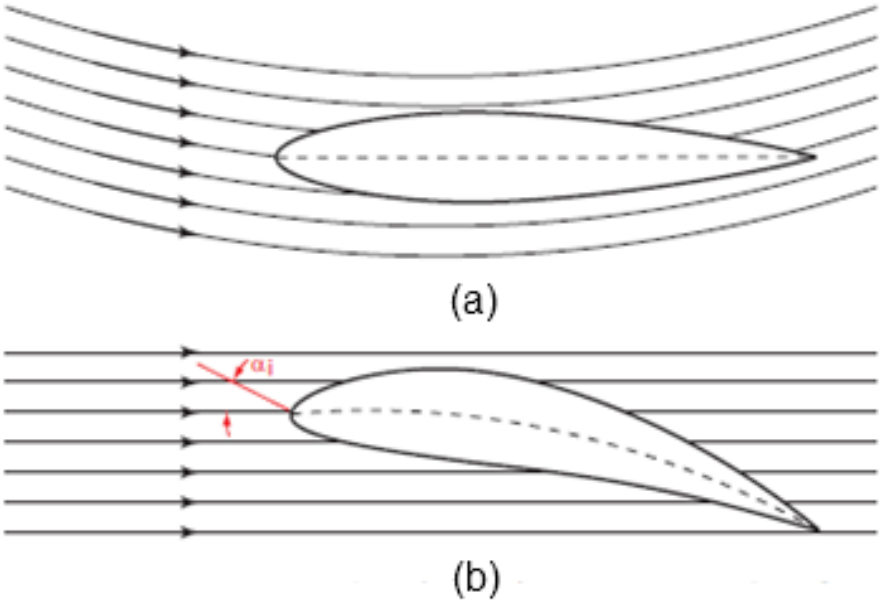

Figure 3-3: Virtual camber and virtual angle of attack as a result of curvilinear flow.

This virtual camber causes an upward shift of the lift curve and introduces an aerodynamic moment [29]. The effect depends on the ratio of blade chord to turbine radius. If the ratio is larger, then flow curvature has a greater effect. Therefore on a V-rotor with non-tapered blades, it will have larger impact closer to the base.

The original approach to capturing this effect was to model the virtual camber [100] and further modification of this work introduced an adjustment to α [101, 102]. The real impact of flow curvature is a contribution to bound circulation and this was originally explored by Strickland in an investigation of the circulatory and non-circulatory effects of the aerodynamics of a flat plate in an unsteady motion [103]. Recently, by considering the effects of augmenting bound circulation, Ferreira provided thorough insights into how flow curvature affects the aerofoil and the rotor flow field [97]. He concluded that the constant change in bound circulation will not have an effect on energy extraction, but does affect the pressure distribution on the aerofoil.

The modelling approach adopted for this thesis is limited by the approximations of actuator surface theory. Therefore, the amendment to bound circulation must be captured in some approximate way. A basic approximation, that was proposed by Sharpe [104], is to model the effects of flow curvature as a contribution to the normal force of an aerofoil acting towards the centre of rotation. Therefore the normal force is increased in the upstream pass and decreased in the downstream pass. Sharpe's analysis in [29] provides the expression in (3-6) for the contribution to normal force coefficient from flow curvature, C_{N_fc}, where c is chord length and r is local VAWT radius.

$$C_{N\_fc} = 0.25\left(\frac{\mathrm{dC_L}}{\mathrm{d\alpha}}\right)\frac{\mathrm{c}}{\mathrm{r}}\left(\frac{\omega \mathrm{r}}{\mathrm{W}}\right) \quad \textbf{(3-6)}$$

3.3.4 Flow Expansion

Flow expansion is the tendency for the flow to expand in the plane of rotation as it passes through the rotor. The velocity of the wind slows as it approaches and passes a rotor and the mass flow rate must remain constant, therefore when modelling the airflow as a collection of aerodynamically independent streamtubes (see Section 3.4.1) the cross sectional area upstream must be larger than the cross sectional area downstream. This phenomenon is directly related to the degree of slowing of the free stream wind speed so can be classified in terms of induction. In [105], Read and Sharpe proposed a method of capturing flow expansion in a VAWT momentum model based on the induction factors by imposing the condition that boundaries of the streamtubes are straight. Flow expansion is an important feature for the current work not only for improved aerodynamic estimation of VAWTs but also because flow expansion alters the azimuthal positions that are spanned by each streamtube. Therefore in order to select the correct pitch value from

β(θ) for a particular streamtube or alternatively to understand which portion of the rotor cycle is being represented by a streamtube, flow expansion must be considered. Sharpe provided full details of his straight streamtube flow expansion model in [33] and this approach is fully developed in Section 4.4.1.

3.3.5 Dynamic Stall

Dynamic stall is a complex unsteady aerodynamic phenomenon that can occur when the angle of attack of the wind speed incident on an aerofoil changes rapidly. The rate of change of α as the blade passes the static stall angle, α_{ss}, has an influence on the manner in which the boundary layer separates or re-attaches. With continuously varying inflow conditions, it is important that dynamic stall is effectively modelled to capture the aerodynamic performance of VAWTs, particularly for low λ.

3.3.5.1 The Dynamic Stall Phenomenon

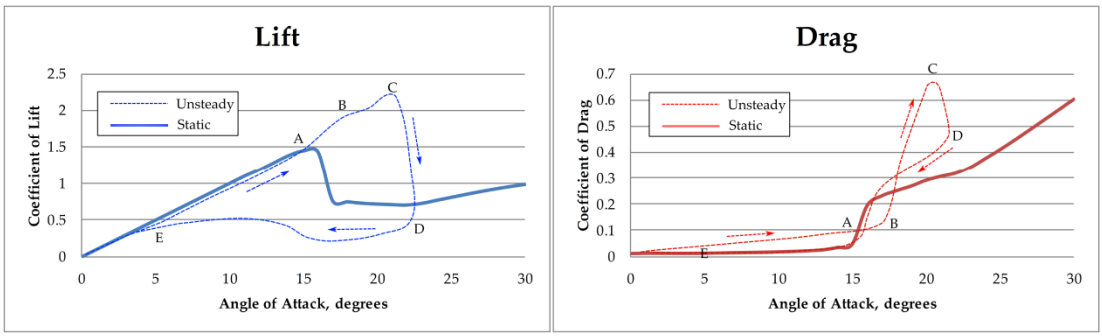

Figure 3-4: Schematic illustration of unsteady and static aerodynamic loading [106]

The characteristic feature of dynamic stall that distinguishes it from static stall is the shedding of a vortex structure at the leading edge [107]. Leishman [106] identifies five stages of the dynamic stall process, which are explained here with reference to Figure 3-4:

Stage 1 – Initial increase past α_{ss} (A): Flow reversal takes place inside the boundary layer but separation has not begun yet. Consequently unsteady lift and drag exceed corresponding static values.

Stage 2 – Formation of vortex at the leading edge (B): The main impact on the aerodynamic forces is a significant increase in drag while lift remains high.

Stage 3 – Vortex convection (B to C): The disturbance convects along the low pressure surface of the blade as α increases generating additional lift and drag.

Stage 4 – Vortex shedding (C to D): When the vortex reaches the trailing edge it is shed into the wake and the low pressure surface becomes fully separated. Lift drops sharply to a value lower than the corresponding static lift. Drag also drops but remains above the static value.

Stage 5 – Reattachment (E): When α is low enough, flow reattaches from front to back. Drag matches the static performance for most $\alpha < \alpha_{ss}$, but lift remains significantly lower than the static lift forces until reattachment takes place.

3.3.5.2 Dynamic Stall Models

Due to the non-linear physics of dynamic stall and the wide range of parameters influencing the impact of such unsteady behaviour, the only way to capture the full detail of dynamic stall is with numerical solutions to the Navier-Stokes equations. These require prohibitively expensive computational effort and have been used in the past to reveal the physics of dynamic stall rather than to model the effects within a design tool. A general review of these numerical approaches is provided in [30].

A wide selection of 'semi-empirical' dynamic stall models exists that aim to model, with various levels of detail, the impacts of dynamic stall. They can be separated into the following three categories underlying in increasing order of complexity:

1. Redefining angle of attack – This approach was initially developed by Gormont [108] for helicopter performance prediction. It is also known as the Boeing-Vertol model. A dynamic angle of attack is defined which is a combination of a so-called 'gamma function', obtained empirically from experimental tests, and the rate of change of α. This dynamic angle of attack is used to look up the static coefficient curves and amplify the static coefficient values. Therefore the delay in onset of stall is captured and the delay increases with increasing pitch rate. Also, dynamic aerodynamic forces demonstrate the characteristic hysteresis loops. With very little computational effort or empirical aerofoil data, this method captures the main impacts of dynamic stall on aerodynamic performance, but lacks physical basis.

2. Modelling of the aerodynamic curves – Tran and Petot developed the ONERA model [109]. This approach describes the aerodynamic force coefficient curves using first-order differential equations for low α and second-order differential equations for higher α where stall would occur. As with the Gormont model, there are no physical mechanisms dictating the differential equations, instead a prohibitively large number of empirical parameters must be calibrated. Comparisons with measurements revealed that this mathematical approach did capture the general features of dynamic stall including lift overshoot and hysteresis effects, but they were not quantitatively accurate [110].

3. Modelling the underlying physical features of dynamic stall – One of the early attempts to model the underlying physics of dynamic stall is the Beddoes Time Delay model [111]. The model uses two non-dimensional time delays. The first represents the time delay between the static stall being exceeded and the initial separation occurring (A to B in Figure 3-4). The

second represents the time taken for the vortex shedding stage to occur (C to D). The time delays are obtained from statistical analysis of a wide range of aerofoils so this is a robust approach for predicting dynamic stall. A far more comprehensive model is the Leishman-Beddoes model [112] which has a modular form with separate subsystems designed to deal with each stage outlined in Figure 3-4. This approach is capable of predicting unsteady lift, pitching moment and drag characteristics. The emphasis in this model was to provide a more complete physical representation of the overall unsteady aerodynamic problem of dynamic stall while minimising the calibration effort required by employing a low number of empirical coefficients. The original model required four empirical coefficients, which is relatively low compared to previous models. A range of dynamic stall models derived from the Leishman-Beddoes approach have been developed including the Oye model [113] and the Riso model [114]. A general review is provided in [106]. While these Beddoes-Leishman derived models capture some nature of dynamic stall, the additional detail revealed regarding the wake and the nonlinear response of the lift and drag characteristics are not necessary for the aims of this research which are to explore the design space of VAWTs and generate approximations of rotor aerodynamics to feed controller design studies.

3.3.5.3 Gormont Model Applied to VAWTs

The equations involved in Gormont's model are provided here as adapted by Strickland [103] to suit VAWT dynamics.

These equations are applied when $\alpha > \alpha_{ss}$. The dynamic angle of attack, α_{dyn}, is given by

$$\alpha_{dyn} = \alpha - \tau\left(\left|\frac{c\dot{\alpha}}{2W}\right|\right)^{0.5} \quad \textbf{(3-7)}$$

for $\dot{\alpha} > 0$, and

$$\alpha_{dyn} = \alpha + \frac{\tau}{2}\left(\left|\frac{c\dot{\alpha}}{2W}\right|\right)^{0.5} \quad \textbf{(3-8)}$$

for $\dot{\alpha} < 0$. τ refers to an empirical function of local Mach number and blade thickness, t/c, where t is aerofoil thickness and c is chord length. For $t/c > 0.1$ and low Mach number, the values of τ_L and τ_D associated with lift and drag in stall respectively are

$$\tau_L = 1.4 - 6\left(0.06 - \frac{t}{c}\right) \quad \textbf{(3-9)}$$

$$\tau_D = 1 - 2.5\left(0.06 - \frac{t}{c}\right) \quad \textbf{(3-10)}$$

The dynamic coefficients of lift and drag are given by using the value of the static lift and drag curves that are associated with α_{dyn}

$$C_L = C_{L\_static}[\alpha_{dyn}] \cdot \left(\frac{\alpha}{\alpha_{dyn} - \alpha_0}\right) \quad \textbf{(3-11)}$$

$$C_D = C_{D\_static}[\alpha_{dyn}] \quad \textbf{(3-12)}$$

α_0 refers to the effective blade angle of attack for zero lift. One drawback of this model of dynamic stall is that the drag characteristics are not amplified so dynamic drag coefficients are underestimated. Consider again Figure 3-4 that was generated using the Beddoes Lieshman approach [106]. The sharp increase in drag due to dynamic stall in portion BC of Figure 3-4 b) cannot be accurately captured with Gormont's model.

Motivated by observations that high-level turbulence acts to inhibit the effects of dynamic stall on a VAWT, Paraschivoiu suggested that in BEM models, a dynamic stall model should be switched off for the portion of rotation $195^o < \theta < 315^o$ [30].

As mentioned earlier, the original Gormont model was developed for helicopter rotors which experience a significantly lower range of α than

VAWTs. Masse claimed that using Gormont's model for VAWTs could lead to an over-prediction of the effects of dynamic stall. In [115] he proposed an adaptation of the Gormont model whereby the dynamic aerodynamic force coefficients are modified by linearly interpolating between the static coefficients and the dynamic coefficients predicted by the Gormont model. Berg [116] used the same adaptation with a different empirical constant to demonstrate satisfactory prediction of the experimental performance of the Sandia 17m ϕ-rotor VAWT.

In this thesis, the Gormont model with Strickland's adaptation is employed to describe the dynamic stall of VAWTs because its form is well suited to the BEM approach and it has been demonstrated to be reasonably accurate [30, 117]. The analysis in this thesis is intended as an exploration for control studies rather than a comprehensive design study for one particular VAWT configuration, therefore a basic Gormont dynamic stall model which captures the main elements of dynamic stall is adequate and the modifications of Paraschivoiu and Masse are neglected.

3.4 Aerodynamic Modelling of VAWTs

There are three main approaches to model aerodynamic performance of a wind turbine:

Computational fluid dynamics (CFD) techniques – CFD methods attempt to solve the Navier-Stokes equations describing fluid interaction with a wind turbine. As with simulation of any complex fluid phenomena, the CFD approach provides detailed simulation of the physics involved, however, this comes at the cost of requiring substantial computing power. The unsteady aerodynamics associated with wind turbines including flow separation during stall and preserved concentrated vorticity structures in the wake

reserves CFD modelling of wind turbines for the future as computing power continues to accelerate.

Wake modelling – By modelling the wake trailed from a turbine, the wind field local to the blades can be induced. This can be coupled with blade element theory to calculate the aerodynamic forces and turbine performance. The wake can be modelled by employing dynamic inflow models or vortex wake models. Dynamic inflow modelling [118] is based on the capturing the aerodynamic lag imposed by vortical structures without establishing their strength in terms of circulation. Essentially the method involves solving a differential equation that relates the inflow to the blade location and pitch value. Vortex wake modelling is a more physical treatment of the turbine wake which represents the strength and spatial location of the vortical elements that are trailed by each blade and convected into the downstream wake, then employs the Biot-Savart law to determine the induced velocity field. Vortex methods have been developed to suit various fluid flow challenges and the first application of vortex methods for VAWTs was reported by Larsen [119]. The initial analysis was for 2D flow and extensions followed for 3D flow [120] and wake expansion [121]. Owing to the proven success of wake models, they are used for full design of wind turbines, however as with CFD approaches they remain computationally demanding.

Momentum based models – An estimate of the local wind field at the blades in terms of an induction factor is generated by balancing the rate of change in momentum of the overall wind flow with the local aerodynamic forces produced by the blades on the air. The most commonly used momentum model in VAWT analysis is the double multiple streamtube (DMS) approach, which models a VAWT rotor as a set of two tandem actuator surfaces. This method is reviewed in the following section. Another approach is the

actuator cylinder model [122] which maintains the cylindrical form swept out by a blade segment. Momentum modelling is much simpler than CFD and wake modelling methods. However it can provide reasonable estimations of turbine loads and performance.

In this thesis, a model is required that is reasonably accurate, with the main purpose of carrying out general rotor design analysis and control studies, which do not require all the information provided by CFD and vortex models. Therefore the DMS momentum approach is selected. Although it is a well-established method, contributions are required to capture V-rotor loading and implement blade pitching.

3.4.1 The Double Multiple Streamtube Method

The form of aerodynamic estimation model that is utilised for this thesis is based on momentum principles coupled with blade element theory. The method which combines these techniques is known as blade element – momentum theory (BEM). It was first used to analyse propellers by Glauert in 1959 [123]. BEM analysis is now a powerful tool for aerodynamic estimation of HAWTs [2] and it can be used to determine the aerodynamic forces on the blades and hence, the torque and power generated. The rotor is modelled as an actuator surface which absorbs energy from the wind and for an accurate BEM analysis a reliable estimate of how much the turbine slows the wind speed is required. The reduced wind speed in the windward direction local to the actuator surface, U_{blade}, is given by

$$U_{blade} = U_{inf}(1 - a) \quad \textbf{(3-13)}$$

where U_{inf} is the unaffected free stream wind velocity and $a \in [-1,1]$ is the induction factor. a is determined by equating the stream wise aerodynamic

forces on the blades with the rate of change of momentum of air. A value of $a < 0$ would imply that the rotor causes the wind to speed up.

The idea underlying any momentum balance modelling approach such as BEM is that the rotor is modelled as a porous actuator disk which extracts energy from the airflow. This terminology was developed for HAWTs with blades that sweep out disks. For VAWTs, the swept area depends on the rotor type. An H-rotor sweeps out a rectangle while a V-rotor sweeps out a trapezium. Therefore, in this thesis, the rotor is said to be modelled as a collection of actuator surfaces, with each one modelling the energy extraction for a portion of the swept area.

Double multiple streamtube (DMS) modelling is an extension of BEM that is suitable for VAWTs. The swept area of a VAWT is approximated as one collection of actuator surfaces upstream and another collection of actuator surfaces downstream and BEM principles are applied at each actuator surface. The two key components of DMS are multiple streamtubes and two tandem actuator surfaces for each streamtube. Imposing independent streamtubes permits variation in the induction factor with θ, which captures the cyclical nature of the aerodynamics. The representation of a VAWT rotor as upwind and downwind actuator surfaces is intuitively accurate because the airflow along any windward streamline is intercepted by a blade twice. Hence, the first actuator surface models energy extracted from the airflow upstream and the second actuator surface models the energy extracted downstream.

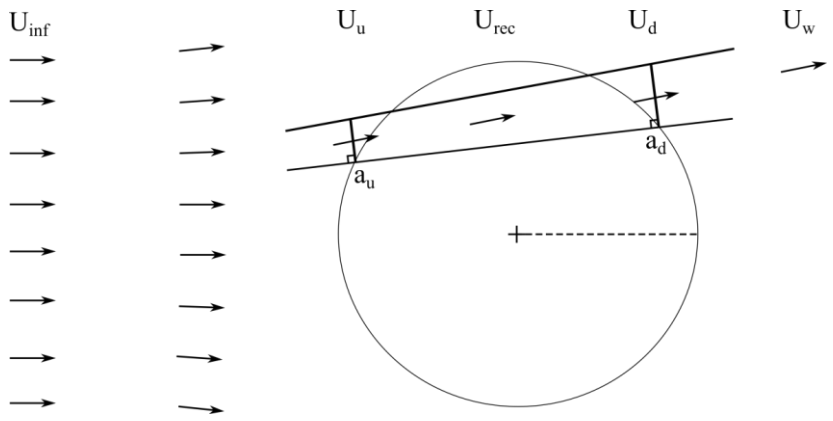

Figure 3-5: Velocity in free stream, upstream, pressure recovery equilibrium, downstream and wake positions.

One assumption that must be made to allow the use of straight streamtubes while capturing streamtube expansion is that the direction of the incoming wind field must be allowed to diverge to account for the flow expansion. Therfore, it is not precisely the undisturbed wind field U_{inf} that is used for the calculations to determine flow characteristics upstream. It is assumed that this deformation of the wind field does not affect the magnitude of U_{inf}. Figure 3-5 is a diagram showing how U_{inf} is allowed to deform before any induction calculations.

For each streamtube, a downstream actuator surface is located in the wake of an upstream actuator surface. The wind speed at the upstream surface, U_u, is the deformed version of U_{inf} reduced by the upstream induction factor, a_u.

$$U_u = U_{inf}(1 - a_u) \tag{3-14}$$

Implicit to the DMS method of analysis is the assumption that there is sufficient slowing of the wind between actuator surfaces for pressure to recover to the ambient value between the surfaces as shown in Figure 3-5. Standard momentum theory demonstrates that this recovered wind speed, U_{rec}, is a function of the upstream induction factor, a_u [124]

$$U_{rec} = U_{inf}(1 - 2a_u) \quad \textbf{(3-15)}$$

Therefore, a scheme which determines a_u can be used to calculate the U_{rec} where the pressure has recovered. The pressure recovery assumption allows U_{rec} to be used as the input wind speed for a scheme to determine downwind induction factor, a_d, which is used to determine the wind speed at the downwind actuator surface U_d

$$U_d = U_{rec}(1 - a_d) \quad \textbf{(3-16)}$$

The ordered nature of the calculation of tandem induction factors, and hence energy extraction for each streamtube, is one of the benefits of the DMS method. It captures the fact that blades downwind are operating in the wake of upwind energy extraction.

Once the local wind field is known for all blade locations, the aerodynamic forces and ultimately the contributions to moments such as torque and bending moments can be calculated.

3.4.2 Review of the DMS Method

The development of the DMS method from basic BEM principles evolved over a ten year period between the 1970s and 1980s. During this period, key aspects of VAWT aerodynamics were identified and formulated in an actuator surface framework.

BEM was first applied to VAWT analysis in 1974 by Templin in his single streamtube model [125]. The blades were divided into sections and the performance at any 2D horizontal cross section was determined by considering the turbine as one actuator surface. This lacked the ability to capture the azimuthal variation in induction and hence loading. A natural development of this was the multiple streamtube model, which separates the swept volume into a series of adjacent and aerodynamically independent

streamtubes. This was first proposed for VAWTs in a paper on aerodynamics of general wind turbines by Wilson and Lissaman [49] while Strickland published the first paper devoted exclusively to multiple streamtube analysis of a Darrieus rotor [126]. The latter proved to be a substantial improvement on single streamtube analysis. It more precisely estimates distributed effects such as blade forces and rotor wake velocity distributions, and it is adaptable to inclusion of spatial variations. However, in general these multiple streamtube models overestimated performance and downwind blade loading. Enhancement has been made to include effects of aerofoil geometry such as support struts and blade aspect ratio [127] and the effects of Reynolds number [128].

A development of the single surface model was made by Lapin in 1975 who modelled the VAWT rotor as two actuator surfaces in tandem [129]. The first surface models energy extracted from the airflow upstream and the second surface models the energy extracted during the downstream pass. This was complimented by Holme [57], in which a vortex model was employed to demonstrate that half of the velocity decrease occurred within a VAWT rotor.

Read and Sharpe [105] published the first DMS model which combined the multiple streamtube approach with the tandem actuator surface idea for each streamtube. Therefore the model accounted for both the variation of induced velocity in the cross-streamwise direction as well as the streamwise direction. This model also made provisions to account for flow expansion. The approach involved streamtubes with straight boundaries that had a smaller cross sectional area upstream compared to downstream. This refinement showed a small improvement in overall performance compared to the previous momentum models for VAWTs, but was capable of much

greater accuracy when predicting the local induced velocity at a blade and hence showed in more detail the variation of the blade forces. Full details of applying streamtube expansion in an actuator surface DMS model are provided in Section 4.4.1.

The tandem actuator approach was also adopted by both Paraschivoiu in a model called CARDAA [130] and Stacey and Musgrove [131]. Both of these models lacked streamtube expansion or multiple streamtubes. A similar tandem actuator approach was adopted by Berg in [116] but this model assumed a predefined variation of a with θ. McCoy and Loth also proposed a double actuator surface model [132] based on a predefined variation of a with θ. McCoy and Loth's theoretical inviscid aerodynamic optimisation concluded that the Betz limit could be breached by modelling a VAWT in this manner, however, the effect of flow curvature and, more importantly, flow expansion were neglected. Newman suggested that the double surface approach implies the theoretical maximum power coefficient for VAWTs is 16/25 [133] and that using increasingly more actuator surfaces permits the power coefficient to approach 8/12 [134]. These demonstrations of exceeding the Betz limit were for idealised situations that lack any account for the tendency of flow expansion. The early double actuator surface momentum models were reasonable for estimating aerodynamic performance of a VAWT for λ ranging from 3.5 to 8. Accurate modelling of aerodynamics at low λ would require a better way to capture the true variation in induced velocity and better understanding of operation in stall.

Paraschivoiu published a full DMS model combining multiple streamtubes and tandem actuator surfaces [84] and this model is called CARDAAV. It captured the influence of secondary effects, which are geometric features such as presence of struts and spoilers, tower and blade

geometry. This model also included a dynamic stall module which improves estimations for low λ. Sharpe refined the DMS method to include flow curvature effects and tip losses [104]. Another improvement to Paraschivoiu's work was to include expansion of the streamtubes in the plane of rotation [135] based on Read and Sharpe's work [105] and this model was called CARDAAX. Paraschivoiu published an overview of momentum based prediction models for VAWTs in 1988 [136]. By 1990 the DMS method with full explanation of streamtube expansion, secondary effects, dynamic stall, flow curvature and tip losses was provided by Sharpe in his contribution to Freris' textbook [29]. A more up to date account of the DMS method with details of the available dynamic stall models was published by Paraschivoiu [30].

Shires has used an actuator surface approach to aid design of a V-rotor [18]. In his paper, Shires demonstrated reasonable matching of DMS aerodynamic estimations with test data from old curved blade VAWT data but it was noted that aerodynamic estimations for the prototype aerogenerator are not accurate. This model does not use multiple streamtubes, and instead a single induction value is used for each half-cycle.

The DMS model developed for this thesis must also permit variable pitch of the blades. Kirke and Lazauskas have implemented variable pitch in a DMS model [80] for passive pitch H-rotors. The model includes flow curvature, streamtube expansion and dynamic stall effects. Their simulations suggest that variable pitch could improve C_{Pmax} from 0.3 to 0.45, but no validation of this DMS model was included in their model. The following year the authors provided test results showing that their passive pitch turbine only achieved a C_{Pmax} of 0.25 [82]. This could be in part due to the difficulty for a passive pitch system to implement the optimal pitch regime

due to the inherent lag between the forces influencing β and the instantaneous value of β.

The combination of V-rotor geometry with variable pitch in an aerodynamic code has not been fully addressed previously. The aerodynamics are complex, in particular, when streamtube expansion is considered, see Section 4.4.2.

3.4.3 Flow State Induction Factor Method

Traditional actuator surface momentum aerodynamic estimation models use an iterative scheme to determine the induction factor, a [124]. In this thesis an alternative approach called the flow state method [28] is used, which was previously developed for use in a VAWT single surface multiple streamtube momentum model. Essentially, windward force due to momentum theory and windward force due to blade element theory are expressed as a function of a and the values of a are determined where the expressions are equal. Multiple crossing points can occur when stall sets in and during flow reattachment. This method is so called because knowledge of the current flow state is used to select the appropriate induction factor in these situations. The design tool in this thesis, which is developed fully in Chapter 4, is the first time the flow state method is adopted for a DMS model. Section 4.5 presents the equations required to implement this method, and demonstrates how the correct induction factor is selected when multiple solutions exist.

3.4.4 Appraisal of Momentum Modelling for VAWTs

Recently momentum based modelling of VAWTs has been subject to severe criticism. This section discusses this criticism and aims to discuss why a DMS approach was selected for this thesis.

In his thesis [97], Ferreira argues that the DMS approach is fundamentally flawed for two main reasons:

1. Streamtube VAWT models incorporate incorrect knowledge of the wake. A DMS model associates blade loading directly with energy conversion. Ferreira argues that blade loading is decoupled from the energy extraction process and at the rotor scale, the wake development expresses the energy exchange process and since the wake develops due to vorticity shed at the periphery portion of the path of rotation, it is only by understanding the release and convection of this shed vorticity that one can gain a better insight into the energy conversion process. Ferreira concludes that a direct consequence of neglecting the shed vorticity at the outer sections of a VAWT path of rotation is that modelling lateral expansion of the wake becomes very difficult.

2. Averaging of forces is non-physical. Ferreira also states that complete interaction of air and blade should be calculated for one instance rather than averaging forces and considering local forces for one small segment of blade. Ferreira sums it up well by stating that DMS leads to high a downstream as a result of analysing induction as a local property and completely independent of the remaining flow. It is true that there is significant difference between a heavily loaded rotor and induction experienced by the blade during the downwind passage.

While these are valid criticisms, engineering models are judged by the purposes to which they are put. The aim of the current thesis is to develop an aerodynamic estimation code as a means of exploring the VAWT design space and the potential of pitch control for VAWTs. The relative simplicity of the DMS approach compared to CFD and vorticity based models is attractive

because the chosen approach has to be adapted to suit both V-rotors and blade pitching.

Although DMS models do not currently capture the genuine source of wake expansion, a suitable approximation of flow expansion is incorporated in the formulation of the DMS geometry by Read and Sharpe [105] which permits expansion based on the assumption of straight streamtubes. This formulation is explained fully in Section 4.4.1.

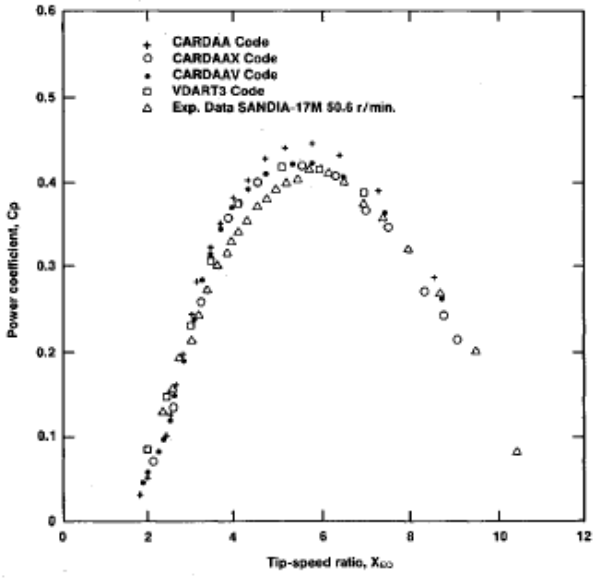

Figure 3-6: Performance comparison between theoretical results and experimental data for the Sandia 17-m turbine [136].

It is apparent from validation of the early DMS models that despite the unrealistic averaging of forces, this approach captures the general performance of VAWTs relatively well. Figure 3-6 is taken from Paraschivoiu's 1988 review paper [136] and it shows how C_P-λ estimations from a range of DMS codes and a vorticity code compare with experimental test data for the Sandia 17m ϕ-rotor. This plot demonstrates that DMS models are effective at predicting aerodynamic performance of VAWTs. The basic 1981 model [130] (CARDAA code) over-predicts the maximum power

coefficient, but improvements for azimuthal variation of a [84] and streamtube expansion [135] (CARDAAV and CARDAAX code respectively) bring predictions in line with experimental data and a more sophisticated vortex code, VDART3 [137].

3.5 Summary

The phenomena which dominate VAWT aerodynamics and how the double multiple streamtube approach has been developed to capture these are reviewed and discussed in this chapter.

Tip loss is the reduction in aerodynamic performance towards the tips of a wind turbine as the consequence of vorticity shed from the tips. Flow curvature captures the augmentation to aerodynamic performance that occurs as a result of a body moving in a curvilinear path as is experienced by a VAWT blade moving around its circular path of rotation. The flow curvature effects increase with solidity and can be modelled approximately as an augmentation to normal force coefficient. Flow expansion is the tendency for the flow to expand in the plane of rotation as it passes through the rotor thus reducing the volume of wind that interacts with the turbine. A formulation by Read and Sharpe can capture the broad effects of flow expansion in an actuator surface framework by assuming the streamtube boundaries are straight. Dynamic stall is a complex unsteady aerodynamic phenomenon that causes the aerodynamic characteristics of an aerofoil to depend on the rate of change of the angle of attack as it passes the static stall angle. In this thesis, Gormont's model with Strickland's adaption is employed which captures the effect of dynamic stall by generating a dynamic stall angle that is used to look up the static lift curve.

The various methods for capturing VAWT aerodynamics in some form of estimation tool are introduced and the method which is selected for this thesis is the double multiple streamtube model. It models a VAWT as a collection of actuator surfaces which extract energy from the wind, with each surface modelling a small portion of the turbine's swept area. Any small volume of air is assumed to interact with two of the surfaces in tandem modelling the up and downstream passes of the blades. At the core of this model is the determination of induction factors which indicate how much slowing of the wind has occurred. A relatively new approach for calculating induction factors is adopted in this thesis called the flow state model. It captures the hysteresis nature of stall by maintaining the correct flow state throughout onset of stall and flow reattachment.

The double multiple streamtube method was developed throughout the 1970s and 1980s and today is well established, however, no industry standard DMS based VAWT design tool exists. Furthermore, the DMS method was developed for fixed pitch H-rotors and ϕ-rotors. Attempts to capture variable pitch and V-rotor performance in this context have been sparse and lack validation. In the next chapter a bespoke DMS model capable of capturing these features in addition to the key VAWT aerodynamic phenomena is developed.

Chapter 4

StrathDMS Aerodynamic Model Development

4.1 Introduction

A contribution of this thesis is the development of a design tool capable of estimating the aerodynamic performance of variable pitch, piecewise linear bladed VAWTs. The aerodynamic code is referred to as StrathDMS reflecting both its origin in the University of Strathclyde and the double multiple streamtube (DMS) method which underpins the model. StrathDMS is programmed in MATLAB. However, the focus of this chapter is the underlying equations of the model.

StrathDMS is capable of modelling the aerodynamics of the V-rotor geometry and variable pitch regimes, which no available design tool is capable of so doing. Further novelty is provided by the incorporating the impact of wind shear and the introduction of the modelling issue referred to here as fanning, a consequence of varying degrees of streamtube expansion along a blade, which is significant for tapered blades and V-rotors. In

addition, the flow state method [28] for calculating induction factors is applied to the DMS method for the first time.

This chapter begins with a brief overview of StrathDMS to introduce the key elements in Section 4.2. In Section 4.3 the geometry of the model is provided including the mesh representing the swept area, expansion of streamtubes and the geometry of the airflow local to a VAWT blade. In Section 0 a brief description is provided of the aerofoil data used throughout this thesis. In Section 4.5 the flow state method for determining induction factors is discussed. In Section 4.6 it is shown how variable pitch is integrated into this modelling framework. Section 4.7 discusses the outputs that can be extracted from StrathDMS. Section 4.8 investigates the impact of tip loss and dynamic stall. This chapter finishes with an extensive validation in Section 4.9.

4.2 StrathDMS Procedure

StrathDMS is an aerodynamic estimation tool that is based on the DMS method and is suitable for modelling variable pitch, piecewise linear blade VAWTs. The code is built in MATLAB. This section provides the broad structure of StrathDMS which helps to understand how the novel contributions add to the general DMS approach.

The structure of StrathDMS consists of three separate phases that are represented graphically in Figure 4-1. In Phase 1 the model is initiated by reading in the rotor geometry, the environmental conditions, the pitch regime (Section 4.6), the rotor mesh discretisation parameters (Section 4.4.1) and the aerofoil lift and drag characteristics. In Phase 2 the local fluid flow is determined at each mesh point in the swept area by calculating appropriate induction factors by applying the flow state method for each actuator surface

(Section 4.4.3). This phase is run for one λ and at the end of that phase, all local flow velocities, angles and aerodynamic forces are stored for that λ. Finally in phase 3, the moment contributions from each actuator surface are calculated, and these are combined to determine the performance of the rotor in terms of torque, thrust and loading (Section 4.7.2). Phases 2 and 3 can be run for a range of λ to create global performance information such as C_P-λ and C_Q-λ curves.

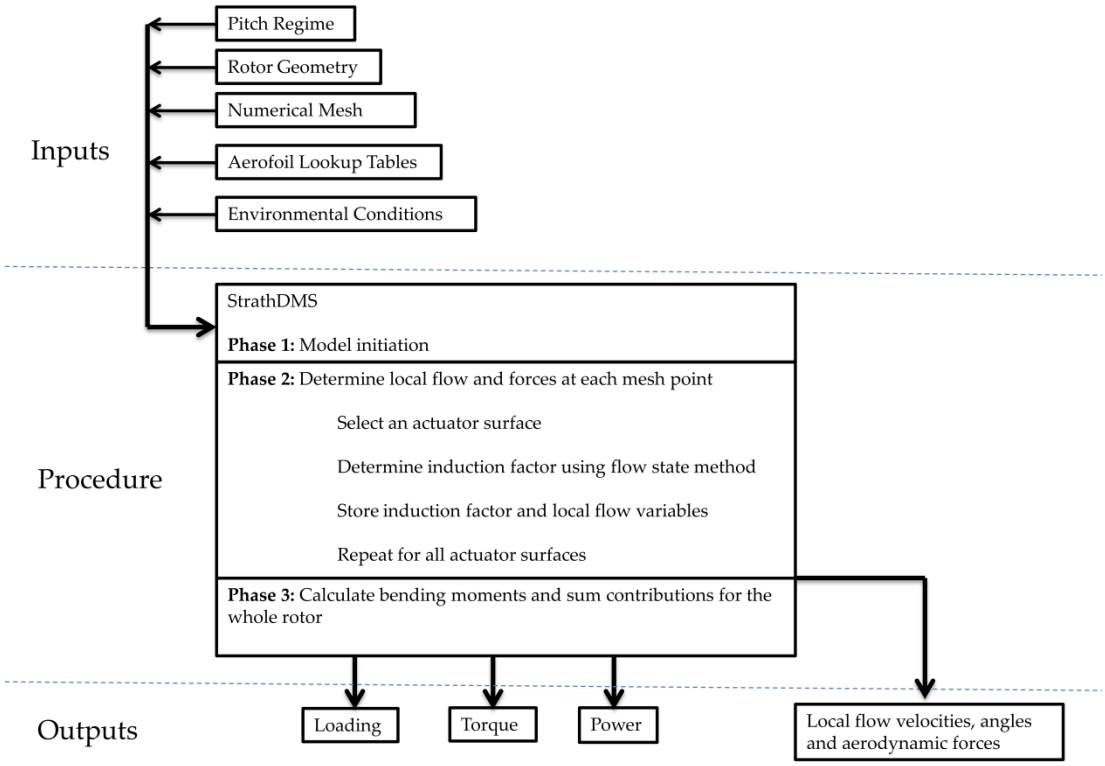

Figure 4-1: StrathDMS aerodynamic estimation code structure.

The StrathDMS procedure runs very quickly so it is a useful tool for exploring a wide range of rotor designs and pitch regimes. On a standard 1GHz processor, StrathDMS will generate all local flow variables and calculate the aerodynamic performance of a VAWT rotor for a particular λ in less than 1 minute. This is based on discretisation of the swept area into a mesh with 640 grid points.

4.3 StrathDMS Assumptions

The following key assumptions are made within the StrathDMS procedure:

1. Pressure recovers to ambient value between tandem actuator surfaces.

As was explained in Section 3.4.1, an inherent assumption that is made in most DMS models is that there is sufficient slowing of the wind for pressure to recover to the ambient value between tandem actuator discs within the rotor. This is necessary in order to calculate a recovered wind speed that can be used for the downwind calculation. However, certain portions of the rotor in the periphery region will have limited space between the discs. This assumption will lead to over predicting the recovered wind speed available downwind.

2. Flow expansion only occurs in the horizontal (x-y) plane

StrathDMS accounts for flow expansion, however it is limited to the horizontal (x-y) plane. A full 3D flow is also likely to expand in the vertical direction in response to a blockage of the flow field. The consequences of neglecting vertical expansion are a small overestimation in the aerodynamic performance of a rotor and a minor error in the extent of the fanning as explained in Section 4.4.2.

3. Induction factor is restricted to positive values.

A negative induction factor is a logical concept and it represents the situation where the rotor increases the energy in the flow. StrathDMS limits induction factors to positive values as a trade-off. The extra detail that is captured by allowing negative induction factors is more accurate modelling of conditions far from design such as extremely high run off tip speed ratios. This extra detail would come at the cost of significantly increasing the time taken to run

simulations because the flow state method must carry out calculations for all potential induction factors.

4. Tangential induction is neglected so that induction only occurs in the streamwise direction.

The BEM method for HAWTs permits calculation of a tangential induction factor that quantifies rotation of the wake [2]. This induced flow orthogonal to streamwise induction conserves angular momentum as a reaction to the wind field rotating the blades. A similar mechanism is at work with VAWTs, however the wake would be deflected rather than rotated. More sophisticated VAWT models have accounted for tangential induction such as Madsen's actuator cylinder model [122] and Ferreira's Modified DMS model [8]. Ferreira's numerical simulations in [8] demonstrate that the impact of neglecting tangential induction factor are to underestimate the tangential force coefficient downstream and overestimate the tangential force coefficient for certain regions of the upwind pass, however, the tangential forces for a significant region of the most upstream position are not affected. Therefore StrathDMS focuses on an accurate representation of the induction factor in the streamwise direction only.

4.4 Geometry

This section outlines how the swept area is discretised into a collection of actuator surfaces and explains the order of calculation of induction factors that must be followed to capture streamtube expansion. The fanning phenomenon is explained, which occurs when there is variation in the degree of streamtube expansion along a VAWT blade. Finally the local flow geometry is provided for a single actuator surface modelling a small portion of the total swept area.

4.4.1 Rotor Mesh and Streamtube Expansion

The rotor is discretised into a mesh by dividing the blades into segments and at the height of each segment, the incident wind is separated into aerodynamically independent streamtubes. N_s is the number of blade segments bounded by N_s+1 blade stations. N_t is the number of azimuthal positions, which dictates the number of streamtubes to be $N_t/2 + 1$ as explained in the following example. Figure 4-2 illustrates the mesh for a V-rotor blade and swept area in the y-z plane when $N_s = 10$ and $N_t = 16$. For a particular blade segment, there is one central streamtube straddled by pairs of streamtubes that get progressively thinner towards the edge of the swept area. Each actuator surface is associated with one azimuthal position and all streamtubes have two actuator surfaces in tandem apart from the outer streamtubes that only have one (8 and 9 Figure 4-2). Therefore choosing $N_t = 16$ creates 9 streamtubes.

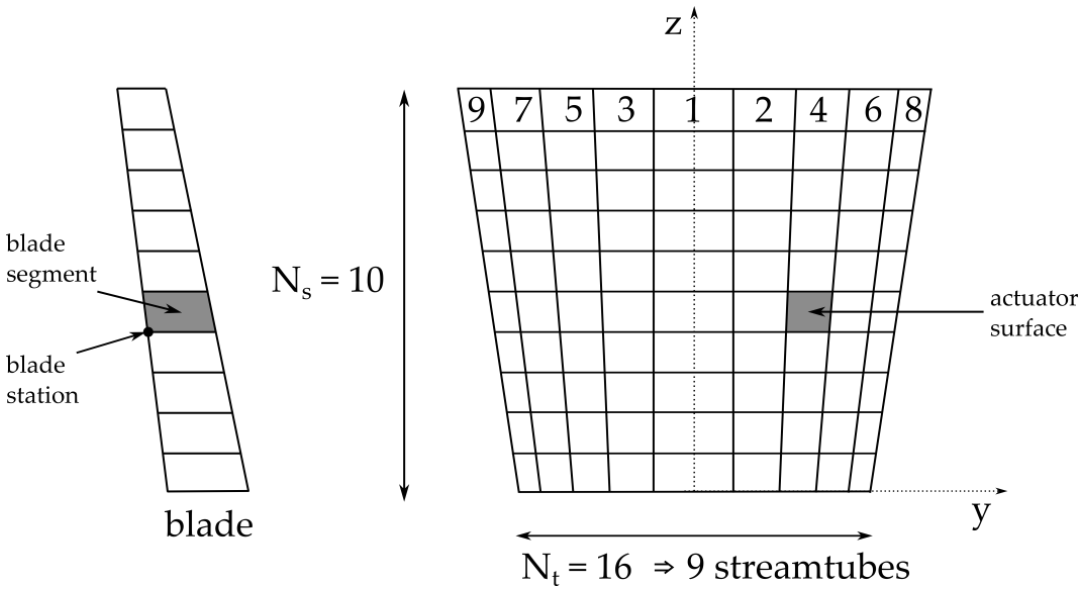

Figure 4-2: Rotor mesh definitions for a V-rotor blade and swept area.

The convention for angles follows Sharpe's formulation in [29] which includes a model of streamtube expansion based on the assumption of

straight streamtubes. Sharpe's approach of working from the central streamtube outwards allows identification of the location of the intersection of the streamtube boundaries with the path of rotation before moving on to the next streamtube. This is critical for implementing and designing pitch regimes as will be discussed in Section 4.6.

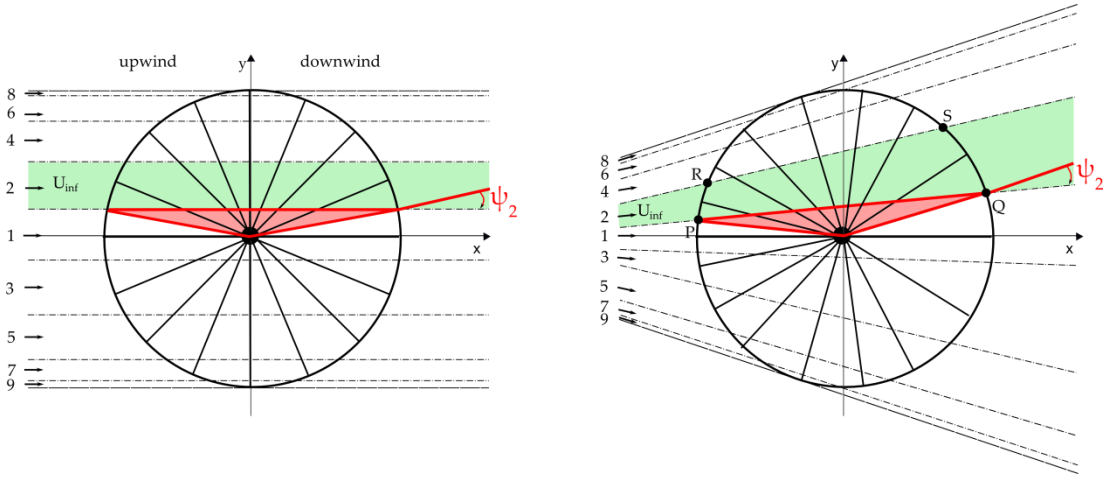

a) No streamtube expansion **b) With streamtube expansion**

Figure 4-3: plan view of a VAWT path of rotation in the x – y plane with and without streamtube expansion.

Conservation of mass flow within a streamtube implies that flow diverges in the downwind direction because the velocity decreases. Therefore a DMS model which captures flow expansion must have upwind surface areas which are smaller than the downwind surface areas. Figure 4-3 illustrates this for the choice $N_t = 16$ in the x-y plane. The linearly increasing cross sectional area of each streamtube causes more of the rotor cycle to be modelled as downwind where energy has already been extracted from the flow. The symmetrical expansion is a consequence of neglecting tangential induction. In actual fact there would be a skewing of the wake to conserve angular momentum. If the blades of the rotor illustrated in Figure 4-3 are

rotating anticlockwise then wake would be deflected along the positive y axis.

Flow expansion is well understood, as outlined in Section 3.3.4 but, difficulty arises when applying it to momentum models. In general, if flow expansion is to be taken into account, there is a difficulty with the definition of the boundaries between different streamtubes, as the azimuthal position of these boundaries depends on the amount of flow expansion and thereby on the induction factors. As explained in [29], making the approximation that the streamtubes are straight, and calculating induction factors in a specific order can overcome this difficulty. The streamtube numbers in Figure 4-3 indicate the order that is followed. There is one central streamtube straddling the x-axis, followed by consecutive pairs of streamtubes all the way out to the outer region of the path of rotation. The induction factors for the central streamtube are determined, and this dictates the degree of expansion of the first streamtube. Thus, the locations of the boundary of the second and third streamtubes are known. The induction factors for streamtubes two and three are calculated before considering streamtubes four and five. This process continues until all induction factors are determined.

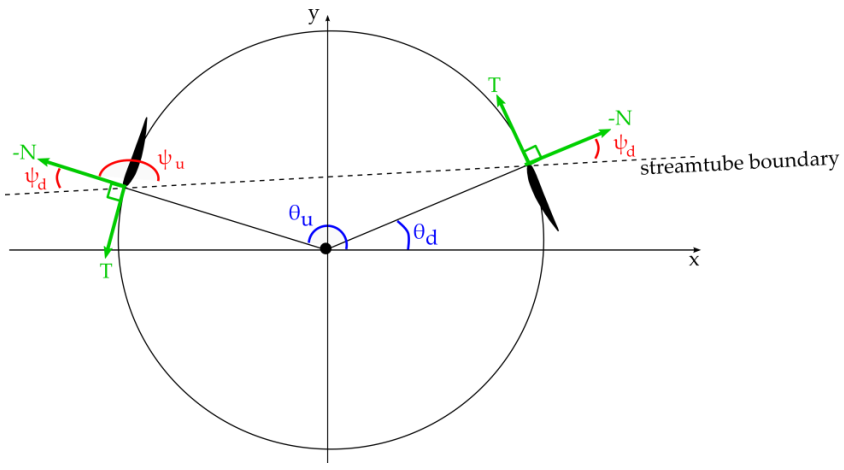

Figure 4-4: θ defined relative to x-axis and ψ defined relative to straight streamtube.

The objective of a DMS model is to balance blade element forces with the thrust in the direction of the streamtube and a consequence of flow expansion is that the direction of the incoming U_{inf} deforms in a manner that tends to point it away from the central streamtube. θ is defined relative to the original direction of U_{inf} and for induction factor calculations a new angle must be introduced in terms of the straight streamtube. Momentum balance can be defined instead in terms of the angle ψ between a radial line protruding from the path of rotation at a streamtube boundary and the straight streamtube pointing downwind, as shown in Figure 4-4. The normal and tangential aerodynamic forces can be transformed into the streamtube direction using ψ. The central streamtube is assumed to have $\psi = 0^{o}$. This new angle is used to calculate the up and downwind induction factors and the degree of streamtube expansion for that streamtube.

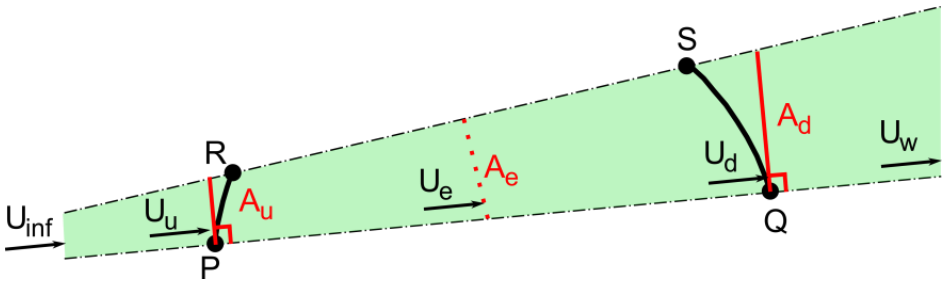

Figure 4-5: The second streamtube with local wind vectors and actuator surface areas.

In order to demonstrate how to calculate the upwind and downwind actuator surface areas, the second streamtube is shown again in Figure 4-5 with local free stream wind velocities and actuator surface areas labelled. The upstream induction factor, a_u, must be determined before calculating the downstream induction factor, a_d, as explained in the DMS overview in Section 3.4.1. The procedure for determining the induction factors is provided in Section 4.5. Once both induction factors have been calculated for one streamtube, the wind speeds U_u and U_d are known. Now the equilibrium

wind speed, U_e, and equilibrium streamtube area, A_e, can be introduced. Based on the straight streamtube assumption, when expansion occurs there is exactly one location between the actuator surfaces that maintains the area of that streamtube without expansion. That location is referred to as the equilibrium. A_e is the average of the up and downstream areas so

$$2A_e = A_u + A_d \tag{4-1}$$

The streamtubes are assumed to be enclosed and density of air does not vary so conservation of mass flow in the form of (4-2) applies.

$$U_u A_u = U_e A_e = U_d A_d \tag{4-2}$$

Combining (4-1)and (4-2)

$$2A_e = \frac{A_e U_e}{U_u} + \frac{A_e U_e}{U_d} \tag{4-3}$$

Simplifying,

$$U_e = \frac{2U_u U_d}{U_u + U_d} \tag{4-4}$$

It must be noted that U_e should not be confused with U_{rec} which is the wind speed between the tandem actuator surfaces where pressure has recovered. A_e is independent of the induction factors because the straight streamlines pivot about this point for different induction factors

$$A_e = r|\cos\psi|\delta_\psi\delta_h \tag{4-5}$$

Where δ_ψ is 2π divided by the number of actuator surfaces for a blade segment, i.e., $\delta_\psi = 2\pi/ N_t$, and δ_h is the vertical height of a streamtube. Conservation of mass flow in the form of (4-2) can be used to determine the areas of the streamtubes up and downstream, A_u and A_d, respectively.

As already mentioned, the amount of flow expansion of the central streamtube is determined before considering the adjacent outer streamtubes.

Therefore the series of arcs subtended by actuator surfaces is built up cumulatively as the procedure progresses from the centre streamtube towards the edge of the swept area. Consider again Figure 4-5, the location of P and Q will be determined while dealing with the first streamtube. Then once the current U_u and U_d are obtained, the conservation of mass flow can be used to define expansion factors up and downstream, χ_u and χ_d respectively.

$$\chi_u = \frac{2U_d}{U_u + U_d} \tag{4-6}$$

$$\chi_d = \frac{2U_u}{U_u + U_d} \tag{4-7}$$

These are used to determine the location of the points of intersection between the next streamtube and the circular path of rotation, R and S. θ_R is used to denote the azimuthal position of the boundary point R.

$$Quadrants\ 1\ and\ 2 \begin{cases} \theta_R = \theta_P - \chi_u \delta_\psi \\ \theta_S = \theta_Q + \chi_d \delta_\psi \end{cases} \tag{4-8}$$

$$Quadrants\ 3\ and\ 4 \begin{cases} \theta_R = \theta_P + \chi_u \delta_\psi \\ \theta_S = \theta_Q - \chi_d \delta_\psi \end{cases} \tag{4-9}$$

While Sharpe's formulation was presented for non-pitched blades in [29], the cumulative nature permits a feature which is convenient when implementing pitch regimes. One of the boundaries of a streamtube is known before any calculations are performed for that streamtube. Therefore, this position can be used to set the pitch angle from a continuous relationship, $\beta(\theta)$, to specify the pitch angle applied for a specific actuator surface. This ensures the correct β is applied as the streamtubes deform to account for flow expansion. Knowing which θ are associated with which

streamtubes is central to implementing variable pitch in an actuator surface framework. More details on this on this are provided in Section 4.6.

4.4.2 Fanning Phenomenon

When modelling a VAWT with an actuator surface model which permits streamtube expansion based on induction factors, variation in induction factors along a VAWT blade will lead to varying degrees of streamtube expansion. No investigation of this phenomenon, which will be referred to as fanning, has been previously reported in the context of BEM modelling. Fanning is particularly significant with tapered blades and V-rotors where induction factors tend to decrease towards the tip due to the lower solidity, and stall sets in at different locations along the blade. The consequence of this is that actuator surfaces will subtend different arc sizes at different blade segments.

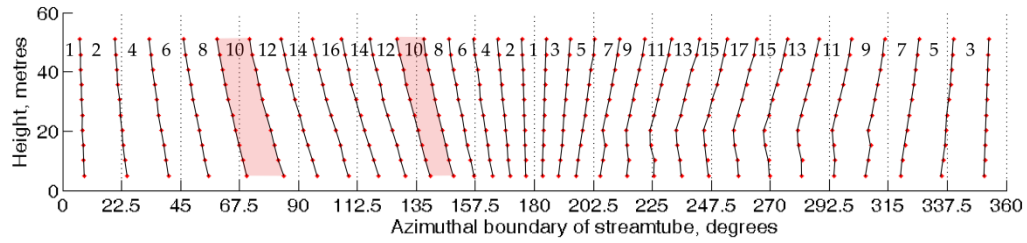

Figure 4-6: Exploded view of the azimuthal position of the intersections of the streamtubes and the circular path of rotation for the test V-rotor, $\lambda = 4.5$.

The issue of fanning is illustrated in Figure 4-6 which is a collection of points indicating the azimuthal positions of intersections of streamtube boundaries with the circular path of rotation for a 1MW rated V-rotor at λ = 4.5 when N_t = 32. The VAWT, to which Figure 4-6 applies, is the test turbine of Chapter 6. The choice of N_t creates 17 streamtubes for any blade segment. The numbers 1 through 17 refer to the streamtube numbers. All actuator surfaces with streamtube number 10 are highlighted. The highlighted

surfaces near $\theta = 135^o$ are the upwind surfaces that share streamtube number 10 and the highlighted surfaces near $\theta = 67.5^o$ are the downwind surfaces that share streamtube number 10.

The effect of streamtube expansion for any particular horizontal cross section of the swept area of a VAWT is to decrease the arc subtended by the upstream actuator surface and increase the arc subtended by the downwind surface. In Figure 4-6, streamtube expansion in the horizontal plane leads to closer spacing between two adjacent points upwind and larger spacing between the two points corresponding to the same streamtube number downwind. At any height, streamtube 10, which is highlighted in Figure 4-6, subtends a smaller arc upstream near $\theta = 140^o$ and a smaller arc downstream near $\theta = 70^o$. Figure 4-6 represents a V-rotor and when the whole blade is considered, the surfaces with the same streamtube number appear to fan away from $\theta = 180^o$. The fanning is a consequence of the higher solidity towards the root of the V-rotor producing higher induction factors in this region. Consequently, more streamtube expansion occurs towards the root of the blade.

The complexity of fanning is further exacerbated by the way in which stall sets in at different locations along a V-rotor blade. In Figure 4-6 stall has set in on the lower half of the blades between $200^o < \theta < 300^o$ causing a region of low induction factors and hence very little streamtube expansion.

Fanning complicates the representation of a VAWT blade using an actuator surface framework. Any vertical line in Figure 4-6 indicates an azimuthal position that must be constant for the whole blade at one particular instant. It is clear from following the vertical line at $\theta = 135^o$ that for a blade at this azimuthal position, any of the blade below 22m is in

streamtube number 12 while the rest of the blade above 22m is in streamtube number 10.

Fanning causes the same streamtube number to subtend different arcs at different positions along the blade as illustrated by Figure 4-7. It shows the plan-view of the same 1MW rated V-rotor at λ = 4.5. In this plot, the circular swept path at the root and the tip are included, and the arcs subtended by the actuator surfaces which share the streamtube number 4 are highlighted. The dotted circle is swept out by the root and solid circle is swept out by the tip. From Figure 4-6, at the root, streamtube 4 subtends $25^o < \theta < 41^o$ downwind and $165^o < \theta < 171^o$ upwind. At the tip, streamtube 4 subtends $20^o < \theta < 33^o$ downwind and $156^o < \theta < 166^o$ upwind. Therefore, only the range $25^o < \theta < 33^o$ downwind and $165^o < \theta < 166^o$ upwind, where the shaded segments overlap in Figure 4-7, are azimuthal positions where the root and the tip share the streamtube number 4.

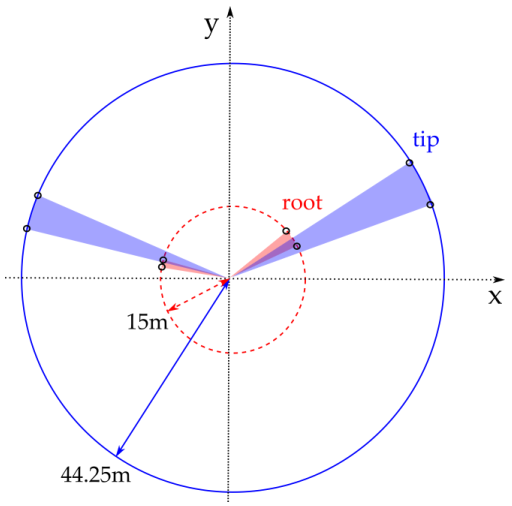

Figure 4-7: Plan view of a V-rotor and the arcs subtended by the same streamtube number at the root and the tip.

The fanning effect of an actuator surface model is particularly important when applying or designing a variable pitch regime. When applying a predefined pitch regime, as explained in Section 4.6.1, care must

be taken to apply a pitch angle for a different portion of the path of rotation at different blade segments. Alternatively, when using the actuator surface framework to design a pitch regime which optimises performance, as explained in Section 4.6.2, it is reasonable to identify the optimal β for a column of surfaces, with each surface optimised individually, then retrospectively consider the azimuthal positions that these optimal β were implemented at and combine them in such a way that generates an averaged β for any specific θ.

4.4.3 Local Flow Geometry

The airflow local to the aerofoil depends on the induction factor. The subsequent section outlines how to determine the correct induction factor, but first it must be explained how the local flow characteristics and aerodynamic forces for any particular induction factor are determined.

The conventions for blade angles and aerodynamic forces are illustrated in Figure 4-8 for a blade in a downstream position with a positive pitch angle. All angles (with the exception of θ) are measured with a clockwise direction of positivity. Blade pitch angle, β, is measured from the tangent to rotation to the chord line. Flow angle, φ, is measured from the tangent to rotation to the net wind speed vector, W. Angle of attack, α, is measured from the chord line to W. For the purposes of this convention, α is restricted to the interval [-180°, 180°]. Since clockwise rotation is considered positive, the situation illustrated in Figure 4-8 shows a negative α. For an un-pitched blade, positive normal direction points towards the centre of rotation and positive tangential direction points along the chordline protruding from the leading edge.

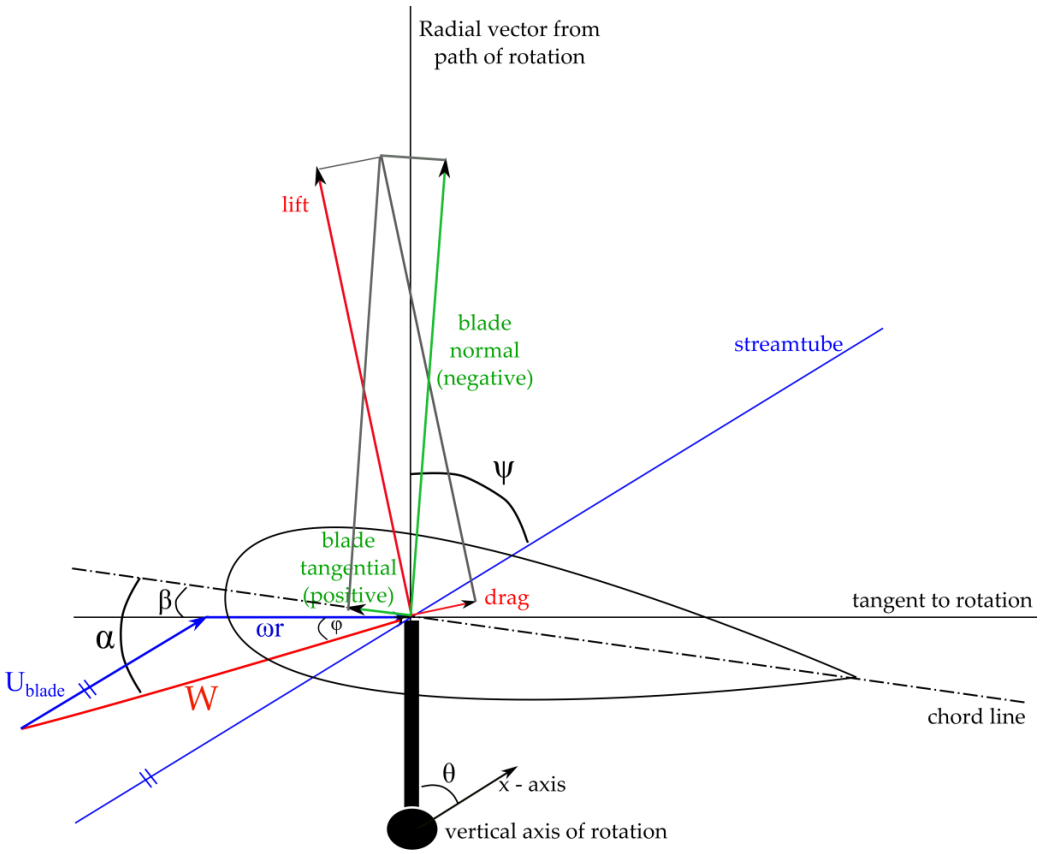

Figure 4-8: Aerofoil flow variables convention for a blade in the first quadrant at an azimuthal position close to θ=45°. The blade is downstream so φ, lift and normal force are all negative. The tail is pitched in so β is positive.

The net wind incident on a VAWT blade, *W*, is the resultant from the addition of two wind vectors; the incident wind in the streamtube direction local to the blade, U_{blade}, and wind due to rotation of the blade, ωr, which is tangential to the path of rotation. U_{blade} is U_u upstream and U_d downstream.

In order to determine φ, the orthogonal components of *W* parallel and perpendicular to the tangent to the direction of rotation are required as defined in Figure 4-9. The component perpendicular to the tangent of rotation must lie in the plane containing the aerofoil cross section. Therefore, for a V-rotor, this component is transformed by cos(γ).

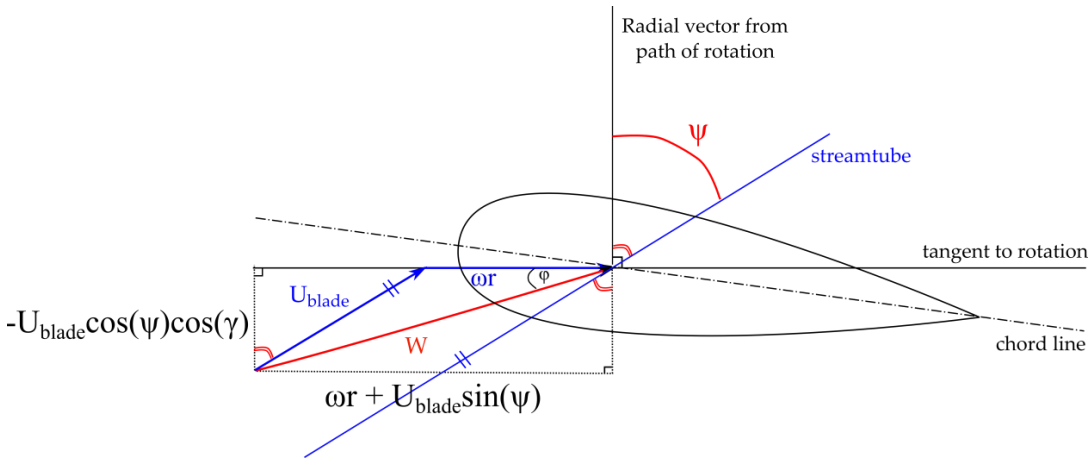

Figure 4-9: Orthogonal components of *W* parallel and perpendicular to the tangent to rotation.

The flow angle, φ, can be expressed in terms of these orthogonal components as in (4-10). Due to the consistent convention used defining angles, (4-10) can be used for any azimuthal position. The resulting φ are positive upstream and negative downstream.

$$\varphi = \tan^{-1}\left(\frac{-U_{blade}\cos\psi\cos\gamma}{U_{blade}\sin\psi + \omega r}\right) \quad \textbf{(4-10)}$$

From φ and the pitch angle, β, angle of attack, α, is determined by

$$\alpha = \varphi - \beta \quad \textbf{(4-11)}$$

These three angles are demonstrated for a blade at $\theta = 45^{o}$ in Figure 4-8. In this case φ is negative and β is positive so α is negative.

Together, *W* and α dictate the aerodynamic forces acting on an aerofoil. The aerodynamic forces acting on a blade at an azimuthal position in the first quadrant are illustrated by Figure 4-8. Drag, *D*, is parallel to *W* and lift, *L*, is perpendicular to *D*, with the sign of α dictating the direction of the lift. Lift and drag coefficients, C_L and C_D, are taken from aerofoil coefficient lookup tables based on α and (4-12) is used to transform these into normal and tangential force coefficients, C_N and C_T. Using α for this rotation

transforms the blade lift and drag forces into normal and tangential in the blade frame of reference.

$$C_N = C_L(\alpha)\cos\alpha + C_D(\alpha)\sin\alpha$$
$$C_T = C_L(\alpha)\sin\alpha - C_D(\alpha)\cos\alpha \quad \textbf{(4-12)}$$

When the blade is pitched by β, the coefficients, C_R, for the force acting radially towards the centre of rotation, and C_S, for the force acting tangentially to the path of rotation and pointing in the direction of rotation, are required. They are related to C_N and C_T by (4-13)

$$C_R = C_N\cos\beta - C_T\sin\beta$$
$$C_S = C_N\sin\beta + C_T\cos\beta \quad \textbf{(4-13)}$$

4.4.4 Aerofoil Data

The performance of any rotor is influenced by the choice of aerofoils. StrathDMS models aerofoil performance using look up tables that contain the coefficients of lift and drag for a range of α and Reynolds number. The simulations within this thesis use symmetric NACA aerofoils and lift and drag coefficients obtained from wind tunnel testing can be found in [138].

As a demonstration of the quality of data used in the simulations for this thesis, the lookup tables for the symmetrical NACA0012 used in StrathDMS are provided in Appendix A.

Reynolds number has a significant impact on the aerodynamic characteristics of the aerofoil and the effective wind speed, and hence Reynolds number varies as the blade rotates. Therefore it is important that a VAWT aerodynamic estimation code utilizes the correct Reynolds number for each point in the path of rotation. StrathDMS recalculates the Reynolds number at each location around the path of rotation and for every value of a as the flow state method is carried out.

4.5 Implementing the Flow State Method for Calculating Induction Factors

The flow state method for determining induction factors as introduced by McIntosh et. al. [28] is applied to the double multiple streamtube method for the first time in StrathDMS. The method generates two functions of induction factor, the first is force in the windward direction from momentum considerations and the second is force in the windward direction from blade element considerations. The induction factor at which these functions intersect is selected for that actuator surface. In this section, the two separate ways to express windward force as a function of induction factor are presented. Subsequently, it is demonstrated that this method selects the correct induction factor for situations with multiple solutions. The notation used in this section refers to an upstream actuator surface. The same principles apply downstream.

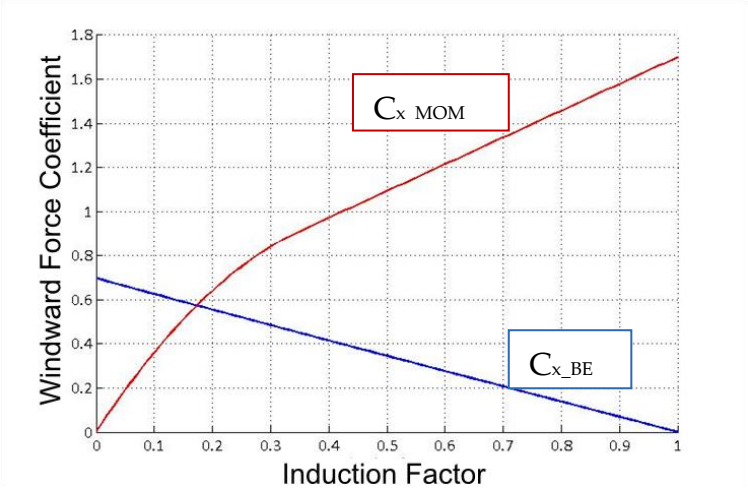

Figure 4-10: An interception diagram depicting force in the windward direction plotted against induction factor from momentum equations and blade element equations. Turbine simulated here: H-rotor with 50m blades, 25m radius, 2m chord. $\lambda = 4$ and $\theta = 180^{o}$.

Force in the windward direction due to momentum considerations is based on standard momentum theory coupled with Glauert's correction [2].

Standard momentum theory implies that the coefficient of thrust in the windward direction is given by

$$C_x = 4a(1-a) \tag{4-14}$$

and U_{rec}, the wind speed in the wake of the actuator surface when pressure has recovered, is

$$U_{rec} = U_{inf}(1-2a_u) \tag{4-15}$$

For $a > 0.5$, the wind speed in the wake would have reversed according to (4-15). This is clearly nonsense and occurs because the momentum based assumptions have completely broken down. In fact, the air chooses to flow around the turbine instead of through it. The assumption of enclosed streamtubes has broken down and while the blades experience a high thrust, very little energy is converted to torque. An empirical correction for high induction factors was provided by Glauert in 1926 [139] with a positive correlation between a and C_x for high a. The standard momentum parabola is extended from a near 0.35, rising towards $C_x = 1.7$ as a approaches 1.

For the flow state method, an injective function $C_x(a)$ is required. For $a < a_{thresh}$ the standard function provided in (4-14) is used. For $a > a_{thresh}$ a tangential extension from the standard parabola is used. Constraining the tangent to pass through $C_x = 1.7$ at $a = 1$ forces

$$a_{thresh} = 1 - \frac{\sqrt{1.7}}{2} \tag{4-16}$$

The equation of the straight line capturing Glauert's correction is

$$C_x = 1.21536a + 0.48463 \tag{4-17}$$

Together, (4-14) and (4-17) are referred to as C_{x_MOM} and they are illustrated together in Figure 4-10.

In order to determine the induction factor that balances momentum and blade element forces, thrust due to blade element considerations is required as a function of induction factor. Instantaneous force in the streamwise direction due to normal and tangential blade element forces is given by (4-18). As before, δ_ψ is 2π divided by the number of actuator surfaces for a blade segment, i.e., $\delta_\psi = 2\pi/ N_t$ so $B\delta_\psi/2\pi$ is an averaging factor that accounts for the proportion of time a streamtube has a blade in it.

$$F_{x\_BE} = (-F_R \cos\psi \cos\gamma - F_S \sin\psi)\frac{B\delta_\psi}{2\pi} \tag{4-18}$$

This expression can be normalised using the following coefficients of force

$$\begin{aligned} C_R &= \frac{F_R}{0.5\rho A_{seg} W^2} \\ C_S &= \frac{F_S}{0.5\rho A_{seg} W^2} \end{aligned} \tag{4-19}$$

Where A_{seg} is the area of a blade segment, and

$$C_x = \frac{F_x}{0.5\rho A_{surface} {U_{inf}}^2} \tag{4-20}$$

where $A_{surface}$ is the area of an actuator surface within a streamtube. For a downwind actuator surface U_{inf} is replaced by U_{rec} in (4-20). Substituting (4-19) and (4-20) into (4-18) generates

$$C_x = \left(\frac{B\delta_\psi}{2\pi}\right)\left(\frac{A_{seg}}{A_{surface}}\right)\left(\frac{W}{U_{inf}}\right)^2 (-C_R \cos\psi \cos\gamma - C_S \sin\psi) \tag{4-21}$$

The following expressions for areas are used where δl is the length of a blade segment.

$$\begin{aligned} A_{seg} &= c\delta l \\ A_{surface} &= r\delta\psi|cos\psi|\delta l \cos\gamma \end{aligned} \tag{4-22}$$

Substituting (4-22) into (4-21) generates the expression for averaged thrust coefficient based on blade element principles, C_{x_BE}. For downstream actuator disks, U_{inf} is replaced with U_{rec}.

$$C_{x\_BE} = \left(\frac{Bc}{2\pi r \cos\gamma}\right)\left(\frac{W}{U_{inf}}\right)^2 |\sec\psi|(-C_R \cos\psi \cos\gamma - C_S \sin\psi) \quad \textbf{(4-23)}$$

Equation (4-23) depends on ψ which is independent of the degree of streamtube expansion. C_{x_BE} is a function of a because W, C_R and C_S are all functions of a. An example of C_{x_BE} is shown as the downward sloping line in Figure 4-10.

With C_{x_MOM} and C_{x_BE} defined, the procedure for determining the correct a can be described. For all a in [0, 1] with a step size of 0.001 U_{blade} is calculated and the task is to determine the a for which $C_{x\_BE} = C_{x\_MOM}$. For any particular induction factor, the local aerodynamic forces are generated as explained in Section 4.4.3. These local aerodynamic forces are used to calculate a value of C_{x_BE} for that induction factor. The sign of $C_{x\_BE} - C_{x\_MOM}$ is evaluated to check if there has been a crossing of the two windward force functions compared to the situation for the previous a. If a crossing has occurred then this value of a is stored as a potential solution. Subsequently the next a is considered. Once all a have been considered, the set of a associated with crossing points is available. In most situations there will be one crossing and that value of a is selected as the induction factor as is demonstrated in Figure 4-10 where there is a unique solution at $a = 0.175$. The following section discusses how to select an induction factor when multiple crossing points exist.

4.5.1 Multiple Solutions

There are situations where multiple crossing points occur and as McIntosh et. al. explained in [28], the advantage of the flow state method is that it

identifies all crossing points and allows the correct value of a to be selected based on the current flow state. Multiple crossing points are a consequence of stall on the blades and can occur during onset of stall or flow reattachment. Each of the triple crossing points defines a different flow state of the blade as illustrated in Figure 4-11. The three potential states are; attached, partial stall and deep stall, however partial stall is unstable and should never emerge as a solution of the flow state scheme [28]. In order to capture the hysteresis effect of stall the correct value is chosen to maintain the flow state from the previous azimuthal location in the path of rotation.

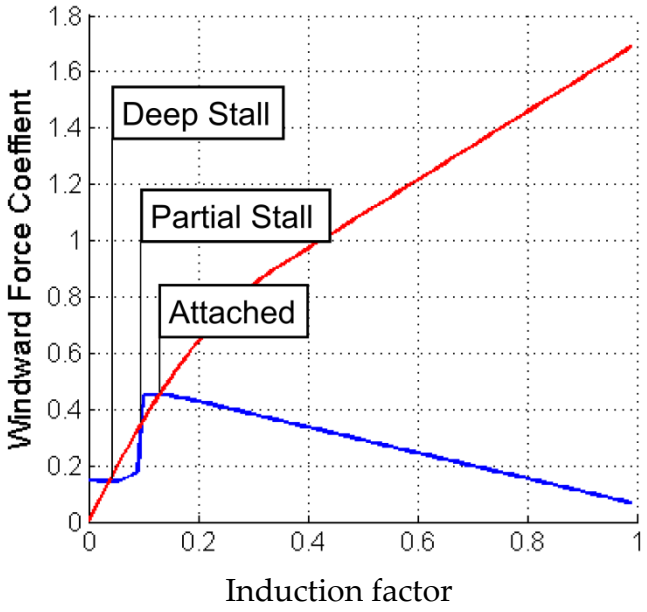

Figure 4-11: Interception diagram for a test H-rotor at an azimuthal location which demonstrates multiple solutions. $\lambda = 2$ and $\theta = 236^{o}$.

A 500kW H-rotor has been designed to demonstrate that StrathDMS selects the correct a when multiple solutions exist. The turbine has 3 blades, 16m radius, a uniform chord length of 2m and NACA 0012 aerofoil data is employed. An interception diagram for $\theta = 236^{o}$ where the H-rotor could be in one of the three potential flow states is illustrated in Figure 4-11. Knowledge that the flow is in the process of reattachment here dictates that

the correct choice of a is the lowest value of the three which is 0.041. This maintains the deep stall state. Figure 4-12 shows how induction factor varies with θ when $\lambda = 2.5$. Figure 4-12 a) shows the full path of rotation and there is a small region upstream between $205^{o} < \theta < 240^{o}$ where there is a significant drop in a due to stall occurring in this region. A closer look at the stalled region is shown in Figure 4-12 b). It includes the multiple solutions that are disregarded by the flow state method. This clearly illustrates that during onset of stall, the attached flow state is sustained, and then when reattachment begins, the blade remains in stall until there are no more multiple solutions.

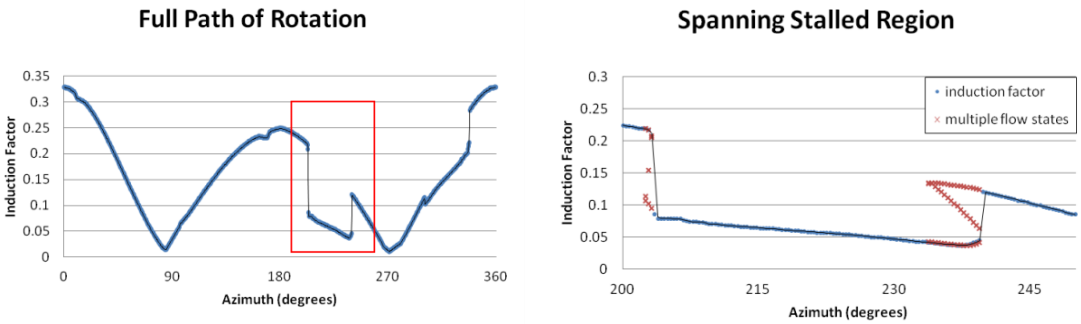

a) b)

Figure 4-12: Capturing the hysteresis effect of stall with the flow state method. $\lambda = 2.5$.

4.6 Implementing Variable Pitch in an Actuator Surface Framework

4.6.1 Implementing a Pitch Regime

In the actuator surface framework, the swept area of a VAWT is modelled as a collection of actuator surfaces. The underlying assumption is that the variation in aerodynamics throughout the portion of the swept area that is modelled by a particular surface can be represented by the blade being sustained at one particular azimuthal location for the time it would take for

the blade to sweep through the appropriate portion of the swept area. In order to implement a pitch regime, $\beta(\theta)$, an azimuthal location must be selected to represent each surface. Consider again Figure 4-5 depicting a streamtube. Since the inner boundary, PQ, of this streamtube is known before calculating the width of this streamtube, it is sensible to select the intersections of the inner boundary with the path of rotation, i.e. positions P and Q, to represent the up and downstream surfaces respectively for this streamtube.

4.6.2 Designing an Optimal Cyclical Pitch Regime

Any optimisation by definition must have an objective function. In this thesis cyclical pitch will be employed to achieve two different objectives in Chapter 6, maximise aerodynamic performance, and minimise cyclical loading without impacting aerodynamic performance. In this section it is shown that the actuator surface framework can be used to represent a VAWT blade in order to select the best β for each θ.

Attempting to use an actuator surface approach to optimise $\beta(\theta)$,seems simple; what β should be selected at each θ? Since the blade can only ever achieve one β at any instant raises the question, how is the blade represented in the actuator surface framework? It is tempting to represent the blade as a column of actuator surfaces. However, as a consequence of the fanning phenomena described in Section 4.4.2 in certain situations a straight blade may straddle multiple columns of actuator surfaces. In these situations it is necessary to carry out separate optimisations for all blade segments associated with one streamtube. This will generate for each of the N_t stations, a set of optimal pitch angles and associated azimuthal positions. These values are averaged using a weighting such that the choice of β for a particular azimuthal location is influenced more by the blade segments

which contribute more towards the objective. The final output of this procedure is a function $\beta(\theta)$ with N_t values which can be used at all heights.

4.6.3 Variable Pitch Effects on Flow Curvature

A method of capturing the effect of flow curvature by augmenting C_N of an aerofoil is presented in Section 3.3.3 and this effect can be amplified or reduced by the pitching of blades as the rotor spins. A simple correction in terms of dβ/dθ can capture the pitching effect.

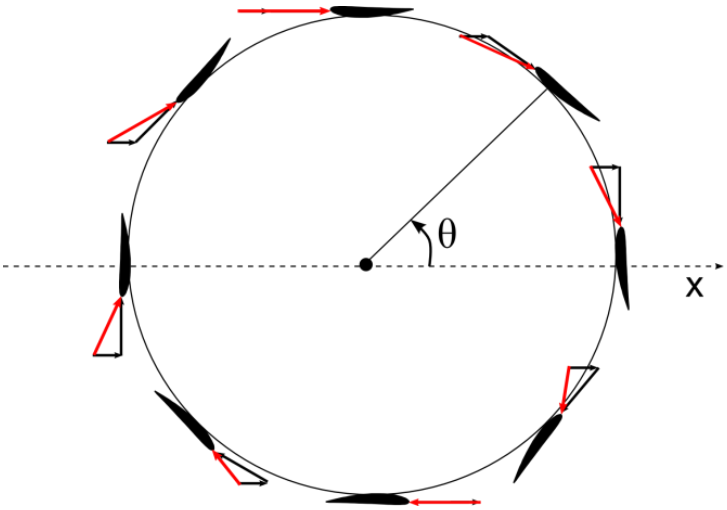

Figure 4-13: Variation in angle of attack with θ

Consider Figure 4-13 which depicts the variation in α with θ. The x-axis divides the path of rotation into an upper half where the blades move towards the wind and a lower half where the blades move with the wind. In the upper half a positive dβ/dθ is required to maintain a constant α as θ increases whereas in the lower half a negative dβ/dθ is required. A convenient detail is that across any arc spanning $d\theta$, a pitch of the magnitude $d\beta$ in the correct direction will counter the effect of flow curvature. Thus dβ/dθ = 1 is required to counter the flow curvature effect. Therefore, a simple correction can be expressed as D_β, which captures the amplification or reduction in the effect of flow curvature.

$$D_\beta = \begin{cases} 1 - \dfrac{d\beta}{d\theta}\ , upper\ half \\ 1 + \dfrac{d\beta}{d\theta}\ , lower\ half \end{cases} \quad \textbf{(4-24)}$$

Including this in (3-6) provides an expression for the contribution to normal force from flow curvature accounting for blade pitch, so C_{N_fc} becomes

$$C_{N\_fc} = \frac{1}{4}\frac{dC_L}{d\alpha}\frac{c}{r}\frac{\omega r}{W}D_\beta \quad \textbf{(4-25)}$$

4.7 Model Output

There is a wide selection of outputs that can be extracted from StrathDMS. These outputs are either local flow variables at the aerofoil scale or measures of global performance which take into account contributions at the rotor scale.

4.7.1 Local Flow Variables

With an induction factor determined for a specific actuator surface, this defines the local flow for the small portion of the swept area that is modelled by that actuator surface. With the local flow defined, all aerodynamic forces are available. The most important variables are depicted in Figure 4-8.

4.7.2 Global Performance

Once the aerodynamic forces at each azimuthal position and all streamtube areas have been stored for a specific λ, the global performance can be calculated.

4.7.2.1 Torque

The instantaneous torque per unit length for a discretised location on the swept area is given by

$$q_{i,j} = \frac{1}{2}\rho {W_{i,j}}^2 D_{Qi,j} \quad \textbf{(4-26)}$$

where i is the blade segment index and j is the azimuthal position index, $A_{i,j}$ is streamtube area and ρ is air density. $D_{Qi,j}$ is an expression that captures the normalised instantaneous forces and moment arms that contribute to the torque provided by a blade segment at a particular location as shown in (4-27). The first component is the tangential force on a blade segment acting at a distance r from the axis of rotation. The second is the normal force acting towards the centre of rotation as a consequence of attaching the blade at the c/2 point while aerodynamic forces act at the c/4 point [33]. This additional contribution to torque only applies for symmetric aerofoils in attached flow.

$$D_{Q\,i,j} = C_{S\,i,j} r_i + \frac{c_i}{4} C_{R\,i,j} \quad \textbf{(4-27)}$$

Trapezoidal loading can be used to determine, $\bar{q}_{i,j}$, the contribution to torque from each blade segment for each location on the swept area (i, j) then total torque provided by the whole turbine, Q, is simply the sum of the individual torque contributions as in (4-28). Finally, power generated for a specific λ is the product of Q and ω.

$$Q = \sum_i \sum_j \bar{q}_{i,j} \quad \textbf{(4-28)}$$

4.7.2.2 Thrust

The rotor decelerates the mass of the wind in the streamwise direction and the reactionary force of the wind on the rotor is thrust. StrathDMS determines thrust on a whole blade for each azimuthal position by summing the instantaneous aerodynamic force in the streamwise direction along the blade. Alternatively the thrust on the whole rotor is determined by summing thrust contributions, that have been time averaged to account for proportion of time each blade spends in each streamtube, for all actuator surfaces across the whole swept area. Both measures of thrust involve an intrinsic approximation. The impact of flow expansion is to cause the streamwise

direction to diverge away from the x-axis. Therefore not all components in the calculation of thrust are acting in the same direction and the expected result is minor over estimation of the thrust.

4.7.2.3 Bending Moments

Aerodynamic forces at discretised stations along the blade can be converted into aerodynamic moments. The conversion from blade normal force, F_N, to flapwise blade bending moment is used to illustrate how to convert instantaneous force per unit length at discretised points at either end of a blade segment into a contribution to the bending moment from that blade segment. The instantaneous normal force (orthogonal to the chord length) per unit blade length at a discrete position along a blade is given by

$$F_{N\,i,j} = \frac{1}{2}\rho {W_{i,j}}^2 c_i C_{N\,i,j} \tag{4-29}$$

This is transformed to a contribution to flapwise blade bending moment from segment i when the blade is in azimuthal position j using (4-30) which is based on trapezoidal distributed loading. d_i is the moment arm at which the instantaneous force per unit length acts. The derivation of this expression is provided in Appendix B: Trapezoidal Loading.

$$\begin{aligned} M_{B-f\,i,j} = {} & \frac{1}{6}F_{N\,i,j}\left({d_{i+1}}^2 - d_{i+1}d_i - 2{d_i}^2\right) \\ & + \frac{1}{6}F_{N\,i+1,j}\left(2{d_{i+1}}^2 + d_{i+1}d_i - {d_i}^2\right) \end{aligned} \tag{4-30}$$

The following moments are used in this thesis:

Overturning moment in the windward direction: $M_{OT\text{-}x}$ – For any single azimuthal position, all blades are considered. For an H-rotor the

instantaneous force considered is the aerodynamic force in the windward direction and the moment arm is the distance from the ground. For a V-rotor there is an additional contribution which is the aerodynamic force in the vertical direction and the moment arm is the horizontal distance to the axis of rotation. To determine $M_{OT\text{-}x}$ for one azimuthal position, the blade segment contributions for a blade at that azimuthal position are summed along with the contributions from the other blades (that will be 120^o apart for a three bladed rotor).

Overturning moment in the cross wind direction: $M_{OT\text{-}y}$ – For any single azimuthal position, all blades are considered. For an H-rotor the instantaneous force considered is the aerodynamic force in the cross wind direction and the moment arm is the distance from the ground. For a V-rotor there is an additional contribution which is the aerodynamic force in the vertical direction and the moment arm is the horizontal distance to the axis of rotation. To determine $M_{OT\text{-}y}$ for one azimuthal position, the blade segment contributions for a blade at that azimuthal position are summed along with the contributions from the other blades (that will be 120^o apart for a three bladed rotor).

Flapwise blade root bending moment: $M_{B\text{-}rf}$ – The flapwise blade bending moment for one segment is calculated using (4-30). The instantaneous force considered is the blade normal force. The moment arm for an H-rotor is the distance to the centre of the blade (a supporting strut in the centre is assumed) and the moment arm for a V-rotor is the distance to the blade root (no supporting struts are assumed). The flapwise blade root bending moment is the combined contribution from all of the blade segments in half of the blade for an H-rotor and the whole blade for a V-rotor.

Edgewise blade root bending moment: $M_{B\text{-}re}$ – The same procedure as for $M_{B\text{-}rf}$ is followed except instantaneous blade tangential aerodynamic force is used.

In-Plane blade root bending moment: $\mathbf{M_{B\text{-}rin}}$ –The in-plane blade bending moment for one segment is calculated using (4-30). The instantaneous force considered is the rotor tangential force. The moment arm for an H-rotor is the distance to the centre of the blade (a supporting strut in the centre is assumed) and the moment arm for a V-rotor is the distance to the blade root (no supporting struts are assumed). The in-plane blade root bending moment is the combined contribution from all of the blade segments in half of the blade for an H-rotor and the whole blade for a V-rotor.

Out-of-Plane blade root bending moment: $\mathbf{M_{B\text{-}rout}}$ – The same procedure as for $M_{B\text{-}rf}$ is followed except instantaneous rotor normal aerodynamic force is used.

4.8 The Impact of Correction Factors on Aerodynamic Estimations

There are certain aerodynamic phenomena that must be captured in order to accurately simulate VAWT performance. Streamtube expansion has already been addressed because it is engrained within the geometry of the turbine mesh. The two phenomena that are modelled with corrections that can be switched on or off are tip loss and dynamic stall. The theory underpinning these phenomena was provided in the review in Section 3.3. This section will present a set of test simulations to demonstrate how the corrections impact aerodynamic estimations and a sensitivity analysis is carried out to reveal what elements of rotor design impact the effect of the corrections. Three

design variables are investigated here; σ, blade length and turbine scale. In addition the hysteresis loop associated with dynamic stall is demonstrated.

4.8.1 Baseline Test Turbine

A baseline H-rotor turbine is designed to investigate the effect of aerodynamic corrections implemented within StrathDMS. The rotor details are provided in Table 4-1. To investigate σ, the chord length of the baseline turbine is varied to achieve $\sigma = 0.1$ and $\sigma = 0.3$. To investigate blade length, a short blade with l = 20m and a long blade with l = 100m are simulated. The baseline turbine is considered medium scale and to investigate turbine scale, σ = 0.2 and blade aspect ratio of 40 are maintained for both a small scale turbine with r = 1m and a large scale turbine with r = 50m. Each simulation is run with $N_s = 26$ and $N_t = 128$.

Table 4-1: Rotor details for the baseline H-rotor turbine

# of Blades	Radius (m)	Chord (m)	Blade Length (m)	Aerofoil
3	18.75	1.25	50	NACA0012

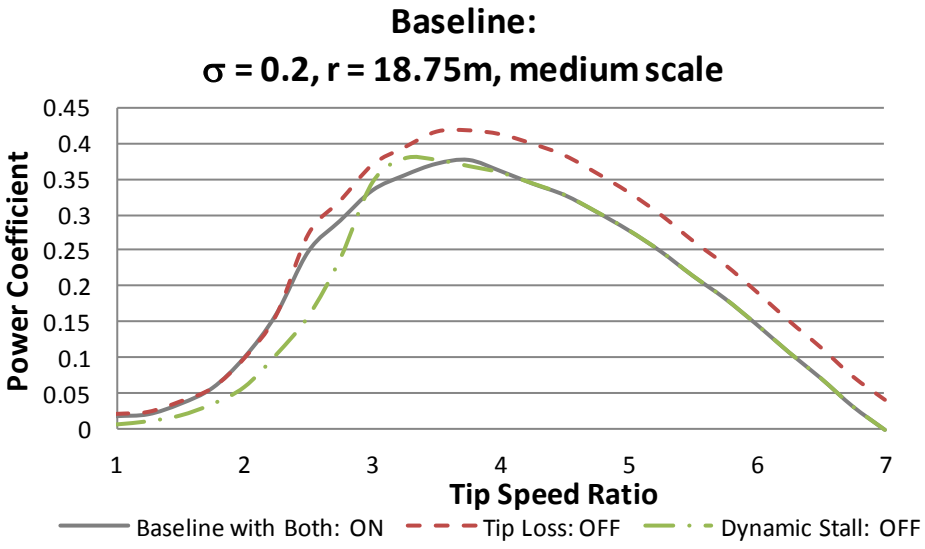

Figure 4-14: Cp-λ for the baseline H-rotor turbine. The effect of tip loss and dynamic stall are displayed.

The C_P-λ curve, which was generated by StrathDMS for the baseline turbine, is presented in Figure 4-14. The solid line shows performance for the full simulation with both tip loss and dynamic stall switched on. C_{Pmax} of 0.38 is attained at λ_{opt} = 3.75. The dashed line shows the performance with tip loss switched off and the dash and dotted line shows the performance when dynamic stall is switched off.

Furthermore, C_P-λ curves have been generated for a range of solidity, blade lengths and turbine scales in Figure 4-15 to Figure 4-17 with the corrections switched on and off. The double line represents the baseline turbine with both corrections switched on. The solid line is the new turbine design with corrections switched on. The dashed line shows the performance of the new design with tip loss switched off and the dashed and dotted line shows the performance of the new design when dynamic stall is switched off. The following sections analyse this output to explore the impact of the corrections.

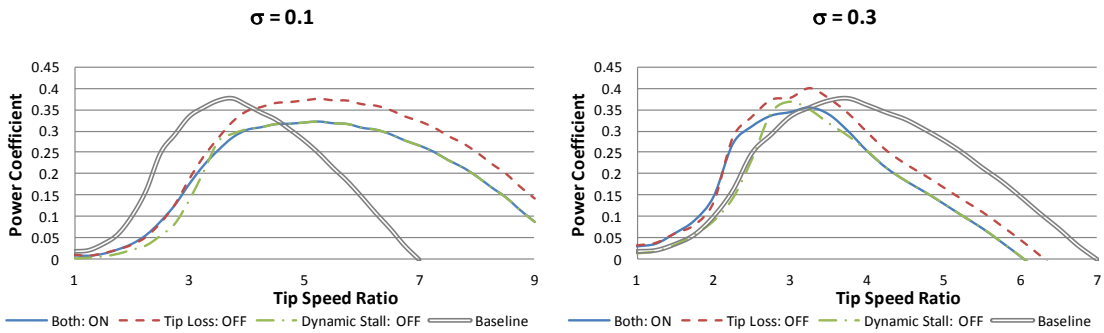

a) Low solidity c = 0.625m **b) High solidity c = 1.875m**

Figure 4-15: The effect of solidity on aerodynamic estimations. All other parameters set to baseline values.

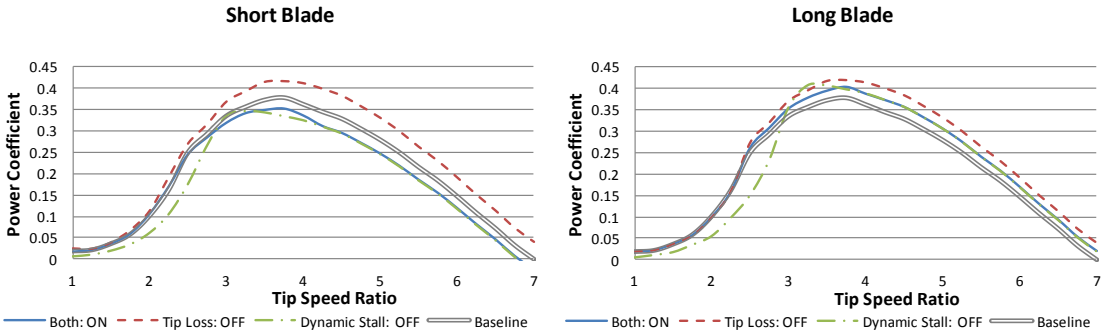

a) Short blade 20m **b) Long blade 100m**

Figure 4-16: The effect of blade length on aerodynamic estimation. All other parameters set to baseline values.

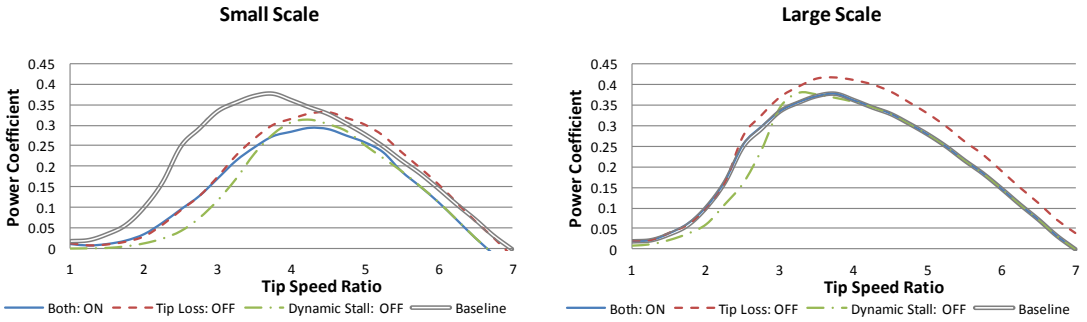

a) Small scale: R = 1m, c = 0.067m, blade length = 2.67m. **b) Large scale: R = 50m, c = 3.33m, blade length = 133.33m.**

Figure 4-17: The effect of turbine scale on aerodynamic estimations.

4.8.2 Tip Loss

It can be seen from Figure 4-14 that tip loss has a significant effect on the aerodynamic performance. C_{Pmax} reduces from 0.42 to 0.38, a reduction of 9.5%. For low λ, tip loss has no effect and for $\lambda > \lambda_{opt}$, it has a gradually diminishing effect. Figure 4-15 and Figure 4-17 demonstrate that σ and turbine scale have very little impact on the effect of tip loss. Figure 4-16 shows that the tip loss correction factor captures the fact that tip loss has a larger impact when the ratio of blade length to radius decreases. The tip loss

correction factor reduces C_{Pmax} by 16% for the short blade, which is more than the baseline, whereas C_{Pmax} reduces by 4.8% for the long blade, which is less than the baseline.

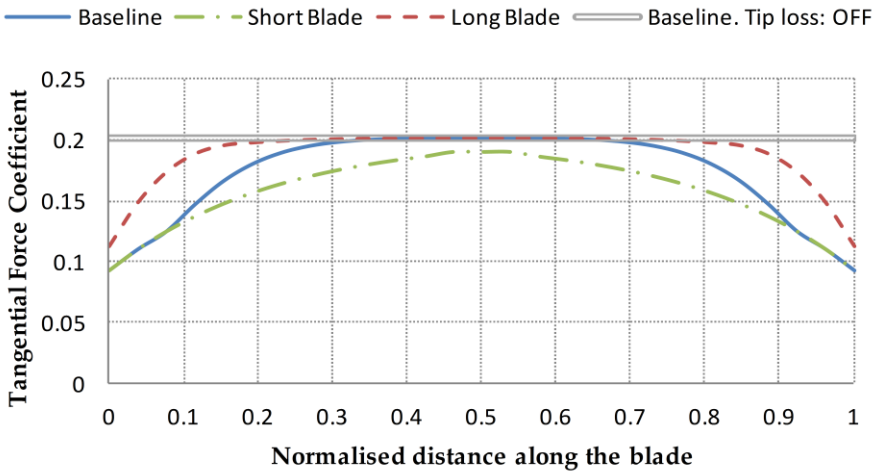

Figure 4-18: Effect of tip loss on C_T for three blade lengths. Baseline turbine at θ = 180°.

For a closer scrutiny of the effect of blade length on tip loss, C_T is plotted against normalised distance along the blade for three different blade lengths at the position θ = 180° in Figure 4-18. C_T is plotted because it is the main contribution to driving torque. On the baseline blade, the impact of tip loss on C_T impacts roughly 25% of the blade at either end. The longer blade has a weaker impact on C_T and it is limited to the final 15% of each blade. The impact of tip loss on the small blade is stronger and it is experienced at all locations along the blade.

4.8.3 Dynamic Stall

As discussed in Section 3.3.5.3, StrathDMS applies Strickland's adaptation of the Gormont dynamic stall model because it sufficiently captures the main elements of dynamic stall which are a delay in the onset of stall, dynamic lift coefficients exceeding static lift values and the hysteresis loop between the onset of stall and flow reattachment. StrathDMS is developed for exploration

of rotor configurations and pitch options rather than comprehensive design studies so the additional modification of the Gormont due to Masse is not included.

In order to apply the Gormont model, the time derivative of α is required. For this step in StrathDMS, induction is neglected. Therefore the time derivative of α can be calculated for each azimuthal position independent of a scheme for determining the local flow field.

The overall impact of dynamic stall on aerodynamic estimation can be seen in Figure 4-14. For low λ, deep stall conditions exist and the effect of dynamic stall is to permit larger C_L and ultimately C_P increases. Then for a small region of λ approaching λ_{opt} ($3 < \lambda < 3.75$ for the baseline turbine), dynamic stall reduces the C_P attained. This causes the peak of the C_P-λ curve to broaden and slightly reduces C_{Pmax}. For $\lambda > \lambda_{opt}$ the range of α experienced by a VAWT blade diminishes until the turbine operates completely out of stall and dynamic stall can have no effect. Figure 4-16 and Figure 4-17 illustrate that blade length and turbine scale have very little impact on the effect of dynamic stall. Figure 4-15 shows that the impact of the dynamic stall correction factor is influenced by the solidity. As σ decreases, the effects of dynamic stall are amplified, so C_P increases further for low λ and the peak is broadened more. The reason for this is that a VAWT with low σ will operate in a low λ, so more stall occurs. A full investigation of the impact of σ on optimal aerodynamic performance of straight bladed VAWTs is provided in Section 5.2.

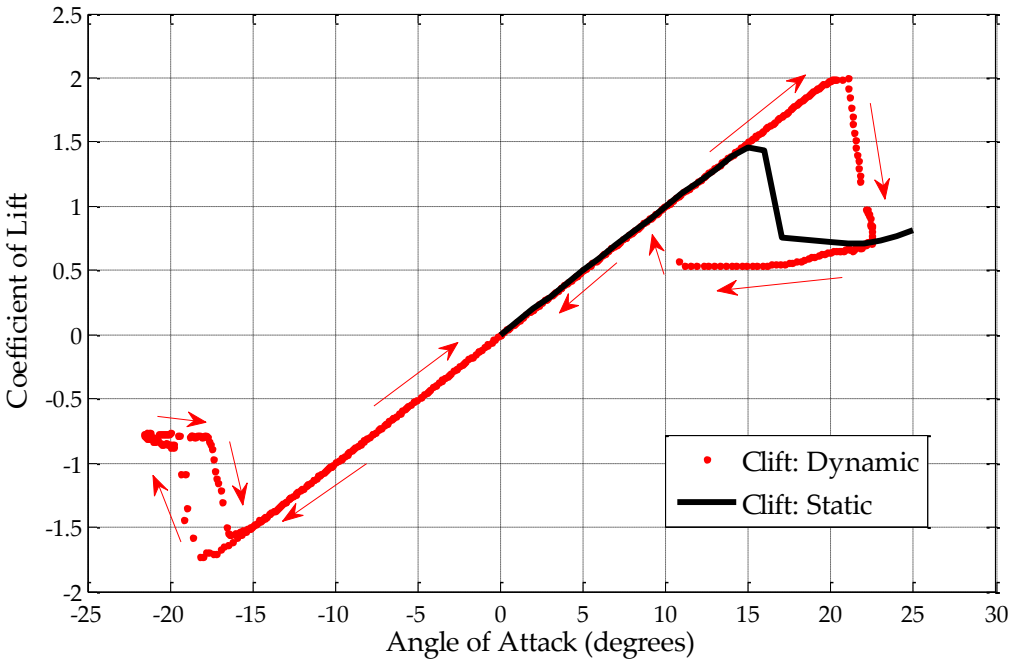

Figure 4-19: Hysteresis loop for baseline turbine at λ = 2.5

A key element of dynamic stall is the hysteresis loop associated with the onset of stall followed by flow reattachment. A plot of C_L against α for the baseline turbine at λ = 2.5 is presented in Figure 4-19 which demonstrates that StrathDMS captures this effect. The solid line is the static lift curve for the NACA 0012 aerofoil that was used to simulate the baseline turbine. The static data demonstrates α_{ss} = 16°. From this static data, Gormont's method is successfully implemented in StrathDMS to generate dynamic lift data which is represented by the data points. The arrows indicate the chronological order that the dynamic data points are generated as the blade rotates. The key aspects of dynamic stall are captured; delay of stall onset to a higher value of α; dynamic lift coefficient exceed the maximum of the static lift data; when stall does occur, the dynamic lift coefficients are significantly lower than the static coefficients; and the stalled condition is maintained until α drops significantly lower than the static stall angle. A hysteresis loop also exists downstream where C_L are negative and in this region the impact of

dynamic stall is reduced. This is a consequence of the use of an empirical factor in the Gormont model with smaller magnitude for this region compared to the upstream region. A reduced impact of dynamic stall is expected downstream because the turbulent wake of the upstream blades and tower will reduce the impact of dynamic stall.

4.9 Model Validation

In order to validate this analytical model, predicted output is compared with real experimental data published for two fixed pitch and two variable pitch VAWTs.

4.9.1 Fixed Pitch Experimental Data

4.9.1.1 Musgrove VAWT 450

The first validation is a comparison of the global aerodynamic performance of the Musgrove VAWT 450. The parameters defining the rotor are provided in Table 4-2 and full details of the turbine geometry and the site test results can be found in [37].

Table 4-2: Rotor details for the Musgrove 450 H-rotor turbine.

# of Blades	Radius (m)	Chord (m)	Blade Length (m)	Aerofoil
2	12.5	1.25	18	NACA0015

The comparison between test data and StrathDMS estimations is provided in Figure 4-20. Drag due to the support structure for this turbine may explain the discrepancy at all λ. This turbine was equipped with a rotor furling mechanism that allowed the blades to hinge at their midpoint to provide overspeed protection. The support for this mechanism and the blade support arms introduced heavy drag penalties. This would be most apparent for high λ where the blades rotate fast and angles of attack are very small and

therefore drag dominates lift. The basic NACA aerofoil data used for this simulations did not account for any extra drag.

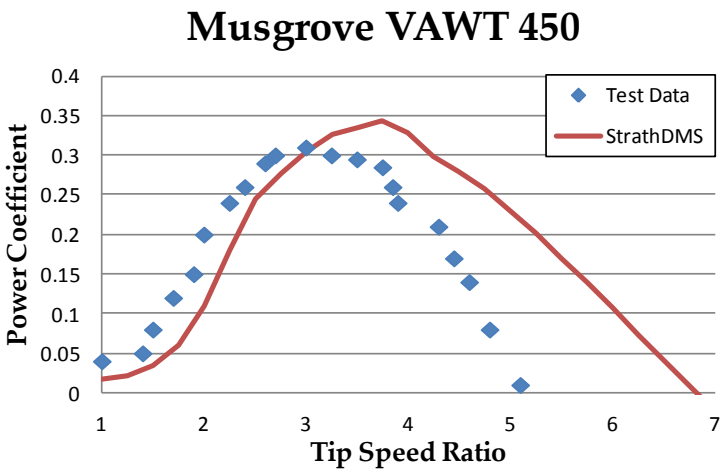

Figure 4-20: Comparison of test data with StrathDMS simulations for the VAWT 450.

4.9.1.2 Musgrove VAWT 850

The larger straight blade VAWT 850 from the Carmarthen Bay test facility is also used to validate StrathDMS. The parameters defining this rotor are provided in Table 4-2 and full details of the turbine geometry and the site test results can be found in [34].

Table 4-3: Rotor details for the Musgrove 850 H-rotor turbine.

# of Blades	Radius (m)	Chord (m)	Blade Length (m)	Aerofoil
2	17.5	2	24.3	NACA0012

The comparison between test data and StrathDMS predictions is provided in Figure 4-21. The C_{Pmax} value and λ_{opt} are predicted well. Prediction is far better here than for the VAWT450. There are two significant differences that may explain the improvement in simulation accuracy. First is that the folding blade overspeed protection was removed for the VAWT850 so there would have been far less parasitic drag. In addition the radius was much bigger. This allows more chance of full pressure recovery between up and down stream. For smaller turbines, a DMS model may overestimate how

much pressure recovery occurs, which would naturally lead to overestimation of aerodynamic performance. While the simulations are very close to experimental data for the VAWT 850, the lack of any means to model the parasitic drag may explain the discrepancy at high λ.

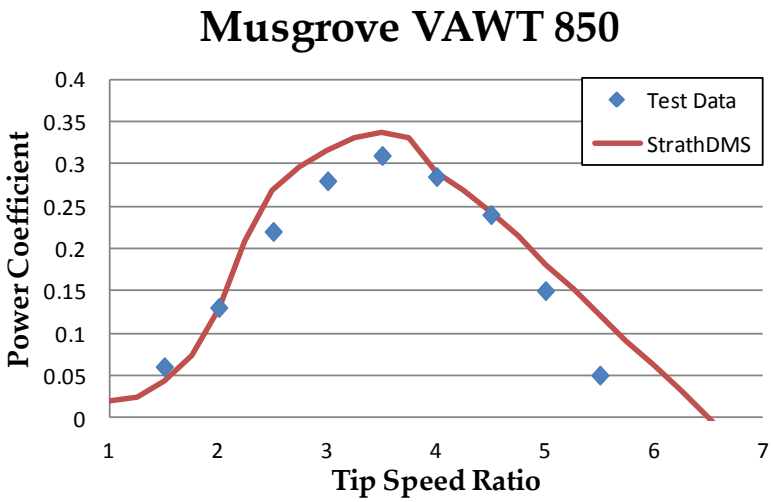

Figure 4-21: Comparison of test data with StrathDMS for the VAWT 850.

4.9.2 Variable Pitch Experimental Data

StrathDMS has the ability to assess the performance of blade pitch regimes. Here two small scale turbines are used to validate the impact of variable pitch on turbine aerodynamic performance.

4.9.2.1 Voith-Schneider Inspired Turbine

Madsen and Lundgren published results from a field test of a small scale variable pitch straight bladed VAWT [24]. Data are available on power coefficient and reduction in wind speed at the blades. The dimensions of the rotor are provided in Table 4-4 and the sinusoidal pitch regime that was selected is given by (4-31). Note that this expression is stated in the convention used in this thesis.

$$\beta(\theta) = 6.6\cos(\theta) + 3.1 \quad \textbf{(4-31)}$$

Table 4-4: Rotor details for the Voith-Schneider turbine built and tested by Madsen and Lundgren.

# of Blades	Radius (m)	Chord (m)	Blade Length (m)	Aerofoil
3	1.4	0.28	3.3	NACA0015

Figure 4-22 is a comparison of experimental results with predicted power coefficients generated by simulating the turbine with StrathDMS. There is spread in the experimental data but it is clear that StrathDMS predicts C_{Pmax} and λ_{opt} with sufficient accuracy. Parasitic losses from the drag on support structures is modelled using the correction proposed by Vandenberghe in [60] as given in (4-32). The justification is that it was generated for application to a similar small pitching VAWT with equal solidity.

$$C_{Ploss} = 0.333(\lambda^3 + \lambda) \quad \textbf{(4-32)}$$

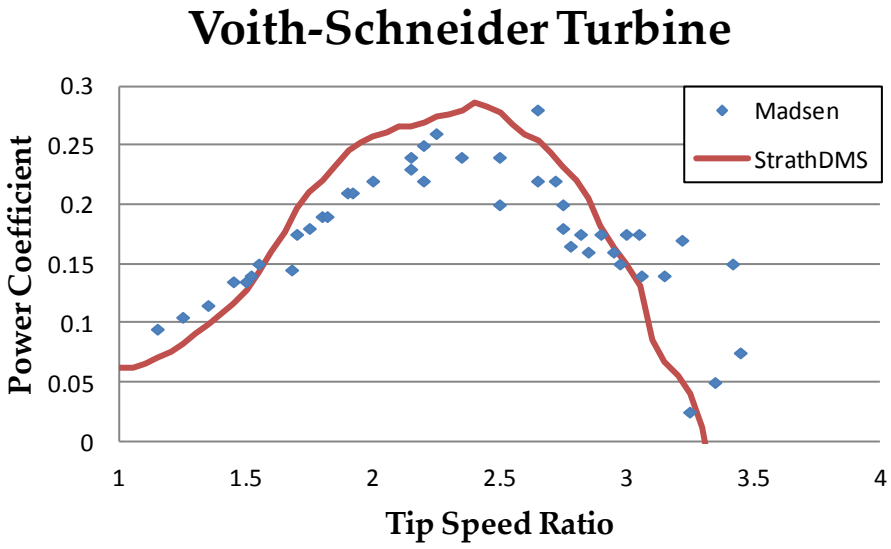

Figure 4-22: Predictions for the Voith-Schneider VAWT generated by StrathDMS compared with experimental data. Power coefficient against tip speed ratio.

Madsen and Lungren also provided measurements of the azimuthal variation of wind blockage provided by the turbine at λ=2.8. This is very useful because it can be used to validate induction factors which are the core of the momentum based modelling approach. Figure 4-23 is a comparison of experimental data with predictions from StrathDMS for the wind local to the blade in the streamwise direction normalised by the free stream velocity. This value is labelled U_{blade}/U_{inf} and is equivalent to 1 – a. StrathDMS clearly generates accurate estimations of the induction factors despite the fact that they are consistently slightly higher than the experimental data. Lower predicted values in this figure implies over-prediction of a, and hence over-prediction of the slowing of U_{inf}. One potential explanation for this is that StrathDMS does not include lateral induction in the y dimension and hence may slightly over-predict how much slowing of the wind there is in the x direction.

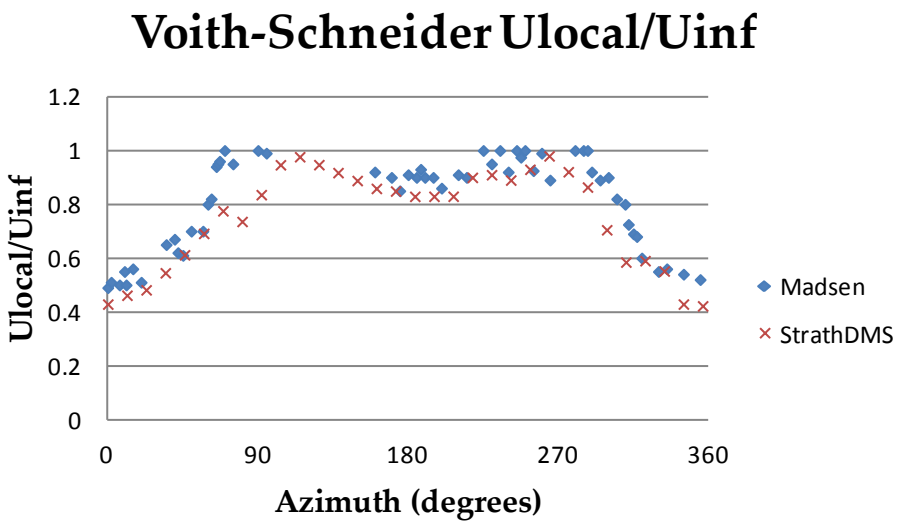

Figure 4-23: Predictions for the Voith-Schneider VAWT generated by StrathDMS compared with experimental data. Wind velocity at blade normalised by free stream wind velocity as a function of azimuthal position for λ = 2.8.

4.9.2.2 Vandenberghe and Dick Turbine

Vandenberghe and Dick published results from wind tunnel tests for a variable pitch VAWT [25]. The dimensions of the rotor are provided in Table 4-5.

Table 4-5: Rotor details for the variable pitch VAWT built and tested by Vandenberghe and Dick.

# of Blades	Radius (m)	Chord (m)	Blade Length (m)	Aerofoil
3	0.5	0.1	0.6	NACA0012

A free vortex model was used by the same group of authors to determine the optimum pitch regime for this turbine [60]. The resulting harmonic pitch control law is given in (4-33). This assumes the convention that $\theta = 0^o$ occurs at 90^o according to the convention in this thesis. (4-33) is the second order optimal pitch regime and to get the first order regime in (4-34), the expression is truncated at the first order θ terms.

$$\beta(\theta) = 2.4 - 2.0\cos(\theta) + 10.3\sin(\theta) - 0.5\cos(2\theta) - 3.4\sin(2\theta) \quad \textbf{(4-33)}$$

$$\beta(\theta) = 2.4 - 2.0\cos(\theta) + 10.3\sin(\theta) \quad \textbf{(4-34)}$$

Figure 4-24 is a comparison of experimental results with predicted power coefficients generated by simulating the Vandenberghe turbine with StrathDMS. Figure 4-24 a) shows results for the first order pitch regime and Figure 4-24 b) shows results for the second order pitch regime. For both a) and b) the correction for structural drag losses given in (4-32) is used. The comparison in a) demonstrates that StrathDMS can accurately predict the maximum C_P, λ_{opt} and performance for the first order pitch regime at all operating regions. The comparison in b) shows that for the second order pitch regime, StrathDMS over-estimates efficiency for the range $1.5 < \lambda < 2.5$

and the predicted λ_{opt} is slightly low. Nevertheless, the predicted C_{Pmax} is accurate and the fall off trend in performance for high λ is accurate.

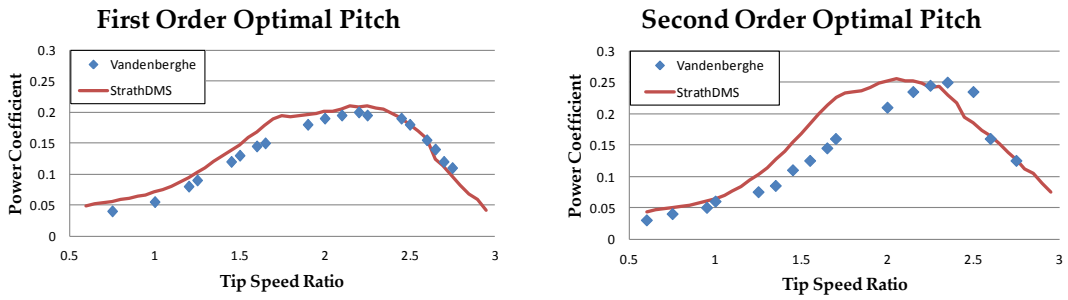

a) First order optimal control regime **b) Second order optimal control regime.**

Figure 4-24: Power coefficient against tip speed ratio for the Vandenberghe and Dick VAWT. Estimated C_P from StrathDMS is compared with experimental results.

4.10 Summary

One of the contributions of this thesis is a bespoke aerodynamic estimation model capable of simulating the performance of variable pitch, piecewise linear blade VAWTs. This chapter outlines the model developed with a particular focus on the novel contributions contained within this model. The model is called StrathDMS and it is built upon the principles of the double multiple streamtube method.

A full account of Sharpe's streamtube expansion formulation is provided. This leads to demonstration of a novel concept called fanning, which explains why it is difficult to accurately define a VAWT blade in an actuator surface model which permits streamtube expansion. The flow state approach to determining induction factors is demonstrated with evidence that the hysteresis associated with stall is captured. Also, a discussion is provided, with regard to the accurate implementation of a pitch regime and to the design of a pitch regime in an actuator surface framework.

Correction factors for tip loss and dynamic stall are developed that can be switched on and off for simulations. A sensitivity analysis is carried out to explore what elements of turbine design have an effect on the impact of these correction factors. Ratio of blade length to radius has a significant impact on tip loss while solidity has a significant impact on dynamic stall effects.

Reynolds number can vary significantly for a VAWT around the path of rotation and StrathDMS captures this by recalculating Reynolds number for each location and for every potential induction factor.

Finally, a validation is presented for StrathDMS. Two medium scale fixed pitch VAWTs and two small scale variable pitch VAWTs are simulated and aerodynamic performance is compared with experimental data. It is clear that this design tool is accurate at predicting overall aerodynamic performance for the whole C_P-λ curve and in particular, defining features such as λ_{opt} and C_{Pmax}. StrathDMS generates far more conservative predictions of aerodynamic performance compared with the majority of published simulations. Furthermore, a comparison with the data from the small scale Voith-Schneider VAWT demonstrated that StrathDMS generates accurate predictions of induction factors when a pitch regime has been implemented.

Chapter 5

Rotor Design and Control Analyses for Fixed Pitch VAWTs

5.1 Introduction

The previous chapter outlined the development of a design tool which can be used to carry out aerodynamic investigations for both stall and pitch controlled piecewise linear blade vertical axis turbines. This chapter focuses exclusively on stall controlled, fixed pitch rotors and consists of three investigations facilitated by the design tool.

The first, in Section 5.2, is a general investigation of how peak aerodynamic performance varies with rotor geometry. A measure of VAWT aerodynamic performance based on lift to drag ratio is defined which permits comparison between H- and V-rotors, and with HAWT performance. The second investigation is a design study of the V-rotor concept in Section 5.3 exploring the impact of wind shear on V-rotor blade design. Finally Section 5.4 utilises aerodynamic performance look up tables, generated by the design code, to drive a dynamic model of a stall regulated V-rotor. The

dynamic model exhibits fluctuating power as a consequence of torque ripple and a control based approach is developed for minimising large fluctuations in power generated from VAWT farms when individual turbines are aggregated.

5.2 Effective Lift to Drag Ratio for VAWTs

This section introduces an effective lift to drag ratio for a VAWT design based on averaged torque per cycle. This metric is used to characterise the relationship between overall optimum aerodynamic performance and design parameters. The DMS aerodynamic estimation model, StrathDMS, is employed to demonstrate the impact of effective lift to drag ratio and solidity (σ = Nc/R) on optimal power performance for the H-rotor. A further study investigates the impact of effective lift to drag ratio and coning angle, γ, for the V-rotor.

For a given blade number and chosen aerofoils, an optimum wind turbine rotor can, within limits, be designed for any desired tip speed ratio. However, a specific λ related to these choices will result in an overall maximum power coefficient. Figure 5-1 is taken from [6] and it demonstrates this λ relationship for HAWT design. This plot shows how lift to drag ratio and number of blades influences maximum achievable C_P and the λ_{opt} at which it occurs. For the optimal rotor design in [6] the approximation is made that all blade segments operate at their maximum lift to drag ratio. As a VAWT operates with intrinsically variable angle of attack in each cycle of rotation, the blade sections cannot operate at a fixed lift to drag. This section defines an effective lift to drag ratio for a VAWT design based on averaged torque per cycle and this metric is then used to characterise the relationship

between overall optimum aerodynamic performance and design parameters for straight blade VAWTs.

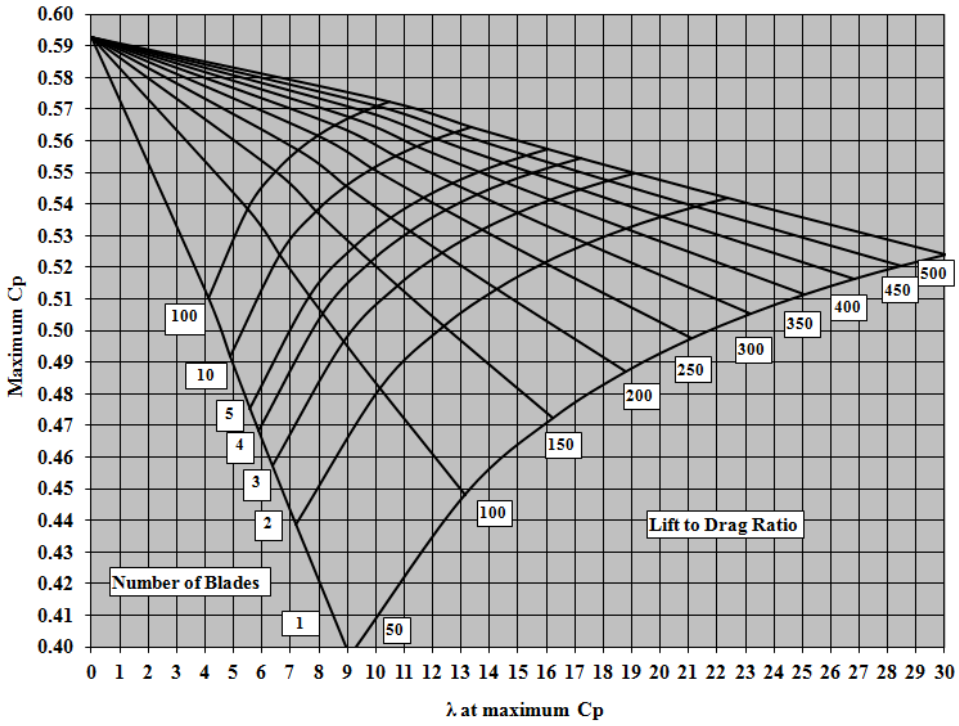

Figure 5-1: Influence of blade number and lift to drag ratio on HAWT C_{Pmax} and λ_{opt} [6]

5.2.1 Definition of Effective Lift to Drag Ratio for VAWTs

Current HAWTs attain a C_{Pmax} exceeding 0.5, at λ_{opt} beyond 8. This is achieved by maintaining a lift to drag ratio between 100 and 120 with the present aerofoils preferred for large HAWT blades [6]. The C_{Pmax} and λ_{opt} of a VAWT also depend on a lift to drag ratio but, because of the variation of angle of attack in each cycle of rotation, the relevant lift to drag ratio is an "effective" one which, unlike the HAWT design, is much lower than the maximum lift to drag ratio of the aerofoil section.

The **effective lift to drag ratio**, L/D_{eff}, for a VAWT is defined as follows. For a given turbine at a particular λ, the averaged torque per cycle is determined and an azimuthal position is found that produces an

instantaneous torque equal to the averaged torque. The lift to drag ratio at this azimuthal position is selected as the indicative lift to drag ratio for that turbine. Averaged torque here refers to the total torque provided by the rotor divided by the number of azimuthal positions. Once an indicative azimuthal position has been selected as the location to calculate L/D_{eff}, the lift provided by the whole blade at that position is divided by the drag created by the whole blade. This is done because a V-rotor will exhibit variation in lift and drag along the blade.

This new measure of aerodynamic performance of a VAWT is used in this section to investigate optimal performance of the H-rotor and V-rotor concepts. Islam et al. [140] investigated how the various lift to drag ratios for different aerofoils affected VAWT performance. In the present investigation one set of aerofoil data is selected and manual adjustment of the drag coefficients allows examination of how variation in L/D_{eff} affects rotor performance.

5.2.2 Simulation Set-Up

In this section the methodology followed to explore the impact of L/D_{eff} on optimal straight blade VAWT aerodynamic performance is outlined.

This is an optimal rotor investigation and the aim is to determine maximum achievable aerodynamic performance so tip loss is switched off. For all simulations in this section, the actuator surface resolution is prescribed by $N_t = 32$ and $N_s = 10$. The aerofoil selected is the NACA0012 and the coefficients associated with base case simulations were discussed in Section 0.

For any given rotor geometry, this investigation considers eight different L/D_{eff} by generating eight different sets of drag coefficients by

adjusting the base case data. The base case drag coefficients are the unadjusted NACA0012 drag coefficients; the infinite lift to drag ratio case has zero as all drag coefficients; the other six sets of drag coefficients are generated by amending the base case drag coefficients by an additive correction of one of the values from the following set [-0.01, -0.005, +0.005, +0.01, +0.02, +0.05].

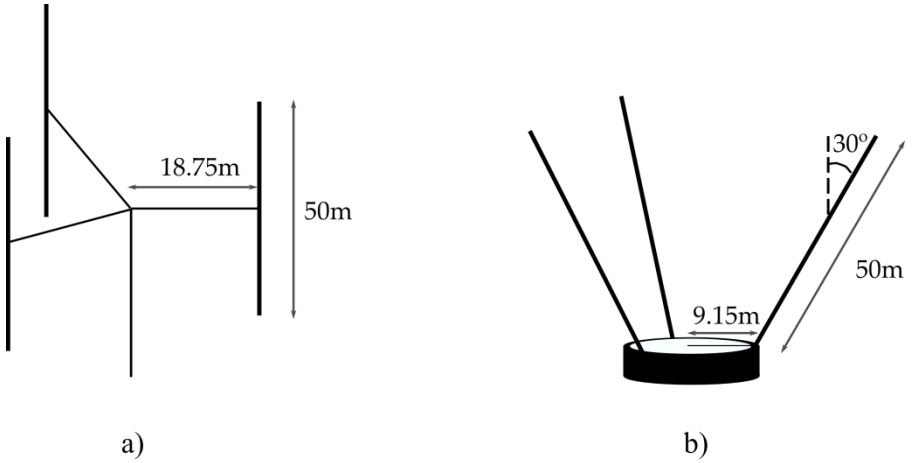

Figure 5-2: Test turbines for the investigation of impact of L/D_{eff} on optimal VAWT aerodynamic performance.

This investigation addresses optimal aerodynamic design of the H-rotor and V-rotor concepts. The first investigation is optimal aerodynamic design of the H-rotor concept. The aim is to identify the effect of L/D_{eff} on optimal H-rotor aerodynamic performance and then investigate the impact of σ on H-rotor design. The second investigation is optimal aerodynamic performance of the V-rotor concept. The aim is to identify the effect of L/D_{eff} on optimal V-rotor aerodynamic performance and then investigate the impact of coning angle on V-rotor design. The baseline rotor configurations are shown in Figure 5-2.

5.2.3 Optimal H-Rotor Design

5.2.3.1 Impact of L/D_{eff} on H-Rotor Aerodynamic Performance

The following procedure is used to determine the optimal H-rotor turbine performance. For any particular λ, the rotor aspect ratio (l/R) and σ are varied in order to determine the aerodynamically optimal rotor geometry that generates a global C_{Pmax} for that λ. Repeating this for a range of λ generates a theoretical idealised C_P-λ curve. The L/D_{eff}, occurring at λ_{opt} for this idealised C_P-λ curve, is indicative of that curve. Subsequently, the aerofoil drag data is shifted by a scalar and the same procedure followed to generate a new ideal C_P-λ curve for a different L/D_{eff}. Eight different idealised C_P-λ curves are generated, each classified by a different L/D_{eff}.

The influence of L/D_{eff} on optimal H-rotor aerodynamic performance is shown in Figure 5-3. The base case simulation attains a global C_{Pmax} of 0.42 at λ_{opt} of 3.3. The infinite lift to drag case demonstrates C_P which approaches 0.5 asymptotically as λ increases, which is an increase of 19%. The lowest lift to drag case results in a C_P-λ performance curve with C_{Pmax} of only 0.22 at λ_{opt} = 2.75. Furthermore, increasing the L/D_{eff} from 15 up to 65 increases λ_{opt} from 2.75 up to 4.5. It is clear that increasing L/D_{eff} increases both the maximum attainable C_P and the optimal rotational speed.

The C_P-λ curves in Figure 5-3 are idealised because σ can vary with λ to attain the optimal C_P for each λ. To illustrate this variation in σ, Figure 5-4 is a plot of optimal σ against λ for the baseline H-rotor with L/D_{eff} = 45. Generally, σ_{opt} decreases as design λ increases. There is a steep decrease in σ_{opt} for design λ between 0.5 and 2.5, then for design λ > 2.5 the σ_{opt} is significantly less sensitive to design λ. This reveals that for VAWTs that are designed to operate with relatively low λ, σ is an important design

parameter. Alternatively the figure suggests that VAWTs that have been built with large σ should be operated at relatively low λ.

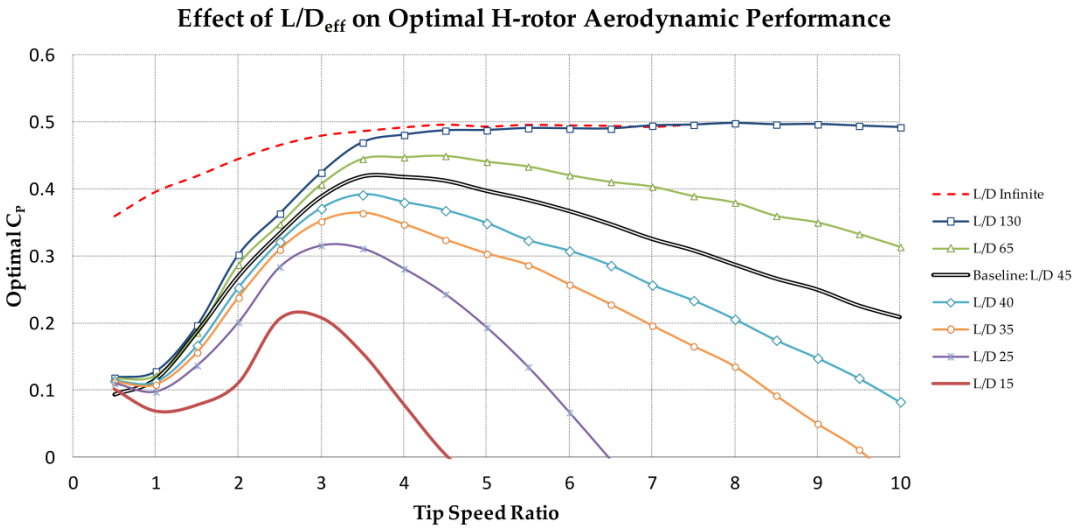

Figure 5-3: Theoretical idealised C_P-λ curves parameterised by L/D_{eff}.

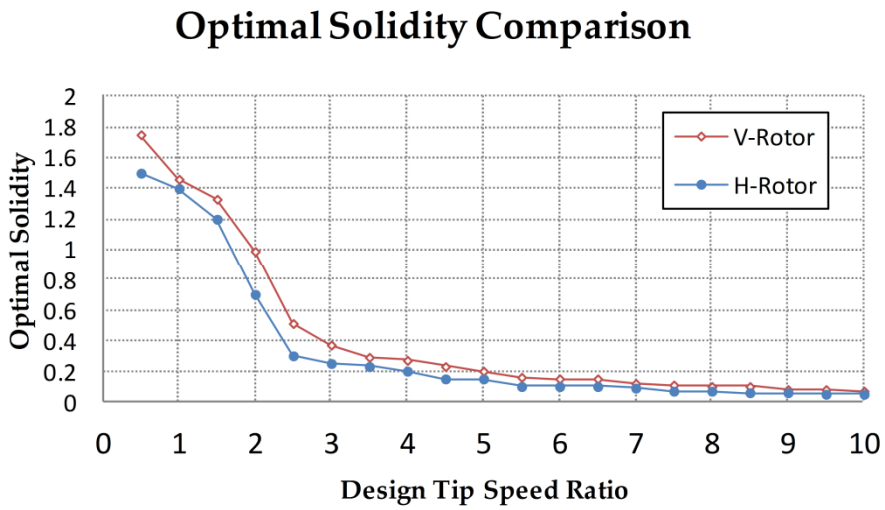

Figure 5-4: Optimal solidity of the test rotors as a function of design tip speed ratio.

5.2.3.2 Impact of Solidity on H-Rotor Design

To assess the impact of σ on H-rotor design, the three blade H-rotor illustrated in Figure 5-2 a) is used which has l/R = 2.67. Chord length is fixed

originally at 0.75m so $\sigma = 0.12$ and a C_P-λ curve is generated using StrathDMS with NACA 0012 aerofoil data to determine (λ_{opt}, C_{Pmax}) for this turbine. Then, as before, the drag coefficients are shifted by a scalar to generate a different (λ_{opt}, C_{Pmax}) for that choice of σ which is classified by a different L/D_{eff}. Subsequently, the same method is repeated as σ varies. Ultimately sets of (λ_{opt}, C_{Pmax}) pairs are generated for each σ. These can be used to examine how optimum performance varies with both L/D_{eff} and σ.

The results of this procedure are presented in Figure 5-5. Each data point indicates a pair (λ_{opt}, C_{Pmax}) for a specific L/D_{eff} and σ. The solid lines connect the data points with the same L/D_{eff} and the dashed lines connect the data points with the same σ. The dashed lines are darker for higher solidity. This family of curves can be used to identify λ_{opt} and the idealised attainable C_{Pmax} if σ and L/D_{eff} are known. The thick double line represents the (λ_{opt}, C_{Pmax}) generated by StrathDMS when the baseline aerofoil data are used. Following this double line from left to right indicates that λ_{opt} increases as solidity decreases and there is a global C_{Pmax} of 0.42 at $\sigma = 0.2$. The other solid lines show the same analysis for different L/D_{eff}. This figure shows that for any L/D_{eff} there is a σ which attains a global C_{Pmax}. The best choice of σ is 0.2, independent of L/D_{eff} apart from the case with $L/D_{eff} = 130$ for which $\sigma = 0.16$ provides the global C_{Pmax}. The dashed lines are almost vertical for high σ indicating that L/D_{eff} has very little impact on λ_{opt} for high solidity turbines. Whereas for low σ, the dashed lines have a positive gradient showing that λ_{opt} is sensitive to L/D_{eff}, so improving L/D_{eff} allows higher λ_{opt} to be designed.

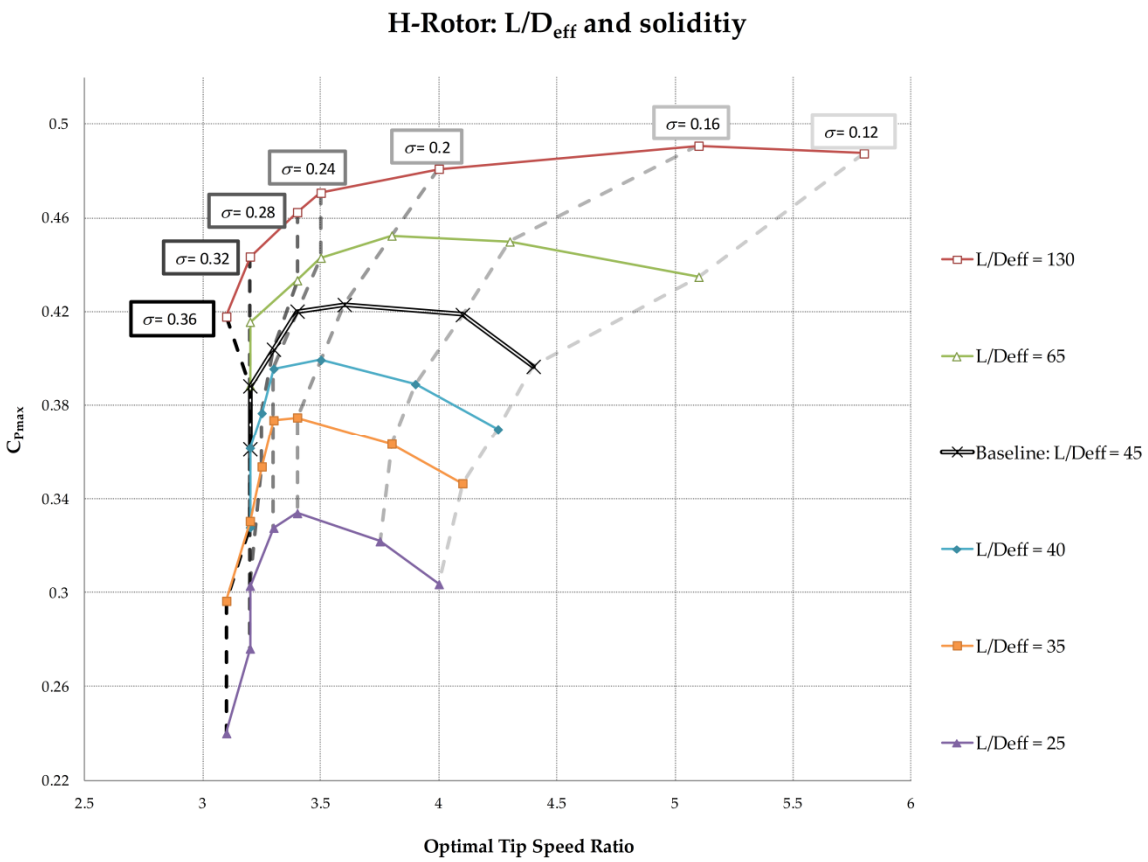

Figure 5-5: Impact of *L/D*$_{eff}$ and solidity on H-Rotor optimal aerodynamic performance.

5.2.4 Optimal V-Rotor Design

5.2.4.1 Impact of L/D$_{eff}$ on V-Rotor Aerodynamic Performance

The V-rotor configuration introduces a new degree of freedom to the geometry of the rotor; γ can vary in addition to σ and L/D_{eff}. While σ will in fact vary along the length of a V-rotor blade due to the change in local radius, σ refers to the tip. A simplification is made for this investigation that the chord length remains constant along the whole blade to reduce the number of degrees of freedom in the design so that a comparison can be made between γ and L/D_{eff}. Therefore, while a single value of σ will classify a particular V-rotor, the local solidity will in fact be larger towards the root.

The same procedure as in Section 5.2.3.1 is followed to determine the optimal aerodynamic performance for a base case V-rotor. Allowing γ to vary in the optimisation of rotor geometry drives it to zero to resemble an H-rotor; therefore a coning angle of 30° is selected for these simulations. As before, the simulation procedure permits different σ at each λ to generate eight different idealised C_P-λ curves, each classified by a different L/D_{eff}.

The impact of L/D_{eff} on optimal V-rotor aerodynamic performance for a turbine with $\gamma = 30^o$ is shown in Figure 5-6. The base case simulation attains a global C_{Pmax} of 0.34 at λ_{opt} of 5.5. The infinite L/D_{eff} case demonstrates C_P which approaches 0.45 asymptotically as λ increases, which is an increase of 32%. The lowest L/D_{eff} case results in a C_P-λ performance curve with C_{Pmax} of only 0.15 at $\lambda_{opt} = 3.5$. L/D_{eff} has a significant effect on the maximum aerodynamic performance that can be attained by a V-rotor VAWT. Furthermore, increasing the L/D_{eff} from 10 up to 70 increases λ_{opt} from 3.5 up to 6.5. It is clear that increasing L/D_{eff} increases both the maximum attainable power coefficient and the optimal rotational speed. Comparing these idealised C_P-λ pairs with a similar analysis for H-rotors in Figure 5-3, the H-rotor can attain significantly higher C_P values but the V-rotor achieves optimal performance at much higher λ which can potentially bring down the cost of the drive train by reducing the overall weight.

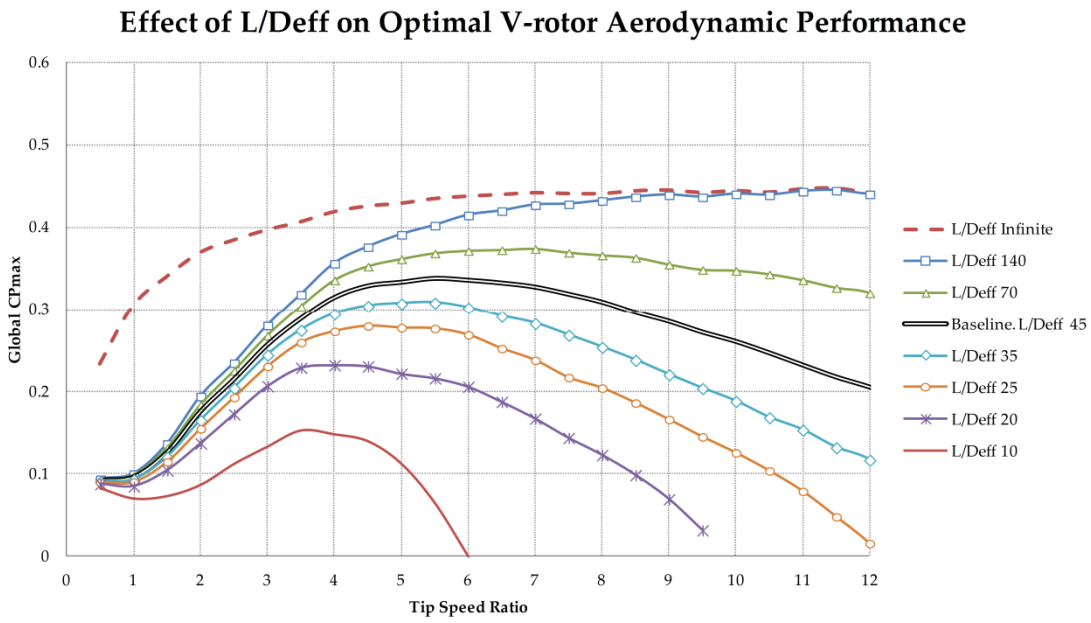

Figure 5-6: Idealised C_P-λ curves parameterised by L/D_{eff} for a V-rotor with $\gamma = 30^o$.

The C_P-λ curves here are idealised because σ can vary with λ to attain the optimal C_P for each λ. To illustrate this variation in σ, Figure 5-4 includes σ_{opt} against design λ for the baseline V-rotor with $\gamma = 30^o$ and $L/D_{eff} = 45$. As with the H-rotor, σ_{opt} decreases as design λ increases and high solidity V-rotor turbines are much more sensitive to design λ. The V-rotor has a consistently higher optimal solidity.

5.2.4.2 Impact of Coning Angle on V-Rotor Design

To assess the impact of γ, the base case V-rotor illustrated in Figure 5-2 b) is used with fixed blade length. In order to compare results with the H-rotor, it is important that a comparable V-rotor is designed. The swept area of 1875m^2 is maintained so both turbines interact with the same volume of air in any given period. The blade length of 50m is kept the same. The coning angle of $\gamma = 30^o$ dictates that the root radius is 9.15m. For this base case V-rotor, the same procedure as in Section 5.2.3.2 is followed with γ varied instead of σ. σ

can vary when searching for the global C_{Pmax} for a particular γ. For each γ this generates a set of (λ_{opt}, C_{Pmax}) with each one classified by a different L/D_{eff}. As γ varies in this investigation, the blade length changes to maintain a constant swept area with a constant root radius. Ultimately sets of (λ_{opt}, C_{Pmax}) pairs are generated for each γ. These can be used to examine how optimum performance varies with both L/D_{eff} and γ.

The results of this procedure are presented in Figure 5-7. Each data point represents a pair of (λ_{opt}, C_{Pmax}) for a specific L/D_{eff} and γ and the solid lines connect the data points with the same L/D_{eff}. The dashed lines represent the data points with the same γ and the dashed lines are lighter for higher γ. This family of curves can be used to identify λ_{opt} and the idealised attainable C_{Pmax} if γ and L/D_{eff} are known. The thick double line represents the (λ_{opt}, C_{Pmax}) generated by StrathDMS when the baseline aerofoil data are used. Following this double line from top to bottom it is observed that the achievable C_{Pmax} decreases with an increase in γ and $\gamma = 30^{o}$ is associated with the maximum λ_{opt} of 5.75. The other solid lines show the same analysis for different L/D_{eff}. This figure shows that for any L/D_{eff} there is a γ which attains a global maximum λ_{opt}. The dashed lines are almost vertical for $\gamma = 0^{o}$ when $L/D_{eff} < 45$ so λ_{opt} is not sensitive to L/D_{eff}. However, when L/D_{eff} is improved or γ is introduced, λ_{opt} becomes sensitive to L/D_{eff}.

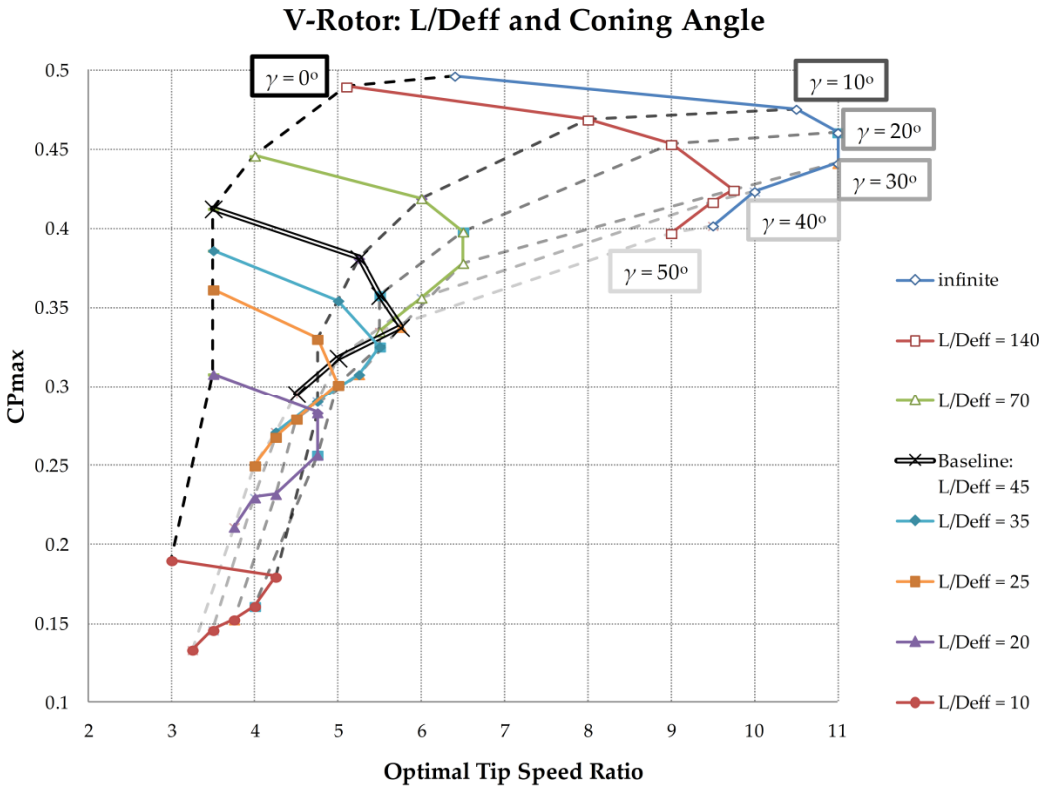

Figure 5-7: Impact of L/D_{eff} and γ on V-rotor optimal aerodynamic performance.

5.3 Impact of Wind Shear on V-Rotor Design

Within the atmospheric boundary layer, the variation of wind speed with vertical height is called wind shear. There is a tendency for wind speed to increase with distance from the ground and this can be approximated as a logarithmic relationship as illustrated in Figure 5-8 a). Wind shear has a significant impact on wind turbine design, especially for large MW scale rotors. In terms of HAWT design, wind shear contributes to fatigue of the blade by inducing cyclic loading [141]. The situation is different with VAWTs. Instead of experiencing a range of wind speeds caused by wind shear, any particular VAWT blade segment will experience a more steady incoming wind because the height of each blade segment is fixed for the

entire rotor cycle. This investigation exploits this difference and proposes VAWT blades that are designed to suit the logarithmic form of wind shear as shown in Figure 5-8 c).

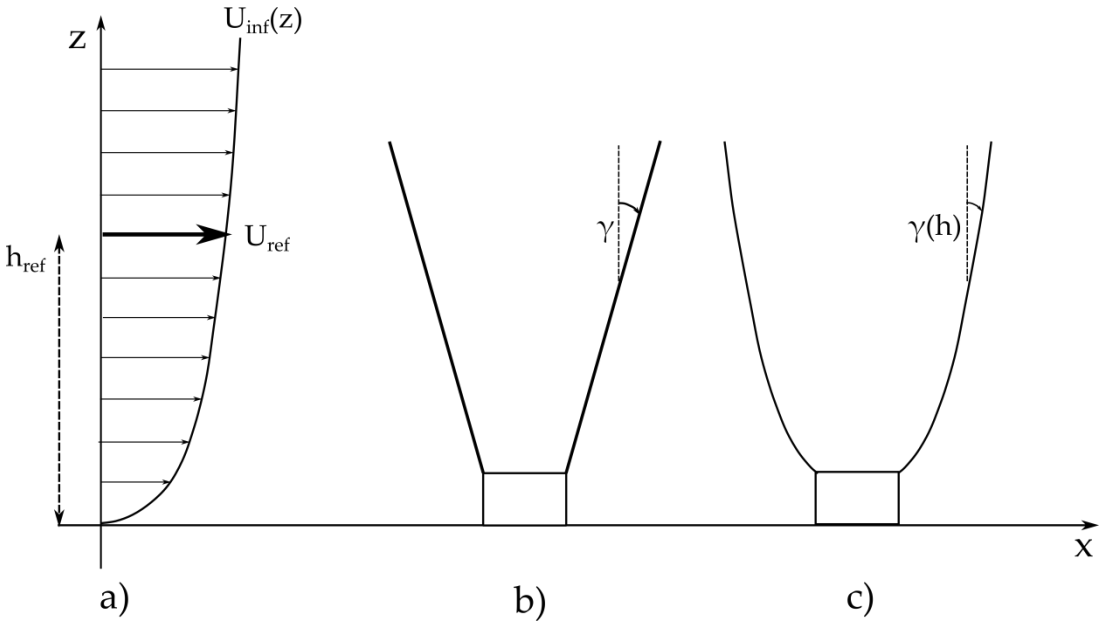

Figure 5-8: a) wind shear profile b) straight blade V-rotor c) logarithmic blade VAWT

This section begins with an introduction to wind shear. A curved blade is introduced and is referred to as a logarithmic blade because it reflects the logarithmic nature of the variation of wind speed with height. The performance of a rotor with this blade is compared to that of a similar sized V-rotor with straight blades. Subsequently, a sensitivity analysis is carried out to determine which factors of logarithmic blade design and the wind shear model have the most significant impact on potential performance improvements.

5.3.1 Wind Shear

Variation in wind speed with height is a consequence of complex processes occurring near the earth's surface [2]. Geostrophic wind is approximately

1km above the earth and is sufficiently high that it is not impacted by these surface processes. The region of the atmosphere below the geostrophic winds is known as the atmospheric boundary layer. Within the boundary layer, wind shear has a strong impact and its effects are significantly influenced by surface roughness. Surface roughness is a measure of the texture of a surface and it is characterised by the surface roughness length, z_0.Typical z_0 for a range of terrains are provided in Table 5-1 [2].

Table 5-1: Example surface roughness lengths

Terrain	Surface Roughness Length [m]
Cities, forests	0.7
Suburbs, wooded countryside	0.3
Villages, countryside	0.1
Open farmland, few trees and buildings	0.03
Flat grassy plains	0.01
Flat desert, rough sea 0.001	0.001

A suitable model for U_{inf} which accounts for wind shear is to describe the variation in wind speed as the logarithmic function of height given by (5-1). This model assumes a reference wind speed, U_{ref}, has been measured at some reference height, z_{ref} as illustrated in Figure 5-8 a).

$$U_{inf}(z) = U_{ref}\frac{\left(ln\frac{z}{z_0}\right)}{\left(ln\frac{z_{ref}}{z_0}\right)} \tag{5-1}$$

This logarithmic model of wind shear is implemented in StrathDMS by calculating a new $U_{inf}(z)$ for each blade segment.

5.3.2 Baseline Turbine and Simulation Set-Up

The swept area of a straight blade H- or V-rotor VAWT can be uniquely defined based on the following four parameters; height of the base, h_{base}; height of the rotor, h_{rotor}; radius at the base of the rotor, r_{base}; and radius at the tip, r_{tip}. These four design parameters are illustrated in Figure 5-9 and they can be used to infer the coning angle, γ. If the restriction to straight blades is relaxed then curved blades can be used while sustaining the same values for the four aforementioned rotor design parameters (although the swept area will change). A suitable comparison of rotors is to hold h_{base}, h_{rotor}, r_{base} and r_{tip} constant and compare the performance with a straight and logarithmic blade.

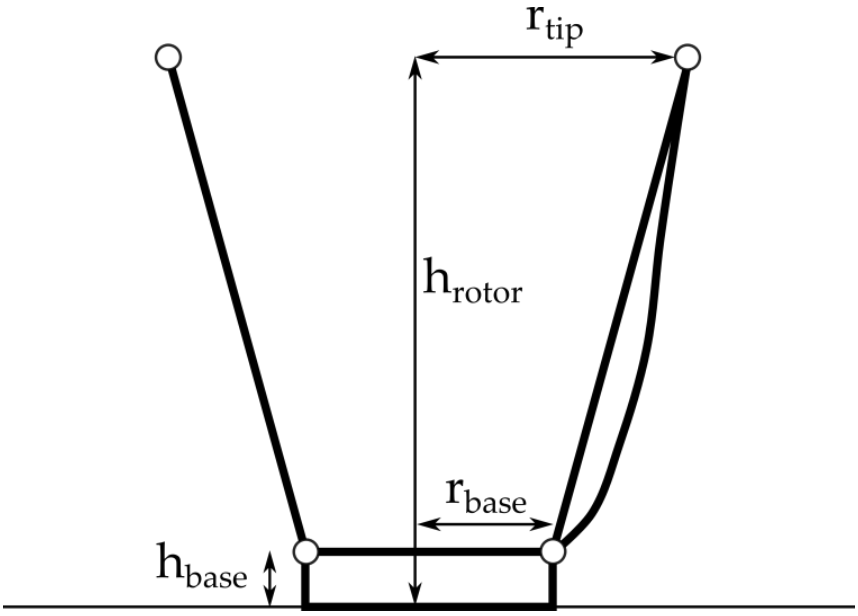

Figure 5-9: The rotor design parameters that remain the same with a straight blade and a logarithmic blade

For investigations throughout this section a baseline V-rotor is designed and the design parameters are provided in Table 5-2. The baseline values for the wind shear model are given in Table 5-3.

Table 5-2: Parameters for the baseline V-rotor design.

h_{base}	h_{rotor}	r_{base}	r_{tip}	γ	B	σ
20m	140m	15m	47m	15°	3	0.2

Table 5-3: Parameters for the baseline wind shear profile.

z_0	U_{ref}	z_{ref}
0.01m	12ms^{-1}	100m

In this section, all rotors considered have σ = 0.2 at the blade tip because the analysis in Section 5.2.3.2 demonstrates that it is a good choice for straight blade VAWT aerodynamics. Chord length is uniform along the blade and a NACA0012 profile is used for all simulations. For these investigations, StrathDMS is run with N_t = 32 and N_z = 30. Dynamic stall and tip loss are both switched on.

5.3.3 The Logarithmic Blade

A blade referred to as the logarithmic blade is proposed here to investigate if performance of a VAWT could be improved by incorporating the variation in the wind field due to wind shear into the design process for fixed pitch VAWT blades.

5.3.3.1 Design of a Logarithmic Blade

By using the form of the wind profile to determine how radius increases with height a blade is designed and referred to as the logarithmic blade. The form of the logarithmic blade is given in (5-2). Given the height and radius at the root and the tip of the rotor, this function describes the variation in radius with height of the logarithmic blade. The radius at any particular height is determined based on the variation in wind between that height and the root normalised by the total change in wind speed across the span of the whole

rotor. Since the wind shear is approximated by a logarithmic function given in (5-1), the radius reflects the assumed logarithmic nature of the wind.

$$r(z) = r_{base} + \left(\frac{U_{inf}(z) - U_{inf}(h_{base})}{U_{inf}(h_{rotor}) - U_{inf}(h_{base})} \right) \cdot \left(r_{tip} - r_{base} \right) \quad (5\text{-}2)$$

With the wind shear parameters; z_0, U_{ref} and z_{ref} defined and the rotor design parameters; r_{base}, r_{tip}, h_{base} and h_{rotor} defined, (5-2) describes the shape of the logarithmic blade. The same rotor design parameters r_{base}, r_{tip}, h_{base} and h_{rotor} can be used for both a straight blade and a logarithmic blade so they are kept the same for any comparisons.

5.3.3.2 Straight Blade and Logarithmic Blade Comparison

The first application of the logarithmic blade is to compare it with the baseline straight blade rotor defined by values in Table 5-2 by estimating performance of both with StrathDMS. The power generated and C_P are used to compare the overall performance. Analyses of the angle of attack and torque coefficient for blade segments at different positions along the blade are used to illustrate differences in performance.

The overall performance of the straight blade and the logarithmic blade for the baseline V-rotor dimensions are presented in Table 5-4. The logarithmic blade increases the power generated by 19.9%. This significant improvement in performance is misleading because the curved form of the logarithmic blade increases the swept area. A better comparison is C_P which does increase by 3.2% when the logarithmic blade is used.

Table 5-4: Power performance of straight and logarithmic blade for baseline V-rotor.

	Straight Blade	Logarithmic Blade	Change (%)
Power [MW]	2.719	3.259	19.9
Swept Area [m²]	7,457	8,633	15.8
Blade Length [m]	124.2	125.5	1
C_{Pmax}	0.312	0.322	3.2

In terms of rotor design, increasing swept area is appealing because it allows more wind to interact with the rotor. However, this comes at the cost of the extra material required to increase the size of the rotor. The logarithmic blade increases the swept area by 15.8% with only a 1% increase in blade length. In comparison, if a HAWT with the same swept area of 7,457m² were to increase blade length by 1%, the swept area would increase by only 2%.

The C_P-λ curves generated by StrathDMS for the straight blade and the logarithmic blade for the baseline V-rotor dimensions are shown in Figure 5-10. The logarithmic blade attains a higher C_{Pmax} and it consistently achieves higher C_P for $\lambda < 4.5$. For higher λ the straight blade achieves higher C_P.

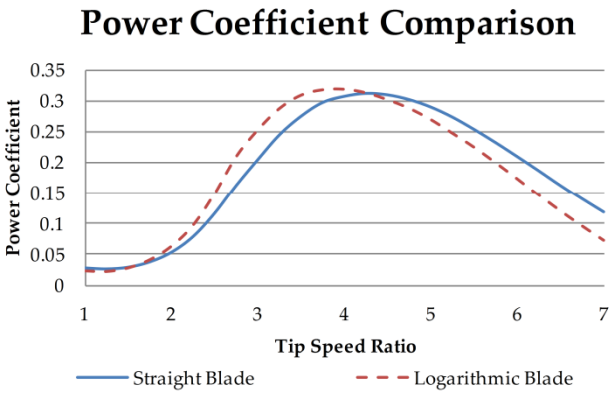

Figure 5-10: C_P-λ curves for the baseline V-rotor dimensions.

In order to identify why performance improves with the logarithmic blade, Figure 5-11 plots α and torque coefficient against θ for λ = 3.5 at three different positions along the blade; root, middle and tip. The plots a), c) and e) of α reveal that the logarithmic blade reduces $|\alpha|$ significantly at the root and at the middle but there is very little difference at the tip. This is due to the fact that the logarithmic blade increases the local radius compared to the straight blade for the bottom half of the blade. Therefore there is a larger component of wind due to rotation influencing the effective wind (see Figure 4-9), decreasing φ, and α directly since this is a fixed pitch turbine. The plots in Figure 5-11 b), d) and f) show how the different blade types impacts torque contribution. At the blade root, reduction of $|\alpha|$ with the logarithmic blade has diminished the torque contribution between $90^o < \theta < 135^o$ and stall occurs for both blades between $180^o < \theta < 255^o$. Downwind the logarithmic blade does not experience such deep stall and it provides more torque between $290^o < \theta < 5^o$.At the middle of the blade, the logarithmic blade avoids stall for the whole rotor cycle. This is kinder to the blade, but the straight blade does provide more torque for all of the downwind portion and between $90^o < \theta < 185^o$. At the tip due to the fact that both blades experience similar α, the torque contributions are very similar. The ability of the logarithmic blade to avoid stall explains why it achieves better C_P for low λ.

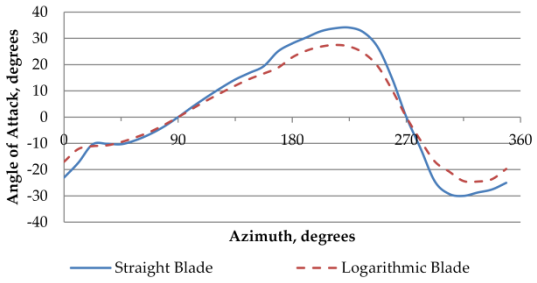

a) α against θ at blade root

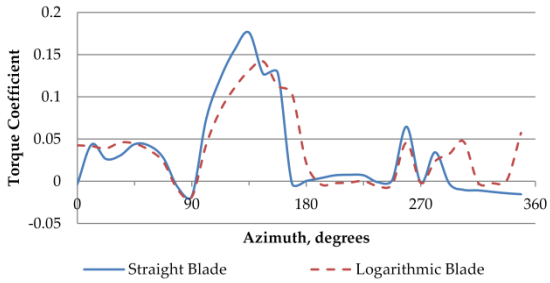

b) C_Q against θ at blade root

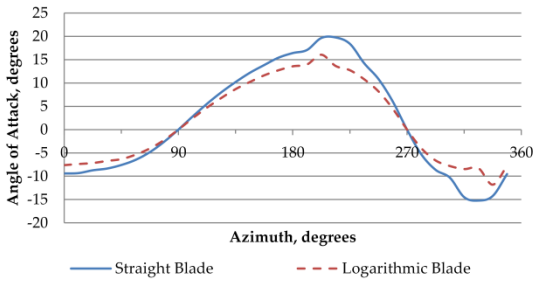

c) α against θ at blade midpoint

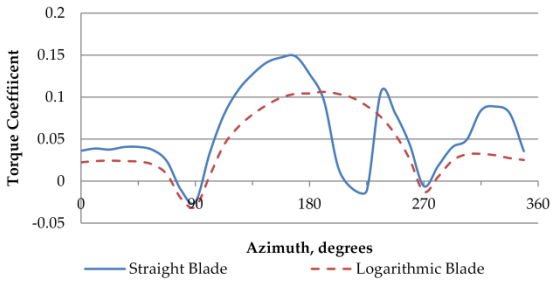

d) C_Q against θ at blade midpoint

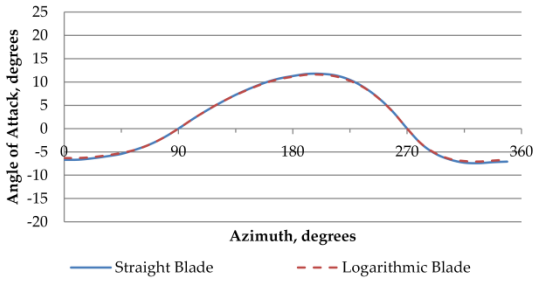

e) α against θ at blade tip

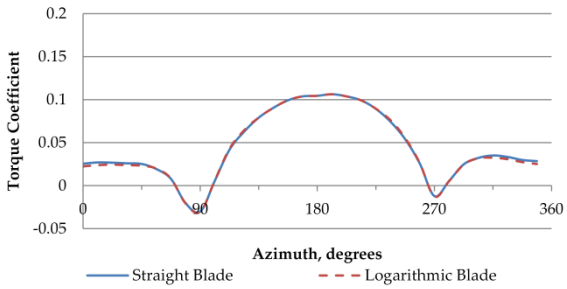

f) C_Q against θ at blade tip

Figure 5-11: Variation of α and Torque Coefficient with θ at different points along the baseline rotors, λ = 3.5.

5.3.3.3 Logarithmic Blade Design Sensitivity Analysis

A sensitivity analysis is conducted to investigate which parameters of the V-rotor design and the wind shear model are most significant. All other parameters are held at the baseline values while one parameter varies to quantify how it impacts on performance of the logarithmic blade compared to the straight blade.

The impact of the rotor design parameters are analysed first before investigating the impact of the wind shear model parameters.

The four design parameters that define the swept area of a straight blade V-rotor design are h_{base}, h_{rotor}, r_{base} and γ. Since they can be combined to calculate r_{tip}, they can be used with (5-1) to generate a logarithmic blade. Each

design parameter is allowed to vary between 0.25 and 2 times of the baseline value with a resolution of 0.25. For example, r_{base} is varied between 3.75m and 30m with a resolution of 3.75m. For each value of r_{base} the procedure outlined in Section 5.3.3.1 is followed to design a logarithmic and associated straight blade. Both are simulated in StrathDMS and the difference in C_P is stored.

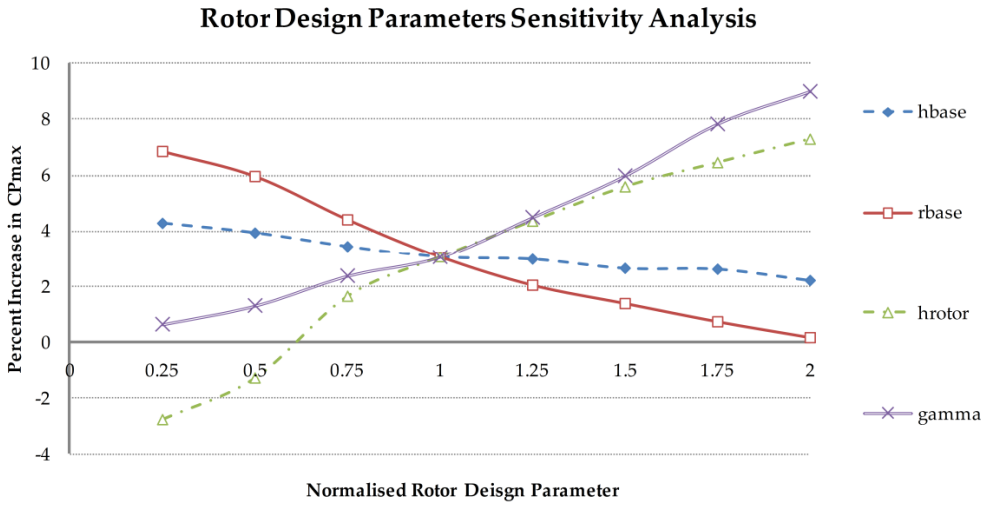

Figure 5-12: Sensitivity of the rotor design parameters.

In Figure 5-12 the percentage increase in C_{Pmax} when a logarithmic blade is used compared to a straight blade is plotted as each rotor design parameter is allowed to vary. All lines pass through (1, 3.2%) because this refers to the baseline case, investigated in the previous section, where the logarithmic blade provides a 3.2% increase in C_P.

The decreasing solid line in Figure 5-12 illustrates the impact of r_{base}. The logarithmic blade can increase C_{Pmax} by 7% when r_{base} = 3.75m. As r_{base} increases, the logarithmic blade has less impact and by r_{base} = 30m the logarithmic blade only increases C_{Pmax} incrementally. A V-rotor with uniform blade thickness and low r_{base} will have a relatively high local solidity towards the root of the blade and the logarithmic blade significantly increases r in this

region of the rotor. This helps to alleviate performance penalties by reducing the high local solidity near the blade root.

The decreasing dashed line illustrates the impact of h_{base}. As h_{base} increases, the logarithmic blade has less potential for improvement in C_{Pmax}. This shows that the logarithmic blade has higher potential to improve performance when the root of the blade operates closer to the earth's surface, where increases in wind speed with height are at their largest.

The increasing solid line illustrates the impact of γ. For γ = 3.75°, the logarithmic blade does not significantly alter the swept area but it still improves C_{Pmax} by 0.75%. For V-rotors with larger γ, to achieve good aerodynamic performance, a certain chord length must be selected which achieves solidity of 0.2 near the tip because the top half of the blade does most of the aerodynamic work. If the chord length is uniform, the root of the blade will have large local solidity. This issue is exacerbated for larger values of γ. The logarithmic blade increases r near the root of the blade and hence decreases local solidity, so it has higher potential for improvement for larger γ. For γ = 30° the logarithmic blade increases C_{Pmax} by 9%.

The increasing dashed-dotted line illustrates the impact of h_{rotor}. The logarithmic blade decreases C_{Pmax} when h_{rotor} = 30m and h_{rotor} = 60m. Then as h_{rotor} increases past 90m the logarithmic blade begins to increase C_{Pmax}. For h_{rotor} = 240m the logarithmic blade increases C_{Pmax} by 7.2%. This variation in the influence of h_{rotor} is a consequence of restricting the same r_{tip} for both blade types. When h_{rotor} is small, the blade operates entirely in heights where the effects of wind shear are significant; however the restriction on r limits the potential of the logarithmic blade. In the case of h_{rotor} = 30m, the maximum r can be is r_{tip} = 23m (when all other parameters are kept at the baseline values).

However, when h_{rotor} = 240m the logarithmic blade permits much larger values of r at the low z where wind shear effects are most significant.

A similar sensitivity analysis is carried out for the parameters that influence the wind shear model. These parameters are z_0, U_{ref} and z_{ref} and instead of applying normalised variation in the parameters, a range is selected for each parameter. The range for these parameters is provided in Table 5-5.

Table 5-5: Wind shear model parameter ranges for sensitivity analysis.

Wind Shear Model Parameter	Range
z_0 [m]	0.005, 0.01, 0.05, 0.1, 0.25, 0.5, 0.75, 1
z_{ref} [m]	10, 25, 50, 75, 100, 125, 150, 175, 200
U_{ref} [ms^{-1}]	6, 7, 8, 9, 10, 11, 12

In Figure 5-13 the values of C_{Pmax} for each blade are displayed as the three wind shear parameters are varied and all other design parameters are held at the baseline values. The difference in wind shear conditions leads to different logarithmic blades according to (5-2).

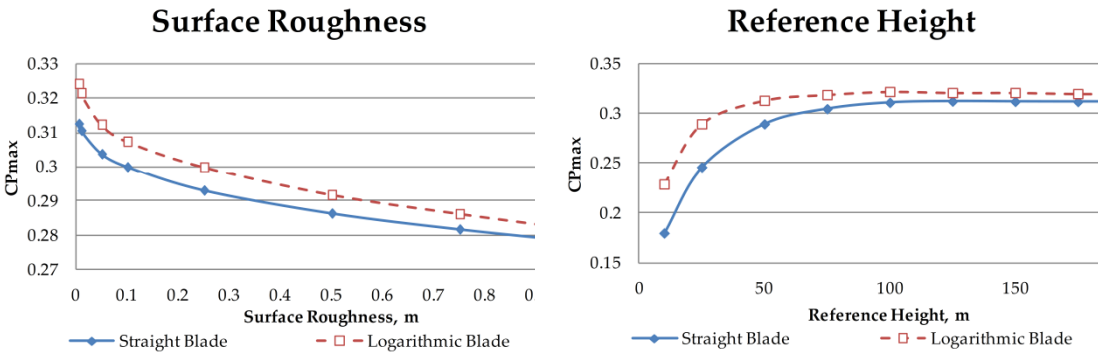

a) Influence of z_0 on aerodynamic performance

b) Influence of z_{ref} on aerodynamic performance

Figure 5-13: Sensitivity of the wind shear model parameters.

Figure 5-13 a) shows the impact of z_0 on performance of both blades. Increasing z_0 diminishes performance of both blades with performance more sensitive to z_0 for low values of z_0. The logarithmic blade displays a consistent increase in C_{Pmax} as z_0 varies. Figure 5-13 b) shows the impact of z_{ref} on performance of both blades. Both blades display an asymptotic increase in C_{Pmax} as z_{ref} increases. The logarithmic blade increases C_{Pmax} by 27.5% compared to the straight blade when z_{ref} = 10m and only increases C_{Pmax} by 2.6% when z_{ref} = 200m. The logarithmic blade can provide larger improvements to V-rotor performance when z_{ref} is low because a low value of z_{ref} will have a wider variation of $U_{inf}(z)$ across the baseline rotor with tips at z = 120m. The third variable that impacts the wind shear profile, U_{ref}, has no impact on performance of both blades. This is a consequence of the nature of the expression in (5-2) which describes a logarithmic blade. When this equation is applied to two rotors which have all design and wind shear parameters held constant apart from U_{ref}, the same logarithmic blade will be generated. The logarithmic blade reflects the logarithmic variation in wind speed with height and this is independent of U_{ref}. Therefore the improvement in performance provided by a logarithmic blade is independent of U_{ref}.

5.4 Phase-Shifting Control for Aggregated VAWTs

A significant disadvantage for many types of VAWTs is that the generated power is inherently periodic in nature. This power quality issue is exacerbated as the turbines increase in size and are aggregated requiring the transmission system to withstand large transients. This section proposes a control based approach to mitigating these power fluctuations by adjusting the drive train torque demand for each individual turbine in order to maintain a suitable phase difference between the individual rotor cycles.

A model of a multiple VAWT farm is developed which is used to design the controller and assess its performance. The individual turbines are two bladed 5MW, stall controlled, variable speed VAWTs. The fixed-pitch rotor aerodynamics for a turbine are determined from StrathDMS. Since the controller for the group of VAWTs is very slow acting, a simple lumped parameter ODE model of the turbine dynamics is sufficient. A stochastic wind speed model is used in the farm model.

5.4.1 The Phase-shifting Control Concept

The angle of attack and net wind speed incident on a VAWT aerofoil are periodic in nature. Consequently the torque generated pulsates in phase with the rotation of the rotor. This effect is known as torque ripple and has been introduced in Section 2.2.2 as one of the major design challenges for VAWTs. The problems caused by torque ripple are exacerbated when VAWTs are aggregated because peaks in power generated have the potential to coincide causing large surges in power through the wind farm transmission system. Peaks in power coinciding is a significant issue for three key reasons. Firstly the magnitude of the deviations from the mean power is extremely high as is demonstrated in Section 5.4.2.2. Secondly, aggregated VAWTs will all operate at slightly different speeds so over a sufficient portion of time it is guaranteed that the rotors will come in and out of phase. Thirdly, these surges are deterministic, so unlike stochastic perturbations of a system that tend to cancel out, when these cycles in power get close to being in phase, they will sustain a similar phase.

Skewed or helical blades are one way of providing some smoothing of the periodic power generated by a single turbine. This is unlikely to be economical at the multi-megawatt scale due to the increase in length required, complexity of manufacture and loss of aerodynamic performance.

Adjusting ω can also mitigate torque ripple. When operated according to a constant speed strategy, the periodic torque perturbations can be absorbed by allowing the rotor speed to vary relative to the constant speed set point. However, the capacity factor for a turbine operated in this manner is low because the turbine rarely operates at λ_{opt}. The alternative is to operate the turbine according to a variable speed strategy where the rotor speed is reduced as wind speed increases above rated, so λ decreases and the turbine is driven into stall. However, it was explained in Section 2.5.4 that the dynamics in the stall region are unstable [77], and therefore the controller needs to regulate the rotor speed more tightly. Essentially, the controller objective is to maintain constant power by tracking the constant power curve. As wind speed increases, this causes the rotor speed to decrease into stall. Because the dynamics are unstable, it is not possible to let the rotor speed vary to reduce the large torque oscillations. Furthermore, they are at too high a frequency to be actively regulated by the controller. Consequently, it is no longer possible to absorb the periodic torque perturbations by allowing the rotor speed to vary.

A new approach to smoothing the power fluctuations from aggregated VAWTs is proposed, whereby a controller for a small group of turbines is designed which controls the drive-train torque demand to each individual VAWT in order to maintain a set phase difference between each power output cycle. The primary aim of this controller is to smooth the aggregated power output from the wind farm while maintaining the overall performance of the turbines in a group.

The equation describing the motion of each blade is (5-3) where f is the viscous damping term.

$$\omega = \frac{1}{J}\int \left(Q_A - (Q_{DT} + f\omega)\right)dt \qquad \textbf{(5-3)}$$

In steady operation $Q_A = (Q_{DT} + f\omega)$ and the blades rotate with a constant angular velocity. Allowing Q_{DT} to decrease will cause the rotor blades to accelerate. Thus the phase of a VAWT power output can be altered by manipulating Q_{DT}.

Figure 5-14 depicts the non-physical situation where the power cycles are exact sinusoids. Initially, there are two turbines with the peaks in power output in-phase. The period of one rotor cycle for both turbines is $t_1 - t_0$. At time t_1, the drive-train torque of turbine 2 is increased to reduce its rotor speed. By time t_2, turbine 2 is π out-of-phase relative to turbine 1. The drive-train torque is then reduced to its original setting so that the peaks in the power output remain π out-of-phase. The aggregated power from the two turbines when they are in phase between t_0 and t_1 has fluctuations that can be twice the maximum output of each individual turbine, whereas by t_2 the aggregated power fluctuations are eliminated because the individual turbine power fluctuations are out-of-phase.

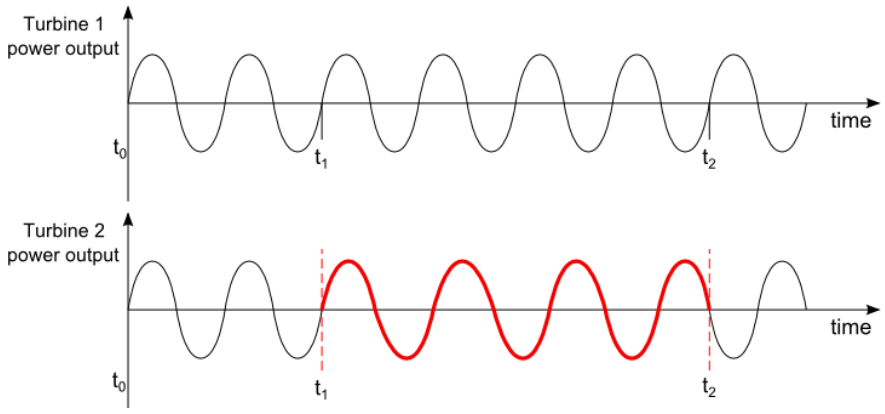

Figure 5-14: Idealised sinusoidal power output from two VAWT models. Turbine 2 has a higher drive train torque demand between times t_1 and t_2.

Manipulating Q_{DT} to alter a power output phase relative to another cyclical power output is referred to as **phase-shifting**. Aggregating wind turbines essentially sums the power outputs [142]. Thus aggregation of multiple VAWTs has the potential of producing power flows with current transients exceeding safety levels in the power lines. The idea of the proposed phase-shifting control is to combine multiple identical VAWTs in such a way that the aggregated power output is smoothed without impacting the average power generated.

5.4.2 VAWT Farm Model

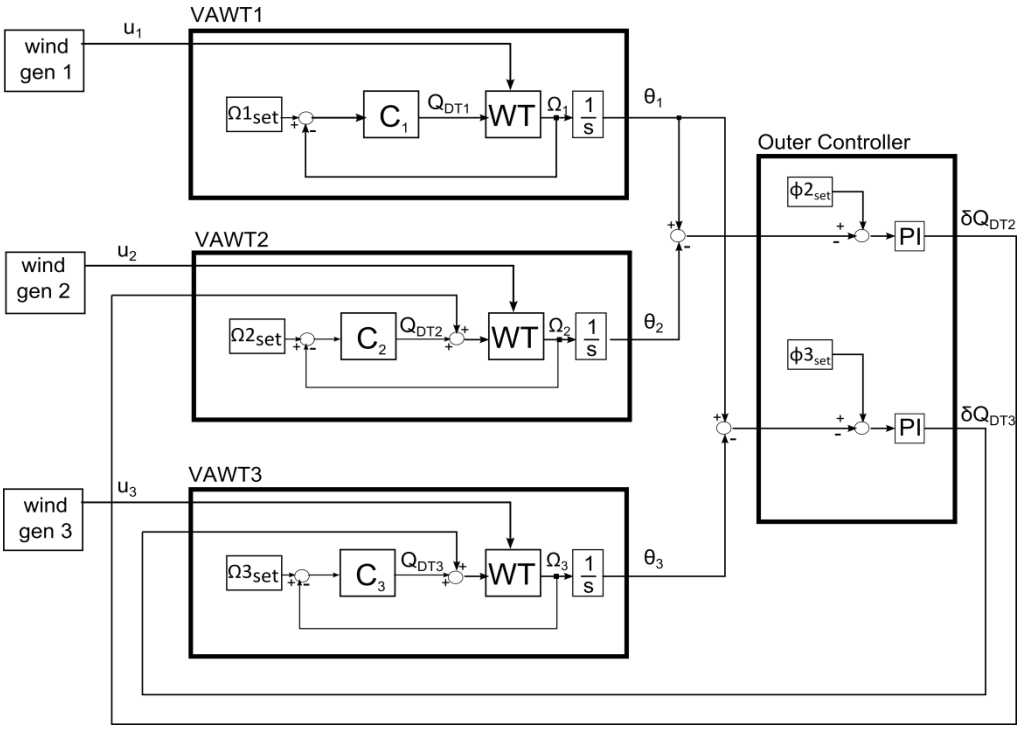

Figure 5-15: Structure of the VAWT farm

To demonstrate the phase-shifting control concept a VAWT farm is developed consisting of three subcomponents; a stochastic wind model; an individual VAWT model; and an outer controller that interacts with multiple VAWTS in the farm. An example VAWT farm is illustrated in Figure 5-15

and full details of the VAWT farm subcomponents is provided in Appendix C: Phase-shifting VAWT Control.

5.4.2.1 Stochastic Wind Speed Model

The wind speed model uses a predefined mean wind speed and turbulence intensity of 10% to produce a stochastically varying time series of wind speed. The wind speed model generates an effective point wind speed [2] that is spatially filtered so that the spectrum of torque generated by a uniform wind field with that wind speed is the same as a spatially varying wind speed.

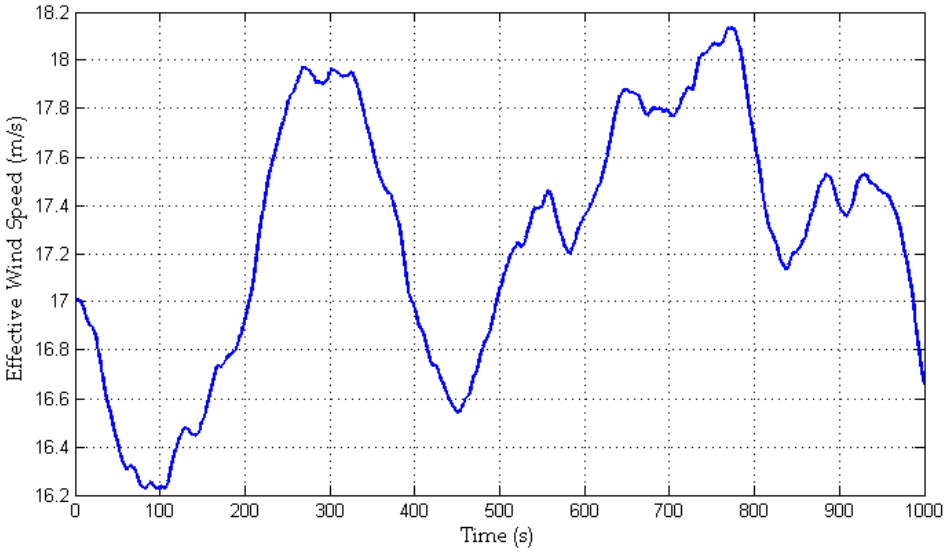

Figure 5-16: Effective wind speed time series

To demonstrate the wind simulated for this analysis, Figure 5-16 is a wind speed time series for a mean wind speed of 16ms^{-1} with a turbulence intensity of 10%. The Simulink wind speed model is provided in Appendix C.2. In order to simulate different wind speeds for each individual turbine in a VAWT farm, an independent wind model is used for each turbine. The same mean wind speed and turbulence intensity are used for each turbine. The aggregated turbines being modelled here would naturally be located

close together and hence would experience similar wind profiles. A more realistic approach for capturing the wind for aggregated turbines would be to use three correlated wind speeds that are generated from the same underlying wind model. This is suggested as further work.

5.4.2.2 Individual V-Rotor VAWT Model

The wind turbine considered in this study is a 5MW V-rotor. The blades are tapered and untwisted. The turbine parameters are provided in Table 5-6.

Table 5-6: Parameters of the V rotor VAWT used in this study.

Number of blades	2
Length of blade	100m
Blade chord at root	10.5m
Blade chord at tip	3.8m
Inclination to the vertical	36^{o}
Radius at rood	23m
Rated Power	5MW

A simple lumped parameter ODE Simulink model is developed to investigate phase-shifting control. The full Simulink model of the individual VAWT is provided in Appendix C: Phase-shifting VAWT Control. The individual VAWT model consists of a rotor model incorporating rotor aerodynamics generated from StrathDMS, a drive train model which implements (5-3), and an inner controller consisting of a feedback loop with a PI controller.

The power output from one individual VAWT model with a mean wind speed of 16 ms^{-1} is provided in Figure 5-17. At this wind speed, the

VAWT model exhibits an average power output of 5MW with periodic power fluctuations exceeding the average by up to 2.5MW. One of the blade azimuthal positions is used to indicate the azimuthal position of the rotor. However, the second blade is positioned exactly π radians out of phase causing symmetry in the power output produced upstream and downstream. The periodic nature of the generated power is clear from Figure 5-17 and for every half cycle there is a peak in power output.

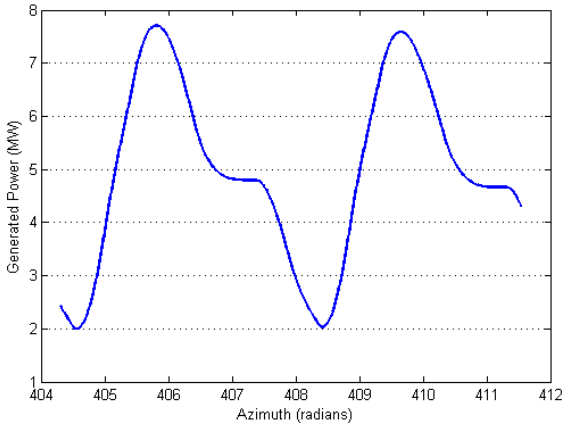

Figure 5-17: One power cycle from an individual VAWT in a mean wind speed of 16ms^{-1} with turbulence intensity of 10%.

5.4.2.3 Outer Controller

The objective of the outer controller is to regulate the relative phases of two turbines in the farm so that overlapping of peaks in the generated power from individual machines is avoided. This phase-shifting controller is discussed in Section 5.4.3.2.

5.4.3 Hierarchical Control Design

The VAWT farm incorporates a layered control scheme for maintaining constant average power of individual VAWTs while ensuring smooth aggregated wind farm power output. The controller for the VAWT farm has a hierarchical structure with inner and outer controllers. Each individual

VAWT has its own inner controller which regulates the individual turbine speed. The outer controller interacts with multiple wind turbines in the farm and attempts to maintain a certain difference in the phase of the periodic power output by each turbine in order to smooth the aggregated power output. The speed of this outer phase-shifting controller for a group of wind turbines is much slower than the individual wind turbine central controllers due to the large inertia of the rotors. The inner and outer controllers are, thereby, effectively decoupled.

5.4.3.1 Individual VAWT Control

The objective of the inner control system in a variable speed, stall regulated wind turbine depends on the wind speed [77]. The operating strategy consists of thee modes, each of which is brought about by the inner controller:

i) For drive train torque to track the CPmax curve for low winds;

ii) To allow the turbine to hold a steady rotor speed for medium winds;

iii) For aerodynamic torque to track constant power for high winds.

The three operating regions are depicted in Figure 5-18 which shows torque against rotor speed for various wind speeds. The controller aims to maximise energy capture by tracking the C_{Pmax} curve in low wind speeds. However, in high wind speeds the turbine follows the constant power strategy towards the stall region to minimise drive-train transient loads. The transition region between these two strategies is for the rotor speed to be held at a constant speed.

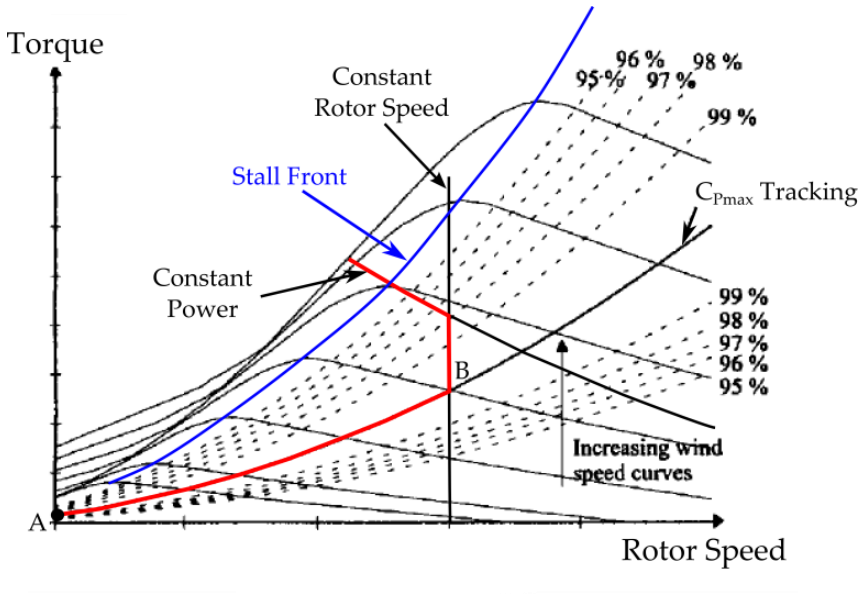

Figure 5-18: The operating strategy for a variable speed stall regulated wind turbine. [77]

The inner controller has the ability of controlling the turbine in each of the three different operating regions mentioned above. Hazardous power surges due to aggregation issues are not significant at low wind speeds due to the low individual power outputs and torque ripple can be absorbed in the constant rotor speed region, so this work focuses on operation in high winds. Therefore the inner controller adopts the third operation strategy and attempts to track constant power.

As is explained in Section 2.5.4, a consequence of stall regulation in above rated conditions is that the controller is inherently unstable in that if ω or torque is to deviate from the operating strategy, there is a tendency for these deviations to grow. Therefore the inner controller must be designed to track the operating strategy very closely and ω cannot vary in phase with θ to accommodate torque ripple. Thus, the fluctuations in torque, and hence power, from each individual VAWT are unavoidable.

The inner controller uses PI control and the set points are tuned for above rated stall control, therefore they must ensure close tracking of the

setpoint. The proportional gain is $2*10^9$ and the integral gain is 0.4. These gains differ by many orders of magnitude because the integral action acts on the product of rotor speed and torque whereas the proportional action acts only on the rotor speed. The speed loop has been separated, as is shown in the block diagram in Appendix C.1.4, to allow the weakest possible control that will stabilise the system. This maximises the alleviation of torque ripple that can be achieved through variations in rotor speed dues to slow control action.

5.4.3.2 Phase-Shifting Outer Control

The task of the outer control system is to control the phase difference between the power cycles of two turbines in order to avoid peaks from overlapping and causing unsafe power flows for the transmission system. This is done by adjusting the drive train torque demand setpoint within the individual controller of one of the turbines. The speed of the outer controller must be much slower than the inner controller in order to decouple the dynamics.

The structure of this hierarchical control for a three VAWT farm is illustrated in Figure 5-15. The subscript i refers to the i^{th} turbine. u_i are the effective wind speeds, θ_i are the rotor azimuthal positions, Q_{DTi} are drive train torque demands and δQ_{DTi} are the increments to drive train torque demand. Φ_i is the phase difference between azimuthal position of rotor 1 and rotor i. The outer controller determines an adjustment to the inner feedback loops set points by comparing the azimuthal positions of the rotors relative to one another.

The objective of the outer controller in the three turbine case is to maintain a phase difference between turbine 1 and 2 of $\Phi_2 = \pi/3$. This is a disturbance rejection problem. For turbine 2, the outer controller must reject

the phase change of turbine 1 as a disturbance and attempt to control the phase of turbine 2. This is achieved by measuring the difference in azimuthal positions and subtracting it from the set point. This error signal is fed through a PI controller whose output is labelled δDT_2, the increment to drive-train torque demand for VAWT2. This is fed directly into the drive-train of turbine 2 to accelerate or decelerate the rotor as required. A similar comparison is made between θ_1 and θ_3 with a set point of $\Phi_3 = 2\pi/3$ to generate the outer control adjustment of δDT_3.

5.4.4 Controller Analysis

The performance of the outer controller is constrained by the limitations of the inner individual VAWT controllers. The nonlinear equation of motion in (5-3) can be linearised to reveal the limitations imposed by the inner controller. Differentiating both sides of (5-3)

$$\frac{d\omega}{dt} = \frac{1}{J}\left(Q_A - (Q_{DT} + f\omega)\right) \tag{5-4}$$

The nonlinearity stems from the nature of Q_A and Q_{DT} which are given by

$$Q_A(\omega, U_{inf}, \theta) = \frac{1}{2}\rho A_{swept} {U_{inf}}^2 R C_P(\omega, U_{inf}, \theta) \tag{5-5}$$

$$Q_{DT}(\omega) = C(\omega) \tag{5-6}$$

The function $C(\omega)$ is the action of the inner controller. Q_A will peak once with every rotation of the blades but the mean Q_A will vary on a slower timescale as the wind speed and rotational speed of the blades changes. Changes due to azimuthal variation are relatively fast compared to the speed with which the outer controller will act so the low frequency component of Q_A variation contains the important information for designing the hierarchical controller. Therefore variation due to θ can be neglected. Furthermore, with the assumption that λ remains constant, then C_P remains fixed at the constant

value C_{P0} and Q_A becomes a function of U_{inf} alone. Neglecting viscous damping, the system can be written as

$$\frac{d\omega}{dt} = \frac{1}{J}(Q_A(u) - Q_{DT}(\omega)) \quad \textbf{(5-7)}$$

$$= \frac{1}{J}(Wu^2 - C(\omega)) \quad \textbf{(5-8)}$$

Where u = U_{inf} and W = $0.5\rho A_{swept} R C_{P0}$. Using a Taylor expansion truncated after the linear terms, the system can be linearised about (ω_0, u_0) and expressed with one state variable and one input variable.

$$\frac{d(\omega - \omega_0)}{dt} = -\frac{1}{J}\frac{\partial C}{\partial \omega}\Big|_{\omega_0}(\omega - \omega_0) + \frac{2}{J}Wu_0(u - u_0) \quad \textbf{(5-9)}$$

Which in state space is written as

$$\frac{d\bar{\omega}}{dt} = -\frac{1}{J}\frac{\partial C}{\partial \omega}\Big|_{\omega_0}\bar{\omega} + \frac{2}{J}Wu_0\bar{u} \quad \textbf{(5-10)}$$

The characteristic equation of this linear state space system reveals that there is a pole in the right half plane and the system is unstable whenever $\frac{\partial C}{\partial \omega}\Big|_{\omega_0} > 0$. In the case of a PI controller with K_p and K_i as the proportional and integral controller gains respectively

$$C(\omega) = K_p\omega + K_i\int \omega\, dt \quad \textbf{(5-11)}$$

And

$$\frac{\partial C}{\partial \omega}\Big|_{\omega_0} = K_p + K_i\omega_0 \quad \textbf{(5-12)}$$

Since the controller gains and the steady state rotor speed are always positive, the system is unstable.

When the outer loop is closed, the unstable nature of the underlying inner individual turbine controllers must be accommodated. Therefore the

speed of the outer loop must be much slower than the inner loop and integral gains must be kept relatively low.

In order to determine suitable PI control gains for the outer controller shown in Figure 5-15, a manual tuning procedure is followed. The proportional gain is increased to a point where the rise time is sufficient without causing so much overshoot that the phase differences are vastly apart. Following this, the integral gain is steadily increased through different orders of magnitude to locate a suitable level of integral action. The outcome of this procedure was a proportional gain of 1,000,000 and an integral gain of 100 for both outer PI controllers.

5.4.5 Simulation and Results

The performance of the phase-shifting VAWT farm controller for a three-turbine wind farm is investigated for a range of mean wind speeds. The performance for a twelve-turbine farm is also investigated at a mean wind speed of 16ms^{-1}.

5.4.5.1 Three-Turbine Wind Farm

For the three-turbine farm, the simulation is run for three different wind speeds; a below rated wind speed of 10ms^{-1}, a high wind speed of 16ms^{-1}, and an extreme wind speed of 22ms^{-1}. The aggregated power for three turbines with inner control only is compared with simulations in which the phase-shifting farm controller operates.

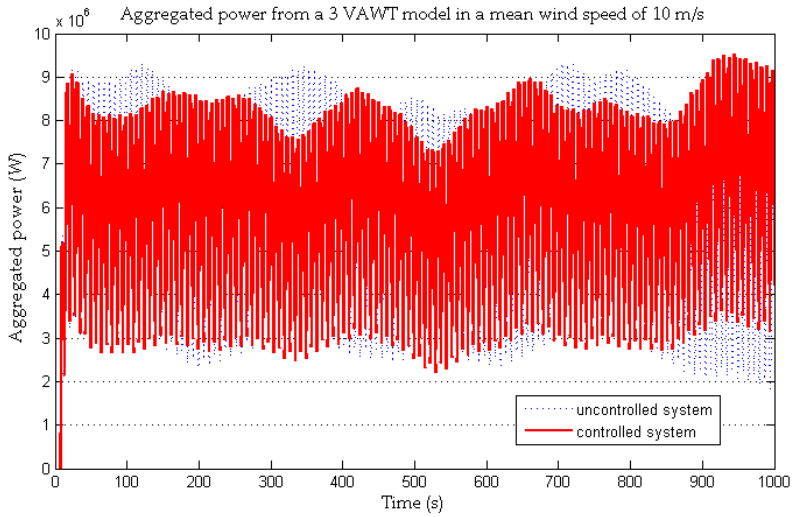

Figure 5-19: Aggregated power output from three VAWTs. Mean wind speed of 10 ms^{-1}.

Figure 5-19 shows the aggregated power output for a three-turbine farm at a mean wind speed of 10 ms^{-1}. The average aggregated power fluctuates about 5.5MW so the individual turbines are operating at below rated power. At this low wind speed, the individual turbines are operating in the constant speed mode. Therefore the individual controllers could be amended to mitigate torque ripple, but this has not been developed here. Furthermore, power transients are not significant because the aggregated power is low.

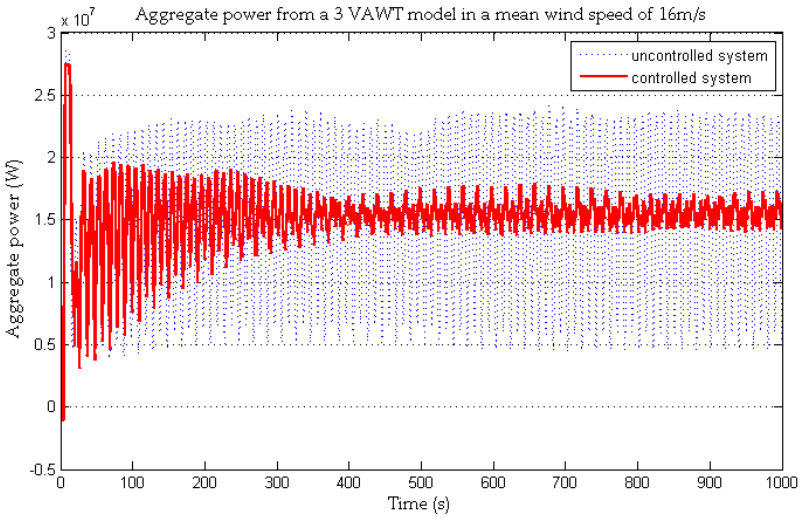

Figure 5-20: Aggregated power output from three VAWTs. Mean wind speed of 16 ms^{-1}.

Once the wind speed rises above rated, each individual turbine adopts constant power tracking control and the power fluctuations become significant. Figure 5-20 demonstrates the effectiveness of the outer controller when the mean wind speed is 16 ms^{-1}. Fluctuations exceeding 10MW above the average aggregated power output are reduced to 3MW without affecting the average aggregate power output of 15MW.

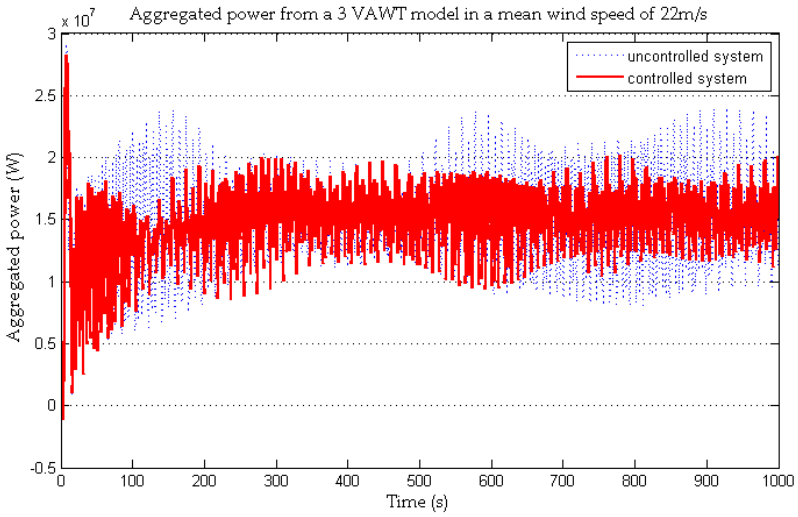

Figure 5-21: Aggregated power output from three VAWTs. Mean wind speed of 22 ms^{-1}.

At extreme wind speeds, the phase-shifting controller is not as effective. This is demonstrated in Figure 5-21 which shows that the outer controller has only reduced fluctuations of aggregate power output of 8MW from the mean down to 5MW from the mean. An inspection of the individual power output at this extreme wind speed reveals that the power variation for one cycle has changed significantly. Figure 5-22 presents the power output from an individual VAWT for one cycle of the rotor at a mean wind speed of 22ms^{-1}. Compared with Figure 5-17, it can be observed that each peak in power output has developed into a double peak. This is due to operation at a lower λ so a wider range of α are experienced and the rotor stalls over an increased range of azimuth angles. A suggestion for further work is to

investigate a new set point and controller gains that improve performance in the high wind speed operation mode.

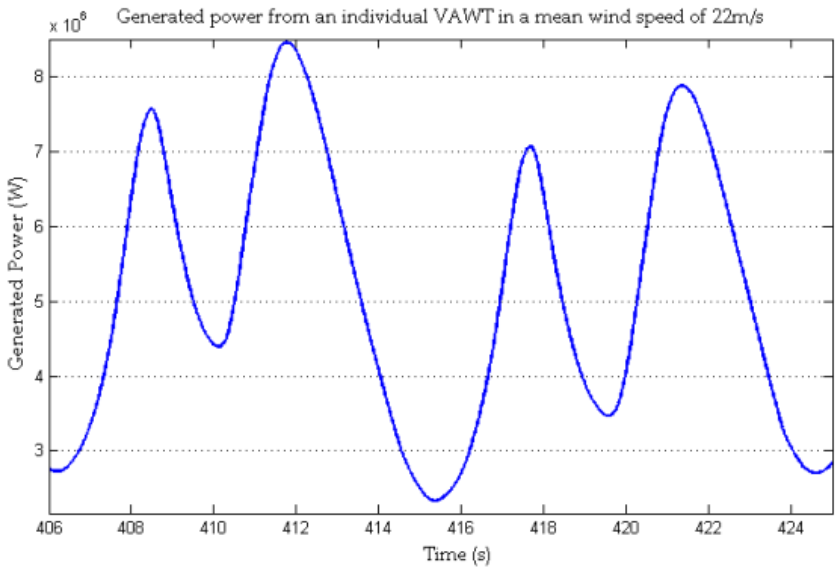

Figure 5-22: One power cycle from an individual VAWT in a mean wind speed of 22 ms^{-1} with turbulence intensity of 10%.

5.4.5.2 Generalisation of Control Scheme for Additional Turbines

The aggregated power output for a twelve-turbine VAWT farm is shown in Figure 5-23 for a mean wind speed of 16 ms^{-1}. The average power is 60MW. The outer controller objective is to phase-shift each turbine power cycle by $\pi/12$ relative to its neighbouring turbine. The outer controller is particularly effective in this case. The uncontrolled output shows power fluctuations exceeding the average by up to 40MW, and the outer controller reduces these to roughly 8MW. As might be expected, the more wind turbines aggregated, the greater the benefit achieved from the phase-shifting wind farm control.

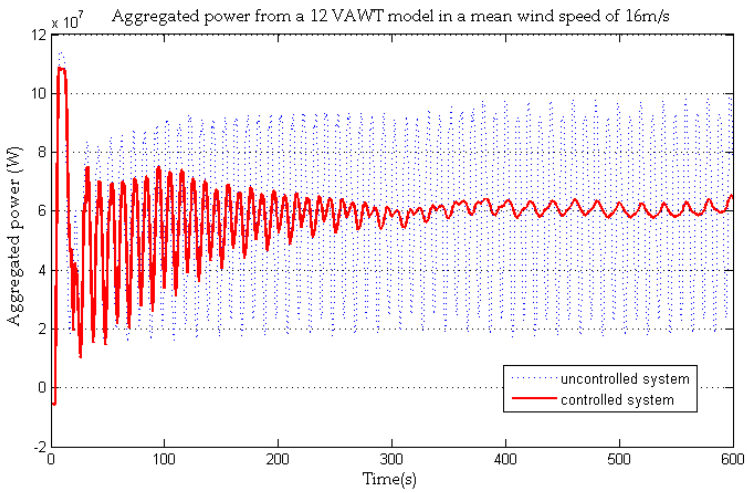

Figure 5-23: Aggregated power output from a twelve VAWT model at a mean wind speed of 16ms^{-1} with and without the phase-shifting outer controller.

The initial case considered is a three-turbine farm with each turbine having two blades. The objective for the phase-shifting controller is to adjust the three phases of the power cycles to be 0, $\pi/3$ and $2\pi/3$ relative to the first turbine so as to cancel the peak aggregation in power output among the three turbines. For the twelve-turbine farm the objective is to maintain a phase difference of $2\pi/(12 \cdot 2)$. For n turbines aggregated, each with m blades equally spaced about the rotor, the relative phase difference target is

$$\phi = \frac{2\pi}{n \cdot m} \qquad \textbf{(5-13)}$$

While it is evident that the effectiveness of this phase-shifting controller increases with the number of turbines in the farm, the number of turbines grouped together needs to be constrained to reduce the size of the network connecting them. It is unlikely that the number would be as large as twelve but that needs to be explored further. The phase-shifting controller should then be applied to groups of turbines within the wind farm.

5.5 Summary

This chapter consist of three investigations for fixed pitch VAWTs that are facilitated by simulating turbine aerodynamic performance with StrathDMS. First a measure of averaged lift to drag ratio is introduced which is suitable for classifying VAWTs and its impact on optimal aerodynamic performance is assessed. The second investigation is the impact of wind shear on V-rotor blade design. The third investigation is a control based approach to mitigating power fluctuations in aggregated VAWTs.

Poor lift to drag ratio underpins some of the most significant disadvantages of VAWT technology. While lift to drag ratio is a standard measure of HAWT performance, very little analysis exists for VAWTs because both lift and drag vary with rotor position. An effective lift to drag ratio is introduced in this chapter as the lift to drag ratio at an azimuthal position which contributes an instantaneous torque that is equal to the averaged torque contribution for a whole rotor cycle. This new measure of VAWT aerodynamic performance is shown to have a significant impact on straight blade VAWT rotor design. The main advantage of improving effective lift to drag ratios for H-rotors is an increase in the achievable aerodynamic performance, while for the V-rotor it would facilitate not only that, but also a significant increase in design tip speed ratio and hence a reduction in the weight and cost of the drive train.

The second investigation in this chapter incorporates the effects of wind shear into the rotor design for V-rotors. Since each location along a VAWT blade operates at a fixed height, there is potential to take the variation in wind speed with height into account to improve VAWT rotor design. A logarithmic blade is designed that reflects the logarithmic nature of wind

shear. For a baseline V-rotor design, it is demonstrated that using this new blade in place of a straight blade increases power generated by 20%. This significant improvement is achieved by increasing the swept area by 16% with only a 1% increase in blade length. Despite the increase in swept area, C_P also increases. Furthermore, stall is avoided towards the root because the logarithmic blade has a larger local radius in this region compared to a straight blade. A sensitivity analysis reveals how the rotor design parameters and wind shear model parameters influence the improvements to aerodynamic performance that the new blade can achieve. The logarithmic blade performance increases when base width or base height decreases and when γ or tip height increases. The achievable improvement with the logarithmic blade increases for lower reference heights in the wind shear model, and it is not affected by z_0 or reference wind speed.

The third investigation in this chapter is a demonstration of the potential, through wind farm control, to reduce the peak transients in power generated when VAWTs are aggregated. The wind farm controller acts to adjust the relative phase of the periodic perturbation of the power generated by the individual wind turbines and thereby smooth the aggregated peaks and troughs. Avoiding unsafe power transients should reduce the cost of the wind farm transmission system. With offshore farms consisting of hundreds of turbines, aggregated power smoothing could contribute to improved safety and cost. A model of a stall regulated, variable speed VAWT farm with three turbines is described. Combining three 5MW turbines, each with power variations of 3MW, has the potential risk of 9MW overshoots and aggregated power output peaking at 24MW. However, the control scheme presented here demonstrates that by adjusting drive-train torque demand to control the phase of the power cycles of groups of turbines, power

overshoots for a farm of three aggregated VAWTs can be restricted to less than 3MW without altering the mean generated power of 15MW and the aggregate power peaks at less than 18MW. For the more general situation with farms containing a larger number of VAWTs, the operating strategy is shown to become more effective, although realistic limits would restrict this farm control method to be applied to small groups of turbines.

Chapter 6

An Exploration of Variable Pitch for VAWTs

6.1 Introduction

Pitch control for wind turbines has the potential to achieve a range of control objectives spanning the whole operating envelope of a variable speed wind turbine and this chapter explores the various ways cyclic blade pitching can be utilised for VAWTs. Employing StrathDMS, which was outlined in Chapter 4, this chapter examines the ways in which pitching can be employed to achieve control objectives to suit both below and above rated operation.

Two example turbines, an H-rotor and a V-rotor, are simulated and cyclic pitch regimes are designed to suit each operating mode of a variable speed operating strategy. In Section 6.2 the range of VAWT control objectives that can be achieved by cyclic pitch are provided. Section 6.3 is a description of the simulation set up including the test turbine dimensions and the numerical resolutions of the simulations. Results are provided in Section 6.4 including a pitch regime suited to each objective and demonstration of the

improvement due to cyclic pitch regime compared to fixed pitch performance.

6.2 Cyclical Pitch Objectives

The operating strategy of a wind turbine depends on the flexibility of operation of the turbine. With constant rotor speed operation, control of the turbine is limited and a wide range of λ is experienced by the rotor. Variable rotor speed operation permits an operating strategy with objectives tailored to different bands of wind speeds as discussed in Section 2.5.3. While HAWTs tend to employ pitch exclusively in the above rated modes, VAWT performance in all modes could be improved with pitching. Cyclic pitch for VAWTs refers to predefined pitch regimes that are functions of azimuthal rotor position, $\beta(\theta)$. Alternatively, responsive pitch refers to manipulation of the pitch regime in response to variation in operating conditions such as wind speed. This chapter explores cyclic pitch exclusively.

Some of the significant improvements in HAWT performance over the past two decades have been due to the move towards pitch control and variable speed operation. These developments have not only improved energy capture, but have achieved load alleviation and power limiting. While variable pitch has been employed in the past for VAWTs, the turbines were limited to fixed speed operation and variable pitch was utilised purely to improve start-up performance and increase aerodynamic performance (see Section 2.4.3 and 2.4.4). With the recent resurgence in interest in VAWTs, it is timely to consider pitching for VAWTs following a typical variable speed strategy with several different modes.

A vorticity code was used by De Vries in [71] to demonstrate that blade pitching is not only able to provide marginal improvements to power

efficiency of a VAWT but it could also provide power limiting in above rated wind speeds. However, with the rise of the Danish concept HAWT in the subsequent decade, interest in variable pitch VAWTs diminished. Investigations and demonstrations were carried out confirming the ability of variable pitch to increase the efficiency of VAWT technology, but very little can be found in the literature addressing how a variable pitch VAWT operating strategy should be designed. The holistic approach of this chapter demonstrates the multifaceted ways in which cyclic pitching can improve VAWT performance.

There are at least five objectives that are achievable with cyclic pitching and they are explored in this chapter.

i) Improve start-up capability, which is a well-documented issue associated with VAWTs [26, 64].

ii) Increase the peak aerodynamic power coefficient, C_{Pmax}.

iii) Alleviate cyclic load fluctuations which are severe for VAWTs due to torque ripple [143]. Responsive pitch would permit regulation of pitch in order to alleviate stochastic transient loads. However, this is beyond the scope of the work described here as transient load alleviation would require a full aeroelastic model.

iv) Power limitation in above rated conditions.

v) Overspeed protection by providing aerodynamic braking.

6.3 Simulation Set Up

In this section, the characteristics for two example VAWTs are described, an H-rotor and a V-rotor, which are modelled in StrathDMS to investigate cyclic

pitch regimes. In addition, the choice of resolution for the StrathDMS simulations is discussed.

It should be noted that throughout this chapter, plots used to demonstrate turbine aerodynamics around the path of rotation, such as α or C_Q plotted against θ, display the behaviour of an individual blade.

6.3.1 Test Turbines

The H-rotor and the V-rotor used to investigate pitch regimes are illustrated in Figure 6-1. The H-rotor is rated at 1MW, has a 30m radius and three blades 50m in length. A uniform chord of 1.25m is selected to ensure that the solidity is such that the design λ is sufficiently high to avoid stall in normal operation. There is 5m clearance between the bottom of the blade and the bottom of the tower. The blades are assumed to be mounted on a cross arm at the centre of the blade. For the purposes of this investigation, drag due to the cross-arm has not been modelled. A V-rotor is also investigated and in order to draw useful comparisons between the H-rotor and a V-rotor, comparable turbines must be used. The first factor that is kept constant is the swept area of 3000m^2 so both turbines interact with the same volume of air over any given period. The choice of coning angle, γ, is a compromise because for a fixed root radius, small values of γ lead to a tall and narrow turbine with high design ω and aerodynamic performance comparable with an H-rotor; whereas large γ leads to a very wide rotor with lower design ω and poorer aerodynamic performance. A choice of γ = 30° is selected and a root radius of 15m dictates that the blade length is 58.5m. The second factor that is chosen to remain the same is the operating λ because the main goal of this work is to investigate pitching regimes. The operating λ has a significant effect on performance of a pitch regime because it dictates the range of flow angle, φ, experienced by the turbine. However, the cost of achieving

comparable λ is that the V-rotor requires wider blades. The effect of γ on both optimal λ and peak performance of VAWTs is discussed in Section 5.2. The V-rotor selected has three blades, each with a 5m chord at the root which linearly tapers to 2.5m at the tip. The higher solidity is designed to ensure both test turbines have the same optimal λ of 4.5. As with the test H-rotor, there is 5m clearance between the bottom of the blade and the bottom of the tower.

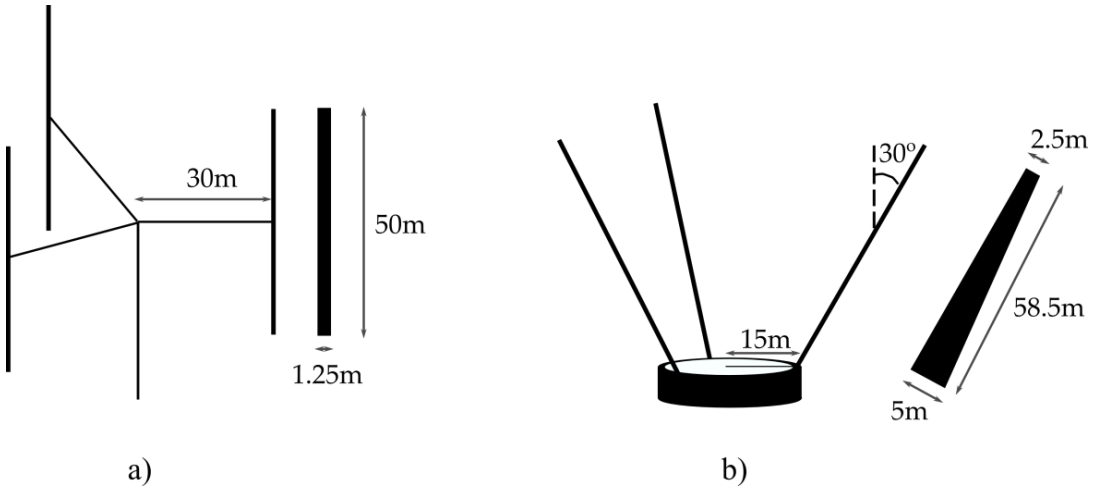

Figure 6-1: Dimensions of the test turbines

Both turbines have NACA0012 aerofoils and at the design λ of 4.5, the Reynolds number at the midpoint of each turbine rotor is 3,000,000. The static stall angle associated with this Reynolds number is 16°. The V-rotor has variation in Reynolds number along the span of the blade. Figure 6-2 illustrates how aerodynamic performance varies with tip speed ratio in the form of power coefficient for the test rotors when no pitch regime is employed. For the H-rotor a $C_{Pmax,}$ of 0.33 occurs at an λ_{opt} of 4.5. For the V-rotor a C_{Pmax} of 0.27 occurs at the same λ_{opt} of 4.5. Due to the lower C_P, the V-rotor has a higher rated wind speed in order to achieve the same rated power of 1MW.

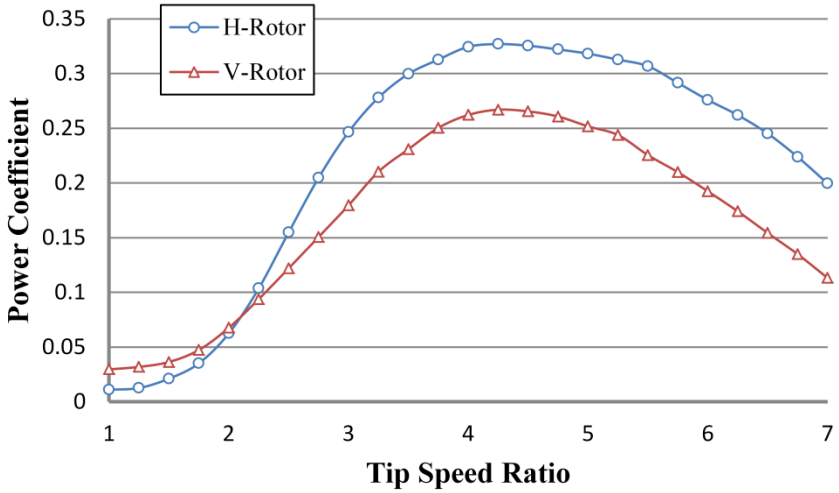

Figure 6-2: Power coefficient against tip speed ratio for the H-rotor and V-rotor test turbines without pitching blades.

6.3.2 Numerical Resolution

In this section, the resolution of the simulations carried out and the number of streamtubes and blade sections used is discussed. For the detailed design of a particular configuration of VAWT and operating strategy, higher resolution, than in the main parts of this chapter, are required. But in the broader context of exploring the options for cyclic pitching, less accuracy is acceptable. In all simulations, N_s = 10 and N_t = 32. The free stream wind speed is 12ms^{-1}.

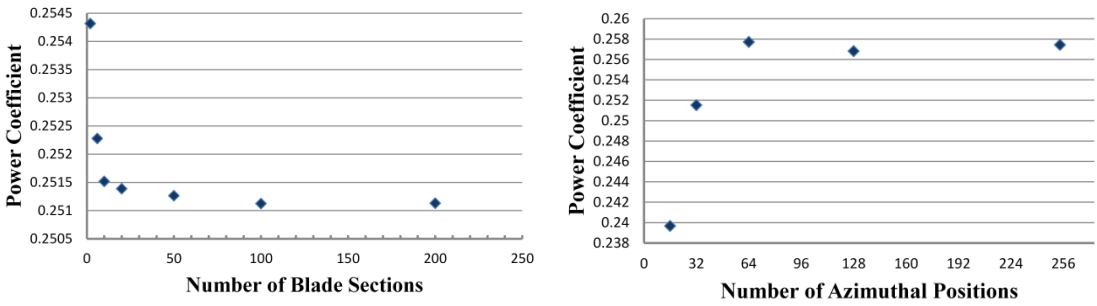

a) Effect of number of blade sections, N_s

b) Effect of number of azimuthal positions, N_t

Figure 6-3: Influence of mesh resolution on accuracy of C_P for the test H-rotor, $\lambda = 3$

A sensitivity analysis is conducted whereby the test H-rotor is simulated using a range of different mesh configurations at λ = 3 and the results are shown in Figure 6-3. It is clear from Figure 6-3 a) that the choice of 10 blade sections is sufficient to capture C_P to suitable accuracy. The effect of the number of azimuthal positions on C_P is presented in Figure 6-3 b) and the selection of 32 azimuthal stations is made as a compromise between predicting C_P to a suitable accuracy, and computational effort. A comparison of instantaneous torque for the H-rotor at λ=3 at two different levels of resolution is depicted in Figure 6-4. The dots represent N_t = 256 and the circles represent N_t = 32. Both cases agree on the general behaviour; that a higher level of torque is reached upstream and stall sets at θ = 180° with dynamic stall temporarily avoiding negative torque. However, the case with more azimuthal positions captures more detail local to the sharp onset of stall and reattachment. The reattachment occurs slightly earlier with N_t = 256 and therefore higher instantaneous torque is generated near θ = 225°.

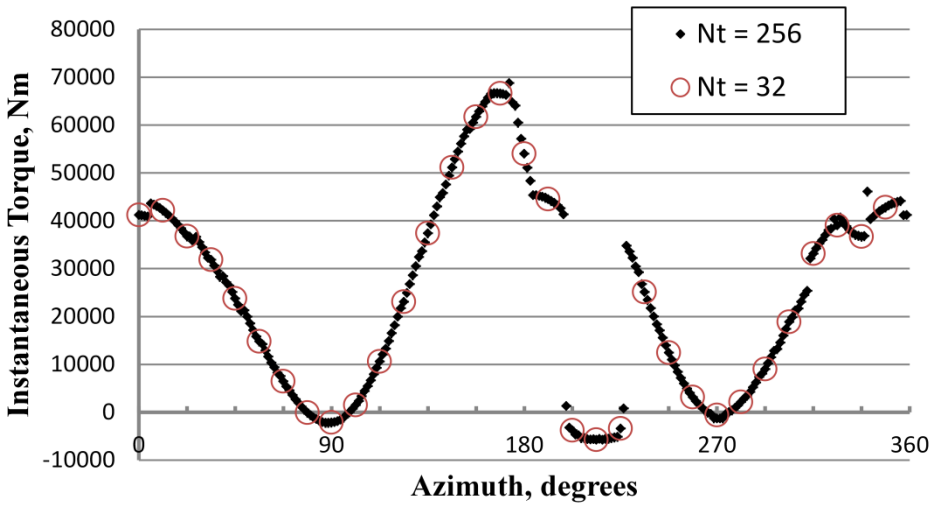

Figure 6-4: Instantaneous torque vs azimuth for an H-rotor at λ = 3. The simulation is run for two different N_t.

6.4 Demonstrating VAWT Control Objectives

In this section, for each of the operating modes of a variable speed pitch regulated wind turbine from start-up in low winds through to shut down in extreme winds, the achievement of the various control objectives for the two test turbines with suitable cyclic pitching regimes are investigated. The control objectives considered are: improving start-up performance; improving peak aerodynamic performance; alleviating cyclic loading; power limiting; and overspeed protection. A different pitch regime is developed to suit each control objective.

6.4.1 Improving Start-Up Performance

Fixed pitch VAWTs suffer from poor start-up capability because the turbine will operate in very low λ during start-up and consequently α will fluctuate between extremely large magnitudes with each rotor cycle. As a turbine starts up, λ must pass through every value from 0 up to the design λ. Figure 6-5 illustrates how the maximum fluctuations in α vary with λ for the test turbines as predicted by StrathDMS. Both turbines display α attaining 180^{o} for low λ, with the maximum values diminishing as λ increases. These extreme fluctuations in α lead to poor aerodynamic performance of the blade. Variable pitch can address this issue but a large range in β is required to avoid excessive α. Kirke designed passive pitch systems for VAWTs to overcome this difficulty [26], however the prototype produced did not achieve good aerodynamic performance in design λ.

The turbine will not be generating power during start up so even a small aerodynamic torque provided by the rotor being capable of overcoming frictional and drag forces is sufficient to achieve start-up. A

suitable objective for a pitch regime in this mode is that it can maintain reasonable torque for a range of low λ.

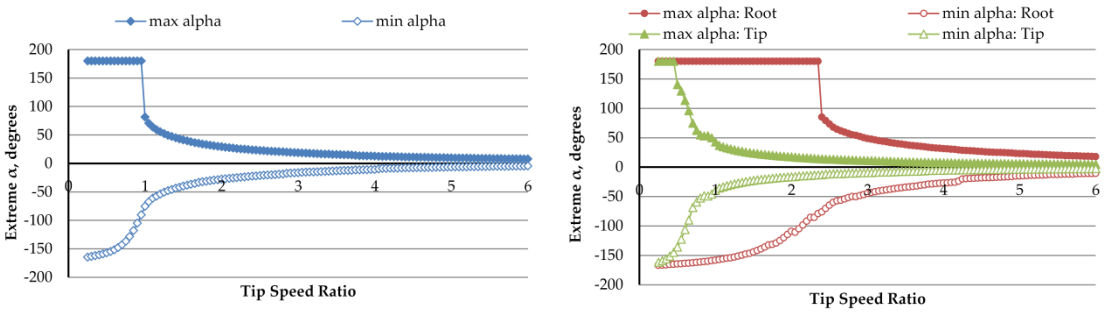

a) H-rotor, mid blade **b) V-rotor, blade root and tip**

Figure 6-5: Variation of extreme α with λ for the test turbines without pitching

Figure 6-5 highlights some features which are useful when designing a pitch regime to improve start-up through low λ. The first observation is that during start-up, the range of α is very sensitive to λ. An optimal pitch regime could be designed to suit a particular λ but this may come at the expense of performance at other λ and the goal in this operating region is to accelerate the rotor through these low λ. For this reason, instead of optimisation design for one particular λ, a pitch regime is searched for which is successful for all $\lambda < 2$. In addition, Figure 6-5 illustrates that there is a significant difference in the variation of α with λ between the H-rotor and the V-Rotor. Excessive α are experienced by the root of the V-rotor for a much wider range of λ compared to the H-rotor because the radius is lower at the root of the V-rotor so the component of wind due to rotation is lower (see Figure 3-2). However, the tip of the V-rotor demonstrates excessive α for a smaller range of λ because γ has the effect of reducing α.

Drawing on the observations outlined above, a pitch regime with the objective of maintaining reasonable torque during start-up is developed as follows. StrathDMS is used to generate the variation in α with θ at a

particular $\lambda < 2$ for the H-rotor without variable pitch. The factor by which α exceeds the static stall angle at the upwind position is stored and $\beta(\theta)$ is designed to divide α by that factor for all θ. This ensures stall will be avoided at all θ while ensuring smooth variation in β. Furthermore, it reflects the non-sinusoidal nature of variation in α. A measure of the performance for any particular $\beta(\theta)$ is the sum of C_Q across all $\lambda < 2$. This process was repeated for all $\lambda < 2$ and the best $\beta(\theta)$ stemmed from $\lambda = 1.5$. The pitch regime selected to improve start-up is illustrated in Figure 6-6. Unlike the H-rotor, in a V-rotor each blade station operates at a different local speed ratio and experiences different φ. Thus, the onset of stall occurs at different azimuthal angles and to different extents at different blade locations for a V-rotor and this makes it problematic to design a pitch regime for the V-rotor based on α. Instead the pitch regime designed for the H-rotor is also used for the V-rotor.

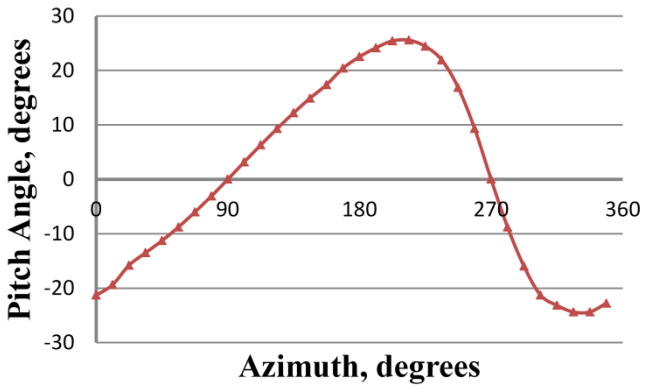

Figure 6-6: The pitch regime used to improve start-up performance at low tip speed ratios.

Figure 6-7 is a plot depicting the impact of applying the pitch regime on torque generated by the test turbines in low λ. Both rotors demonstrate a dip in torque coefficient without variable pitch. Torque is in general slightly higher for the V-rotor throughout this range of λ but there is still a dip in torque coefficient with a local minimum at $\lambda = 1.5$. The pitch regime developed has successfully maintained a reasonable torque coefficient as λ

increases from 0 up to 2 for both turbines. For greater λ, this pitch regime has an adverse effect on performance so a new pitch regime must be adopted.

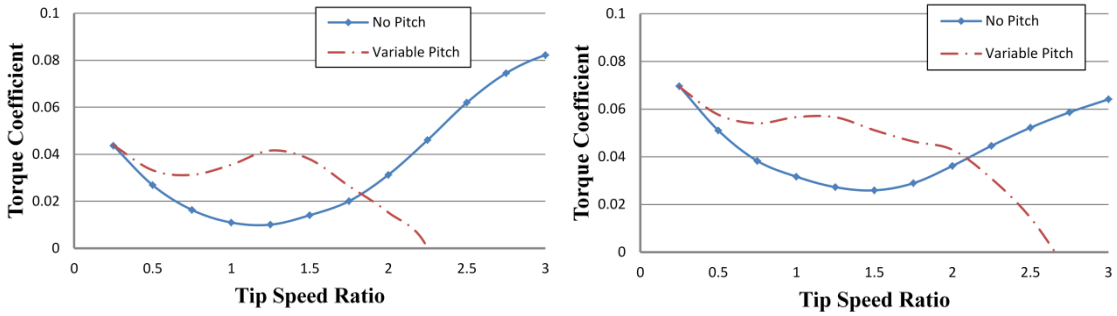

a) H-rotor **b) V- rotor**

Figure 6-7: Torque coefficient vs tip speed ratio with and without the pitch regime for improving start-up applied.

6.4.2 Optimising Peak Aerodynamic Performance

The test VAWTs selected for this investigation are specifically designed to operate at peak aerodynamic performance without going into stall. For this to be the case, the optimal λ must be high enough to maintain low φ. This choice ensures that improvements in performance at design λ due to pitch do not rely on avoiding stall. A distinct pitch regime is required for each rotor to improve aerodynamic performance at design λ. A constrained optimal pitch regime and a fixed pitch regime are also considered in this investigation.

In order to identify the best aerodynamic performance achievable with a fixed offset pitch, the following procedure is used. For both turbines the fixed offset in pitch value is varied and C_P is generated at the optimal λ. The best fixed offset pitch in terms of increasing C_P at λ_{opt} is $\beta = 1.5^o$ for the H-rotor and $\beta = 0.6^o$ for the V-rotor.

The procedure for designing a pitch regime which provides maximum driving torque for each turbine is as follows. While streamtubes are assumed

to be aerodynamically independent, the upstream and downstream actuator surfaces in each streamtube are not independent of each other; an increase in energy extraction upstream will reduce the wind available downstream and thus reduce performance downstream. For each streamtube, β_u and β_d are varied and the combination that maximises the sum of the torque contributions from the tandem actuator surfaces in that streamtube is selected as the pitch values associated with the two azimuthal positions associated with that streamtube at a particular height on the rotor mesh. Since a column of actuator surfaces does not always accurately represent a blade due to the fanning phenomena discussed in Section 4.4.2, an averaging must be involved to transform a column of optimal pitch angles and associated azimuthal positions into one representative pitch angle and azimuthal position. These values are averaged using a weighting based on their proportional contribution to the torque for the given azimuthal location. The choice of β for a particular azimuthal location is thus influenced more by the blade segments that provide the most aerodynamic torque. The final output of this procedure is a function, $\beta(\theta)$, defining the pitch angle at each azimuthal position.

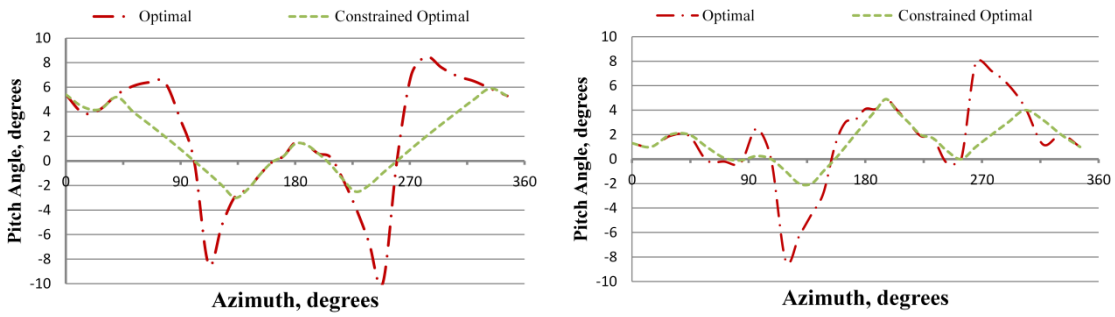

a) H-rotor **b) V-rotor**

Figure 6-8: The pitch regimes used to optimise aerodynamic performance at design tip speed ratio and associated constrained optimal pitch regimes.

The pitch regimes that result from the optimisation procedure are shown as dashed-dotted lines in Figure 6-8. These pitch regimes include sudden reversals in pitch angular velocity and in reality there would be a limit on both $|d\beta/dt|$ and $|\beta|$. Fortunately the regions of the path of rotation that require rapid variations in β are at the region of the swept area where energy extraction tends to be insignificant. With these limitations in mind, a constrained optimal pitch regime is included in this exploration which restricts $|d\beta/dt| < 10^{o}/s$. The constrained optimal pitch regimes are illustrated as dashed lines in Figure 6-8.

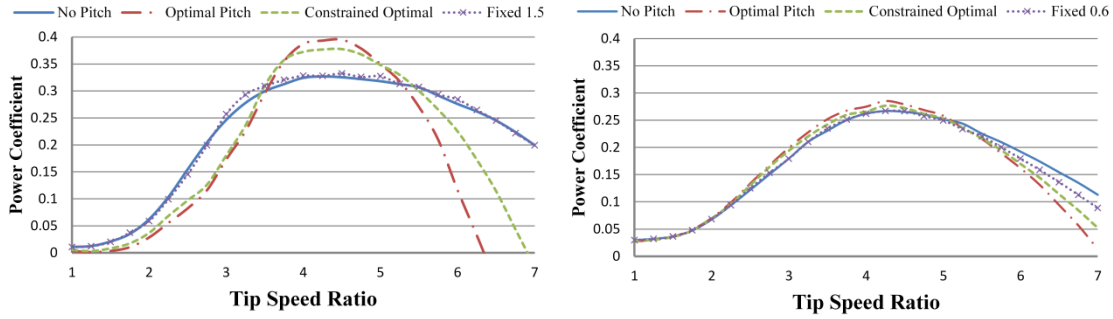

a) H-rotor **b) V-rotor**

Figure 6-9: C_P vs λ with and without the pitch regimes designed to increase maximum C_P.

The set of performance curves for the two test turbines with and without the pitch regimes applied is shown in Figure 6-9. The optimal pitch regimes improve performance at the design λ of 4.5 for both rotors. The H-rotor C_{Pmax} increases from 0.325 to 0.395, a gain of 22%, but the peak has become narrower which is a disadvantage for the control system because it increases the difficulty of C_{Pmax} tracking. Low λ would occur during start-up and high λ should normally only occur in a fixed-speed turbine at low operating wind speeds but might also occur in a variable-speed turbine when the wind drops and the turbine hasn't slowed down yet. It might also occur during runaway conditions, in which case poor performance might be

an advantage. The V-rotor with optimal pitch demonstrated a less significant gain in C_{Pmax}. At the design λ of 4.5, C_{Pmax} increases from 0.265 to 0.279, a gain of 5%. The constrained optimal pitch regimes show improvement in aerodynamic performance while benefitting from easier implementation. The H-rotor C_{Pmax} increases from 0.325 to 0.378, a gain of 16% and the V-rotor C_{Pmax} increases from 0.265 to 0.272, a gain of 3%. Fixed pitch provides an improvement in C_{Pmax} of 2.1% for the H-rotor and 0.54% for the V-rotor.

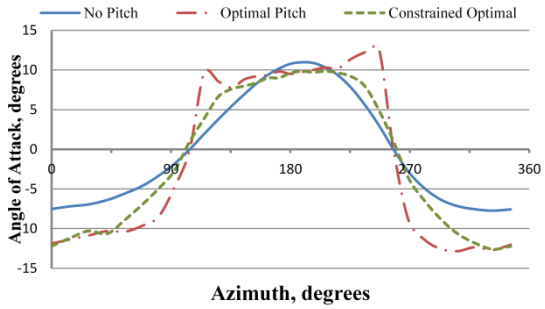

a) α vs θ at the middle blade segment for the H-rotor

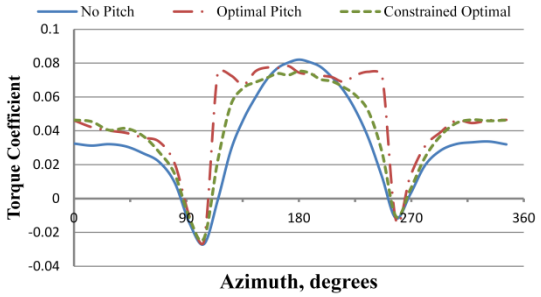

b) C_Q vs θ at the middle blade segment for the H-rotor.

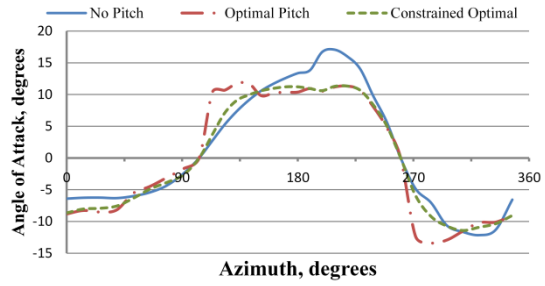

c) α vs θ at the middle blade segment for the V-rotor

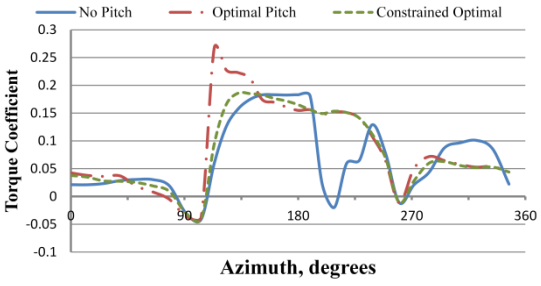

d) C_Q vs θ at the middle blade segment for the V-rotor

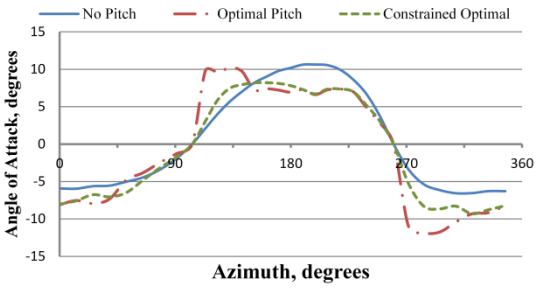

e) α vs θ at the near-tip blade segment for the V-rotor

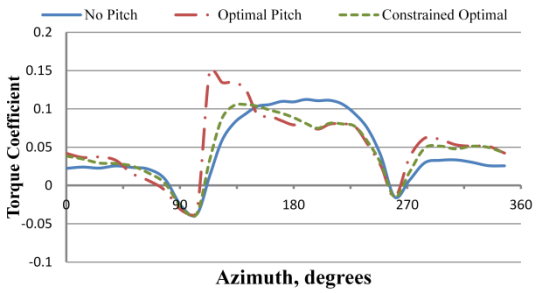

f) C_Q vs θ at the near-tip blade segment for the V-rotor

Figure 6-10: Azimuthal variation of the turbines operating with and without the peak C_P pitch regimes, λ=4.5.

Figure 6-10 depicts the impact of the pitch regime on α and C_Q for both turbines. This permits closer scrutiny of the effect of the pitch regimes on the aerodynamics of the test turbines at λ_{opt} of 4.5. It is evident from Figure 6-10 a) that the optimal H-rotor pitch regime acts to flatten α and maintains a value close to 10° for the upwind sweep. It is interesting to note that the optimal α values upstream are far from the static stall angle of 16° which have the highest lift coefficient. This is because a compromise exists between the performance upstream and downstream. A lower torque in the upstream sweep implies less energy extraction, and thus higher wind speed can pass through to the downwind pass, improving aerodynamic performance downwind. Despite the fact that α is steadily increasing for $140° < \theta < 250°$, C_Q remains relatively flat in this region. This is because the net wind speed drops as the blade moves through this azimuthal range and it suggests that there is an optimal energy extraction for any azimuthal position. The plot of C_Q in Figure 6-10 b) confirms that the pitch regime is successful in generating more torque in most of the blade sweep. The constrained pitch regime demonstrates lower torque than the optimal pitch regime near the outer sections of the path of rotation.

The effect of the pitch regime on α and C_Q for the V-rotor at the middle blade segment is illustrated in Figure 6-10 c) and d) respectively. Both the optimal and the constrained optimal regimes manage to avoid a portion of stall occurring between $190^o < \theta < 250^o$. The effect of the pitch regime on α and C_Q for the V-rotor at the 8th blade segment (near-tip) is illustrated in Figure 6-10 e) and f) respectively. This segment is selected because it displays the same range of α as the H-rotor middle blade segment. The pitch appears to be detrimental to performance in the region $180^o < \theta < 250^o$. This is an interesting result because it reveals that the optimisation has sacrificed performance towards the tip of the blade by reducing $|\alpha|$ in order to avoid stall closer to the root. Avoiding stall in the lower sections of the V-rotor must therefore be more beneficial to aerodynamic performance according to this torque maximising optimisation, instead of attempting to get more from the tip sections which would result in pushing the lower blade further into stall.

6.4.3 Alleviating Cyclic Loading

While it is well established in the literature that blade pitching can improve aerodynamic performance, blade pitching can also be employed to alleviate cyclic loads on the structure. Pitching is capable of redistributing the aerodynamic loads within a VAWT's cycle without significantly compromising on aerodynamic performance [144]. A pitch regime is presented here that aims to minimise the peak flapwise root blade bending moment, $M_{B\text{-}rf}$, which is described in Section 4.7.2.3, without reducing the power performance. To a certain degree, this can be accomplished with a non-zero fixed pitch angle [145]. A fixed pitch regime is therefore also included in this investigation to assess the benefits – in the context of reducing loads – of the additional mechanical complexity required for

variable pitch. An optimisation procedure is followed which generates variable pitch regimes tailored to each test turbine.

In order to identify the best alleviation of cyclical loading achievable with a fixed offset pitch, the following procedure is used. For both turbines the fixed offset pitch value is varied and $M_{B\text{-}rf}$ is generated in StrathDMS for the optimal λ. The most effective fixed offset pitch in terms of reducing the maximum value of $M_{B\text{-}rf}$ is $\beta = 1.3$ for the H-rotor and $\beta = 1.4$ for the V-rotor.

The following optimisation procedure is followed for each turbine to design a pitch regime which minimises the peak $M_{B\text{-}rf}$ without reducing the power performance. First, the pitch regime is assumed to be a combination of sinusoids in the form of (6-1). This form permits a wide range of regimes to be explored which can differ up and downstream and the parameter based structure lends itself to a logical optimisation procedure. The condition that the up and downstream regimes have the same offset, e, ensures smooth transition of $\beta(\theta)$ at the outer azimuthal locations.

$$\beta(\theta) = \begin{cases} e + f_1 \cos\theta + f_2 \sin\theta & \textit{upstream} \\ e + g_1 \cos\theta + g_2 \sin\theta & \textit{downstream} \end{cases} \qquad \textbf{(6-1)}$$

The parameters are varied within a bounded domain with a uniform sampling for each parameter. For each set of parameters, StrathDMS estimates aerodynamic performance of the turbine at $\lambda = 4.5$, with $\beta(\theta)$ implemented as prescribed in Section 4.6.1, to generate the forces on the turbine for the full path of rotation and the largest absolute value of $M_{B\text{-}rf}$ is stored. Among all combinations of (e, f_1, f_2, g_1, g_2), the extreme $M_{B\text{-}rf}$ is minimised subject to the constraint that C_P must remain above 100% of the

C_{Pmax} without a pitch regime. The optimal pitch parameters generated by this procedure for both turbines are provided in Table 6-1 and the associated pitch regimes are illustrated in Figure 6-11.

Table 6-1: Optimal parameters for cyclic load alleviation pitch regime

Parameter	e [deg]	f_1 [deg]	f_2 [deg]	g_1 [deg]	g_2 [deg]	Extreme $M_{B\text{-}rf}$ [MNm]
H-rotor	-0.2	-1.8	0.4	1.2	-0.3	0.55
V-rotor	0.3	-2.8	-0.4	-1.1	-0.8	3.76

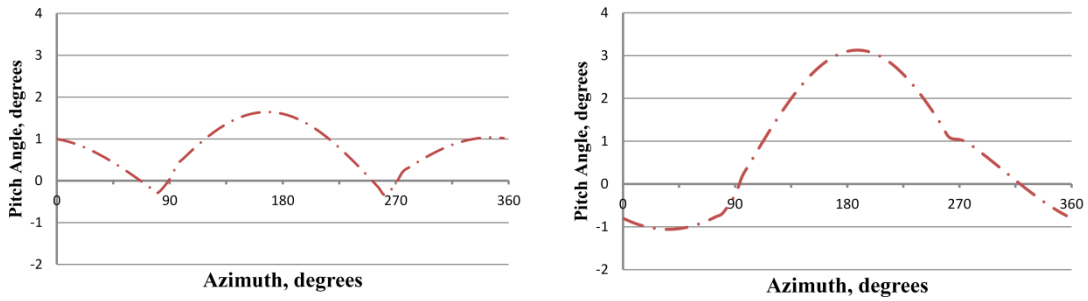

a) H-rotor **b) V- rotor**

Figure 6-11: The pitch regimes designed to alleviate cyclic loading for λ=4.5

Figure 6-12 is a set of performance curves for the two test turbines with and without the pitch regimes applied. Applying the variable pitch regimes causes no significant detriment to aerodynamic performance at any operating λ for either the H or the V-rotor. The fixed pitch has a negligible effect on C_P for the H-rotor. The fixed pitch has a negligible effect on C_P for the V-rotor when $\lambda < 5$ and higher λ show a detrimental effect on aerodynamic performance.

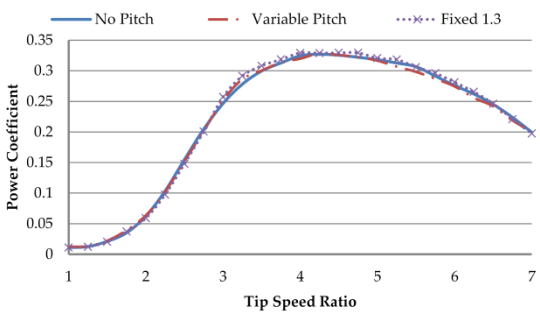

a) H-rotor

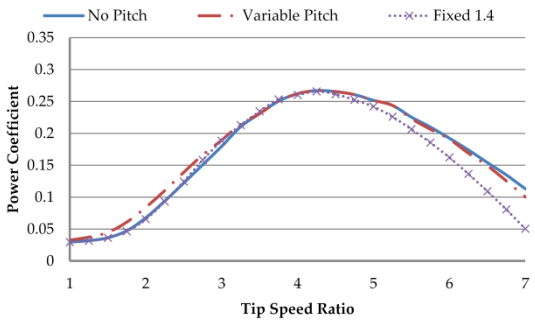

b) V-rotor

Figure 6-12: C_P vs λ with and without the load alleviating pitch regime applied

In Figure 6-13, the impact of the pitch regimes on α and C_Q are illustrated for both turbines operating at optimal λ of 4.5. Figure 6-13 a) and b) are plots of α and C_Q respectively for the H-rotor and Figure 6-13 c) and d) are plots of α and C_Q respectively for the V-rotor. For both turbines, without pitch, the upstream angles of attack are all under the static stall angle and the pitch regime reduces them further in this region in order to impose less reduction of wind speed, so higher winds are experienced in the downwind pass. Ultimately these variable pitch regimes redistribute the energy extraction between the up- and down-stream passes of the blades and it is demonstrated in Figure 6-13 b) and d) that for both turbines, the torque upstream is alleviated and this loss in driving torque is balanced by an improvement in torque downstream.

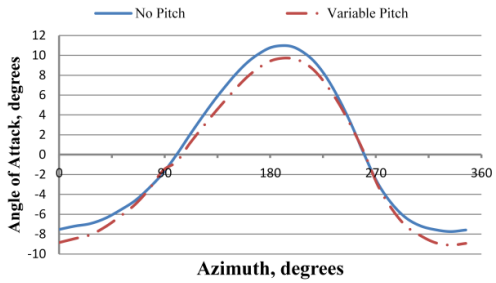

a) α vs θ at the middle blade segment for the H-rotor

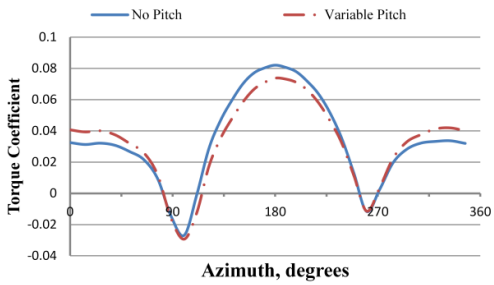

b) C_Q vs θ at the middle blade segment for the H-rotor

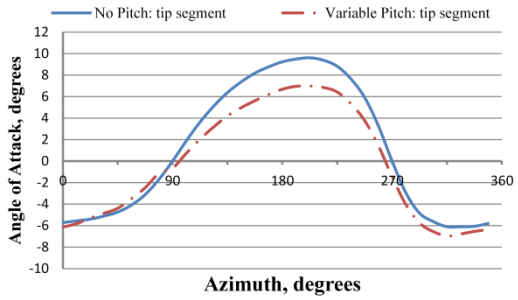

c) α **vs** θ **at the near-tip blade segment for the V-rotor**

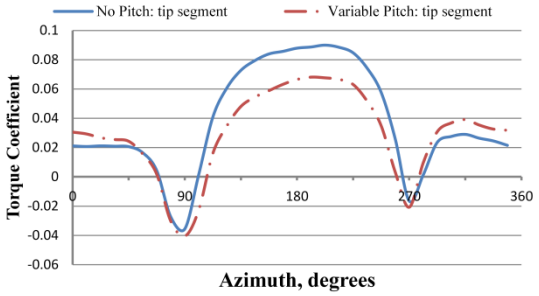

d) C_Q **vs** θ **at the near-tip blade segment for the V-rotor**

Figure 6-13: Azimuthal variation of the turbines operating with and without the load alleviating pitch regime, λ**=4.5**

For both rotors, the loadings that are used to assess the performance of the pitch regime are $M_{B\text{-}rf}$, $M_{B\text{-}re}$, $M_{OT\text{-}x}$ and $M_{OT\text{-}y}$ see Section 4.7.2.3. The impact of the pitch regimes on extreme loading is summarised in Table 6.2 while Figure 6-14 illustrates the dominant bending moments, $M_{B\text{-}rf}$ and $M_{OT\text{-}x}$ for each turbine.

Table 6.2: Extreme values of aerodynamic loads for the turbines with three pitch regimes.

H-rotor	$M_{OT\text{-}x}$ (MNm)			$M_{OT\text{-}y}$ (MNm)			$M_{B\text{-}re}$ (MNm)			$M_{B\text{-}rf}$ (MNm)		
	max	min	range	max	min	range	max	min	range	max	min	range
No Pitch	4.47	3.70	0.77	0.27	-0.29	0.56	0.097	-0.008	0.106	0.66	-0.45	1.11
Variable	4.05	3.57	0.48	0.16	-0.17	0.32	0.062	-0.008	0.070	0.53	-0.48	1.01
Fixed1.3	4.51	3.77	0.74	0.46	-0.1	0.56	0.079	-0.008	0.087	0.59	-0.53	1.12
V-rotor	$M_{OT\text{-}x}$ (MNm)			$M_{OT\text{-}y}$ (MNm)			$M_{B\text{-}re}$ (MNm)			$M_{B\text{-}rf}$ (MNm)		
	max	min	range	max	min	range	max	min	range	max	min	range
No Pitch	7.31	6.00	1.31	0.60	-0.63	1.23	0.73	-0.08	0.81	5.68	-3.67	9.35
Variable	5.70	5.06	0.64	0.14	-0.50	0.64	0.53	-0.08	0.61	3.73	-3.76	7.49
Fixed1.4	7.43	6.14	1.29	1.11	-0.12	1.23	0.64	-0.08	0.72	4.79	-4.82	9.61

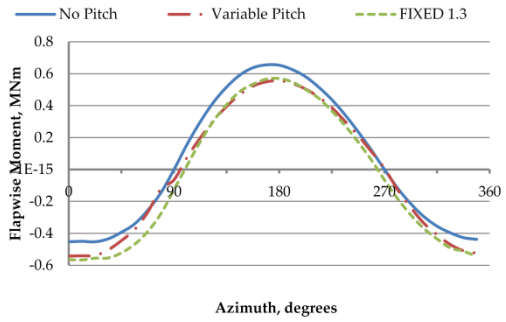

a) $M_{B\text{-}rf}$**, H-rotor**

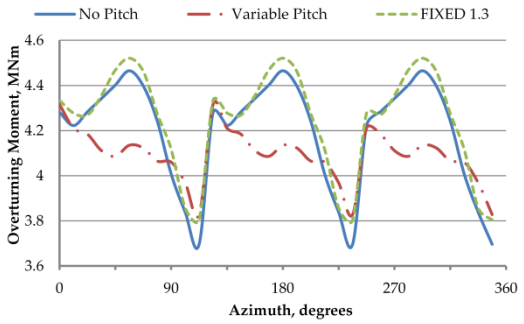

b) $M_{OT\text{-}x}$**, H-rotor**

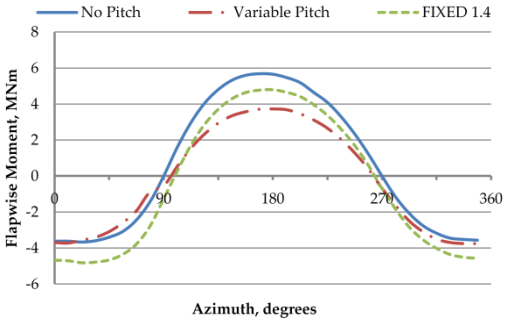

c) $M_{B\text{-}rf}$**, V-rotor**

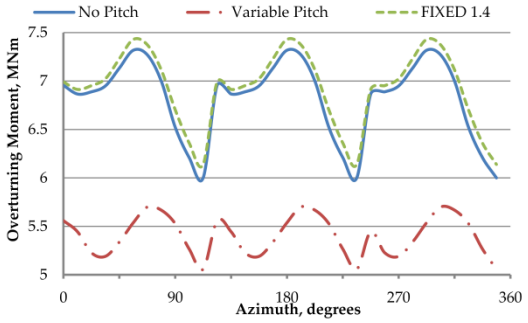

d) $M_{OT\text{-}x}$**, V-rotor**

Figure 6-14: Structural loads with three pitch configurations: no pitch, load smoothing variable pitch, fixed pitch, λ=4.5

In the case of the H-rotor the variable pitch regime is more successful than fixed pitch at reducing all loads. The pitch regime is designed to minimise $M_{B\text{-}rf}$ and from Figure 6-14 a) it appears to shift the azimuthal variation in $M_{B\text{-}rf}$ negatively. This avoids large positive fluctuations upstream. The fixed pitch regime produces a very similar result. The extreme values in Table 6.2 confirm that variable pitch reduces the range of $M_{B\text{-}rf}$ by 9%. In addition, all other measured loads are alleviated. Variable pitch is capable of reducing the range of $M_{OT\text{-}x}$, $M_{OT\text{-}y}$ and $M_{B\text{-}re}$ by 38%, 43% and 34% respectively compared to the zero pitch case.

In the case of the V-rotor the variable pitch regime is again more successful than fixed pitch at reducing all loads. It is evident from Figure

6-14 c) that while fixed pitch simply shifts the variation in $M_{B\text{-}rf}$, variable pitch alleviates the positive fluctuation upstream without increasing any negative fluctuation downstream. The extreme values in Table 6.2 confirm that variable pitch reduces the range of $M_{B\text{-}rf}$ by 20%. This result shows that variable pitch is more effective at reducing $M_{B\text{-}rf}$, without impacting aerodynamic performance, of the V-rotor compared with the H-rotor. Variable pitch is capable of reducing the range of $M_{OT\text{-}x}$, $M_{OT\text{-}y}$ and $M_{B\text{-}re}$ by 51%, 48% and 25% respectively compared to the zero pitch case. The mean $M_{OT\text{-}x}$ of the VAWT can be determined by averaging the values displayed in Figure 6-14 d) and in addition to reducing the range of $M_{OT\text{-}x}$ experienced, applying the variable pitch regime has reduced the mean $M_{OT\text{-}x}$ of the V-rotor from 6.75 MNm to 5.45 MNm, a reduction of 20%.

The reductions in blade and overturning moments achieved with cyclic variable pitch here are significant. However, it must be stressed that this exploration considers only aerodynamic loading from steady uniform winds. The loadings generated here may thus be far from realistic values. Those sources of loading that are absent from this investigation include stochastic aerodynamic loading from turbulence, inertial loading arising from dynamic motion of the flexible members, and the interaction between this and the aerodynamic forces. For this reason it is not considered worthwhile conducting further fatigue analysis based on the loadings provided here, though there seems to be the potential for blade pitching to significantly reduce the aerodynamic loading of a VAWT without reducing aerodynamic performance.

6.4.4 Power Limiting

One of the key features that can be facilitated by variable pitch is the ability to shed energy when the wind speed rises above rated but the turbine is

limited by the power rating of the generator. Power limiting is one of the fundamental objectives of wind turbine control for HAWTs not only due to the steady power generated in above rated conditions, but also because it permits far more flexibility in the design of the operating strategy which oversees the operation of the turbine [77]. A significant benefit of pitch control is that in above rated conditions, the turbine no longer relies on operating in stall to avoid overrating the generator. In terms of the life of the structure, repeatedly going into stall followed by reattachment with every cycle induces significant fatigue effects due to the fluctuating aerodynamic loading. With pitch control, a pitch regime can be designed which reduces $|\alpha|$ towards 0^o so energy is shed without inducing detrimental fluctuating loads on the rotor. This is far more desirable for the life of the structure.

When U_{inf} rises above rated and ω remains constant, λ will tend to decrease. This decreases the aerodynamic performance of the rotor but it may not be enough to achieve the target power output. It is very difficult to achieve constant power above rated with a purely stall regulated turbine [77] and this section presents two alternative approaches to this issue when variable pitch is available. The first is a mechanically simple method of applying a fixed offset β to suit above rated conditions and the second is to apply a $\beta(\theta)$ which drives α to zero.

In this section, the rated wind speed for both test turbines is 12 ms^{-1} and the target is to achieve constant power output for a set of wind speeds above rated wind speed with the rotor speed being held constant at rated ω.

6.4.4.1 Fixed Pitch Power Limiting

The first method of power limiting is the simpler solution. The goal is to apply a fixed offset β that will achieve the target power output for the new λ,

associated with the above rated U_{inf} and ω rated. The results of this procedure are collected in Table 6.3.

Table 6.3: Fixed β, degrees, required to provide power limitation.

U_{inf} [ms^{-1}]	15	18	21	24
λ	3.6	3	2.57	2.25
H-Rotor	6.5	6.5	6.75	7.25
V-Rotor	7.1	6.65	6.7	7.2

An above rated U_{inf} of 18 ms^{-1} is used to illustrate this power limiting mechanism. Without a power limiting mechanism, when the wind speed increases to 18 ms^{-1}, without a change in ω, the turbine λ will drop to 3 for both rotors. From Figure 6-2, the H- and V-rotors have respective C_P of 0.25 and 0.18. Therefore the power generated from the H- and V-rotor is 2.7MW and 1.9MW respectively. Both rotors must shed energy to maintain respective rated powers. In order to investigate how the power limiting procedure works, α and C_Q are presented against θ for the H- and V-rotor, when the wind speed is 18ms^{-1} in Figure 6-15. It is clear from Figure 6-15 a), c) and e) that the procedure simply reduces α by a positive amount at all θ. This method relies on driving the turbine into stall. When a positive fixed β is implemented, it reduces $|\alpha|$ upstream, but increases it downstream to larger negative values. Thus the power limiting is achieved by causing stall to onset in the downwind pass. Figure 6-15 b) is a plot of the effect of power limiting on C_Q at the middle blade segment of the H-rotor at this wind speed. Power limiting has caused stall to set in for most of the downwind sweep, consequently torque is negative in this region. Upwind, torque is significantly reduced between $90^o < \theta < 180^o$ but for the other half of the upwind sweep stall is avoided and torque actually increases. Overall the

reductions in torque dominate and bring down the aerodynamic efficiency of the rotor. The effect of power limiting on the torque provided by the V-rotor at the middle and tip segments are shown in Figure 6-15 d) and f) respectively. As with the H-rotor the result is that positive fixed β causes stall to set in throughout most of the downwind sweep. By comparing these two plots it is evident that there is significant variation in the impact of this method of power limiting along the blade of the V-rotor. At the middle segment deeper stall occurs than at the tip, but at the same time more torque is provided by the upwind sweep at the middle segment than at the tip. Ultimately, as with the H-rotor, the setting in of stall downstream sufficiently reduces aerodynamic performance of the rotor to maintain rated power at this wind speed.

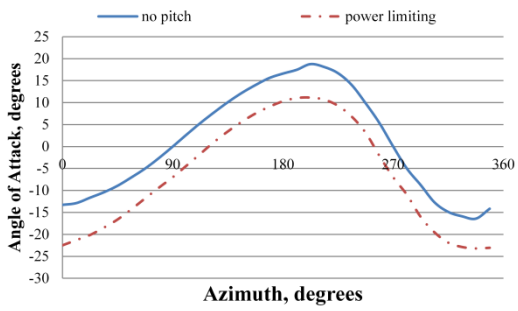

a) α vs θ at the middle blade segment for the H-rotor

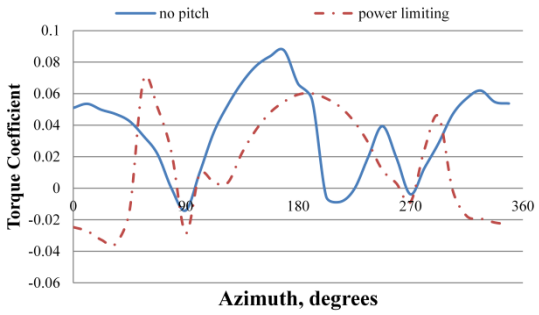

b) C_Q vs θ at the middle blade segment for the H-rotor

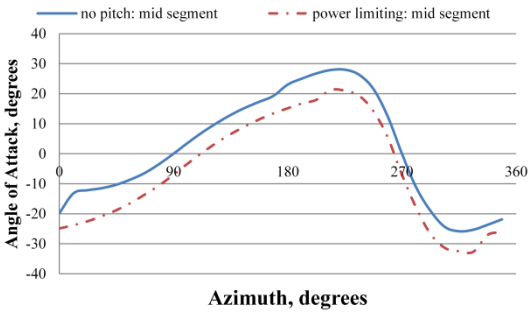

c) α vs θ at the middle blade segment for the V-rotor

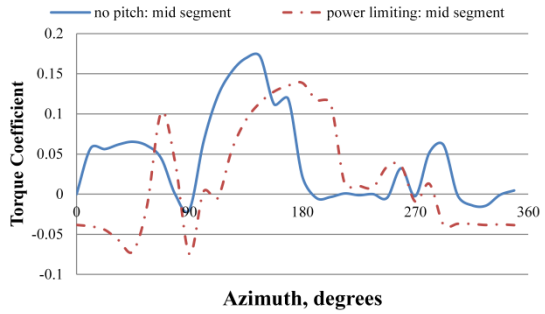

d) C_Q vs θ at the middle blade

segment for the V-rotor

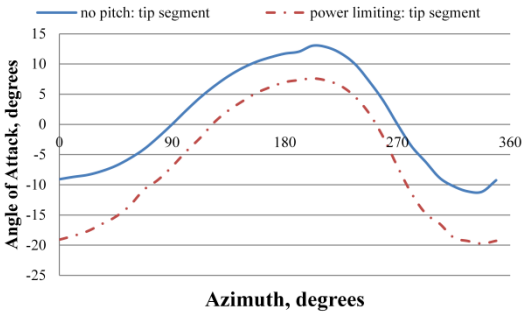

e) α vs θ at the near-tip blade segment for the V-rotor

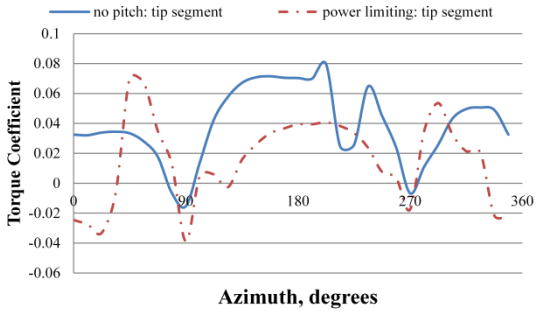

f) C_Q vs θ at the near-tip blade segment for the V-rotor

Figure 6-15: Azimuthal variation of the turbines operating with and without the fixed pitch power limiting pitch regime, λ=3, U_{inf} = 18ms^{-1}.

In order to investigate the impact of power limiting as wind speed increases, the instantaneous torque provided by the H-rotor for the range of above rated wind speeds with power limiting switched on is presented in Figure 6-16. As wind speed increases, deeper stall is occurring downstream but this is accompanied by more torque being provided by the upstream sweep. An important feature highlighted by Figure 6-16 is that there is not a wind speed from the set considered where the entire cycle is in stall. Negative blade damping [146] occurs when the blade remains in stall for the whole path of rotation and it is crucial that the blade moves out of stall for some of the rotor cycle to prevent oscillations of the blade building up.

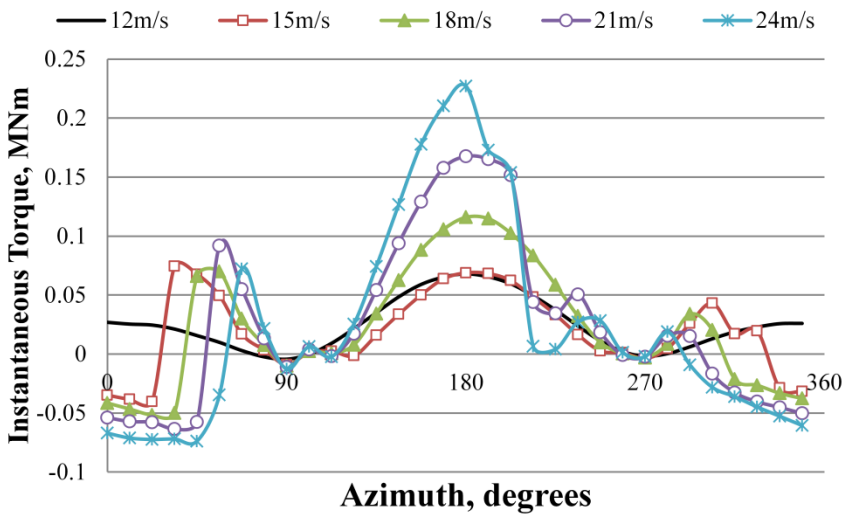

Figure 6-16: Instantaneous torque against azimuth for the middle blade segment of the test H-rotor at different wind speeds with power limiting pitch implemented.

While achieving effective power limiting, the procedure prescribed here does rely on pushing the turbine into stall. Stall induces more cycles in the loading which contributes to blade fatigue and should be avoided, particularly above rated where wind speed and hence loads are extremely large.

6.4.4.2 Driving Angle of Attack to Zero

A more desirable method of power limitation in terms of fatigue alleviation is to implement a variable $\beta(\theta)$ which drives α to 0^o. The objective of the regime is to reduce $|\alpha|$ so lift and hence driving torque is diminished as wind speed increases, instead of driving the turbine into stall.

An unpitched VAWT experiences positive φ upstream and negative φ downstream. The pitch that will be required to reduce $|\alpha|$ is therefore positive β upstream and negative β downstream according to the expression in (2-5). This investigation assumes that a pitch regime suitable for driving α towards 0^o is of the form in (6-2) where ε is a positive real number parameter that is selected to suit the wind speed.

$$\beta(\theta)_\varepsilon = -\varepsilon \cdot \cos(\theta) \quad \textbf{(6-2)}$$

This is a crude pitch regime that does not reflect the difference in flow field up and downstream. However, the reliance on only one constant is well suited to the control task of determining a regime that can be adjusted to suit a change in wind speed.

As with the previous section, a range of above rated wind speeds are considered and the goal is to find a $\beta(\theta)_\varepsilon$ that will achieve the target power output for the new λ, associated with each above rated U_{inf} and ω rated. For each of the above rated wind speeds, ε is varied to find the $\beta(\theta)_\varepsilon$ that achieves the target power output. The results of this procedure are collected in Table 6.4.

Table 6.4: ε, degrees, required to provide power limitation.

U_{inf} [ms^{-1}]	15	18	21	24
λ	3.6	3	2.57	2.25
H-Rotor	7.1	11.5	15.5	20
V-Rotor	24.1	30.1	35.2	40.4

The pitch regimes that successfully provide power limiting above rated by driving α to 0^o are illustrated in Figure 6-17. The H-rotor regimes in a) require up to 20^o pitching to limit the power with this method. The V-rotor regimes in b) require extremely large pitch ranges to permit power limiting with this method. For a wind speed of $24ms^{-1}$, the V-rotor requires $\beta = 40.4^o$ at the most upwind and furthest downwind positions. The root of a V-rotor experiences a very wide range of φ, therefore large values of β are required to ensure the lower portion of the blade is driven towards $\alpha = 0^o$. The excessive range of β required makes this power limiting approach prohibitively mechanically complex.

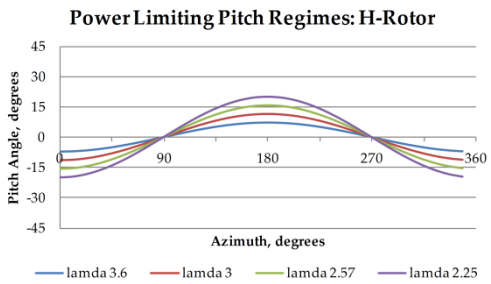

a) H-rotor

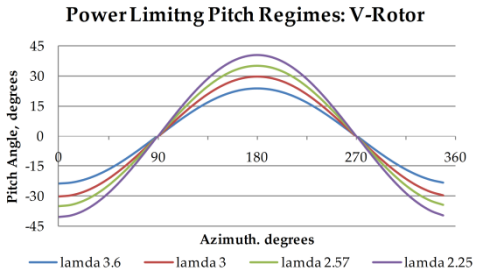

b) V-rotor

Figure 6-17: Power limiting pitch regimes for driving α to 0°

In order to investigate how this approach to power limiting maintains a steady power output as wind speed increases, the instantaneous torque provided by the middle segment of the H-rotor for the range of above rated wind speeds with power limiting switched on is presented in Figure 6-18. As wind speed increases, the torque contribution remains well balanced between the up and downwind portions. There are no sharp drops in the torque contribution because the pitch regime is acting to keep the blade out of stall. Comparing this with Figure 6-16, which shows a similar plot when the simple fixed β approach to power limiting is applied, Figure 6-18 demonstrates that driving α to 0° is beneficial in terms of the life of the structure because this regime avoids any portions of negative torque and any sharp changes in torque.

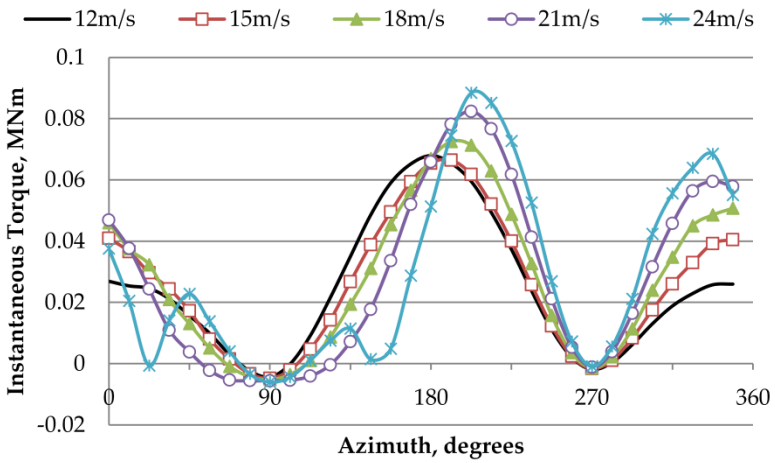

Figure 6-18: Instantaneous torque against θ for the middle blade segment of the test H-rotor at different wind speeds with power limiting pitch implemented.

The $\beta(\theta)$ generated for this investigation are relatively simple cyclic regimes. The simplicity was intentional so that the pitch regime is defined entirely by the direction of the free stream flow, which sets the location of $\theta = 0^{o}$, and ε which can be stored as a function of U_{inf}. In this way the very basics of a responsive pitch regime can be outlined. The pitch regime, based on the parameter ε, can be adjusted according to an estimate of the wind speed. Implementing an above rated responsive operating strategy is beyond the scope of this thesis and is suggested as further work.

Furthermore, there is a continuous range of $\beta(\theta)$ that would achieve the target power output for a given above rated wind speed because pitching can redistribute loading. Therefore, suggested further work is to combine the objectives of achieving a target power output while minimising cyclic loads as in Section 6.4.3. The major disadvantage of this power limiting approach is the prohibitive mechanical complexity required to pitch throughout such a large range of β, so the impact of limitations on $|\beta|$ should be investigated.

6.4.5 Overspeed Protection

A significant benefit of variable pitch wind turbines is that the rotor can provide aerodynamic braking when the turbine requires a shut-down such as during extreme wind conditions. Therefore the requirements of other forms of braking, such as mechanical brakes, can be alleviated. This investigation presents a simple, robust method of providing aerodynamic braking of the test rotors based on sustaining a fixed offset β.

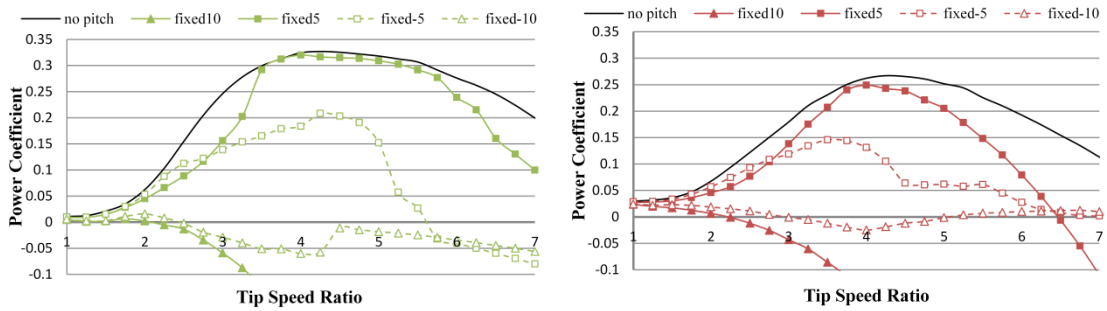

a) H-rotor **b) V-rotor**

Figure 6-19: C_P vs λ for a range of fixed pitch offsets

Figure 6-19 presents C_P against λ for the two test turbines when a range of fixed pitch offsets are applied. Five different simulations are shown for each turbine for fixed β in the set [-10°, -5°, no pitch, 5°, 10°] and it is clear that maintaining a fixed pitch of 10° is sufficient for generating a negative aerodynamic torque and hence providing aerodynamic braking for both VAWTs. In this case, aerodynamic performance is very low because the aerofoils are in such deep stall for the entire downwind pass.

This fixed pitch method of overspeed protection is essentially an extension of the mechanically simple power limiting procedure outlined in

the previous section. While it does rely on pushing the blades into stall in the downstream sweep, the advantage is that it is a robust approach.

By implementing the appropriate control objectives for the whole operating envelope, power curves are generated for the test turbines as illustrated in Figure 6-20. For $U_{inf} < 5ms^{-1}$ the turbine does not switch on. When the turbine first switches on a pitch regime which improves start-up performance is switched on to provide high torque. As U_{inf} increases from 5 ms^{-1} up to rated speed of 12 ms^{-1} the C_{Pmax} is maintained and power increases with the cube of the wind speed. When U_{inf} increases past 12 ms^{-1} power limiting is implemented by either applying the correct fixed pitch or applying the $\beta(\theta)_\varepsilon$ that suitably reduces $|\alpha|$ to maintain the rated power of the turbine. For $U_{inf} > 24ms^{-1}$ the turbine shuts down aided by aerodynamic braking in order to protect the structure in rare extreme gusts.

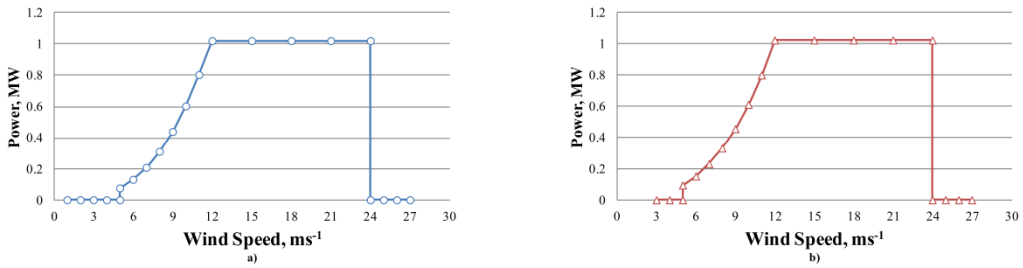

a) H-rotor **b) V-rotor**

Figure 6-20: Power curves for the test turbines

6.5 Summary

In this chapter, StrathDMS is used to demonstrate the range of VAWT control objectives that are achievable using cyclic pitch regimes for two different configurations of VAWT with pitching straight blades, an H-rotor and a V-rotor, each with a swept area of $3000m^2$. The following VAWT control objectives are identified that could be achieved using cyclic blade

pitching: improving start-up by avoiding stall at low tip speed ratios; improving peak aerodynamic performance in below-rated conditions; alleviating cyclic loading on blades and other structural members; power limiting in above rated conditions; and overspeed protection by providing aerodynamic braking.

There is a coupling between the upstream and downstream energy extraction that must be considered when designing a pitch regime for VAWTs for any objective. For example, when optimising aerodynamic performance, operating the turbine at the angle of attack associated with highest lift upstream may improve performance in a localised position, but this extra energy extraction upstream will reduce the energy available downstream and this detriment to performance could dominate. This coupling increases the complexity of searching for an optimal pitch regime and suggests that an optimisation must consider the aggregated effects on performance up- and downstream for each azimuthal position.

The pitch regime designed to improve rotor aerodynamics at low λ successfully improves the torque generated by avoiding stall, though it requires excessive pitch angles in the range of -25° to 25°. An optimisation with the objective of increasing C_{Pmax} by maximising the torque on a streamtube by streamtube basis is successful for both turbines. The α generated for the turbines with optimal pitch regimes applied are significantly lower than the static stall angles that maximise lift. The torque contributions are relatively flat across the upstream sweep for the H-rotor, which suggests that the optimal energy extraction is independent of the azimuthal position in most of the upstream sweep. Improvements in C_{Pmax} from blade pitching are significantly higher for the H-rotor compared to the V-rotor.

Although alleviating cyclic and transient structural loads has become a primary control objective for pitch control of HAWTs, very little work has been done in applying this to VAWT technology. An optimisation procedure is presented which searches for a pitch regime that minimises the peak flapwise blade root bending moment without compromising on C_P. By spreading the energy extraction more evenly around the whole path of rotation, the pitch regimes generated by this procedure successfully alleviate large load fluctuations local to the furthest upstream azimuthal position. It was demonstrated that for VAWTs, overturning moments in the expected windward direction are accompanied by smaller moments in the crosswind direction and flapwise blade bending moments are an order of magnitude larger than edgewise blade bending moments. Cyclic pitching is significantly more successful at alleviating cyclic loading with the V-rotor compared with the H-rotor.

Two different approaches to power limiting are developed. The first is based on varying a fixed pitch angle as the wind speed increases to reduce the aerodynamic torque provided by the rotor and hence maintain a steady power output. It is demonstrated that this approach is effective and robust because the required fixed pitch is insensitive to wind speed; however, it does drive the turbine into stall. The alternative power limiting technique applies a pitch regime which drives α towards 0^o in above rated conditions. This is found to provide significant benefits in terms of fatigue of the structure, but it requires β as high as 40.4^o for a wind speed of 24 ms^{-1}. Overspeed protection is demonstrated for both turbines by applying a fixed pitch value that drives the turbine into such deep stall downstream that C_P is zero or negative for all λ.

Investigating objectives spanning the whole operating envelope of a variable speed VAWT has revealed some significant differences between the H- and V-rotor configurations, and the potential improvements of each from pitching. The V-rotor has better start-up capability. Cyclic blade pitching has the potential to increase C_{Pmax} by a significantly larger proportion with the H-rotor. However, alleviation of cyclic loading with blade pitching is more successful for the V-rotor. Both configurations demonstrate similar potential to be controlled for power limitation and overspeed protection in above rated conditions with cyclic pitching.

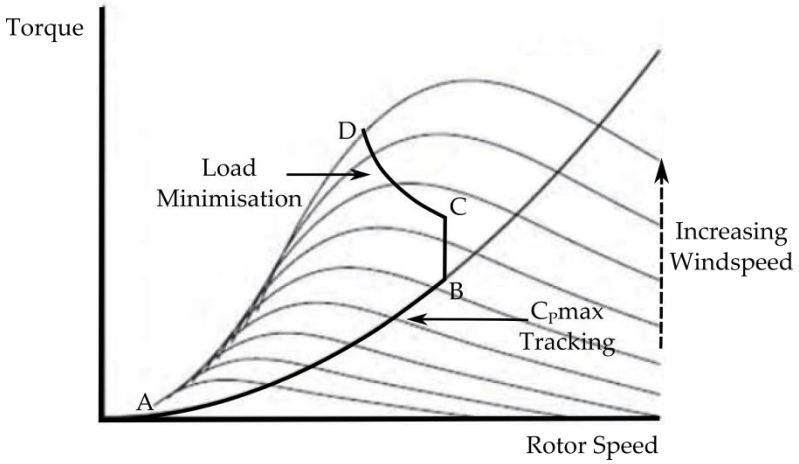

Figure 6-21: A potential operating strategy for a variable speed VAWT

This Chapter has investigated a range of control objectives for a variable speed VAWT in isolation but to design a complete operating strategy for this classification of wind turbine, a process of switching between the modes is necessary. This is a particularly complex task for VAWTs because changes due to azimuthal variation must be reconciled with changes in operational conditions such as free stream wind speed. There are a wide range of options available for how to diverge from the C_{Pmax} tracking region in above rated conditions. One such operating strategy is illustrated in Figure 6-21. The point at which, the strategy moves away from C_{Pmax} tracking is dictated by the rated wind speed of the turbine. A sensible option for

moving towards the stall front above rated may be to follow a strategy that minimises loading because the primary control objective above rated is to protect the turbine in the heavy loaded conditions. One potential criterion would be to diverge from the C_{Pmax} tracking in such a way that minimises the overall fatigue damage. Fatigue is induced by aerodynamic forces and centrifugal forces that scale with rotor speed. Therefore in above rated wind speeds, rotor speed could be reduced to alleviate centrifugal forces and cyclic blade pitching could be employed, as discussed in Section 6.4.3, to minimise aerodynamic forces. A model that estimates dynamic loads could be used to identify a strategy that minimises loading, shown here as the portion CD. The below and above rated strategies would have to be connected by a simple constant rotor speed operating mode shown as BC to mitigate switching issues.

Chapter 7

Conclusion

A significant challenge facing the wind sector today is how to harness offshore wind in a cost effective manner. There is growing support for the argument that engineering current HAWT technology to tolerate the offshore environment is not ideal and a rethink of how to exploit the conditions is required. Despite their inherently poor aerodynamic characteristics, VAWTs have some competitive structural advantages that make them potential candidates for the offshore environment; structural simplicity which improves scalability, and the potential to house the drive train at the base of the structure to provide ease of access and a low centre of gravity.

Current VAWT designs that are emerging to suit this opportunity are relatively simple and many lessons can be drawn on the development of variable speed, pitch regulated HAWTs over the past two decades. This thesis is focused on the areas of aerodynamic modelling, rotor design and control of VAWTs that aim to bring VAWTs in line with the performance of state of the art HAWTs. This Chapter provides the conclusions of the thesis and suggests further work.

7.1 Aerodynamic Estimation Model

Model Development

An aerodynamic estimation tool, based on the double multiple streamtube method, is developed in this thesis and is referred to as StrathDMS. It is capable of modelling piecewise linear blade VAWTs including the H-rotor and V-rotor configurations. The model captures tip loss effects, streamtube expansion and includes Strickland's adaptation of the Gormont dynamic stall model. StrathDMS can model variable pitch of the VAWT blades so it can be used for investigating the impact of predefined pitch regimes or designing a pitch regime to achieve a given objective. The model is validated against previous published experimental data for both fixed and variable pitch VAWTs. The results show that StrathDMS is successful at predicting induced local flow conditions and general performance for the whole range of λ from start-up to run-off. Previous VAWT models generally over-predicted the potential C_P improvements made possible with variable pitch. StrathDMS demonstrates more modest and realistic estimations of VAWT aerodynamic performance. The only experimental VAWT data available is from constant speed machines. A more valuable validation would be to compare StrathDMS predictions with experimental data from a more sophisticated variable speed machine such as the VAWT prototypes that are beginning to emerge for the offshore sector including the Vertiwind turbine or the Modec Skwid turbine.

StrathDMS is a useful tool for prediction of aerodynamic performance and it can be used for basic design studies for VAWT rotors. However, the current model does not account for any structural dynamics and a natural progression of the tool would be to evolve it into an aeroelastic model which

incorporates rotor inertia. An understanding of the relative scale of aerodynamic forces and structural forces and the coupling between them is necessary for much more detailed design of specific rotors as opposed to the general investigations provided in this thesis.

Streamtube Expansion and Fanning

A phenomenon, referred to as fanning, which to date has not been investigated, is identified in this thesis. Fanning is caused by variation in induction factors along a VAWT blade, leading to varying degrees of streamtube expansion for different blade sections. This effect is particularly significant for tapered blades and V-rotors due to the relatively high local solidity near the root leading to higher flow induction in this region. The consequence of fanning is that actuator surfaces that share the same streamtube number at different positions along the blade span will subtend different portions of the rotor cycle. Therefore, particular azimuthal positions can straddle more than one streamtube number. This is important when exploring variable pitch because the same pitch angle must be applied for any particular azimuthal position and this could involve two or more streamtube numbers. The effect of fanning is exacerbated when a larger number of streamtubes is selected for the swept area mesh because streamtubes become narrower.

The flow expansion model used in StrathDMS is implemented in such a way that gives rise to two areas for further work. The first is regarding the resolution of the streamtube mesh. The starting point of a procedure to determine flow conditions for the whole 2D path of rotation is to determine the induction factors and hence, the streamtube widths at the central streamtube which is aligned with the x-axis. Subsequently the procedure determines the widths for the pair of streamtubes straddling the central

streamtube. This process continues out towards the outer points of the path of rotation for a predetermined number of streamtubes. However, an improvement would be to avoid predetermining the number of streamtubes. There is potential for the model to increase the resolution of the mesh in conditions where complex phenomena occur. For example, triggered by high values of angle of attack near the static stall angle, the number of streamtubes could increase to provide more information as unsteady dynamic stall occurs. The second suggestion for further work is to investigate the effects of flow expansion in the z direction. There is a boundary condition at the bottom of the structure therefore a natural procedure would be to determine the vertical expansion at the root of the blade and work up towards the tip.

7.2 Fixed Pitch Straight Blade VAWT Design

Effective Lift to Drag Ratio

Lift to drag ratio is a standard measure of performance for HAWT blades because a blade segment can sustain a relatively steady angle of attack. In the past this ratio has not been used for VAWT blades because the time varying angle of attack leads to variable lift to drag ratios for each blade segment. A new measure, referred to as effective lift to drag ratio, is proposed which classifies a VAWT blade based on the lift to drag ratio which occurs for a particular λ at an azimuthal position that contributes instantaneous aerodynamic torque sufficiently close to the time averaged aerodynamic torque. This new metric permits comparisons of maximum achievable aerodynamic performance for H-rotors, V-rotors and HAWTs. A key conclusion is that the effective lift to drag ratio associated with a V-rotor blade is lower than that of an H-rotor blade, and both are significantly lower than the lift to drag ratios that are achieved by HAWT blades. Increasing

effective lift to drag ratio has the potential to improve the achievable C_P of any straight blade VAWT and for the V-rotor it would significantly increase the design λ to a value comparable with HAWTs. A design study reveals the impact of effective lift to drag ratio and solidity on maximum H-rotor C_P and optimal tip speed ratio. A similar design study for V-rotors reveals the impact of effective lift to drag ratio and coning angle on maximum V-rotor C_P and optimal λ. Theses design studies can be used to determine optimal design choices for straight blade VAWTs in terms of rotor geometry and operational speed.

Impact of Wind Shear on V-Rotor Design

Wind shear is the variation in free stream wind speed with vertical height and it can be modelled reasonably well as a logarithmic function. This issue can be dealt with by HAWT blade pitch control because each blade will periodically experience the full wind speed gradient. The orientation of VAWT rotors is such that each blade segment will always operate at the same height and therefore the conditions imposed by wind shear can be incorporated into the blade design process. As part of this thesis, a blade is designed that incorporates the logarithmic profile describing wind shear. For a baseline V-rotor design it is demonstrated that using this new blade in place of a straight blade increases power generated by 20% according to StrathDMS simulations. This significant improvement is achieved by increasing the swept area by 16% with only a 1% increase in blade length. Aerodynamic efficiency is also improved because the logarithmic blade permits a larger local radius towards the blade root therefore stall is avoided in this region. A sensitivity analysis reveals how the rotor design parameters and wind shear model parameters influence the potential improvements in aerodynamic performance provided by the logarithmic blade.

The impacts of wind shear on VAWT rotor design can be incorporated in many different ways and this work opens up a range of suggestions for further work. In terms of the new logarithmic blade that is designed, a structural analysis should be carried out to determine the natural modes of such a blade shape and investigate what materials may be suitable to determine the cost of achieving the demonstrated aerodynamic advantages. Certain restrictions are imposed for the investigations in this thesis such as predetermining the rotor base radius and tip radius so that the new blade could be compared with a straight blade. These restrictions could be relaxed to evaluate more generally the potential of using the wind shear to improve VAWT rotor design.

Phase-shifting Wind Farm Control

Torque ripple is the tendency for torque and hence power generated by a VAWT to pulsate in phase with the rotor cycle due to the cyclic nature of the aerodynamics. Aggregation of VAWTs can then lead to excessive power surges in the transmission system when rotors are in phase. Torque ripple can be mitigated by permitting sufficient variation in rotor speed to absorb fluctuations in aerodynamic torque provided by the rotor, however, in above rated conditions, this individual turbine control approach is not applicable because the control system is unstable and rotor speed has to be held tight to the rotor speed set point. Another method of mitigating torque ripple is to use a helical rotor which spreads out the range of azimuthal positions where energy is extracted, but this may not be economical at the multi-megawatt scale. This thesis develops a control based approach which mitigates power surges from aggregated straight bladed VAWTs. The controller aims to maintain a phase difference between adjacent rotors within a small cluster of aggregated VAWTs so that peaks in power cycles do not occur

simultaneously. A dynamic model of a farm of stall regulated VAWTs is developed which employs a stochastic wind speed model and StrathDMS provides a model of the rotor aerodynamics. This wind farm model is used for controller design studies. It is demonstrated that a well-tuned controller is able to significantly reduce aggregated power fluctuations without impacting the average wind farm power output in above rated wind speeds. This control approach is not successful for below rated wind speeds but the turbines are operating in the constant speed mode which could be tuned to account for torque ripple. In extremely high wind speeds the farm controller demonstrates limited success because the onset of stall at the low operating tip speed ratios leads to more peaks in the underlying power signal generated by each individual turbine, and hence there is more chance of peaks occurring simultaneously. The phase-shifting concept is applicable for extreme wind speeds but requires a refined configuration. One area for further work is to determine suitable phase difference set points and run a tuning procedure for the extreme wind speed operating conditions. Generalisation of the phase-shifting wind farm controller for more VAWTs demonstrates that the concept is more effective for a larger number of turbines, however there would be realistic limitations on the number of VAWTs that could be connected together in this manner, and for farms with many turbines a clustering formation is recommended whereby groups of turbines are overseen by a phase-shifting controller.

To take the phase-shifting control concept further, a much deeper understanding of the control dynamics are required. The phase shifting controller is a closed-loop feedback system where the input to the plant is an additive perturbation to drive train torque and the controlled variable is the phase difference between rotors. Averaging or linearisation of the azimuthal

variation of the rotor dynamics might be used to generate a transfer function of the plant. Then with the closed-loop transfer function stability limits and non-minimum phase behaviour could be analysed systematically.

7.3 Variable Pitch for VAWTs

Currently variable pitch is employed in state of the art HAWTs to improve performance above rated. The specific control objectives include power limiting, alleviating cyclic and transient loading, influencing structural dynamics and in extremely high winds, providing aerodynamic braking. Theoretically, VAWTs could benefit from all of these performance improvements by employing variable pitch. Variable pitch can also be utilised to improve VAWT performance in below rated wind speed conditions by increasing start-up torque and increasing peak achievable C_P. The only variable pitch objectives that have been investigated for VAWTs to date are the below rated performance improvements by employing passive and active cyclic pitch regimes. There is a significant gap in the knowledge regarding the potential of variable pitch for VAWTs in above rated conditions.

Exploring Cyclic Pitch Objectives

The ability of StrathDMS to accurately predict the performance of variable pitch VAWTs permits an exploration of cyclic pitch options for variable speed VAWTs in this thesis. Two test case turbines are designed, a similarly rated H-rotor and V-rotor, and five control objectives are identified that span the entire operating envelope for any variable speed wind turbine, namely, providing high torque during start-up; maximising power coefficient in below rated conditions; alleviating cyclic loading; power limiting in above

rated conditions; and overspeed protection in extremely high winds. For each turbine and each objective, a cyclic pitch regime is developed.

The pitch regimes designed for below rated objectives are successful. It is demonstrated that high torque can be sustained throughout start-up conditions but very large ranges in pitch angle are required to avoid the deep stall experienced due to the low tip speed ratios. A suggestion for further work is to investigate the potential for variable pitch to improve start-up capability with limitations on the pitch range imposed. It is shown that variable pitch can increase peak power coefficient and an optimisation procedure is presented. No predefined form for the cyclic pitch regime is assumed for this optimisation. The objective function is to maximise torque from each portion of the rotor cycle, and maximising the combined contribution from tandem actuator surfaces captures the coupling between performance up and downstream. The H-rotor demonstrates potential for a larger increase in C_P from variable pitch compared with the V-rotor.

In the past, variable pitch has not been used to achieve the above rated objectives for VAWTs and this thesis demonstrates that these above rated objectives are realisable with cyclic pitch. It is shown that cyclic loading can be alleviated without impacting aerodynamic performance by using variable pitch to distribute the energy extraction and hence loading throughout the rotor cycle. An optimisation procedure is presented with the objective of minimising the blade flapwise root bending moment because it is the most significant blade bending moment. This optimisation procedure could be redefined to minimise any other blade bending moment or rotor overturning moment. The V-rotor demonstrates more potential than the H-rotor with this optimisation, which suggests further work to investigate the sensitivity of this optimisation to rotor support arm configurations.

Two different approaches to power limiting are presented for a particular above rated wind speed; applying a fixed offset pitch angle, or applying a variable pitch regime. The first approach is robust because the necessary fixed pitch angle does not vary considerably when the free stream wind speed increases. However, this approach relies on inducing stall throughout the downwind cycle and stall causes an increased number of load cycles which entails fatigue penalties. The second approach emulates what a HAWT is able to do to in high wind speeds, which is to drive the angle of attack towards zero, and hence reduce the aerodynamic torque provided by the rotor while maintaining low loading on the structure. This can be done by sustaining a relatively large fixed angle of attack for HAWTs, however with VAWTs, due to the positive and negative flow angles in each rotor cycle, a cyclic pitch regime is required attaining a large range of pitch angles. Therefore while, advantageous in terms of the life of the structure, this power limiting solution is prohibitively mechanically complex for VAWTs. A suggestion for further work is to combine the power limiting objective with an optimisation procedure that minimises cyclic loading.

Aerodynamic braking for VAWTs is demonstrated by applying the mechanically simple fixed offset pitch based approach to power limiting. It is simple to apply, which is critical in these extreme conditions and it is demonstrated that it can provide negative aerodynamic torque, or aerodynamic braking for all tip speed ratios.

Significant differences of the potential of blade pitching for the H- and V-rotor configurations are revealed. The V-rotor has better start-up capability. The H-rotor demonstrates greater potential for increasing C_{Pmax} with blade pitching while the V-rotor demonstrates greater potential for alleviating loading with blade pitching. Both configurations demonstrate

similar potential to be controlled for power limitation and overspeed protection in above rated conditions with cyclic pitching. The impact of wind shear may shift the relative advantages of H- and V rotors but this requires further investigation.

Suggested Further Work

With such a significant gap in the knowledge regarding achieving above rated control objectives with variable pitch for VAWTs, there are many ways this work could be taken forward. The most valuable investigation would be to implement some of the pitch regimes suggested in Chapter 6 on a small scale VAWT to demonstrate the ability for blade pitching to achieve above rated control objectives. All the variable pitch investigations in this thesis employ cyclic pitch, however with responsive pitch, a controller could be developed which responds to changes in operating conditions such as wind speed and direction in real time. By creating three dimensional look up tables which provide normalised aerodynamic torque for a whole blade based on tip speed ratio, azimuthal position and pitch angle, StrathDMS could be employed to design responsive pitch strategies. A dynamic model of a pitch regulated VAWT could then be developed to carry out controller design studies.

Designing an optimal pitch regime for a VAWT for all operating conditions is a complex problem. Below rated wind speed, the speed of rotation and cyclic pitch regime must be selected to optimise aerodynamic performance. This is somewhat constrained by the physical impossibility of the instantaneous flips in pitch required to achieve the ideal pitch regime as the blade crosses between the up- and down-wind sweeps and vice-versa. Above rated wind speed, pitching should be used to limit power, and it would be best to attempt to achieve this whilst mitigating the load

fluctuations in these heavily loaded conditions. The pitch regime above rated would have to be a function of wind speed if rotational speed had to be limited because λ would decrease as wind speed increased and the optimal pitch regime is a function of λ. Switching between pitch regimes for operation below and above rated is an interesting challenge which will require further exploration. Another area for further work is the combination of control objectives such as alleviating loads and limiting power.

One major challenge for variable pitch of VAWTs is reconciling between short term azimuthal variations and longer term variations in wind speed and direction. For example, for a VAWT operating at rated, what determines if an increase in effective wind speed experienced by a VAWT blade is due to an increase in the free stream wind speed or turbine state variables such as rate of change of rotor azimuthal position or pitching dynamics? And should the turbine switch to above rated pitching? With a dynamic model of a pitch regulated VAWT, the merits of various approaches to switching between operating modes could be evaluated.

If StrathDMS could be developed into an aeroelastic tool that permits variable pitching, this would allow exploration of the pitch control objectives that currently are achieved with pitch regulated HAWTs, but are omitted from the investigations in this thesis, namely alleviation of transient loading and appropriate influence on structural dynamics such as avoiding blade natural frequencies. Furthermore, a complete operating strategy could be designed based on minimisation of overall fatigue damage in above rated conditions.

7.4 A Future for VAWT Technology?

Wind energy systems have come a long way from the mills that were built 200 years ago. Current wind turbine technology is optimised for maximum power output. However, as turbines begin to be designed exclusively for the offshore environment, reliability and cost reduction, rather than efficiency, could become the driving design factors. Essentially offshore wind turbines must be large and reliable to reduce the cost of energy, and radical new concepts are emerging to address these challenges.

VAWTs are a suitable candidate for the harsh and inaccessible offshore environment and consequently this is a very exciting period for the technology. It is the first time since 1990 that a VAWT with a power rating exceeding one megawatt has been tested [14], and it is tailored for the offshore sector. For utility scale VAWTs to become an investable concept, lessons must be drawn on the development over the past twenty years of the now industry standard three blade, variable speed, pitch regulated HAWT.

The recent interest in VAWTs stems from their potential to reduce the cost of energy for an offshore project, but this remains to be demonstrated. While most major turbine manufacturers, and two new influential market entrants, Samsung and Mitsubishi, strive to engineer the state of the art HAWT to suit offshore conditions, two pioneering groups have embarked on megawatt scale prototyping of offshore VAWTs. The Skwid from Modec is a floating 1.2MW H-rotor and the Vertiwind consortium are testing a 2MW piecewise linear helical rotor as part of the INFLOW project. These utility scale tests are precisely what are required to demonstrate to the market if the VAWT concept really can deliver reductions in offshore wind cost of energy, a claim asserted by many designers and authors for decades. The risk

absorbed by these early adopters may ultimately convince the giants of wind turbine manufacturing that bold engineering now could have an enormous impact on the future of the offshore wind energy sector.

Appendix A: NACA0012 Aerofoil Data

Coefficients of lift and drag for a range of Reynolds numbers and angles of attack for the NACA 0012 aerofoil profile.

Lift:

Alpha	Re 40000	Re 60000	Re 80000	Re 120000	Re 160000	Re 230000
0	0.000	0.000	0.000	0.000	0.000	0.000
1	0.175	0.115	0.100	0.100	0.100	0.100
2	0.295	0.220	0.200	0.200	0.200	0.200
3	0.400	0.340	0.310	0.300	0.300	0.300
4	0.480	0.445	0.420	0.405	0.400	0.400
5	0.560	0.540	0.520	0.500	0.500	0.500
6	0.625	0.620	0.610	0.600	0.600	0.600
7	0.690	0.700	0.700	0.700	0.700	0.700
8	0.740	0.750	0.755	0.775	0.780	0.785
9	0.775	0.780	0.790	0.805	0.810	0.825
10	0.790	0.800	0.815	0.820	0.825	0.845
11	0.800	0.810	0.820	0.825	0.840	0.850
12	0.790	0.800	0.810	0.820	0.825	0.845
13	0.785	0.795	0.805	0.810	0.820	0.830
14	0.780	0.785	0.790	0.800	0.810	0.815
15	0.770	0.775	0.780	0.785	0.790	0.790
16	0.760	0.765	0.770	0.775	0.775	0.775
17	0.750	0.755	0.755	0.760	0.760	0.760

18	0.735	0.740	0.745	0.750	0.750	0.750
19	0.725	0.725	0.725	0.730	0.730	0.730
20	0.720	0.720	0.720	0.720	0.720	0.720
21	0.712	0.712	0.712	0.712	0.712	0.712
22	0.707	0.707	0.707	0.707	0.707	0.707
23	0.728	0.728	0.728	0.728	0.728	0.728
24	0.769	0.769	0.769	0.769	0.769	0.769
25	0.810	0.810	0.810	0.810	0.810	0.810

Alpha	Re 330000	Re 470000	Re 670000	Re 960000	Re 1360000	Re 1940000	Re 2760000
0	0	0	0	0	0	0	0
1	0.100	0.100	0.100	0.100	0.100	0.100	0.100
2	0.200	0.200	0.200	0.200	0.200	0.200	0.200
3	0.300	0.300	0.300	0.300	0.300	0.300	0.300
4	0.400	0.400	0.400	0.400	0.400	0.400	0.400
5	0.500	0.500	0.500	0.500	0.500	0.500	0.500
6	0.600	0.600	0.600	0.600	0.600	0.600	0.600
7	0.700	0.700	0.700	0.700	0.700	0.700	0.700
8	0.790	0.800	0.800	0.800	0.800	0.800	0.800
9	0.840	0.870	0.885	0.895	0.900	0.900	0.900
10	0.860	0.920	0.970	0.985	1.000	1.000	1.000
11	0.865	0.940	1.020	1.060	1.090	1.100	1.100
12	0.860	0.920	1.040	1.130	1.180	1.190	1.200
13	0.845	0.875	0.900	1.050	1.270	1.290	1.300
14	0.820	0.820	0.820	0.905	1.340	1.390	1.400
15	0.790	0.790	0.790	0.800	1.070	1.455	1.490
16	0.775	0.775	0.775	0.775	0.775	1.440	1.520
17	0.760	0.760	0.760	0.760	0.760	0.760	0.760
18	0.750	0.750	0.750	0.750	0.750	0.750	0.750
19	0.730	0.730	0.730	0.730	0.730	0.730	0.730
20	0.720	0.720	0.720	0.720	0.720	0.720	0.720
21	0.712	0.712	0.712	0.712	0.712	0.712	0.712
22	0.707	0.707	0.707	0.707	0.707	0.707	0.707
23	0.728	0.728	0.728	0.728	0.728	0.728	0.728
24	0.769	0.769	0.769	0.769	0.769	0.769	0.769
25	0.810	0.810	0.810	0.810	0.810	0.810	0.810

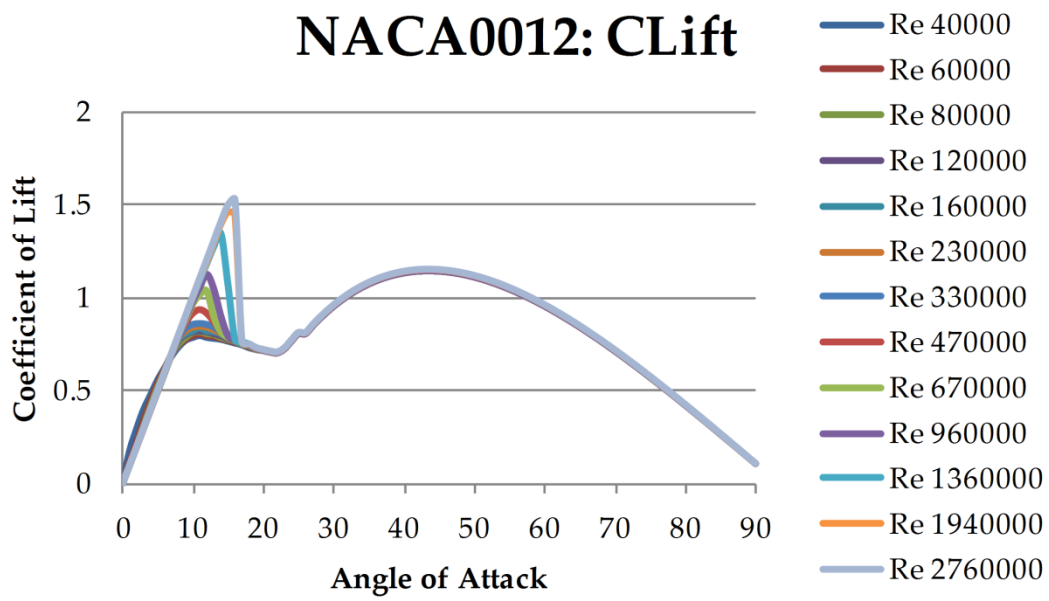

Figure A-0-1: Clift including stalled data

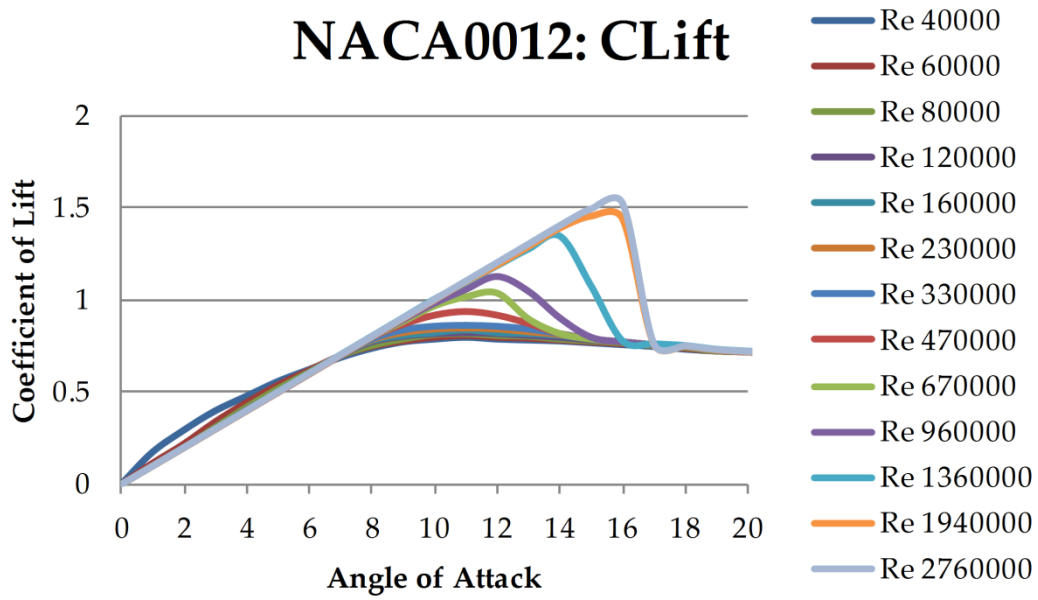

Figure A-0-2: C_L for low alpha

Drag:

Alpha	Re 40000	Re 60000	Re 80000	Re 120000	Re 160000	Re 230000
0	0.025	0.021	0.018	0.016	0.014	0.012
1	0.021	0.020	0.018	0.016	0.014	0.012
2	0.018	0.017	0.017	0.015	0.013	0.011
3	0.017	0.018	0.018	0.016	0.014	0.012
4	0.018	0.017	0.018	0.015	0.014	0.012
5	0.018	0.019	0.018	0.016	0.014	0.013
6	0.020	0.020	0.019	0.018	0.016	0.014
7	0.022	0.022	0.022	0.020	0.018	0.017
8	0.032	0.031	0.028	0.026	0.022	0.020
9	0.044	0.040	0.036	0.032	0.028	0.025
10	0.070	0.063	0.055	0.049	0.042	0.035
11	0.100	0.098	0.090	0.080	0.068	0.056
12	0.130	0.130	0.130	0.125	0.111	0.091
13	0.150	0.150	0.150	0.150	0.148	0.145
14	0.170	0.170	0.170	0.170	0.170	0.170
15	0.190	0.190	0.190	0.190	0.190	0.190
16	0.210	0.210	0.210	0.210	0.210	0.210
17	0.230	0.230	0.230	0.230	0.230	0.230
18	0.250	0.250	0.250	0.250	0.250	0.250
19	0.268	0.268	0.268	0.268	0.268	0.268
20	0.290	0.290	0.290	0.290	0.290	0.290
21	0.305	0.305	0.305	0.305	0.305	0.305
22	0.318	0.318	0.318	0.318	0.318	0.318
23	0.342	0.342	0.342	0.342	0.342	0.342
24	0.375	0.375	0.375	0.375	0.375	0.375
25	0.410	0.410	0.410	0.410	0.410	0.410

Alpha	Re 330000	Re 470000	Re 670000	Re 960000	Re 1360000	Re 1940000	Re 2760000
0	0.011	0.010	0.010	0.010	0.010	0.010	0.009
1	0.011	0.011	0.011	0.011	0.011	0.011	0.009
2	0.010	0.010	0.010	0.010	0.010	0.010	0.009
3	0.011	0.010	0.010	0.010	0.010	0.010	0.010
4	0.011	0.011	0.011	0.011	0.011	0.010	0.010
5	0.012	0.011	0.011	0.011	0.011	0.011	0.010
6	0.013	0.012	0.012	0.012	0.012	0.011	0.011
7	0.015	0.014	0.013	0.013	0.013	0.013	0.011
8	0.018	0.016	0.015	0.014	0.014	0.013	0.012
9	0.022	0.020	0.017	0.016	0.015	0.014	0.013
10	0.029	0.024	0.020	0.018	0.018	0.016	0.014

11	0.044	0.032	0.023	0.021	0.020	0.018	0.016
12	0.070	0.050	0.032	0.025	0.023	0.020	0.018
13	0.130	0.114	0.072	0.041	0.027	0.023	0.021
14	0.170	0.167	0.150	0.098	0.042	0.033	0.026
15	0.190	0.190	0.190	0.185	0.132	0.045	0.033
16	0.210	0.210	0.210	0.210	0.210	0.192	0.045
17	0.230	0.230	0.230	0.230	0.230	0.230	0.230
18	0.250	0.250	0.250	0.250	0.250	0.250	0.250
19	0.268	0.268	0.268	0.268	0.268	0.268	0.268
20	0.290	0.290	0.290	0.290	0.290	0.290	0.290
21	0.305	0.305	0.305	0.305	0.305	0.305	0.305
22	0.318	0.318	0.318	0.318	0.318	0.318	0.318
23	0.342	0.342	0.342	0.342	0.342	0.342	0.342
24	0.375	0.375	0.375	0.375	0.375	0.375	0.375
25	0.410	0.410	0.410	0.410	0.410	0.410	0.410

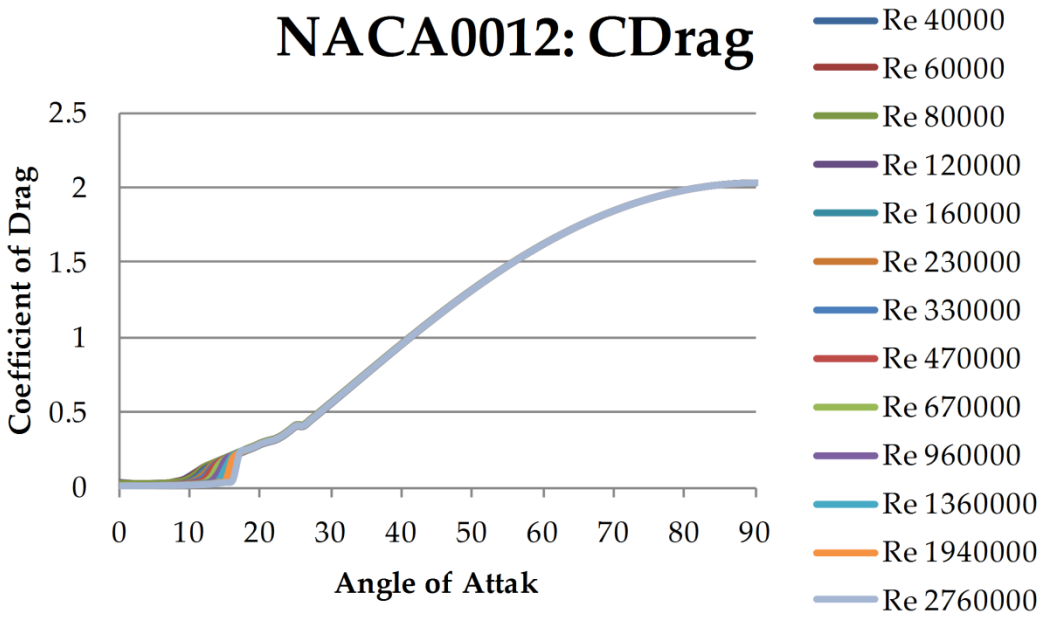

Figure A-0-3: C_D including stalled data

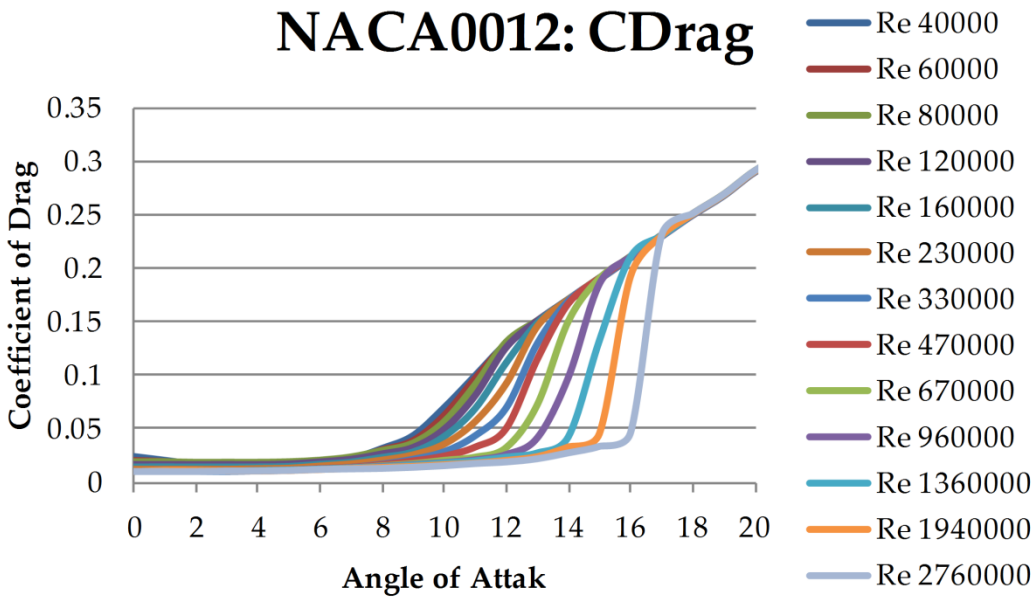

Figure A-0-4: C_D for low alpha

Appendix B: Trapezoidal Loading

This appendix derives equation (4-30), which is an expression for the contribution to a bending moment provided by a blade segment. This derivation is based on trapezoidal loading.

If $x(h)$ is the loading per unit length on a body acting perpendicular to the moment arm h, then the contribution to bending moment for a segment bounded by h_0 and h_1 is

$$\int_{h_0}^{h_1} x(h)hdh \tag{B.1}$$

When $x(h)$ is known at discretised stations along the body then trapezoidal loading can be employed to estimate the contribution to bending moment for the segment. Figure B-0-1 illustrates a structural body and the highlighted segment is bounded by an instantaneous force per unit length of $x(h_i)$ Nm^{-1} acting with moment arm h_i m and an instantaneous force per unit length of $x(h_{i+1})$ Nm^{-1} acting with a moment arm of h_{i+1} m.

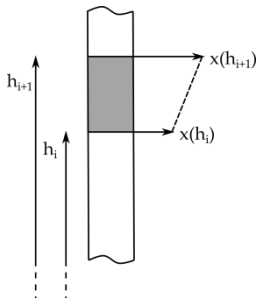

Figure B-0-1: Instantaneous force per unit length, x_i, and moment arm, h_i, for a structural element.

By assuming linear variation between the discretised stations *x(h)* can be expressed as

$$x(h) = x(h_i) + \frac{\left(x(h_{i+1}) - x(h_i)\right)}{(h_{i+1} - h_i)}(h - h_i) \tag{B.2}$$

Using the terminology $x(h_i) = x_i$ and substituting (B.2) into (B.1),

$$\int_{h_i}^{h_{i+1}} x(h)hdh = \int_{h_i}^{h_{i+1}} \left(x_i + \frac{(x_{i+1} - x_i)}{(h_{i+1} - h_i)}(h - h_i) \right) dh \tag{B.3}$$

$$= \left[\frac{h^2}{2} \left(x_i - h_i \frac{(x_{i+1} - x_i)}{(h_{i+1} - h_i)} \right) + \frac{h^3}{3} \frac{(x_{i+1} - x_i)}{(h_{i+1} - h_i)} \right]_{h_i}^{h_{i+1}} \tag{B.4}$$

$$= \frac{\left({h_{i+1}}^2 - {h_i}^2\right)}{2} \left(x_i - h_i \frac{(x_{i+1} - x_i)}{(h_{i+1} - h_i)} \right) + \frac{\left({h_{i+1}}^3 - {h_i}^3\right)}{3} \frac{(x_{i+1} - x_i)}{(h_{i+1} - h_i)} \tag{B.5}$$

Applying difference of squares and difference of cubes

$$= \frac{\left({h_{i+1}}^2 - {h_i}^2\right)}{2} x_i - \frac{(x_{i+1} - x_i)}{2}(h_{i+1} - h_i)h_i + \frac{(x_{i+1} - x_i)}{3}\left({h_{i+1}}^2 + 2h_{i+1}h_i + {h_i}^2\right) \tag{B.6}$$

$$= \frac{x_i}{6}\left({h_{i+1}}^2 - h_{i+1}h_i - 2{h_i}^2\right) + \frac{x_{i+1}}{6}\left(2{h_{i+1}}^2 + h_{i+1}h_i - {h_i}^2\right) \tag{B.7}$$

Appendix C: Phase-shifting VAWT Control Simulink Diagrams

C.1 Individual VAWT Model

C.1.1 VAWT Model

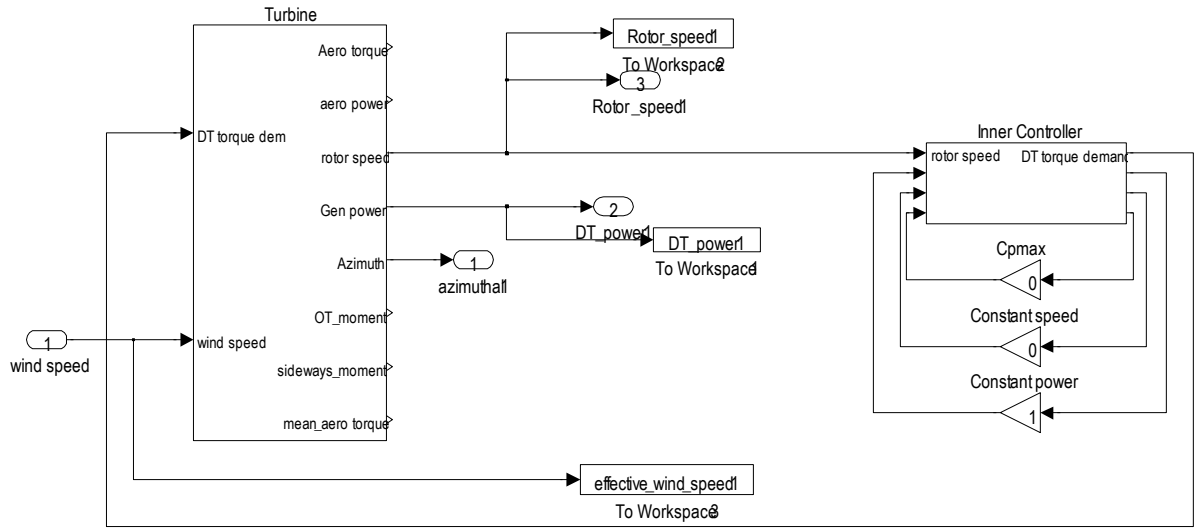

C.1.2 Rotor Dynamics

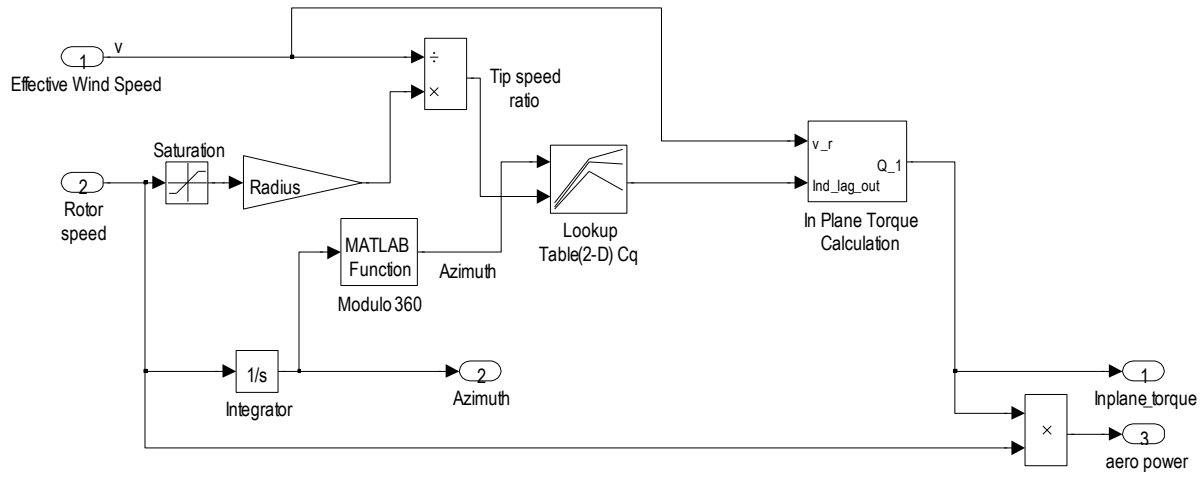

C.1.3 Drive-Train Dynamics

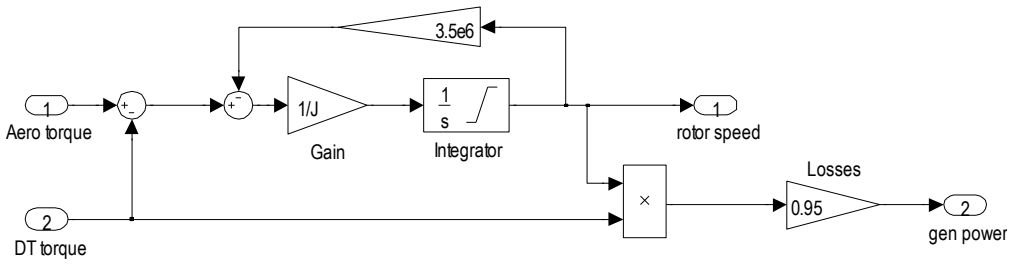

C.1.4 Inner Controller in Constant Power Tracking Mode

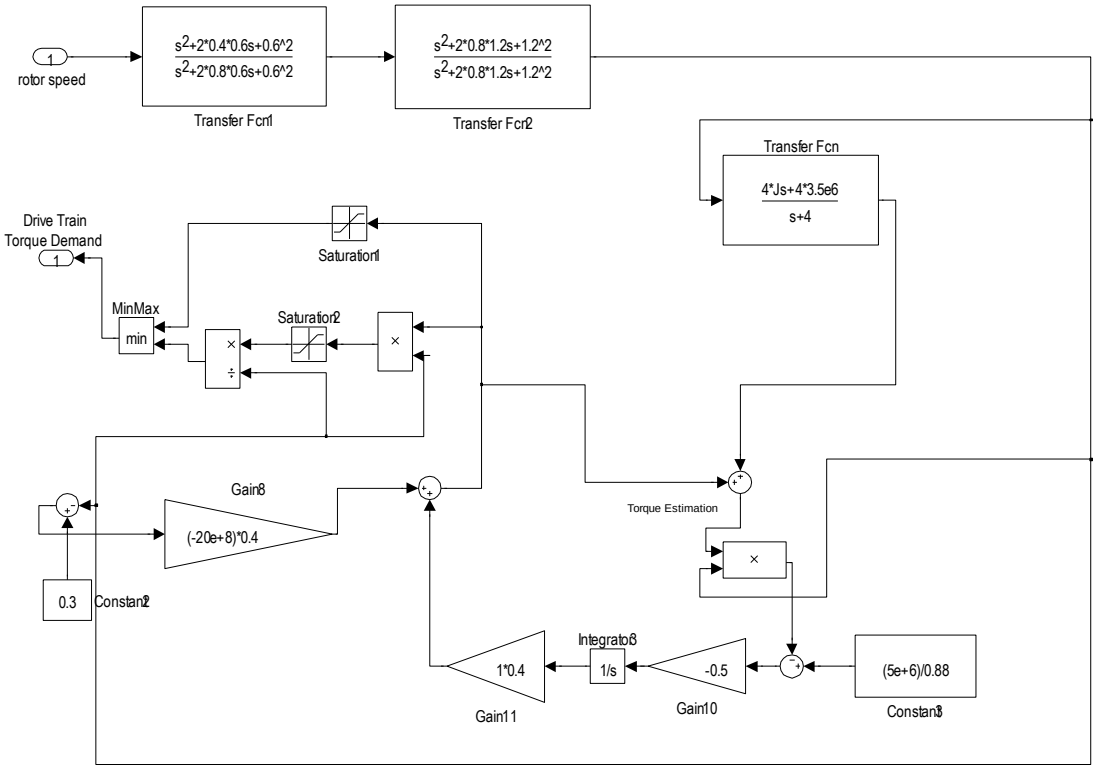

C.2 Stochastic Wind Model

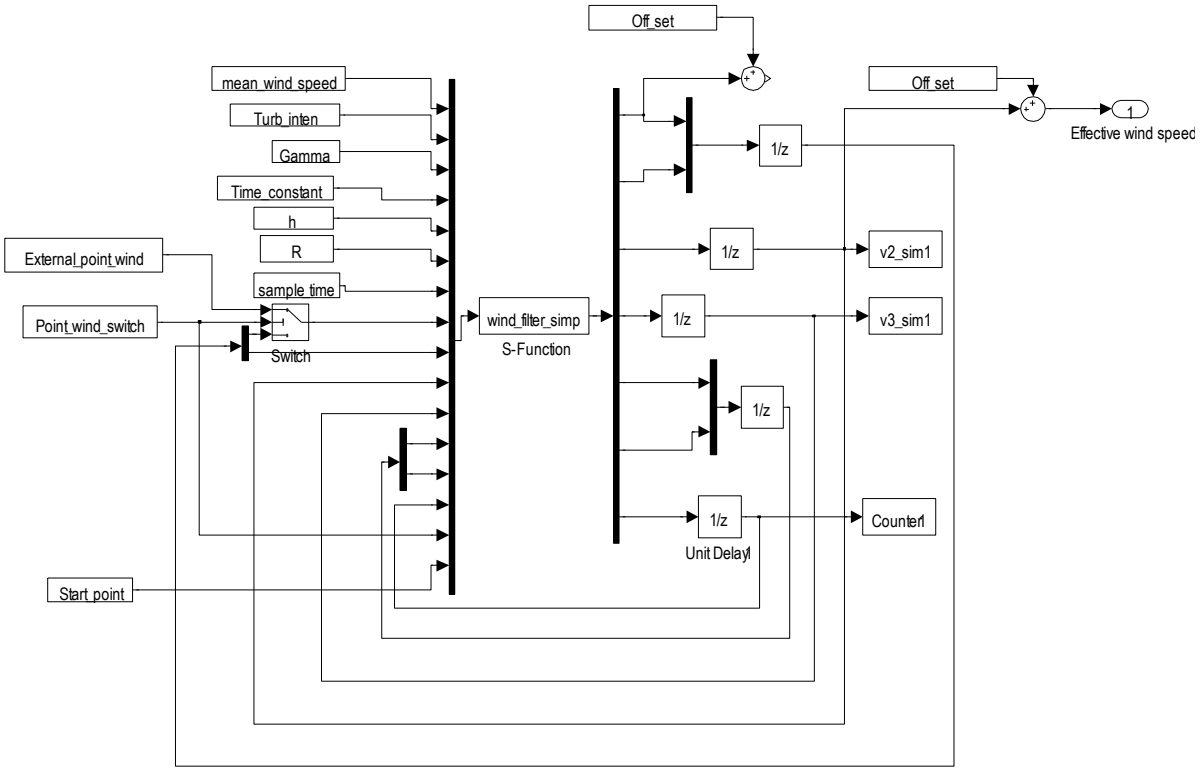

C.3 VAWT Farm Model

C.3.1 VAWT Farm

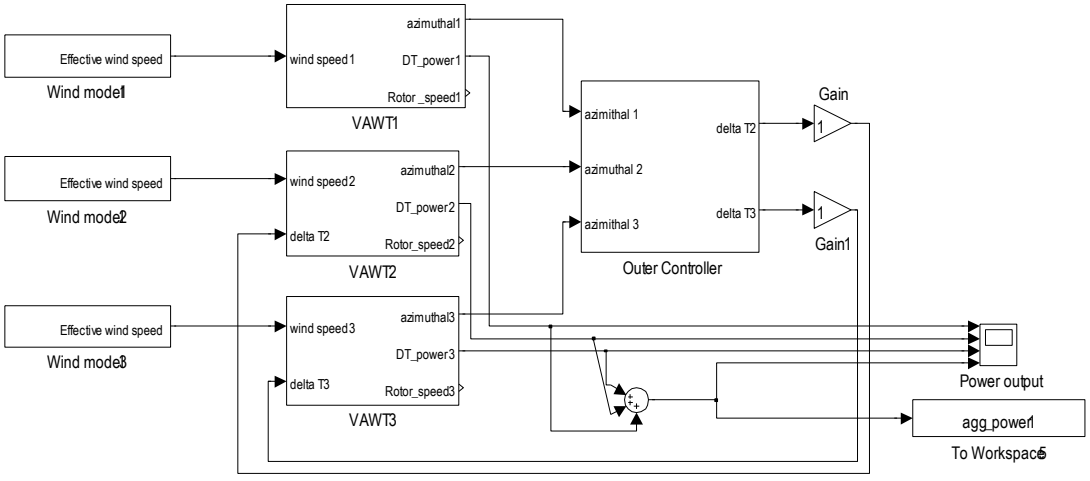

C.3.2 Outer Phase-Shifting Controller

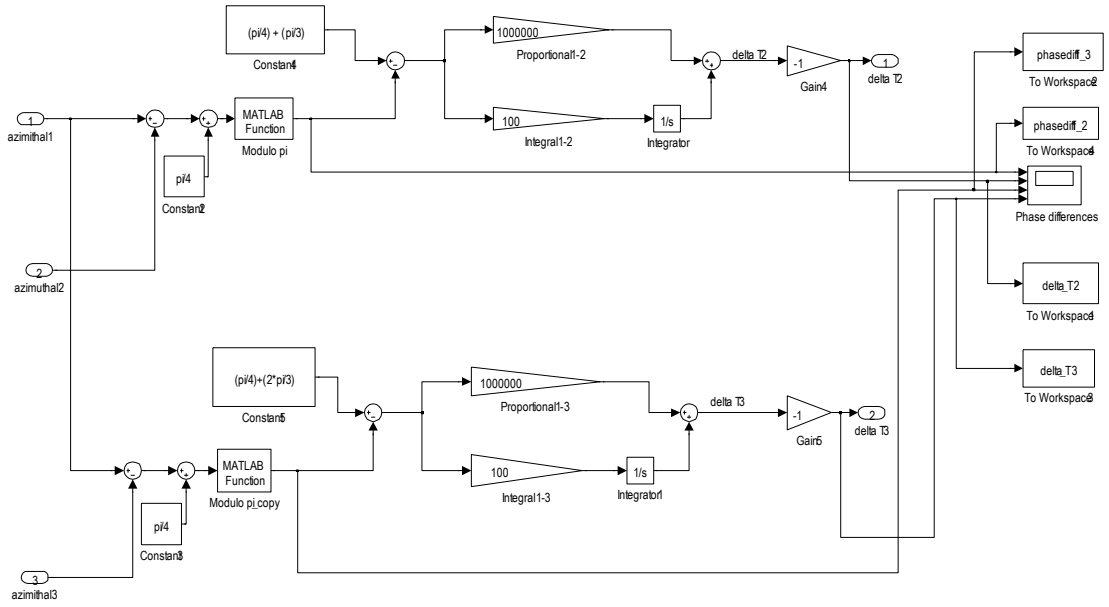

References

1. Twidell, J. and A. Weir, *Renewable energy resources*. 2006: Spon Pr.
2. Burton, T., *Wind energy: handbook*. 2001: Wiley.
3. Williams, A. *How to avoid a £100 million cost over-run on your next offshore wind project*. 2010 28/07/2011; Available from: http://social.windenergyupdate.com/offshore/how-avoid-%C2%A3100-million-cost-over-run-your-next-offshore-wind-project.
4. Marsh, G. and S. Peace, *Tilting at windmills:: Utility-scale VAWTs: towards 10MW and beyond?* Refocus, 2005. **6**(5): p. 37-42.
5. Hibbert, L., *Windmills on the Mind*, in *Professional Engineering*. 2011. p. 42-47.
6. Jamieson, P., *Innovation in Wind Turbine Design*. 2011: Wiley.
7. Islam, M., D. Ting, and A. Fartaj, *Aerodynamic models for Darrieus-type straight-bladed vertical axis wind turbines.* Renewable and Sustainable Energy Reviews, 2008. **12**(4): p. 1087-1109.
8. Ferreira, C., *The near wake of the VAWT: 2D and 3D views of the VAWT aerodynamics*. 2009, Delft University of Technology: F. Coton Associate Editor.
9. Paquette, J. and M. Barone, *Innovative offshore vertical-axis wind turbine rotor project.* EWEA 2012 Annual Event, Copenhagen, Denmark, 2012.
10. Vita, L., *Offshore floating Vertical Axis Wind Turbines with Rotating Platform*, in *DTU Riso*. 2011, Technical University of Denmark. p. 5.
11. Shires, A., *Design optimisation of an offshore vertical axis wind turbine.* Proceedings of the Institution of Civil Engineers, 2013. **166:** : p. 7-18.
12. Paulsen, U.S., et al., *DeepWind 5 MW Baseline design.* Energy Procedia, 2012. **24**: p. 27-35.
13. Nenuphar. *Vertiwind: making floating wind turbine technology competitive for offshore*. 2012 21/10/2013; Available from: http://www.twenties-project.eu/system/files/2_2013-03%20Presentation%20short.pdf.
14. MODEC. *Floating Wind and Current Hybrid Power Generation*. 2013 08/11/2013; Available from: http://www.modec.com/fps/skwid/.
15. Twirl, S. *A new type of offshore wind turbine*. 2012 21/10/2013; Available from: http://www.seatwirl.com/.
16. Ljungstroem, O. *Some innovative concepts in wind turbines of the axial-flow, cross-flow, and combined (dual) flow types*. in *Fifth Bien. Wind Energy Conference and Workshop (WW5)*. 1981.

17. Sharpe, D.J., *Vertical axis turbine apparatus, US 8038383 B2*. 2006.
18. Shires, A., *Development and Evaluation of an Aerodynamic Model for a Novel Vertical Axis Wind Turbine Concept.* Energies, 2013. **6**(5): p. 2501-2520.
19. Leithead, W., S. De la Salle, and D. Reardon, *Role and objectives of control for wind turbines.* Generation, Transmission and Distribution IEE Proceedings, 1991. **138**(2): p. 135-148.
20. Leithead, W., et al. *Wind turbine modelling and control*. in *International Conference on Control*. 1991. Edinburgh: IET.
21. Bossanyi, E., *Wind turbine control for load reduction.* Wind Energy, 2003. **6**(3): p. 229-244.
22. Grylls, W., B. Dale, and P. Sarre. *A theoretical and experimental investigation into the variable pitch vertical axis wind turbine*. in *Proc. 2nd Int. Symposium on Wind energy Systems, Amsterdam*. 1978.
23. McConnell, R.D., *Giromill overview*. 1979, Solar Energy Research Inst., Golden, CO (USA).
24. Madsen, H.A. and K. Lundgren, *The Voith-Schneider Wind Turbine: Some Theoretical and Experimental Results on the Aerodynamics of the Voith-Schneider Wind Turbine*. 1980: Aalborg University Centre, Institute of Industrial Constructions and Energy Technology.
25. Vandenbereghe, D. and E. Dick, *A theoretical and experimental investigation into the straight bladed vertical axis wind turbine with second order harmonic pitch control.* Wind Engineering, 1986. **10**: p. 122-138.
26. Kirke, B.K., *Evaluation of self-starting vertical axis wind turbines for stand-alone applications*. 1998, Griffith University.
27. Pawsey, N.C.K., *Development and evaluation of passive variable-pitch vertical axis wind turbines*. 2002: University of New South Wales.
28. McIntosh, S., H. Babinsky, and T. Bertényi, *Convergence Failure and Stall Hysteresis in Actuator-Disk Momentum Models Applied to Vertical Axis Wind Turbines.* Journal of Solar Energy Engineering, 2009. **131**: p. 034502.
29. Sharpe, D. and L. Freris, *Wind Energy Conversion Systems*. 1990: Prentice Hall.
30. Paraschivoiu, I., *Wind turbine design: with emphasis on Darrieus concept*. 2002: Presses inter Polytechnique.
31. Peace, S. *Another Approach to Wind*. 2004 12/08/2013; Available from: http://www.windturbine-performance.com/www/another%20approach%20to%20wind-apptowind.html.
32. Gipe, P. *Wind-Works*. 21/09/2013; Available from: http://www.wind-works.org/cms/index.php?id=219.

33. Freris, L. and D. Sharpe, *Wind Energy Conversion Systems*. 1990: Prentice Hall.
34. Mays, I.D., et al. *Experience With The VAWT 850 Demonstration Project*. in *EWEC 1990*. 1990.
35. Betz, A. and U.S.N.A.C.f. Aeronautics, *Windmills in the light of modern research*. 1928: National Advisory Committee for Aeronautics.
36. Reuter, R.C., et al., *Torque ripple in a vertical axis wind turbine*. 1978: Sandia Laboratories.
37. Powles, S., C. Anderson, and C. Tan. *Two years of operation of the 25m VAWT at Carmarthen Bay*. in *Conference Proceedings, EWEC, Glasgow, UK*. 1989.
38. Watson, G. *The self-starting capabilities of low-solidity fixed pitch Darrieus rotors*. in *Wind Energy Workshop*. 1979.
39. Sutherland, H.J., D.E. Berg, and T.D. Ashwill, *A retrospective of VAWT technology.* Sandia Report SAND2012-03044 Sandia National Laboratories: Livermore, CA, 2012.
40. Khan, M., et al., *Hydrokinetic energy conversion systems and assessment of horizontal and vertical axis turbines for river and tidal applications: A technology status review.* Applied Energy, 2009. **86**(10): p. 1823-1835.
41. Kaare Jr, F. and E. Evensen, *Turbine driven with a fluid medium*. 2005, Google Patents.
42. Calcagno, G., et al., *Experimental and numerical investigation of an innovative technology for marine current exploitation: the Kobold turbine.* Proc. 16th IOPEC, 2006. **1**.
43. Schönborn, A. and M. Chantzidakis, *Development of a hydraulic control mechanism for cyclic pitch marine current turbines.* Renewable energy, 2007. **32**(4): p. 662-679.
44. Lazauskas, L. and B. Kirke, *Modeling passive variable pitch cross flow hydrokinetic turbines to maximize performance and smooth operation.* Renewable Energy, 2012. **45**: p. 41-50.
45. Musgrove, P., *Wind power: the story so far*. 2007.
46. Savonius, S.J., *Savonius U.S. Patent No. 1,766,765*. 1930, Google Patents.
47. Darrieus, G.J., *Turbine having its rotating shaft transverse to the flow of current*. 1953, Google Patents.
48. Templin, R. and R. Rangi, *Vertical-axis wind turbine development in Canada.* Physical Science, Measurement and Instrumentation, Management and Education-Reviews, IEE Proceedings A, 1983. **130**(9): p. 555-561.
49. Wilson, R. and P. Lissaman, *Applied aerodynamics of wind power machines*. 1974, Oregon State Univ., Corvallis (USA).

50. Sheldahl, R.E. and B. Blackwell, *Free-air performance tests of a 5-metre-diameter Darrieus turbine*, in *NASA STI/Recon Technical Report N*. 1977, Sandia National Laboratories. p. 25632.
51. Worstell, M.H., *Aerodynamic Performance of the 17 Meter Diameter Darrieus Wind Turbine*. 1978, Sandia National Laboratories.
52. Ashwill, T.D., *Measured Data for the Sandia 34-Meter Vertical Axis Wind Turbine*. 1992, Sandia Nationla Laboratories.
53. Carlin, P.W., A.S. Laxson, and E. Muljadi, *The History and State of the Art of Variable Speed Wind Turbine Technology.* Wind Energy, 2003. **6**(2): p. 129-159.
54. Musgrove, P., *Wind energy conversion: recent progress and future prospects.* Solar & wind technology, 1987. **4**(1): p. 37-49.
55. Powles, S., C. Anderson, and C. Tan. *Two years of operation of the 25m VAWT at Carmarthen Bay*. 1989.
56. Price, T.J., *UK Large-scale wind power programme from 1970 to 1990: The Carmarthen Bay experiments and the Musgrove vertical-axis turbines.* Wind Engineering, 2006. **30**(3): p. 225-242.
57. Holme, O. *A contribution to the aerodynamic theory of the vertical-axis wind turbine*. 1977.
58. Drees, H. *The cycloturbine and its potential for broad application*. in *Second International Symposium on Wind Energy Systems, Amsterdam, Netherlands,(Oct. 3-6, 1978) pp. E7-81 to E7-88*. 1978.
59. Brulle, R., *Feasibility investigation of the giromill for generation of electrical power*. 1975, McDonnell Aircraft Co., St. Louis, MO (USA).
60. Vandenberghe, D. and E. Dick, *Optimum pitch control for vertical axis wind turbines.* Wind Engineering, 1987. **11**(5): p. 237-247.
61. *Engineering Village Compendex*. 11/01/2014; Available from: http://www.engineeringvillage.com/.
62. *Science Direct*. 10/01/2014; Available from: http://www.sciencedirect.com/.
63. Bossanyi, E., G. Ramtharan, and B. Savini, *The importance of control in wind turbine design and loading.* 2009.
64. Baker, J., *Features to aid or enable self starting of fixed pitch low solidity vertical axis wind turbines.* Journal of Wind Engineering and Industrial Aerodynamics, 1983. **15**(1): p. 369-380.
65. Robotham, A., J, and D. Sharpe, J,. *The Aerodynamic Control of the 'V' Type Vertical Axis Wind Turbine by Blade Tip Control*. in *British Wind Energy Association*. 1986.
66. Sharpe, D., D. Taylor, and G. Boyle. *Developments with the 'V'-type vertical axis wind turbine*. in *Proc 1987 9th British Wind Energy*

Association Annual Conference, Wind Energy Conversion, JM G alt (ed). 1987.
67. *NOVA project*. 01/08/2011; Available from: http://www.nova-project.co.uk/.
68. Staelens, Y., F. Saeed, and I. Paraschivoiu. *A straight-bladed variable-pitch VAWT concept for improved power generation*. in *Proceedings of the 22nd ASME Wind Energy Symposium held in Conjunction with the 41st Aerospace Sciences Meeting & Exhibit.* . 2003.
69. Fiedler, A.J. and S. Tullis, *Blade offset and pitch effects on a high solidity vertical axis wind turbine.* Wind Engineering, 2009. **33**(3): p. 237-246.
70. Simão Ferreira, C. and F. Scheurich, *Demonstrating that power and instantaneous loads are decoupled in a vertical-axis wind turbine.* Wind Energy, 2013.
71. Vries, O.d., *Fluid dynamic aspects of wind energy conversion*. 1979, DTIC Document.
72. Moran, W., *Giromill wind tunnel test and analysis. Volume 1: Executive summary.* Final Report, Jun. 1976-Oct. 1977 McDonnell Aircraft Co., Saint Louis, MO., 1977. **1**.
73. Brulle, R., *McDonnell 40-kW Giromill Wind System. Phase II. Fabrication and test*. 1980, McDonnell Aircraft Co., St. Louis, MO (USA).
74. Cooper, P. and O.C. Kennedy, *Development and analysis of a novel vertical axis wind turbine.* 2004.
75. Hwang, I.S., et al. *Efficiency Improvement of Cycloidal Wind Turbine by Active Control of Blade Motion*. 2005.
76. Hwang, I.S., et al., *Efficiency improvement of a new vertical axis wind turbine by individual active control of blade motion.* Smart Structures and Materials 2006: Smart Structures and Integrated Systems, 2006. **6173**: p. 316-323.
77. Leithead, W. and B. Connor, *Control of variable speed wind turbines: design task.* International Journal of Control, 2000. **73**(13): p. 1189-1212.
78. Zervos, A., S. Dessipiris, and N. Athanassiadis. *Optimisation of the performance of the variable pitch vertical axis wind turbine*. in *Proc. EWEC conf, Hamburg, FRG, 22e26 Oct*. 1984.
79. Kirke, B. and L. Lazauskas, *Enhancing the performance if a vertical axis wind turbine using a simple variable pitch system.* Wind Engineering, 1991. **15**(4): p. 187-195.
80. Lazauskas, L. and B. Kirke, *Performance optimisation of a self-acting variable pitch vertical axis wind turbine.* Wind Engineering, 1992. **16**(1): p. 10-26.
81. Lazauskas, L., *Three pitch control systems for vertical axis wind turbines compared.* Wind Engineering, 1992. **16**(5): p. 269-282.

82. Kirke, B. and L. Lazauskas, *Experimental verification of a mathematical model for predicting the performance of a self-acting variable pitch vertical axis wind turbine.* Wind Engineering, 1993. **17**(2): p. 58-66.
83. Kosaku, T., M. Sano, and K. Nakatani. *Optimum pitch control for variable-pitch vertical-axis wind turbines by a single stage model on the momentum theory*. 2002. IEEE.
84. Paraschivoiu, I., et al., *Aerodynamic analysis of the Darrieus rotor including secondary effects.* J. Energy;(United States), 1983. **7**(5).
85. Paraschivoiu, I., O. Trifu, and F. Saeed, *H-Darrieus wind turbine with blade pitch control.* International Journal of Rotating Machinery, 2009.
86. Cheng, J., S. Su, and J. Miau, *Application of Variable Blade Pitch Control on Improving the Performance of Vertical Axis Wind Turbine.* Applied Mechanics and Materials, 2012. **229**: p. 2339-2342.
87. Miau, J., et al., *Design and Test of a Vertical-Axis Wind Turbine with Pitch Control.* Applied Mechanics and Materials, 2012. **225**: p. 338-343.
88. Yao, Y.X., et al., *Numerical Study of Pitch Angle on H-Type Vertical Axis Wind Turbine.* Key Engineering Materials, 2012. **499**: p. 259-264.
89. Zhang, L., et al. *Vertical Axis Wind Turbine with Individual Active Blade Pitch Control*. in *Power and Energy Engineering Conference (APPEEC), 2012 Asia-Pacific*. 2012. IEEE.
90. Laks, J.H., L.Y. Pao, and A.D. Wright. *Control of wind turbines: Past, present, and future*. 2009. IEEE.
91. Leithead, W., et al. *Wind turbine modelling and control*. 1991. IET.
92. Leithead, W. and B. Connor, *Control of variable speed wind turbines: dynamic models.* International Journal of Control, 2000. **73**(13): p. 1173-1188.
93. Leithead, W., *Dependence of performance of variable speed wind turbines on the turbulence, dynamics and control.* Generation, Transmission and Distribution [see also IEE Proceedings-Generation, Transmission and Distribution], IEE Proceedings, 1990. **137**(6): p. 403-413.
94. Eriksson, S., H. Bernhoff, and M. Leijon, *A 225 kW direct driven PM generator adapted to a vertical axis wind turbine.* Advances in Power Electronics, 2011. **2011**.
95. McNerney, G.M., *Vertical axis wind turbine control strategy*. 1981, Sandia National Labs., Albuquerque, NM (USA).
96. Goude, A. and F. Bülow, *Robust VAWT control system evaluation by coupled aerodynamic and electrical simulations.* Renewable energy, 2013. **59**: p. 193-201.
97. Simao Ferreira, C., *The near wake of the VAWT: 2D and 3D views of the VAWT aerodynamics.* 2009.

98. Goldstein, S., *On the vortex theory of screw propellers.* Proceedings of the Royal Society of London. Series A, 1929. **123**(792): p. 440.
99. Prandtl, L., et al., *Applied hydro-and aeromechanics*. 1957: Dover publications.
100. Migliore, P. and W. Wolfe. *Some effects of flow curvature on the performance of Darrieus wind turbines*. 1979.
101. Hirsch, C. and A. Mandal. *Flow curvature effect on vertical axis Darrieus wind turbine having high chord-radius ratio*. in *Proceedings of European Wind Energy Conference*. 1984.
102. Cardona, J.L., *Flow curvature and dynamic stall simulated with an aerodynamic free-vortex model for VAWT.* Wind Engineering, 1984. **8**: p. 135-143.
103. Strickland, J.H., B. Webster, and T. Nguyen, *Vortex model of the Darrieus turbine: An analytical and experimental study.* NASA STI/Recon Technical Report N, 1980. **80**: p. 25887.
104. Sharpe, D. *Refinements and developments of the multiple streamtube theory for the aerodynamic performance of vertical axis wind turbines*. in *6th BWEA Wind Energy Conference*. 1984.
105. Read, S. and D. Sharpe. *An extended multiple streamtube theory for vertical axis wind turbines*. 1980.
106. Leishman, J.G., *Challenges in modelling the unsteady aerodynamics of wind turbines.* Wind energy, 2002. **5**(2-3): p. 85-132.
107. McCroskey, W., *The phenomenon of dynamic stall*. 1981, DTIC Document.
108. Gormont, R.E., *A mathematical model of unsteady aerodynamics and radial flow for application to helicopter rotors*. 1973, DTIC Document.
109. Tran, C. and D. Petot, *Semi-empirical model for the dynamic stall of airfoils in view of the application to the calculation of responses of a helicopter blade in forward flight.* 1980.
110. McAlister, K.W., O. Lambert, and D. Petot, *Application of the ONERA model of dynamic stall*. 1984, DTIC Document.
111. Beddoes, T., *A synthesis of unsteady aerodynamic effects including stall hysteresis.* Vertica, 1976. **1**(2): p. 113-123.
112. Leishman, J. and T. Beddoes. *A generalised model for airfoil unsteady aerodynamic behaviour and dynamic stall using the indicial method*. in *Proceedings of the 42nd Annual Forum of the American Helicopter Society, Washington DC*. 1986.
113. Øye, S. *Dynamic stall simulated as time lag of separation*. in *Proceedings of the 4th IEA Symposium on the aerodynamics of wind turbines*. 1991.

114. Hansen, M., M. Gaunaa, and H. Madsen, *A Beddoes-Leishman type dynamic stall model in state-space and indicial formulations, Report No.* R-1354 (EN), Risø National Laboratory, 2004.
115. Massé, B., *Description de deux programmes d'ordinateur pour le calcul des performances et des charges aérodynamiques pour les éoliennes à axe vertical*. 1981: Institut de recherche de l'Hydro-Québec.
116. Berg, D. *Improved double-multiple streamtube model for the Darrieus-type vertical axis wind turbine*. 1983.
117. Masson, C., C. Leclerc, and I. Paraschivoiu, *Appropriate dynamic-stall models for performance predictions of VAWTs with NLF blades.* International Journal of Rotating Machinery, 1997. **4**(2): p. 129-139.
118. Carpenter, P.J. and B. Fridovich, *Effect of a rapid blade-pitch increase on the thrust and induced-velocity response of a full-scale helicopter rotor*. 1953: National Advisory Committee for Aeronautics.
119. Larsen, H., *Summary of a Vortex Theory for the Cyclogiro.* Proceedings of the Second US National Conferences on Wind Engineering Research, Colorado State University, 1975. **8**: p. 1-3.
120. Strickland, J., B. Webster, and T. Nguyen, *A vortex model of the Darrieus turbine: an analytical and experimental study.* Journal of Fluids Engineering, 1979. **101**: p. 500.
121. Wilson, R. and S. Walker, *Fixed-wake analysis of the Darrieus rotor*. 1981, Sandia National Labs., Albuquerque, NM (USA); Oregon State Univ., Corvallis (USA). Dept. of Mechanical Engineering.
122. Madsen, H.A., *The actuator cylinder: A flow model for vertical axis wind turbines*. 1982: Institute of Industrial Constructions and Energy Technology, Aalborg University Centre.
123. Glauert, H., *The Elements of Airfoil and Airscrew Theory*. 1959: Cambridge University Press.
124. Hansen, M.O.L., *Aerodynamics of wind turbines*. 2008: Earthscan/James & James.
125. Templin, R., *Aerodynamic performance theory for the NRC vertical-axis wind turbine.* NASA STI/Recon Technical Report N, 1974. **76**: p. 16618.
126. Strickland, J.H., *Darrieus turbine: a performance prediction model using multiple streamtubes*. 1975, Sandia Labs., Albuquerque, N. Mex.(USA).
127. Muraca, R., M. Stephens, and J. Dagenhart, *Theoretical performance of cross-wind axis turbines with results for a catenary vertical axis configuration.* 1975.
128. Sharpe, D., *An aerodynamic performance theory for the Darrieus wind turbine.* Int. Symp. on Wind Energy Systems, 1976(Sept. St John's College Cambridge, England).

129. Lapin, E., *Theoretical performance of vertical axis wind turbines.* American Society of Mechanical Engineers, 1975. **1**.
130. Paraschivoiu, I. *Double-multiple streamtube model for Darrieus wind turbines*. 1981.
131. Stacey, G. and P. Musgrove, J. *Developments on Vertical Axis Wind Turbine Streamtube Theories*. in *British Wind Energy Association*. 1986.
132. McCoy, H. and J. Loth, *Up-and down-wind rotor half interference model for VAWT.* AIAA Pap.;(United States), 1981. **81**(CONF-811205-).
133. Newman, B., *Actuator-disc theory for vertical-axis wind turbines.* Journal of Wind Engineering and Industrial Aerodynamics, 1983. **15**(1-3): p. 347-355.
134. Newman, B., *Multiple actuator-disc theory for wind turbines.* Journal of Wind Engineering and Industrial Aerodynamics, 1986. **24**(3): p. 215-225.
135. Paraschivoiu, I. and P. Fraunie, *Streamtube expansion effects on the Darrieus wind turbine.* J. Propul. Pow.;(United States), 1985. **1**.
136. Paraschivoiu, I., *Double-multiple streamtube model for studying vertical-axis wind turbines.* Journal of Propulsion Power, 1988. **4**: p. 370-377.
137. Touryan, K., J. Strickland, and D. Berg, *Electric power from vertical-axis wind turbines.* Journal of Propulsion Power, 1987. **3**: p. 481-493.
138. Sheldahl, R.E. and P.C. Klimas, *Aerodynamic characteristics of seven symmetrical airfoil sections through 180-degree angle of attack for use in aerodynamic analysis of vertical axis wind turbines*. 1981, Sandia National Labs., Albuquerque, NM (USA).
139. Glauert, H., *The analysis of experimental results in the windmill brake and vortex ring states of an airscrew.* Reports and Memoranda, 1926(1026): p. 1-10.
140. Islam, M., D.S.K. Ting, and A. Fartaj, *Desirable airfoil features for smaller-capacity straight-bladed VAWT.* Wind Engineering, 2007. **31**(3): p. 165-196.
141. Manwell, J.F., J.G. McGowan, and A.L. Rogers, *Wind energy explained*. 2002: Wiley Online Library.
142. Slootweg, J., et al. *Aggregated modelling of wind parks with variable speed wind turbines in power system dynamics simulations*. Proceedings of the 14th Power Systems Computation Conference, 2002.
143. Freris, L., *Wind energy conversion systems*. 1990, New York: Prentice Hall.
144. Ferreira, C.S. and F. Scheurich, *Demonstrating that power and instantaneous loads are decoupled in a vertical-axis wind turbine.* Wind Energy, 2013.

145. Loth, J.L. and H. McCoy, *Optimization of Darrieus turbines with an upwind and downwind momentum model.* Journal of Energy, 1983. **7**(4): p. 313-318.
146. Anderson, C., H. Heerkes, and R. Yemm. *The use of blade-mounted dampers to eliminate edgewise stall vibration*. in *EWEC-CONFERENCE-*. 1999.